An investigation into the role of dendrimers as potential enhancers of the dermal delivery of topically applied chlorhexidine.

Amy Maryanne Judd

December 2013

Thesis submitted for degree of Doctor of Philosophy

Keele University

SUBMISSION OF THESIS FOR A RESEARCH DEGREE

Part I. DECLARATION by the candidate for a research degree. To be bound in the thesis

Degree for which thesis being submitted **Doctor of Philosophy**

Title of thesis **An investigation into the role of dendrimers as potential enhancers of the dermal delivery of topically applied chlorhexidine.**

Date of submission 31/10/13 Original registration date 21/09/09
(Date of submission must comply with Regulation 2D)

Name of candidate Amy Maryanne Judd

Research Institute ISTM Name of Lead Supervisor Dr. Gary Moss

I certify that:

(a) The thesis being submitted for examination is my own account of my own research
(b) My research has been conducted ethically. Where relevant a letter from the approving body confirming that ethical approval has been given has been bound in the thesis as an Annex
(c) The data and results presented are the genuine data and results actually obtained by me during the conduct of the research
(d) Where I have drawn on the work, ideas and results of others this has been appropriately acknowledged in the thesis
(e) Where any collaboration has taken place with one or more other researchers, I have included within an 'Acknowledgments' section in the thesis a clear statement of their contributions, in line with the relevant statement in the Code of Practice (see Note overleaf).
(f) The greater portion of the work described in the thesis has been undertaken subsequent to my registration for the higher degree for which I am submitting for examination
(g) Where part of the work described in the thesis has previously been incorporated in another thesis submitted by me for a higher degree (if any), this has been identified and acknowledged in the thesis
(h) The thesis submitted is within the required word limit as specified in the Regulations

Total words in submitted thesis (including text and footnotes, but excluding references and appendices) 75, 622

Signature of candidate  Date 19/11/13

Note
Extract from Code of Practice: If the research degree is set within a broader programme of work involving a group of investigators – particularly if this programme of work predates the candidate's registration – the candidate should provide an explicit statement (in an 'Acknowledgments' section) of the respective roles of the candidate and these other individuals in relevant aspects of the work reported in the thesis. For example, it should make clear, where relevant, the candidate's role in designing the study, developing data collection instruments, collecting primary data, analysing such data, and formulating conclusions from the analysis. Others involved in these aspects of the research should be named, and their contributions relative to that of the candidate should be specified (*this does not apply to the ordinary supervision, only if the supervisor or supervisory team has had greater than usual involvement*).

Thesis Abstract

The reduction of bacteria on the skin results in prophylactic and therapeutic benefits by reducing the occurrence of skin infections. Currently, chlorhexidine digluconate, a conventional topical antiseptic, permeates the skin poorly leaving viable opportunistic pathogens below the superficial layers of the *stratum corneum.* The aim of this study was to use polyamidoamine (PAMAM) dendrimers to enhance the topical delivery of chlorhexidine digluconate to improve its antimicrobial efficacy.

This study has characterised the antimicrobial inhibition and mechanism of action of PAMAM dendrimers against clinically relevant skin pathogens. This thesis has showed that the PAMAM dendrimers antimicrobial effect is concentration and generation dependent (i.e. increasing number of surface groups) and that the mechanism of inhibition is through severe outer and inner bacterial membrane permeabilisation and disruption. A topical skin pre-treatment of various antimicrobial concentrations of PAMAM dendrimer followed by a clinical dose of chlorhexidine digluconate (2% w/v aq soln.) resulted in a significant increase in permeation of chlorhexidine digluconate *in vitro* using a Franz diffusion cell model. This study also reports possible mechanisms of penetration enhancement exerted by the PAMAM dendrimer and shows evidence that their effect upon the skin is multifactorial. A novel time-of-flight secondary ion mass spectrometry method was developed and employed that chemically mapped the distribution of chlorhexidine digluconate within skin tissue after topical application. The chemical distribution images showed an enhanced deposition of chlorhexidine

digluconate within the upper skin strata after topical application of PAMAM dendrimer, supporting the Franz diffusion cell findings.

Further, this study investigated the co-application of PAMAM dendrimer-chlorhexidine digluconate to the skin and found that a one-step application significantly increased the deposition of chlorhexidine digluconate within the upper skin strata. PAMAM dendrimers have the capacity to be versatile topically-applied polyvalent biocides/drug delivery platforms that have many biomedical applications.

List of Figures

List of Tables

Abbreviations

5-FU	5-Fluorouracil
8-MOP	8-Methoxypsoralene
AFM	Atomic Force Microscopy
AMP	Antimicrobial Peptide
ANOVA	Analysis of Variance
ATCC	American Type Culture Collection
ATP	Adenosine Triphosphate
ATR-FTIR	Attenuated Total Reflectance Fourier Transform Infra-red spectroscopy
AUC	Area Under Curve
CDC	Centre for Disease Control
CFU	Colony Forming Unit
CHG	Chlorhexidine Digluconate
CHX	Chlorhexidine (Base)
CLSI	Clinical and Laboratory Standards Institute
CLSM	Confocal Laser Scanning Microscopy
CMO	Chief Medical Officer
CRM	Confocal Raman Microscopy
DF	Degrees of Freedom
DMSO	Dimethylsulfoxide
DNA	Deoxyribonucleic Acid
DOC	Deoxycholate
DPPG	Dipalmitoylphosphatidylglycerol
DPX	Dibutyl Phthalate in Xylene
DSC	Differential Scanning Calorimetry
EC_{50}	Half Maximal Effective Concentration

EDTA	Ethylenediaminetetraacetic Acid
EPSRC	Engineering and Physical Sciences Research Council
FDA	Food and Drug Administration
G	Generation
HCAI	Healthcare Acquired Infection
HCEC	Human Corneal Epithelial Cells
HEC	Hydroxyethyl Cellulose
HEMA	Hydroxyethyl Methacrylate
HPC	Hydroxyl Propyl Cellulose
HPLC	High Performance Liquid Chromatography
HPMC	Hydroxyl Propyl Methyl Cellulose
IC50	Inhibitory Concentration at 50%
IPM	Isopropyl Myristate
IR	Infra Red
LOD	Limits of Detection
LOQ	Limits Of Quantification
LPS	Lipopolysaccharide
LSD	Least Significant Difference
MALDI IMS	Matrix-Assisted Laser Desorption/Ionisation Imaging Mass Spectrometry
MALDI TOF	Matrix-Assisted Laser Desorption/Ionisation - Time of Flight mass spectrometry
MCE	Mixed Cellulose Esters
MHA	Mueller-Hinton Agar
MHB	Mueller-Hinton Broth
MIC	Minimum Inhibitory Concentration
MRI	Magnetic Resonance Imaging

MRSA	Multi-drug Resistant *Staphylococcus aureus*
NCHG	Nanocomposite Biocompatible Hydrogels
NIPAM	N-isopropylacrylamide
NSAID	Non-steroidal Anti-inflammatory Drug
OCT	Optimal Cutting Temperature
OCT	Optical Coherence Tomography
OECD	Organisation for Economic Cooperation and Development
ONPG	*Ortho*-Nitrophenyl-β-Galactoside
PAMAM	Polyamidoamine
PBS	Phosphate-Buffered Saline
PEGDMA	Polyethyleneglycol Dimethylacrylate
PEGDMA	Polyethyleneglycol
PES	Pig Ear Skin
PHA	Polyhydroxyalkonoate
PITC	Phenylisothiocyanate
PLGA	Poly-lactic-co-glycolic acid
PNBCA	Poly n-butylcyanoacrylate
PPI	Poly(propylene imine)
PS-OCT	Polarisation Sensitive Optical Coherence Tomography
PVDF	Polyvinyldifluoride
RH	Relative Humidity
RI	Refractive Index
RNA	Ribonucleic Acid
ROI	Region of Interest
ROS	Reactive Oxygen Species

RSD	Relative Standard Deviation
SAXD	Small Angle x-ray Diffusion
SC	*Stratum Corneum*
SD	Standard Deviation
SDS	Sodium Dodecyl Sulphate
SEM	Scanning Electron Microscope
SEM	Standard Error of the Mean
SLN	Solid Lipid Nanoparticles
SMZ	Sulfamethoxazole
SSTI	Skin and Soft Tissue Infection
TC	Total Ion Count
TCA	Trichloroacetic Acid
TEER	Transepithelial Electrical Resistance
TEWL	Trans-epidermal Water Loss
ToF-SIMS	Time-of-Flight, Secondary Ion Mass Spectrometry
TSA	Tryptone Soya Agar
TSB	Tryptone Soya Broth
UV	Ultra Violet
UV - VIS	Ultra Violet - Visible light
VC	Vehicle Control
WHO	World Health Organisation
XRD	x - Ray Diffraction

Acknowledgements

I would like to thank Dr Ka-Wai Wan for the initial input into the project and for the support within the first 18 months of my PhD. I would also like to thank Dr Gary Moss for taking the project on half way through and for the supervision until the end. I gratefully acknowledge the support and guidance of my co-supervisor Professor Jon Heylings who was instrumental to the success of this project. I would also like to thank everyone from DTL, my industrial collaborator, for their hours of support, teaching and guidance, in particular Mr Dave Fox, Mr Thomas Brackin, Ms Rebecca Burton, Mr Abbid Majid and Ann Pillai.

I am also appreciative of the technical expertise from the following people; Dr Katherine Haxton (PAMAM dendrimer synthesis), Dr Ravi Pathak , Dr Mark Cresswell and Mrs Gayle Wilson (all for their organic chemistry knowledge), Mr David Griffiths (histology), Dr Dan Bray (statistics), Dr Andrew Morris and Dr Ellie Wong (microbiology) and Mrs Karen Walker (SEM work). I would like to thank Dr David Scurr from the University of Nottingham for his significant contribution with the ToF-SIMS operation. I am also grateful to Dr Ying Yang for allowing me to use her OCT and for the subsequent support in publishing the work.

I am indebted to the laboratory technicians; Ms Lynsey Wheeldon (for lending me all manner of laboratory equipment), Mr Mark Arrowsmith (for use of the ATR-FTIR) and to Mr Nigel Bowers for whom I owe a bottle of whiskey for allowing me to descend upon his microbiology laboratory over the past three summers.

I also would like to thank Dr Tizzard from the National Crystallography Centre at Southampton University for conducting the XRD analysis and the EPSRC Mass Spectrometry centre at Swansea University for their MALDI-ToF analysis.

To the people who kept me sane (controversial) during the past 3.5 years; Dr Stuart Jenkins (who had the misfortune to be seated next to me), Dr Joanna Miest, Dr Doug Paton, Dr Andrew Morris, Dr Dan Bray, Lynsey Wheeldon, Tim Hinchcliffe, Dr Clare Hoskins, Tracey Coppins, Sile Griffin, Alan Weighman, Chris Adams, Sarah Harris and Dr Clare McArthur. I am eternally grateful for the support of my family and my husband, David Holmes. Dave's unwavering support and patience has meant everything to me and I would never have reached this point without him.

1.0 General introduction

1.1 The barrier to topical drug delivery of antimicrobial compounds.

Human skin is the largest organ of the body and plays a vital role as the interface between the internal and external environments (Figure 1.1). The skin protects the human body from the invasion of harmful exogenous chemicals, microorganisms and even radiation. It has a multitude of functions including thermoregulation and is an important sensory organ that can detect pressure, heat and pain. It provides around 10 % of the body mass of an individual and covers an area of approximately 1.7 m^2 in adults, thus making it an accessible and large surface area for the delivery of therapeutics (Williams, 2003). For efficacious topical and transdermal drug delivery systems, a drug must permeate the *Stratum corneum* (SC).

The SC, the outer layer of the skin, is only 15-20 µm thick, yet provides the main barrier against the ingress of permeants (Hadgraft, 2001). It is sometimes described as a 'brick wall' with anucleate keratinized corneocytes as the "bricks" and the densely packed intercellular lipids making up the 'mortar' (Elias, 1983). The corneocytes are elongated and flattened cells that are approximately 0.2-1.5 µm thick and have a diameter of 34-46 µm. It is the corneoctyes that account for most of the weight of the SC as they are filled with keratin (Alibardi *et al.* 2004). The corneocytes act as spacers and consist of a layer of lipids covalently bound to the cell envelope that act as a scaffold for the extracellular lipid matrix (Prausnitz and Langer, 2008). This acts as a template for the organisation of the non-polar intercellular lipids. The intercellular lipids are organised around the dense envelope of keratinized corneocytes. This tortuous

pathway around the corneocytes along the intercellular lipid lamellae is a significant route for many permeating substances (Bouwstra and Ponec, 2006). The intercellular lipids act as an organised and rigid domain that prevent the loss of moisture from the skin and prevents the ingress of xenobiotic permeants such as actives found in antiseptic products. The lipids of the SC are made up of a complex mixture of ceramides, cholesterol and free fatty acids. The latter, some argue, demonstrate antimicrobial effects and contribute to the prevention of the colonisation of pathogens (Bergsson *et al.* 2002).

Ceramides account for 50 % of the lipid content of the SC and play an important role in the structure of the intercellular lipids (Schurer and Elias, 1991). There are at least six different ceramides with differing head groups and lengths of fatty acid chains that contribute to the barrier nature of the intercellular lipids (Bouwstra *et al.* 1998). It is ceramide 1 that contains linoleic acid linked to a fatty acid chain of 30 to 34 carbon atoms that is assumed to have the most important role in barrier function (Bouwstra *et al.* 1995). Secondly, the intercellular lipids consist of cholesterol sulphate at around 1-7 % depending on the skin site (Lampe *et al.* 1983).

Cholesterol within the SC is very important as it regulates the proteases in the desquamation process of the SC. In patients that have recessive x-linked ichthyosis an increase of cholesterol sulphate accumulates within the SC that leads to thickening of the SC and hyperkeratosis (Sato *et al.* 1998). Cholesterol allows for the solubilisation of free fatty acids and regulates the phase behaviour of the SC lipids (Norlén *et al.* 1999). Therefore, the amount of cholesterol within the SC is important for maintaining the barrier homeostasis of the skin.

Free fatty acids are products from the hydrolysis of phospholipids by phospholipase and they consist of long chain (>18 carbon atoms) saturated species (Fluhr *et al.* 2001). To investigate the importance of free fatty acids to the skin barrier the production of free fatty acids was inhibited using 5-(tetradecyloxy)-2-furancarboxylic acid to inhibit acetyl CoA carboxylase. The authors found that the skin barrier was impaired by up to 50 % and recovery of the SC was significantly delayed after disruption of the free fatty acids within the SC (Mao-Qiang *et al.* 1993).

It has also been shown that the ratio of free fatty acids to cholesterol and to ceramides is also of importance for the maintenance of the SC barrier function and alteration of the ratio of free fatty acids found within the SC can increase the trans-epidermal water loss (TEWL), an indicator of barrier impairment (Lavrijsen *et al.* 1995). The free fatty acids are also important in the maintenance of an 'acid mantle' whereby the external SC has an acidic pH of 4 to 6 (Ohman and Vahlquist, 1994). Alterations to the pH of the SC results in a decrease in its barrier integrity and cohesion. It was reported that if neutralisation of the SC occurs for only 3 h, the skin barrier is impaired (Fluhr *et al.* 2001).

As well as the composition and molar ratios of the SC lipids, the phase behaviour and therefore structural organisation is also important for the maintenance of SC barrier integrity. Using small angle X-ray diffraction (SAXD) it was found that in healthy human skin, SC lipids are structured in two lamellar phases found in two periodicities of 6 nm, short periodicity phase and 13 nm, long periodicity phase (Bouwstra *et al.*, 1991). The characteristic 13 nm long periodicity phase has been identified in many species' lipid lamellar thus it is assumed that

this phase is of great importance to the barrier function of the SC and therefore the permeation of substances across the tortuous path (Bouwstra *et al.* 1998).

The SC previously described as a ‘brick wall’ is the rate limiting barrier and quite a predicament for researchers within topical and transdermal drug delivery. It is not just composition and structure that contributes to the skin barrier homeostasis. The terminal differentiation process involves the proliferation of keratinocytes from the basal layer moving upwards to become anucelate corneocytes at the SC surface (Egelrud, 2000). This upward movement process terminates in desquamation i.e. sloughing of the outer SC layers. The SC turnover is around 14 days (Marks, 2004).

The continuous upward movement of the corneocytes that are then sloughed from the body prevents the ingress of microorganisms and can help to eliminate cancerous cells and particulate debris from the skin (Prow *et al.* 2011). Using a mathematical model of SC turnover and drug absorption it was shown that the continuous turnover and thus sloughing of skin cells does significantly impede the absorption of highly lipophilic or high molecular weight drugs (Reddy *et al.* 2000). This is due to highly lipophilic drugs forming a reservoir within the intercellular lipid matrix of the SC. High molecular weight drugs with slow diffusivity through the SC are not absorbed within the 14 day SC turn over.

The SC is a challenging barrier to topical drug delivery therefore enhancement strategies to overcome the skin’s barrier function are required.

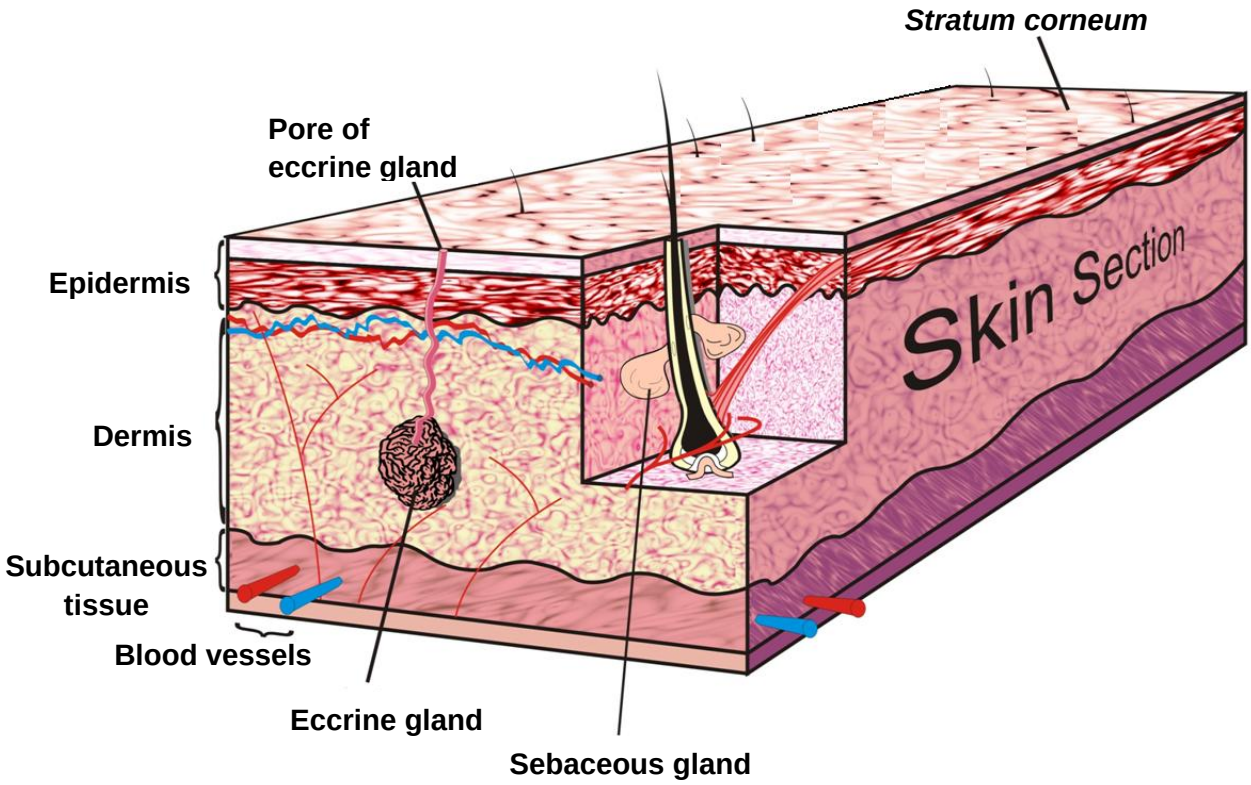

Figure 1.1 Schematic of a skin section.

When considering the skin as a permeable drug delivery site, it should be noted that there are many biomolecules within the skin that could potentially affect the therapeutic drug or the excipients. These could include; free fatty acids, waxes, glycerides, phospholipids, hydrocarbons (e.g. squalene) and also sterols. Further, it is likely that Ca, Na, K, Cl, NH_3, phosphate, thiocyanates, urea, uric acid, creatine, amino acids, lactic acid, glucose and vitamins (Wheatley, 1963) and (Rothman, 1954) will be encountered within the superficial layers of the SC by the active drug and excipients in the formulation. Molecules naturally found on the skin surface have the potential to interact with the formulation affecting its bioavailability by forming insoluble complexes.

1.2 Topical and transdermal drug delivery.

Drugs can permeate through three possible routes across the SC for dermal absorption. The three routes are intercellular, intracellular and transappendageal as illustrated in Figure 1.2 (Williams, 2003). It is the tortuous intercellular channels of extruded lipid lamellae that are said to be the primary route for the dermal delivery of lipophilic drugs (Stoughton, 1989). It is the only continuous phase across the skin, though the long tortuous path length and dense packing of ~10 lipid bilayers compacted between each corneocyte cell still provides a significant permeability barrier (Karande *et al.*, 2006). The stacking of the corneocytes is also important as they dictate the tortuous path taken by the drug (Christophers *et al.* 1974). The intercellular lipid channels are reported to be between 0.4 – 40 nm in width and this characteristic prevents the ingress of high molecular weight drugs and nanoparticles (Cevc and Vierl, 2010 and Van der Merwe *et al.* 2006).

The transcellular pathway affords a polar route through the intact SC. For a drug to penetrate the SC using the transcellular route it would be required to diffuse across the hydrophilic, keratin filled environment of the corneocytes. The corneocytes are surrounded by the extruded lipid lamellae therefore any hydrophilic drug diffusing through the intracellular route would not only have to traverse the aqueous environments of the corneocytes but also partition into the lipid rich extracellular matrix (Williams, 2003). Though this would be the shortest path length for a drug to traverse the SC, a limiting factor is that a drug would have to partition into the corneocyte, diffuse across the corneocyte and then partition back into the lipid bilayer before diffusing across the bilayer and partition back into

a corneocyte and so forth (Figure 1.2). The rate-limiting barrier for a hydrophilic drug traversing the intracellular route is the lipid bilayer and would require a drug to have an optimal hydrophilic, lipophilic balance (Heisig *et al.* 1996). It is for this reason that hydrophilic drugs generally exhibit poor permeability across the SC (Prausnitz *et al.* 2004).

The transappendageal route can include pilosebaceous units and apocrine/ eccrine sweat glands that emerge from the dermis that can be used by drugs to avoid traversing the SC for drug absorption. Eccrine sweat glands are distributed across the skin surface however their openings are very small and sensible sweat is continuously being excreted from the gland. This would reduce the likelihood of a drug to penetrate the skin using this path (Meiden *et al.* 2005). The pilosebaceous units or the follicular route provide a pathway for the drug or vesicle without the requirement to traverse the SC. The drug can permeate down the follicle to the dermis where there is a concentration gradient due to a copious blood supply allowing ‘sink’ conditions (Lauer *et al.* 1995).

Siddiqui *et al.* (1989) demonstrated that the transappendageal routes are only minor contributors (5-10 %) in the steady state flux of steroids through excised human skin implying that the follicular pathway for topical and transdermal drug delivery systems is not significant. Recently Knorr *et al.* (2009), argued that the calculation claiming that the follicular penetration route accounts for only 0.1 % of the skin surface area and did not take into consideration that hair follicles represent invaginations offering a significant increase in skin surface area for permeants. The transappendageal or ‘shunt’ route is important for liposomes and other vesicles that are too large to penetrate the SC (Lieb *et al.* 1992).

Fluorescently labelled polystyrene nanoparticles of various diameters were shown to preferentially accumulate within the follicular openings of the skin (Alvarez-Roman *et al.* 2004a and Alvarez-Roman *et al.* 2004b). Nanoparticles with a 320 nm diameter were shown to deliver a fluorescent dye more effectively than the free solution if the skin was massaged after application (Lademann *et al.* 2007). The authors suggested that the physical motion of the hairs pumped the nanoparticles deeper within the follicle resulting in an enhanced delivery.

It is likely that the penetration pathways for topical and transdermal drug delivery are not mutually exclusive but that a number contribute to the ingress of the topically applied drugs and that it is dependent on the physiochemical properties of a drug.

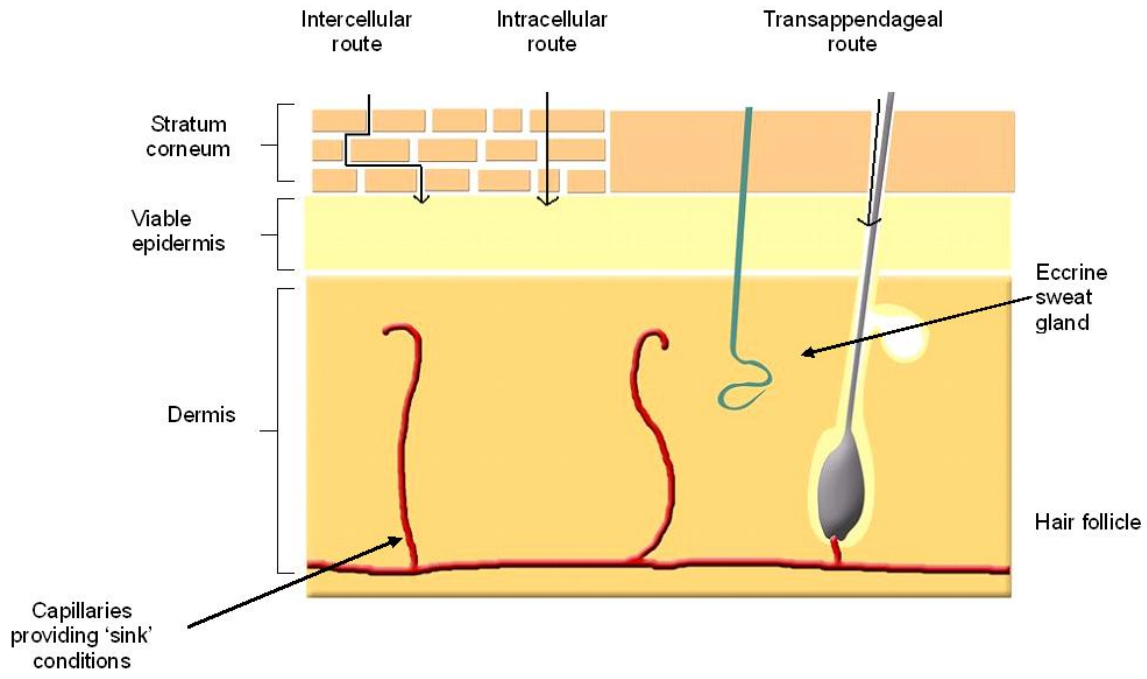

Figure 1.2. A schematic of the permeation routes through the skin.

1.3 Physicochemical influences on the topical delivery of drugs within and across the skin.

The physicochemical properties that can affect the permeation of drugs within the skin are molecular mass, ionisation at physiological pH, the partition coefficient and the solubility/melting point (Beetge *et al.* 2000). It is the partitioning coefficient (log P) that determines how well a drug will partition into the SC and is the governing factor in determining which pathway the drug will take through the skin (Barry, 1987). Those with a high partition coefficient, i.e. hydrophobic drugs, are likely to take the intercellular pathway where as those with a low partition coefficient, hydrophilic drugs, will take the intracellular pathway. For a drug to be a likely candidate for transdermal or topical delivery it would ideally have a balanced hydrophilic/lipophilic character with a log P value of 2 or at the very least between 1 - 3 (Guy and Hadgraft, 1989 and Finnin and Morgan, 1999).

Beetge and co-workers (2000) demonstrated with a range of non-steroidal anti-inflammatory drugs (NSAIDs) that with increasing log P values the blood-plasma concentration values decreased, with a minor discrepancy between indomethacin and ibuprofen that both have very similar log P values. The biocide used in this project, chlorhexidine (CHX) has an octanol/water partition coefficient of 0.754 (free base) and CHX digluconate (CHG) has a log P value of 0.037 (Farkas *et al.* 2007) therefore the free base and its salt do not possess an optimal partition coefficient for topical drug delivery.

The molecular mass of a drug is also a major factor in its success as a transdermally delivered drug. It is thought that one reason there are so few transdermal drug delivery systems on the market is because there are so few ideal therapeutic candidates <400 Daltons (Potts and Guy, 1992). There is said to be a 500 Dalton cut off for drugs to be able to be absorbed after topical application (Bos

and Meinardi, 2000). Once below this cut-off point, NSAIDs with a molecular weight from 206.30 Da up to 357.80 Da resulted in no significant variation of drug flux due to the molecular mass (Beetge *et al.* 2000). Drugs possessing ideal characteristics for topical or transdermal drug delivery typically possess low melting points $\leq$ 200 ºC (Finnin and Morgan, 1999). Unionised forms of a drug should be able to permeate the skin more effectively than ionized forms according to the pH-partition hypothesis, principally via the intercellular route (Smith and Irwin, 2000). It is possible for drugs that are ionised at physiological pH to permeate the skin as it has been reported that ionised drugs can permeate the skin via the intercellular lipid route due to ion pairing (Hadgraft and Valenta, 2000). Other reasons relating to the measured drug dose achieved in plasma after transdermal drug delivery include individual differences in permeability that are intrinsic, or in the case of skin disease.

1.3 Micro-flora of the skin.

Human skin is the host to a large and diverse population of microorganisms. It provides conditions for growth such as an uneven skin surface with sporadic openings of many pores and ducts. It is also irrigated with various fluids such as eccrine sweat, sebum and apocrine sweat which provide a film of nutrition across the surface of the skin. Nutrition is available for microbes in the form of dead squamous cells from the SC which can support a vast microbial flora (Gibbs and Stuttard, 1967).

The three major determinants of cutaneous habitats for bacteria have been identified as: ability to maintain a reduced environment; availability of moisture; and the presence of sebaceous lipids (Leydon *et al.* 1983). One study by Gao and

co-workers (2007) identified 182 species of microorganisms found on the skin belonging to 8 different phyla. Of the 1,221 clones analysed, 54 % of them belonged to the genera of *Propionibacteria, Corynebacteria, Staphylococcus* and *Streptococcus*. The various layers of the skin host a diverse flora of commensual and pathogenic bacteria, not just the superficial layers of the SC (Grice *et al.* 2008*)*. The inaccessible proportion of bacteria (Figure 1.3) inhabiting the furrows and appendages of the skin was termed “hidden” flora by Reybrouck (1986) and this hidden flora remains undetected to conventional skin sampling such as swabbing. The depth of hair bulbs and apocrine sweat glands that are thought to be bacteria reservoirs are situated 400-700 µm (Figure 1.3) within the dermis (Touitou, *et al.* 1998). A topically-applied antimicrobial compound must reach this depth within the skin to reduce the resident microbial flora. Deep and efficient antisepsis is required to prevent the repopulation of the skin surface. For bacteria such as coagulase negative staphylococci (i.e. Methicillin-resistant Staphylococcus aureus) this re-population would occur within hours after the skin surface disinfection (Brown *et al.* 1989).

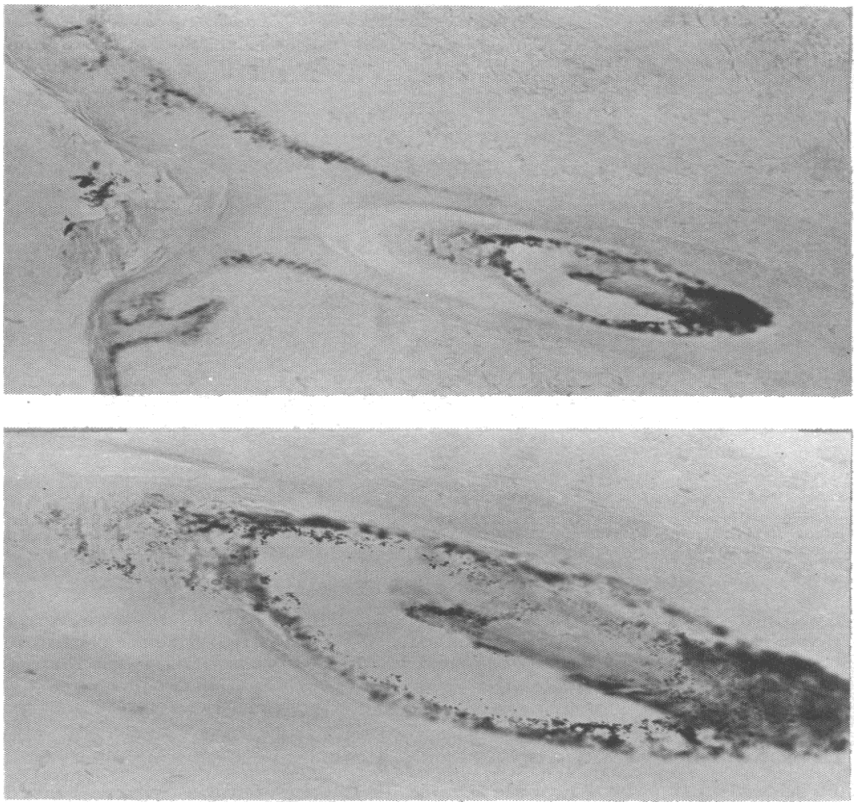

Figure 1.3. Large hair follicle showing Gram stained bacilli and cocci deep within the follicle taken from an abdomen skin biopsy. *Top – magnification x116; bottom x336. Image taken from Selwyn and Ellis (1972).*

1.4 Skin and soft tissue infections- invasion of pathogenic bacteria.

Though the skin is an effective barrier against the ingress of microorganisms, occasionally it can succumb to infection through a reduction of integrity to the skin barrier. Skin and soft tissue infections can range from non-complex cellulitis through to deep-seated subcutaneous tissue infections (Stulberg *et al.* 2002). Microorganisms that can cause infections of the skin include –

- **Viruses**- Can cause childhood illnesses such as measles and chickenpox, or are known to cause non-cancerous tumours such as warts.
- **Bacterial infections**- Often it is the Staphylococcal species that is the source of skin infections such as *Staphylococcus aureus,* or the

streptococcus species such as *Streptococcus pyogenes.* An example of a skin infection caused by both of the aforementioned organisms is impetigo.

- **Fungal infections**- Are very common. An example being ring worm that is an infection of the keratin layer caused by *Fungi imperfecti.*

  (Fitzpatrick *et al.* 2005)

Bacteria that have colonised the skin rarely cause infection if the individual is not immuno-compromised (Hoffman, 2001). Dermatological infections have multifactorial causes but generally older patients, very young patients or the immuno-compromised are those at the greatest risk of developing an infection (Pratt *et al.* 2005). Skin and soft tissue infections (SSTI's) can arise from a number of sources including animal or human bites, animal contact, infections due to an immuno-compromised patient, or surgical site incision infections (Stevens *et al.* 2005). With regards to the latter two sources, it is typically the patient's own resident microbial flora that invades and infects the epidermis (Dryden, 2009). SSTI's exist as a significant problem to inpatients as well as outpatients and are increasingly acquired within the community (Rajan, 2012).

S. *aureus* is the most common pathogen identified as causing SSTI's and is the result of colonisation due to a breach of the skin barrier, i.e. surgical site incision or trauma. If a patient is colonised by S. *aureus* they are at a higher risk of obtaining a surgical site infection than those who are not, particularly when the colonization density is greater than $1x10^6$ colony-forming units per anatomical site (Paulson, 2002). A Study of dissemination of S. *aureus* after inoculation of the skin in a mouse model by Hahn *et al.* (2009) showed that within six hours the pathogen had invaded the tape-stripped epidermis and had disseminated rapidly to the

spleen and kidneys before severe cutaneous damage and complete necrosis of the dermis 48 hours after inoculation. In humans from colonisation and thus infection, typically of the subcutaneous plane, there is a three day incubation period until the patient develops symptoms (Stone *et al.* 2000).

S. aureus is responsible for a range of minor non-complex infections such as impetigo, folliculitis, subcutaneous abscesses and furnacles that would not require systemic antibiotic therapy but a topical localised treatment. An example of a severe infection as a result of *S. aureus* would be staphylococcal scalded skin syndrome triggered by the microorganism's associated exfoliative toxins. The syndrome is characterised by the splitting of the epidermis just above the granular layer resulting in excessive desquamation (Patel and Finlay, 2003). *S*. *aureus* α-toxin enhances transient membrane permeability to large molecules and causes vacuole formation and defects in mitochondrial enzymes resulting in a severe drop of Adenosine-5'-triphosphate (ATP) within viable keratinocytes (Suriyaphol *et al.* 2009). Such SSTI's could then develop into serious systemic infections such as septicaemia, meningitis and osteomyelitis which could potentially lead to death as a result of staphylococcal toxic shock syndrome (Iwatsuki *et al.* 2006). Increasing antibiotic resistance, particularly with regards to *S. aureus* and *Streptococcus pyogenes* to methicillin and erythromycin respectively, is of great concern as the opportunistic pathogens are frequently responsible for complex STTI's (Stevens *et al.* 2005). Further, methicillin resistant *Staphylococcus aureus* (MRSA) is also now the predominant cause of community-acquired SSTI's (Eady and Cove, 2003 and King *et al.* 2006). A bacterial skin infection can have serious consequences on a patient's health and can place additional stress and anxiety on the family. MRSA bacteraemia cases with skin infection identified as the source, increased from

25 % to 32 % from October to December 2011 (Health Protection Agency, 2011). On average, a single infection acquired in hospital costs between £4000 and £10,000 and just 40 MRSA bacteraemia cases would incur an additional cost between £160,000- £400,000 for that Trust (Department of Health, 2006).

With antibiotic resistance increasing amongst skin pathogens it is of paramount importance to prevent SSTI's through effective skin antisepsis. Also of great importance is to develop novel strategies for the treatment of antibiotic resistant strains of bacteria through mechanisms that are low risk for microbial acquisition of resistance.

1.5 Chlorhexidine.

Chlorhexidine (CHX) is a cationic bisbiguanide that demonstrates a broad spectrum of antimicrobial activity but exhibits low level toxicity to mammalian cells (Figure 1.4). It has been used throughout the global healthcare sector since it was first synthesised in 1954 by Rose and Swain (Davies *et al.* 1954). It also has a strong affinity for the skin, thus it has been used extensively in topical antimicrobial formulations (Denton, 1991). It is typically used as the digluconate, acetate or hydrochloride salt form due to solubility issues with the free base. It is active against an extensive range of microorganisms such as vegetative gram positive and gram negative bacteria, fungi such as yeast, dermatophytes and some lipophilic viruses (Ranganathan, 1996). CHX has a cationic charge at physiological pH thus it has the ability to bind to negative surfaces such as the cell wall of bacteria (Jones, 2007). For example the cell wall of *S. aureus* contains teichoic acids that are highly anionic conferring a net negative charge over the cell membrane (Gross *et al.* 2001). It is this strong affinity that allows CHX to retain low

toxicity towards mammalian cells whilst remaining biocidal against a broad range of microorganisms.

The mechanism of action of CHX is bacterial cell membrane disruption. In bacteriostatic concentrations, the binding of the biguanide groups of the drug to the membrane phospholipids of the bacteria induces structural modifications that allow the leakage of low molecular weight intracellular contents such as potassium ions (Carlotti and Maffart, 1996). If the concentration of CHX is high, i.e. bactericidal concentrations, it will cause a high degree of structural damage to the cell membrane leading to cytoplasmic leakage and precipitation (Kuyyakamond and Quesnel, 1992).

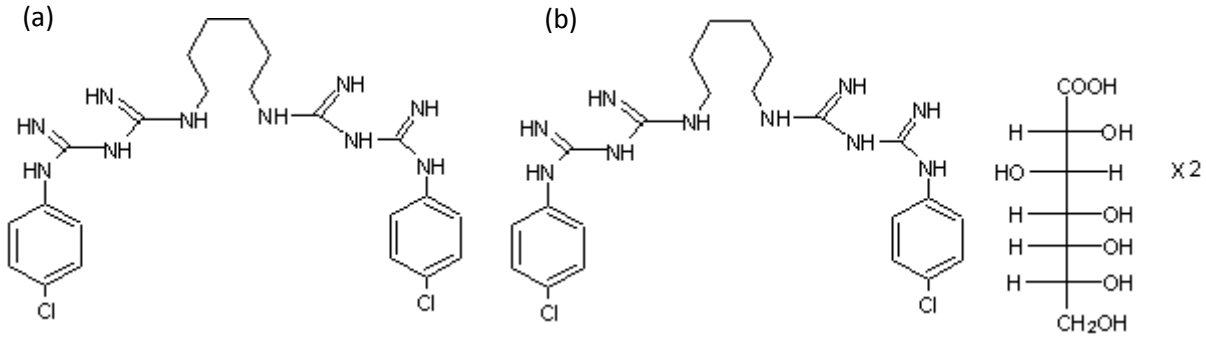

Figure 1.4. Chemical structure of CHX free base and its commonly used salt CHG. *(a) Structure of CHX free base and (b) structure of CHG.*

The physicochemical characteristics of CHX impart poor percutaneous absorption characteristics within the skin. CHG is water-soluble and is typically used in topical preparations. The physicochemical characteristics of CHG are not ideal for percutaneous permeation as it is in the ionized form when topically applied under physiological skin conditions (Smith and Irwin, 2000). CHG has a molecular weight of 897.8 g/mol which exceeds the optimal molecular weight for effective skin permeation that is described as a maximum of 500 g/mol (Bos and

Meinardi, 2000). Furthermore, a log P (octanol/water) of 0.0133 is also less than optimal for percutaneous absorption (Farkas *et al.* 2007) as outlined in Section 1.2. Typically when drugs are ionised at skin pH, counter ions are utilised to neutralise the drug for enhanced deposition within the skin (Valenta *et al.* 2000). This is not a viable option for CHX as many counter anions form insoluble salts and neutralise CHX diminishing its antimicrobial properties (Denton, 1991). Further, CHX and its salts have been shown to aggregate at concentrations above > 40 mM therefore self-aggregation may contribute to the low skin penetration observed for CHG (Zeng *et al.* 2009, Heard and Ashworth, 1968, and Perrin and Witzke, 1971).

CHX is known for its poor permeability into human skin as demonstrated by Karpanen *et al.* (2008). Using *ex vivo* human skin in a diffusion cell the authors found that CHG only permeated to a high enough concentration to kill microorganisms in the top 100 µm of the skin and below 300 µm the concentration of CHG was less than 0.002 µg/mg tissue as detected by high performance liquid chromatography (HPLC) (Karpanen *et al.* 2008). Lafforgue *et al.* (1997) used an *ex vivo* rat skin model to demonstrate low permeation of CHG across and within the rat skin. After a 48 h contact time, a concentration of 26 .63 ± 13.17 µg/cm^2 of CHG was detected within the whole rat skin and a concentration of 4.03 ± 0.6 µg/cm^2 of CHG was detected within the receptor fluid. Wang *et al.* 1990 investigated the permeation of CHX phosphanilate (CHP), a new salt of CHX, using *ex vivo* human skin in a static diffusion cell. After 48 h there was almost no CHP that had permeated the intact SC, however in damaged skin with the SC enzymatically removed CHP was detected throughout the skin strata and typically remained within the dermis (Wang *et al.* 1990).

Percutaneous absorption of CHG *in vivo* was shown to be negligible after researchers bathed neonatal rhesus monkeys in an 8 % CHG skin cleanser every day for 90 days (twice the concentration used typically) (Gongwer *et al.* 1980). A low concentration of CHG was detected within the skin 0.118 ± 0.051 µg/mg of tissue (*n*=5) after 90 days. The absorption of CHG across new-born infants' skin was also investigated by venepuncture to obtain a blood sample after bathing the babies with a CHG containing wash, hibiscrub® (4 % CHG). Low concentrations of CHG almost at the limits of detection were detected within the blood serum samples for 5 out of 24 babies tested. No toxicity was observed as a result (Cowen *et al.* 1979). Further, in 1978 Chow *et al.* studied the distribution of CHX radio-labelled with C-14 after topical application in an *in vivo* rat model. It was found that over a 5 day period less than 5 % had been absorbed and the radiolabelled CHX was excreted within the faeces (Chow *et al.* 1978). More recently, Lee *et al.* (2011) studied the blood concentrations of CHX after hospitalised children underwent daily CHX bathing. Though low levels of CHX were detected in 15 % of the blood samples, there was no evidence that CHX accumulates within the bloodstream of children as young as three months following percutaneous absorption. This study was conducted on children with intact skin. There are very few studies within the literature investigating the percutaneous absorption of CHX despite the antimicrobial compound being widely used within the healthcare sector across the globe. The studies carried out within the literature show that CHX penetration within intact skin is minimal.

If topical antimicrobial compounds do not permeate the upper strata of the skin in high enough concentrations, the bacteria in reservoirs found deep within the dermal structures are potentially left viable. Viable opportunistic pathogens are

then free to directly infect the impaired epidermis. The reasons for the lack of skin permeation for CHG are due to sub-optimal physiochemical characteristics for topical drug delivery that includes; high molecular weight, polycationic charge and a low log P. This is discussed in detail in the introduction to Chapter 3.0. Despite poor skin permeation there are many products on the market in which CHX is the active antimicrobial. Table 1.1 lists topical antiseptic preparations available on the UK market as listed within Martindale: Drug reference (Sweetman, 2011). Though none of the listed products contain a penetration enhancer *per se*, excipients such as surfactants, glycerol, propanol and lipophilic perfumes (e.g. essential oils) found within the formulations are known to act as penetration enhancers (Williams and Barry, 2012). CHX has many applications including hand washing, pre-operative skin preparation, vaginal antisepsis, gingivitis treatment and body washes for prevention of SSTI's (Milstone, 2008).

The Centre for Disease Control and Prevention (CDC) made recommendations to use hand soap containing CHX due to its residual activity reinforcing the effectiveness of CHX as a topical antiseptic (Boyce and Pittete, 2002). There are many cases highlighting the superior efficacy of CHX for example CHX was incorporated into an alcohol hand rub and was successfully implemented as part of a hand hygiene programme in an Australian hospital that had an MRSA endemic. The study found that healthcare worker compliance to hand hygiene had doubled within 12 months and the number of patients with reported MRSA bacteraemia was reduced by 57 %. Clinical MRSA isolates had also dropped by 40 % hospital-wide (Johnson *et al.* 2005). When compared to povidone-iodine, CHG was shown to significantly reduce the number of vascular

catheter-related infections by 49 % when 4143 catheter insertions were studied (Chaiyakunapruk *et al.* 2002).

More recent patient studies where CHX was successfully implemented to combat infections include the significant reduction of periprosthetic hip arthroplasty infections (Kapadia *et al.* 2013), and the reduction of multi-drug resistant microorganism infections and hospital acquired bacteraemia cases (Climo *et al.* 2013). A detailed review of the scientific support for the use of CHX within the healthcare sector can be found in Weinstein *et al.* (2008). CHX has repeatedly been shown to significantly decrease the number of healthcare acquired infections across hundreds of publications that act as evidence for the necessity of CHX as an antiseptic in the health care sector (Milstone *et al.* 2008).

Table 1.1 A table of CHX containing topical antiseptic formulations available within the UK. *All CHX containing topical antiseptic preparations that are currently available within the UK as listed within Martindale: The drug reference (Sweetman, 2011).*

Skin disinfectant product	Dosage form	CHX salt and concentration within formulation	Skin disinfection use
CHX listed as a single ingredient in commercially available topical preparations in the UK			
Acriflex®	Cream	CHG 0.25 % (w/w)	Burns and scalds
Cepton®	Lotion	CHG 0.1 % (w/v)	Acne and spots
	Wash	CHG 1 % (w/v)	Acne and spots
CX powder®	Powder	CHX acetate 1 % (w/w)	Dusting powder for general skin antisepsis
Eczmol®	Cream	CHG 1 % w/w	Eczema
Hibiscrub®	Liquid	CHG 4 % (w/v)	General skin disinfection
Hydrex®	Liquid	CHG 0.5 % (w/v)	General skin disinfection
Savlon wound wash®	Liquid spray	CHG 0.45 % (w/v)	Wound cleansing
Spotoway®	Cream	CHG 1 % (w/w)	Localised spot treatment
Steripod CHG®	Liquid	CHG 1 % (w/v)	General antisepsis
CHX listed as a multiple ingredient in commercially available topical preparations in the UK			
Cathejell with lidocaine®	Gel	CHX HCL 0.05 % (w/w)	Anaesthetic
Chloroprep®	Liquid	CHG 2 % (w/v)	Pre-operative skin antisepsis
Cyteal®	Liquid	CHG 0.1 % (w/v)	Liquid
Dermol®	Cream	CHX HCL 0.1 % (w/w)	Eczema
	Lotion	CHX HCL 0.1 % (w/w)	
Germolene®	Cream	CHG 0.25 % (w/v)	Haemorrhoids
Hibi Hand Rub®	Liquid	CHG 2 % (w/w)	General antisepsis
Instillagel®	Gel	CHG 0.25 % (w/w)	Anaesthetic
Nystaform®	Ointment	CHX acetate 1 % (w/w)	General antisepsis
Quinoderm®	Liquid	CHG 0.15 % (w/v)	Acne and spots
Tisept®	Liquid	CHG 0.015 % (w/v)	Wound cleansing
Torbetol®	Liquid	CHG 0.75 % (v/v)	Acne
Savlon antiseptic®	Cream	CHG 0.1 % (w/w)	General antisepsis
	Liquid	CHG 0.3 % (w/v)	General antisepsis

Resistance to antimicrobial compounds including preservatives and disinfectants is an increasing problem. Though resistance or reduced susceptibility to CHX is rare it is being increasingly observed for the *Pseudomonas* species. It was demonstrated that *Pseudomonas stutzeri* developed resistance to CHX acetate after repeated exposure to sub-lethal concentrations *in vitro*. It is thought that a decrease in susceptibility was due to alterations of the cell envelope increasing its hydrophobicity. This strain has also developed a reduced susceptibility to antibiotics and to other non-antibiotic compounds including triclosan and cetylpyridinium chloride (Tattawasart *et al.* 1999). Further the same group demonstrated that *Pseudomonas aeruginosa* also developed stable resistance to CHX acetate on repeated exposure to sub-lethal concentrations. The authors stated that *Pseudomonas aeruginosa* may develop resistance to CHX from 'residual' concentrations and that the also Gram negative, *Escherichia coli,* did not develop a reduced susceptibility (Thomas *et al.* 2000).

Other strains that have reduced susceptibility to CHX include the oral pathogen *Porphyromanas gingivalis* that produced vesicles to bind to CHX reducing the bacteria's susceptibility to CHG (Grenier *et al.* 2007). It should also be noted that contaminated CHX disinfectants have caused nosocomial infections due to contamination with a range of resistant opportunistic pathogens including *Burkholderia stabalis* (Heo *et al.* 2008), *Serratia marcescens* (Vigeant *et al.* 1998) and *Pseudomonas cepacia* (Sobel *et al.* 1982). The occurrence of resistance or lowered susceptibility of microorganisms to CHX is still very infrequent but the aforementioned reports do highlight the requirement of sensible disinfectant use. Concentrations that are significantly higher than the minimum inhibitory concentrations should be used and care should be taken not to leave sub-lethal

concentrations as a residue. To avoid contamination issues strict aseptic manufacturing practices, correct storage conditions and accurate dilutions with sterile diluent should also be followed to prevent bacterial resistance.

There is also evidence of microbial degradation of CHX. *Pseudomonas* species isolated from river bed sludge were shown to degrade CHX into a number of intermediates (Tanaka *et al.* 2005). Copious use of CHX as a disinfectant results in washing CHX into the waterways. It was found that the inhibitory concentrations for these CHX intermediates increased ten-fold for a range of bacteria when compared to the parent CHX. In the case of *Pseudomonas aeruginosa* and *Serratia marcescens* CHX had a minimum inhibitory concentration (MIC) of 100 µg/mL whilst the intermediates degraded by the *Pseudomonas* species had a MIC of >1000 µg/mL (Tanaka *et al.* 2005 and Tanaka *et al.* 2006). The products of microbial degradation of CHX were also isolated and identified from an ultrasonic hand washer using three dimensional HPLC (Ogase *et al.* 1992). The causative and resistant strain was identified as *Achromobacter xylosoxidans* and the authors suggested the presence of CHX degrading enzymes degrade CHX into *p*-chloroaniline and *p*-chlorophenol. Though the studies mentioned provide evidence for microbial degradation of CHX there are still limited studies conducted in the area of investigating the microbial degradation of antimicrobial compounds. Further, no studies have been conducted investigating the effect that cutaneous enzymes have upon CHX.

Investigations into the efficacy of CHX particularly using time-kill assays is a controversial area. Kampf has published many papers questioning the use of CHX. In particular, Kampf (2008) made a bold statement calling for healthcare

workers to remove CHX from their formulations until further efficacy data is available. He argues that the studies conducted in which the CDC based their recommendations are flawed due to a lack of validity of the results. CHX salts at different concentrations are known to be very difficult to neutralise (Kampf, 1998 and Kampf, 2006) and that all the studies conducted on the efficacy of CHX did not validate the neutraliser step nor demonstrate the required efficacy. A neutraliser validation study should always be conducted first before determining the antimicrobial efficacy of a biocide within a particular time frame, e.g. European study EN1500. Such preliminary data is rarely published although it is often available by request from the author. Nevertheless, even if the neutraliser validation study was neglected, the results should not be disregarded as the compound still exhibits antimicrobial affects but just possibly not within the stated time frame of the bacteria-CHG contact time (i.e. 30 seconds for the EN 1500 test). There are, however, an overwhelming number of studies within the literature supporting the clinical use of CHX.

1.5.1 Contra-indications for the use of CHX.

CHX is routinely used in the healthcare sector as well as in consumer products (e.g. mouthwash, hand sanitiser) and it appears to have a good record with regards to minimal adverse reactions. In rare cases, typically after parenteral or mucosal exposure to CHX, anaphylaxis has been observed. Krautheim *et al.* (2004) published a comprehensive review on CHX anaphylaxis that details 26 case reports. More recently further case reports have been published (Khan *et al.* 2011, Lloyd-Lavery and Reed, 2012 and Bae *et al.* 2008). Life threatening and immediate adverse side effects are rare however there is a growing concern with

the use of CHX incorporated into medical devices such as catheters and medicinal products; in October 2012, the MHRA (Medicines and Healthcare products Regulatory Agency) released a safety alert regarding CHX incorporated products. All allergic reactions to CHX must now be reported to the MHRA to determine whether CHX should be incorporated into products that are exposed to mucosal membranes or parenteral routes.

Minor adverse effects associated with CHX use on intact skin include contact dermatitis; the prevalence of contact dermatitis caused by CHX is very low. At St John's Institute of Dermatology over a 19 year period there were only five reported cases (Goon *et al.* 2004). In a further study sensitization and dermatitis was investigated at the Turku University Hospital Dermatology Department, where out of 7610 patients in the study only 26 patients were found to sensitized to CHX (0.47 %) and CHX containing topical products were found to have caused contact dermatitis in 5 patients (Liippo *et al.* 2011). Further, infrequent cases of CHX causing photosensitivity have been reported (Wahlberg and Wennersten, 1971), as well as contact urticaria (Wong *et al.* 1990).

CHX has a number of contra-indications; firstly it should not be used for antisepsis before a lumbar puncture as it can cause damage to the meninges on contact. It should also be avoided for use on the eyes and new tissue other than at very low concentrations ($\leq$0.05 %) as it has been shown to be cytotoxic (Salami *et al.* 2006). CHX must also never be used on the mucosa epithelia of the middle ear as it can damage the cells of the middle ear thus demonstrating ototoxicity (Igarashi and Oka 1988). After a number of case reports detailing the patients'

allergic response to CHX digluconate that had been incorporated into an antiseptic urethral gel, it is now considered that CHX should not be applied to mucosal surfaces of the body due to the possibility of inciting anaphylaxis (Jayatthillake *et al.* 2003 and Okano *et al.* 1989). Irrespective of the rare anaphylaxis cases and infrequent dermatitis cases documented there are a significant number of products on the market containing CHX that have been used globally for over 2 decades; even CHX containing chewing gum- CHewX® is available on the Swiss market (Imfeld, 2006). CHX remains a low cost and effective antiseptic that is well tolerated by consumers and patients across the world (Weinstein *et al.* 2008). The benefits of the antibacterial compound clearly outweigh the risks.

1.6 Controlled release strategies used in the drug delivery of CHX.

To overcome conditions that are less than favourable for drug delivery researchers have turned to colloids to enhance a drug's therapeutic affect and to allow targeted delivery. Most colloids can be modified for a tailored affect and many have enhanced properties over conventional dosage forms.

To overcome the challenges in formulating CHX, such as adsorption to surfaces, incompatibility with anionic components and poor skin permeation, researchers have investigated ways to enhance the controlled and sustained delivery of CHX to a localized target, i.e. the skin, root canal or biofilms. Liposomes with encapsulated radiolabelled C^{14} CHX were optimised to determine the most effective liposomal compositions, i.e. cationic or anionic constituents (Jones *et al.* 1997). Liposomes (containing dipalmitoylphosphatidylglycerol (DPPG), cholesterol and stearylamine) were shown to increase the delivery of

CHG to the biofilms of skin-associated opportunistic pathogens (Jones *et al.* 1997).

CHX-containing liposomes were developed in the early 1990's. A patent on liposomes containing either CHG or CHX diacetate or a naturally occurring surfactant was published 15 years ago. The authors cited advantages as reduced side effects and increase in the sustained release of CHG or CHX diacetate (Gonzalez *et al.* 1998). The same authors then incorporated CHG containing liposomes into skin cleansing tissues for use on the face (Gonzalez *et al.* 2000). Human albumin microspheres were also shown to provide controlled and sustained release of CHX dihydrochloride that exhibited enhanced efficacy against Gram negative and Gram positive opportunistic pathogens that cause urinary tract infections. The microspheres were also investigated as a biocidal catheter coating (Egbaria and Freidman, 1990 (a) and 1990 (b)).

1.6.1 Delivery of CHX from Hydrogels.

Hydrogels are typically biodegradable, biocompatible and non-immunogenic three dimensional cross-linked polymer networks that swell in the presence of water (Bako *et al.* 2008). They can be designed to be pH or thermo sensitive for controlled drug release (Zhao *et al.* 2009, Gupta *et al.* 2002 and Xu *et al.* 2006). Their mucoadhesive and hydrophilic nature has been exploited for the controlled and sustained release of CHX and CHG after topical application. They are commonly investigated for the treatment or prevention of periodontal infection (Xia *et al.* 2010, Vitkova *et al.* 2011 and Vitkova *et al.* 2013).

Bako and co-workers (2008) designed nanocomposite biocompatible hydrogels (NCHG) for the sustained release of CHX once applied to periodontal infection. Nanoparticles were formed from hydroxyethyl methacrylate (HEMA) and polyethyleneglycol dimethylacrylate (PEGDMA) and were loaded with CHX. The nanoparticles were then added to a matrix to form a hydrogel through photopolymerization using the same monomers, and CHX was again incorporated within the matrix. The NCHG allowed for the sustained release of CHX (release over a 48 h period) when compared to the control hydrogel (24 h release period) and it was found that 60 % of the loaded drug was released. The swelling of the NCHG was observed to be much slower than the control hydrogel, though the NCHG had a higher water adsorbing capacity (Bako *et al.* 2008).

Further Ma *et al*. (2007) developed a thermo-sensitive hydrogel (liquid at room temperature then rapidly gels at body temperature) for the prolonged release of CHG incorporated within β-cyclodextrin inclusion complex that were then added to a chitosan matrix containing a growth factor recombined human bone morphogenetic protein. The *in vitro* release profile for CHG was shown to be sustained and controlled over a 1 month period from the NCHG. The authors believe that the chitosan thermo-sensitive hydrogel may have vast potential for treatment against periodontal infections (Ma *et al.* 2007). One strategy to prevent infection has been to use thermo-sensitive hydrogels as wound dressings or to act as a coating for medical devices (Jones *et al.* 2008). NIPAA based hydrogels were incorporated with CHX diacetate (1 % w/w) and were shown to possess ideal thermo-responsive behaviour resulting in antimicrobial properties through CHX diacetate release. Pulsatile biocide release may aid the prevention of resistant

bacterial strains as it refrains from prolonged release of possible sub-lethal concentrations of a biocide.

There are numerous hydrogel systems that have been developed for enhanced topical skin delivery of CHX however very few have been tested using an *in vitro* skin diffusion model. A thermo-sensitive vinyl-ether based hydrogel was designed for CHX release and a high CHX acetate loading was achieved (~36 mg of CHX per gram of gel). CHX acetate was released over a 27 day period in a concentration that was above the MIC for two microorganisms found within the human mouth *Streptococcus mutans* and *Lactobacillus casei* (Kiremitçi *et al.* 2007).

Hydrogels containing porous (type I) collagen matrices were developed for the sustained release of CHG (Sulea *et al.* 2011). It was determined that an enhanced release of CHG occurred from slightly basic hydrogels when compared to acidic hydrogels. The CHG release was also enhanced with increasing CHG concentration within the porous collagen matrices within the hydrogel. Another example of a hydrogel designed for CHG release is the chitosan hydrogel to enhance the mucosal delivery of CHG (Şenel *et al.* 2000). Hydrogels containing 1-2 % chitosan were prepared and characterised to determine the antifungal effects and release of CHG from the gels *in vitro*. Chitosan gels released CHG over a 3 h period without a lag period as did chitosan based films resulting in a prolonged release of CHG (Şenel *et al.* 2000). Reports of CHX having been incorporated into various hydrogel systems are within the literature however there does seem to be few studies using an *in vitro* diffusion cell model to characterise the release into biological membranes (i.e excised skin). It would be of interest to

determine the efficacy of more hydrogel systems using *ex vivo* skin in diffusion cells or *in vivo* studies.

1.6.2 Polymeric CHX delivery systems.

Polyurethane films inclusive of CHX acetate were also developed for controlled drug delivery (Huynh *et al.* 2010). The authors showed that modulation of CHX acetate release was possible depending on the structure of the polyurethane films. It was determined that CHX acetate had no interaction with the polyurethane as illustrated by differential scanning calorimetry (DSC) and attenuated total reflectance Fourier transform infrared spectroscopy (ATR-FTIR) and therefore sustained drug release was observed over 29 days. CHX and CHG were incorporated within poly(lactic-co-glycolic acid) (PLGA) microspheres for sustained release over a two week period. The addition of cyclodextrins reduced the immediate burst release of CHG and CHX resulting in controlled release of CHX for the prevention or treatment of periodontal disease (Yue *et al.* 2004). Sustained release of CHX has been demonstrated by incorporation in to cold cured polymerizing methylacrylate systems (Riggs *et al.* 2000). The sustained release of CHX digluconate was achieved from a device coated in chitosan, poly (lactic-co-glycolic acid) (PLGA), and polymethyl methacrylate (PMMA). By controlling the pore size of the PLGA and PMMA upon the device they could effectively control the release rate of CHX. (Lee *et al.* 2005a).

Delivery of CHX from poly (Ɛ-caprolactone) nanocapsules to artificially contaminated porcine skin achieved superior results compared to the CHX in free solution (Lboutounne *et al.* 2002). The nanocapsules encapsulating CHX preferentially accumulated into hair follicles, which act as bacteria reservoirs thus

ensuring targeted delivery. CHX loaded nanocapsules developed by Lboutounne *et al.* (2002) were later formulated into a hand rub (Nanochlorex®) and tested against the resident skin pathogen *Staphylococcus epidermidis* after contamination onto *ex vivo* porcine skin (Nhung *et al.* 2007). Sustained antimicrobial activity was observed for Nanochlorex® with a statistically increased $\log_{10}$ reduction of *S. epidermidis.* Farkas *et al.* (2004) utilised a vesicular phospholipid gel for the enhanced delivery of CHX. It was determined that multilamellar lipid vesicles significantly enhanced the delivery of CHG across dialysis membrane in a diffusion cell due to increased dispersity and fluidity.

More recently preparations containing polymeric thermo-sensitive modified poly-*N*-isopropylacrylamides microspheres were investigated for the sustained release of CHX base at different skin temperatures (Musial *et al.* 2012). The polymeric system at skin temperature released CHX at around 60-130 minutes after application. At a lower temperature the CHX was released and localised between 80- 90 minutes. The system is an example of controlled release however a long lag time may impede the delivery and localisation of CHX at the target site of the skin.

There are many examples of colloidal CHX delivery systems and the benefits of such colloid systems used in topical and transdermal drug delivery include:

- Targeting of drugs to a localised infected area
- Reducing drug degradation rates
- Improving drug release profile
- Minimising adverse effects on the skin

(Nhung *et al.* 2007)

1.6.3 Other strategies employed for enhanced delivery of CHX.

Other penetration enhancers have been used to increase the delivery of CHG into the upper skin strata. Eucalyptus oil was shown to enhance the penetration of CHG into the deeper layers of the skin (Karpanen *et al.* 2010). After CHG (2% w/v) was dosed along with 50 % (v/v) of eucalyptus oil the concentration of CHG within the top 100 µm of the skin after 30 minutes was 0.398 ± 0.076 µg/mg tissue (SEM) compared to 0.077 ± 0.015 µg/mg tissue (SEM) when CHG was dosed alone (Karpanen *et al.* 2010) and (Karpanen *et al.* 2008). Further, after 2 minutes a higher concentration of CHG was observed within the skin after dosing CHG in a eucalyptus oil (10 % v/v) and isopropanol (70 % v/v) vehicle (Karpanen *et al.* 2010). The same authors also compared the topical delivery of CHG from aqueous and alcohol vehicles. It was reported that following a two minute exposure the concentration of CHG recovered in the top 100 µm of the skin was 0.023 ± 0.007 µg/mg tissue (mean ± SEM) and 0.157 ± 0.047 µg/mg tissue (mean ± SEM) for CHG (2 % w/v) in a 70 % (v/v) isopropanol vehicle and CHG (2 % w/v) in an aqueous solution (Karpanen *et al.* 2009). At 30 minutes there was no statistical difference in the concentration of CHG within the skin after application from an aqueous or alcoholic vehicle.

1.7 Nanomaterials used for topical and transdermal drug delivery.

Nanomaterials are increasingly being studied for use as topical and transdermal drug delivery systems for improved drug delivery kinetics (Figure 1.5). The nanoparticle skin delivery field is in its infancy but has the potential to yield fruitful drug delivery systems. Conventional passive skin penetration enhancers such as the chemical penetration enhancer azone and dimethylsulfoxide (DMSO)

and physical methods such as iontophoresis have not achieved commercial success as a result of high cost or biocompatibility problems. Nanomaterials' unique physiochemical properties exerted by their large surface area are advantageous for use as a passive topical or transdermal drug delivery platform (Bouchemal *et al.* 2004). Their constituents, for example lipids within liposomes and surfactants within niosomes may penetrate the SC and act as a penetration enhancer after nanoparticle ruption on the SC surface (Jain, 2012). These constituents are known to fluidise the intercellular matrix and enhance drug penetration within the skin (Benson, 2005). Further, nanoparticles may act as a depot for sustained skin drug delivery or act as a rate limiting barrier deposited across the SC surface for controlled release (Jain, 2012). Previously a range of nanomaterials have been explored as drug delivery systems for the skin (Figure 1.5) in an attempt to obtain controlled and targeted drug delivery for enhanced therapeutic efficacy.

Nanoemulsions (droplet size between 20-200 nm) are increasingly utilised for the topical delivery of drugs due to advantages such as enhanced drug solubility, good thermodynamic stability and enhanced skin penetration when compared to conventional dosage forms (Sarker, 2005, Shakeel *et al.* 2007, Shakeel *et al.* 2010 and Sakeena *et al.* 2010). Nanoemulsions enhanced the flux of ketoprofen six fold compared to the control after application to mouse skin *in vitro* (Kim *et al.* 2008). The authors suggested the permeation enhancement was due to the impact of the particle's size and a contributing factor may be due to the incorporation of known penetration enhancers such as oils and surfactants. Nanoemulsions also enhanced (between 5 and 15 fold when compared to control) the topical delivery of the hydrophilic compound inulin *in vitro* using hairy mouse

skin (Wu *et al.* 2001). The authors believe the penetration enhancement of inulin was due to co-transport of the drug *via* the follicular transport route (due to water-in-oil nanoemulsions' compatibility with sebum) and through surfactant-induced SC perturbations. A full review on nanoemulsions was compiled by Shah and co-workers (2010).

Nanocapsules are lipophilic droplets coated in a polymeric membrane to form a vesicular polymeric drug carrier. Nanocapsules have a number of advantageous properties for drug delivery; they are biocompatible and biodegradable, they can act as a reservoir for sustained drug delivery, the drug is encapsulated therefore localised tissue irritation is avoided, high drug loading capability and the polymer coating offers protection from drug degradation (Couvreur *et al*. 2006). Poly n-butylcyanoacrylate (PNBCA) nanocapsules with encapsulated indomethacin (0.5 % w/v) were applied to excised rat skin *in vitro.* After an 8 h contact time the cumulative concentration of indomethacin that had permeated the rat skin after application encapsulated within the PNBCA nanocapsules was ~9 times higher than when compared to the control (Miyazaki *et al.* 2003). Further, poly(ε-caprolactone)-nanocapsules were encapsulated with sunscreen (Parsol MCX) and were shown to exhibit enhanced photo-protection when compared to a standard topical gel (Alvarez-Roman *et al.* 2001).

One strategy that has received a great deal of attention over the last three decades for enhanced skin delivery of therapeutics is vesicular systems. Vesicles aid the penetration of drugs into the SC but also reduce percutaneous absorption for enhanced skin delivery of therapeutics by acting as a reservoir within the upper skin strata (Lboutounne *et al.* 2004). Liposomes are microscopic phospholipid

bubbles with a lipid bilayer membrane as an outer structure (Torchilin, 2005). Liposomes have been utilised for the enhanced topical skin delivery of many therapeutic entities (Schreier and Bouwstra, 1994, Mezei and Gulasekharam, 1980, Tabbakhian *et al.* 2006, El Maghraby *et al.* 2008). There are a number of proposed mechanisms of action of liposomes including: intact vesicular penetration within the SC, a penetration enhancing effect caused by interaction of the lipids within the endogenous SC lipids, the adsorption effect and preferential accumulation of the liposomes within the transappendageal route (Elsayed *et al.* 2007).

More recently, adaptations of the classical liposome have been developed using a range of constituent materials within the bilayer including; transfersomes (Maghraby *et al.* 2001), niosomes (Balakrishnan *et al.* 2009), cubosomes (Esposito *et al.* 2005) and ethosomes (Elsayed *et al.* 2006). All of the aforementioned vesicles resulted in enhanced drug deposition within the upper skin strata. Samad and co-workers wrote a comprehensive review on vesicular drug delivery for enhanced topical drug delivery (Samad *et al.* 2007).

Solid lipid nanoparticles (SLNs) have been investigated since the early nineties as an alternative to polymeric drug carriers. SLNs offer the advantages of being biocompatible and biodegradable, a high surface area, protection of labile drugs and they form an occlusive film across the skin surface for enhanced drug deposition and skin hydration (Müller *et al.* 2002 and Mehnert and Mäder, 2001). SLNs have been used to act as a topical drug carrier for enhanced deposition within the upper skin strata for many compounds including vitamin A (Jenning *et al.* 2000), sunscreen-oxybenzone (Wissing and Müller, 2002) and isotretinoin (Liu

et al. 2007). Though SLNs are produced from physiological materials and do not require organic solvents, they do suffer from low drug loading and physical instability during storage (Mehnert and Mäder, 2001). SLNs may exist as alternative colloidal structures such as liposomes, micelles and nanocrystals (Guterres *et al.* 2007). This added complexity of alternative lipid structure formation may be a reason for SNPs not being incorporated into a single pharmaceutical product on the market (though they have been used in >30 cosmetic formulations) (Pardeike *et al.* 2009).

Polymeric nanoparticles (nanospheres, dendrimers, hydrogels etc.) have also been investigated for use as topical drug delivery systems through encapsulation, adsorption or dispersion within the polymeric chains of the nanoparticle (Guterres *et al.* 2007). Advances in polymer chemistry have allowed for the design of novel transdermal and topical drug delivery systems. Encapsulation of drugs within a polymeric nanoparticle can modify the physiochemical characteristics and may act as a penetration enhancer due to the possession of a higher thermodynamic activity when compared to the free solution (Naik *et al.* 2004).

poly-lactic-co-glycolic acid (PLGA) nanoparticles have been used as a drug delivery system for various hair growth treatments using excised human scalp *in vitro* (Tsjimoto *et al.* 2007). It was found that the encapsulated hair growth drugs within the PLGA nanoparticles had an enhanced deposition (2-2.5 fold enhancement) within hair follicle when compared to the control. PLGA nanoparticles encapsulating drugs have been utilised to enhance the penetration of a range of therapeutics within the SC and markedly within the follicular route

(Haddadi *et al.* 2008, Naik *et al.* 2004 and De Jalón *et al.* 2001). Further, various other block co-polymers have been utilised to encapsulate drugs for skin delivery (Rastogi *et al.* 2009 and Choi *et al.* 2012).

Polymeric drug delivery systems designed for skin delivery may take many different forms. Conventional transdermal patches are typically based on a polymeric matrix with the active drug dispersed or dissolved within the matrix (Jones, 2004). The ratio and type of polymers used can be manipulated to control the partitioning and diffusion of the compound from the patch into and across the SC (Arora *et al.* 2002). Therapeutic polymers are also incorporated to act as an anti-nucleant for the prevention of crystallisation of the drug when formulated into a super-saturated topical formulation (Pellet *et al.* 1994 and Raghavan *et al.* 2000). Though on a micro-scale, it is worth mentioning the recent development of polymeric microneedles that have been utilised for physical skin delivery to circumvent the SC (Park *et al.* 2005, Lee *et al.* 2012, and Lee *et al.* 2008). Polymeric microneedles have the advantage of being biodegradable, biocompatible and cheaper to manufacture than their silicon counterparts (Van der Maaden *et al.* 2012). A comprehensive state of the art review was recently published on polymeric microneedles (Ochoa *et al.* 2012).

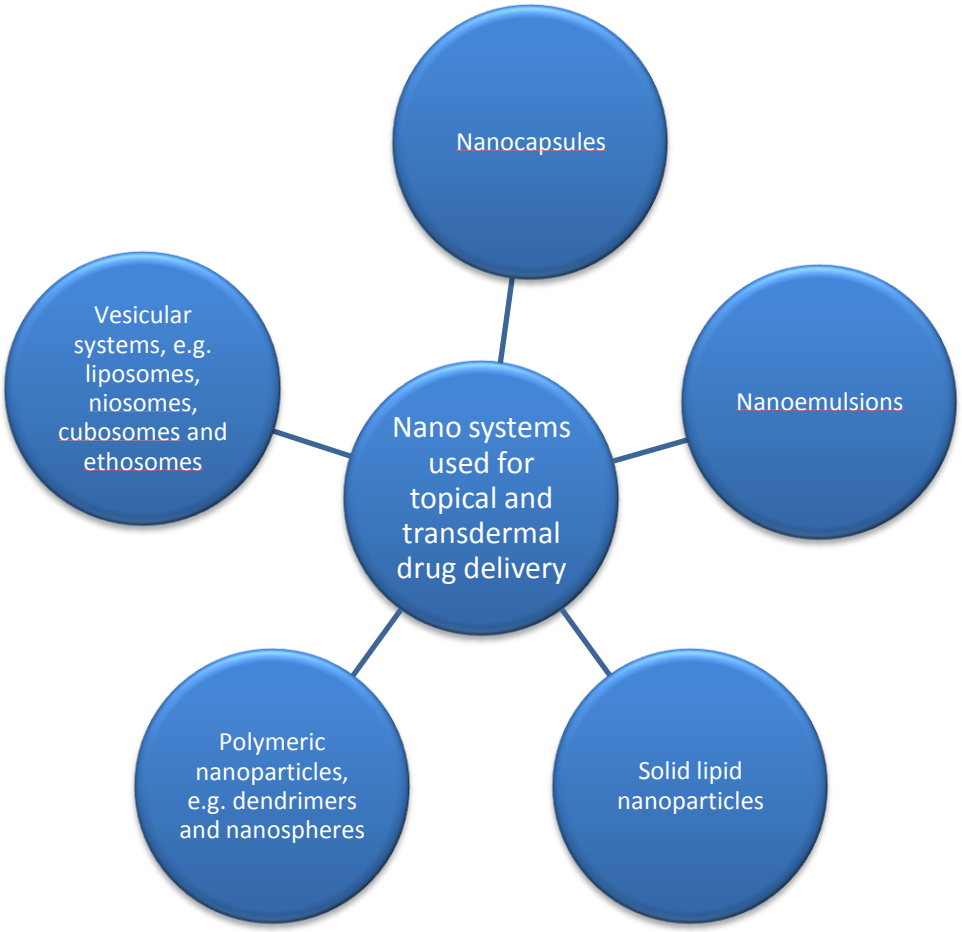

Figure 1.5 Schematic of commonly used nano-particulate topical and transdermal drug delivery systems.

1.8 Introduction to PAMAM dendrimers; the chosen novel strategy for enhanced topical drug delivery.

The novel strategy employed to enhance the deposition of a topical antiseptic are a type of dendrimer called polyamidoamine (PAMAM) dendrimer Figure 1.6). Though PAMAM dendrimers were first synthesised in the mid-eighties it was only recently that PAMAM dendrimers were investigated as a novel dendritic penetration enhancer used to improve drug delivery kinetics (See section 3.1 for detailed discussion). PAMAM dendrimers are highly branched polymeric molecules that are composed of multiple branched monomers that derive from a central core. A dendrimer can be thought of as three sections: a focal core,

internal branches of repeating units and peripheral functional groups. The number of branch points emanating from the core defines the generation of the dendrimers, e.g. G1, G2, G3, etc. (Lee *et al.* 2005b) as observed in Figure 1.7.

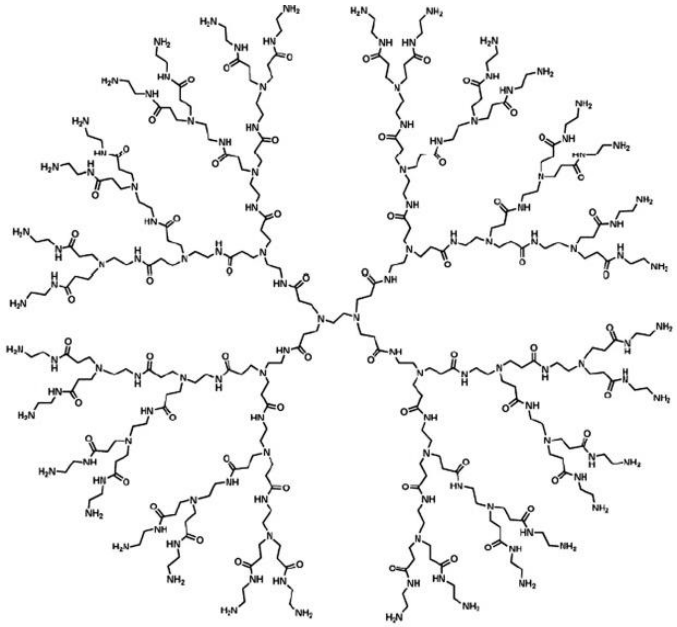

Figure 1.6 Chemical structure of a generation 3 polyamidoamine (PAMAM) dendrimer. *An ethylenediamine core with repeating monomers of ethylenediamine and methyl acrylate, terminating in amine groups.*

The physicochemical properties of PAMAM dendrimers that make them unique are listed below:-

- Uniform molecular weight with a narrow molecular weight distribution – i.e. they are monodispersed.
- They have predictable three-dimensional architecture.
- The diameter and generation number increases systematically.
- The step-by-step controlled synthesis allows for site selective functionalities.
- In high generation dendrimers (> G4) isolated interior pockets allow the dendrimers to host small guest molecules.

- The solubility of dendrimers can be controlled by the peripheral functional groups, e.g. by adding hydrophilic functional groups the water solubility can be increased.

  (Jang *et al.* 2009)

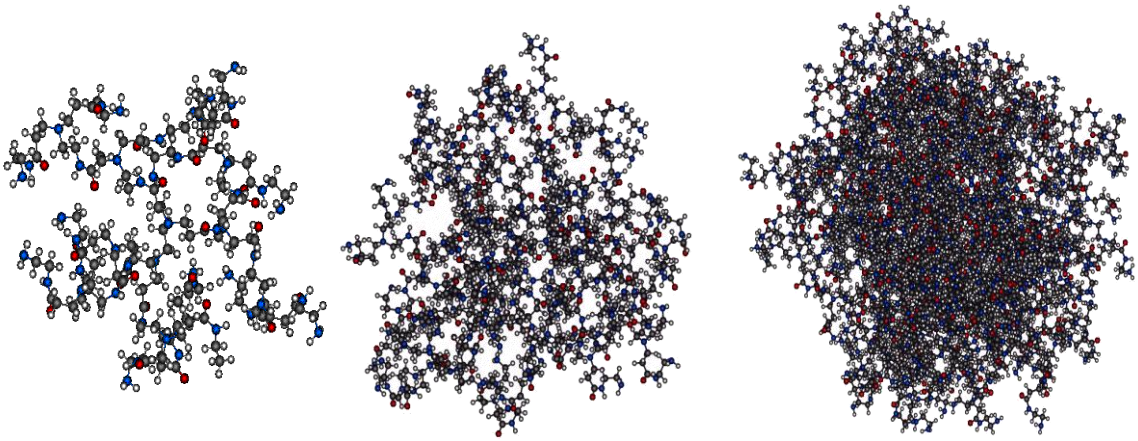

Generation 2 Generation 4 Generation 6

Figure 1.7. Generation 2, 4 and 6 PAMAM dendrimers observed as molecular dynamic simulations (Adapted from Maiti *et al.* 2004).

PAMAM dendrimers have been utilised within this investigation and they are the most studied dendrimer within the literature. A search for the term 'PAMAM dendrimer' on ScienceDirect retrieved 2,616 publications (March 2013). PAMAM dendrimers can be commercially purchased from Dendritech in the US as they are now manufactured on a kilogram scale. PAMAM dendrimers can also be synthesised within the laboratory using a divergent method developed by Donald Tomalia that was published in 1985 (Tomalia *et al.* 1985).The divergent method for PAMAM dendrimer synthesis (aka Starburst® dendrimers) was first developed by D. Tomalia in 1978 in the Dow chemical laboratories. It is a synthetic pathway of iterative alkylation and amidation reactions; each resulting in one new generation

as illustrated in Figure 1.8. PAMAM dendrimers contain an initiator core that is typically a molecule of ammonia or ethylenediamine.

The PAMAM dendrimers used within this project have ethylenediamine (1,2-diaminoethane) as a core/monomer and methyl acrylate as a monomer. The first reaction for PAMAM dendrimer synthesis is a Michael addition between the primary amine groups of the ethylenediamine and the methyl acrylate which results in a half generation carboxyl group terminated PAMAM dendrimer. Amidation of a half generation carboxyl terminated PAMAM dendrimer with excess ethylenediamine results in an amine terminated full generation PAMAM dendrimer (Figure 1.8). These two reactions are then repeated to form half and full generation PAMAM dendrimers up to generation 12, under optimal synthetic conditions (Tomalia *et al.* 1993).

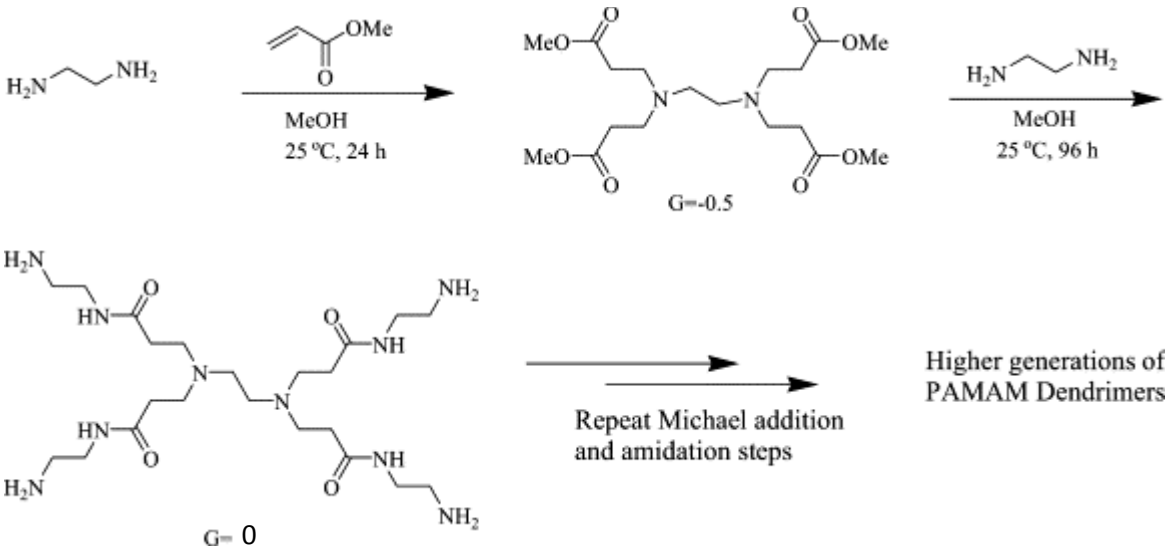

Figure 1.8. Schematic of the synthetic steps for the divergent approach in synthesising PAMAM dendrimers. *An iterative reaction of alkylation and amidation forms a full generation amine terminated PAMAM dendrimer. Schematic taken from Fréchet and Tomalia (2001).*

The physiochemical characteristics of PAMAM dendrimers can be found in Table 1.2. The number of surface groups, in this case primary amine groups, doubles and the molecular weight increases exponentially with each iterative step of alkylation and amidation and thus an increase in the generation (Lothian-Tomalia *et al.* 1997). The PAMAM dendrimers used within this thesis are generations 2-5 with diameters ranging from 2.6-5.7 nm. The most commonly used PAMAM dendrimer within this thesis is generation 3 that is 3.6 nm in diameter (Table 1.2). For scale this is approximately equivalent to the diameter of insulin and around half the diameter of a lipid bilayer (Esfand and Tomalia, 2001).

Table 1.2. Theoretical physiochemical characteristics of PAMAM dendrimers from generation 0-10. *Table taken from Fréchet and Tomalia, 2001*.

Generation	Surface groups (Z)	Molecular formula	MW	Diameter (nm)
0	4	$C_{22}H_{48}N_{10}O_4$	517	1.4
1	8	$C_{62}H_{128}N_{26}O_{12}$	1,430	1.9
2	16	$C_{142}H_{288}N_{58}O_{28}$	3,256	2.6
3	32	$C_{302}H_{608}N_{122}O_{60}$	6,909	3.6
4	64	$C_{622}H_{1248}N_{250}O_{124}$	14,215	4.4
5	128	$C_{1262}H_{2528}N_{506}O_{252}$	28,826	5.7
6	256	$C_{2542}H_{5088}N_{1018}O_{508}$	58,048	7.2
7	512	$C_{5102}H_{10208}N_{2042}O_{1020}$	116,493	8.8
8	1,024	$C_{10222}H_{20448}N_{4090}O_{2044}$	233,383	9.8
9	2,048	$C_{20462}H_{40926}N_{8186}O_{4092}$	467,162	11.4
10	4,096	$C_{40942}H_{81888}N_{16378}O_{8188}$	934,720	Around 13.0

The *in vitro* toxicity of PAMAM dendrimers has been investigated in a number of studies and the cytotoxicity appears to be dependent on the concentration and generation (molecular weight and number of surface groups) of the PAMAM dendrimer (Mukherjee and Byrne, 2012). It has been established that cationic dendrimers are more toxic than their anionic counterparts (Jevprasephant

et al. 2003 and Duncan and Izzo, 2005). There is however a discrepancy between the reported toxic concentrations of PAMAM dendrimers. Full generation cationic PAMAM dendrimers above generation 1 were shown to be haemolytic at a concentration of 1 mg/mL by Malik and co-workers (2000). Also the cytotoxicity was measured as the IC_{50} concentration (mg/mL) after a 72 h MTT ((3-(4,5-Dimethylthiazol-2-yl)-2,5-diphenyltetrazolium bromide) assay using B16F10 cells (mouse melanoma cells). The IC_{50} concentration for G1, G2, G3 and G4-PAMAM-NH_2 was calculated as >2, >2, 0.05 and 0.05 mg/mL respectively. The lower generation PAMAM dendrimers did not incite cytotoxicity up to a concentration of 2 mg/mL and this was also observed for the half generation carboxyl terminated PAMAM dendrimers (Malik *et al.* 2000). A more recent *in vitro* study on rat red blood cell lysis using G4-PAMAM-NH_2 dendrimer showed no effects of haemolysis up to a concentration of 10 µM L^{-1} over 24 h (Labieniec *et al.* 2008). When the toxicity of PAMAM dendrimers was investigated using a lactate dehydrogenase assay on caco-2 cell (human intestinal adenocarcinoma) monolayers G2-PAMAM-NH_2 and G3-PAMAM-NH_2 dendrimers exhibited toxicity at a concentration of >10 and >0.1 mM respectively (Elsayed *et al.* 2002).

More recently, G4, G5 and G6-PAMAM-NH_2 dendrimers were tested for induction of cytotoxic responses as a product of the formation of reactive oxygen species (ROS) after endocytosis (Mukherjee and Byrne, 2012). It was found that these higher generation PAMAM dendrimers incited toxicity at a concentration of 1 mM due to the formation of ROS resulting in mitochondrial membrane disruption (Mukherjee and Byrne, 2012). Calabretta *et al.* (2007) found no cytotoxicity for G5-PAMAM-NH_2 up to a concentration of 1 µg/mL against human corneal epithelial

cells (though below this concentration they exhibit antimicrobial properties against *P.* aeruginosa) though at the highest tested concentration 10 µg/mL 25 % of HCECs survived that was comparable to the positive control benzalkonium chloride.

Few studies have been conducted *in vivo* on PAMAM dendrimer toxicology, though when PAMAM dendrimers up to Generation 5 (G7-PAMAM-NH_2 dendrimer potentially induced problems as 1 in 5 mice died in that treatment group) were injected into mice at a dose of 10 mg/kg^{-1} they appeared to be non-toxic (Bos and Heegaard, 2004, Roberts *et al.* 1996 and Bourne *et al.* 2000). Chauhan *et al.* (2010) and colleagues found G4-PAMAM-NH_2 and G4-PAMAM-OH dendrimers to be non-toxic in general after an *in vivo* study in mice at a low, medium and high dosages. It was found that at the high concentration treatment group of G4-PAMAM-NH_2 dendrimer some toxicity was observed (i.e. declined glucose levels) though this was seen to recover after a 15 day recovery time. A full review on the toxicity of dendrimers was recently compiled by Jain and co-workers (Jain *et al.* 2010).

With regards to the PAMAM dendrimer toxicity after application to the skin surface, it is expected to be low as the PAMAM dendrimers' penetration across or within the skin is low (for a detailed discussion on the potential for PAMAM dendrimers to penetrate the skin, see section 4.1) (Sun *et al.* 2012). As outlined in Sections 1.1 and 1.2 the SC is a formidable barrier composed of anucleate corneocytes and a dense intercellular lipid network that prevents the ingress of large and highly charged macromolecules such as PAMAM dendrimers. Bos and Meinardi (2001) stated that for significant transdermal drug delivery a permeating

compound must be below 500 Da in order to traverse the SC; a G3-PAMAM-NH_2 dendrimer is ~6,909 Da. The toxicity of PAMAM dendrimers *in vivo* has not been realised and it should also be considered that if a commercially available and widely accepted ethanolic hand gel (60-80 % ethanol v/v) was applied to a cell line, low cell viability would be the result and toxicity inferred.

Due to their unique physiochemical characteristics dendrimers have been investigated for use in a wide range of biomedical applications. These include the use as an improved magnetic resonance imaging (MRI) contrast agent through covalent conjugation to, for example Gd(III)-diethylenetriamine (GD(III)-DTPA) or GD(III)-tetracarboxymethyl-1,4,7,10-tetraazacyclododecane (GD(III)-DOTA) (Venditto *et al.* 2005) and (Wiener *et al.* 2005). After conjugation of an MRI contrast agent to a PAMAM dendrimer it was reported to result in increased blood circulation times that allows for an extended imaging time frame. Another advantage of the PAMAM conjugated MRI contrast agent was greater contrast and enhanced images as PAMAM dendrimers possess high relaxivities (Wiener *et al.* 1996). PAMAM dendrimers have also found use as effective DNA transfecting agents through electrostatic complexation of the primary amine groups on the dendrimer surface and the negatively charged phosphate groups of the nucleic acids (Bielinska *et al.* 1999 and Eichman *et al.* 2000). PAMAM dendrimers have been used frequently as drug delivery agents and less commonly as biocides. A detailed discussion on dendrimer-biocides can be found within the introduction in Chapter 2. Further, the efficacy and suitability of PAMAM dendrimers as a topical drug delivery system has been discussed in further detail within the introduction to Chapter 3.

1.8.1 Aims and objectives of the study.

The prevalence of healthcare-acquired infections, in particular, multi-drug resistant strains has given rise to considerable concern and the issue is persistently highlighted by the media. There is a clear need for innovation in infection control to enhance and increase the current armoury of anti-infective agents (Davies, 2013). The aim of this project is to develop a novel topical antimicrobial formulation that utilises dendritic architectures as a platform to enhance the permeation of anti-infective agents into the skin. PAMAM dendrimers have previously been shown to be antimicrobial (Calabretta *et al.* 2007 and Wang *et al.* 2010) however their antimicrobial efficacy against opportunistic skin pathogens and their mechanism of action have yet to be fully elucidated.

An objective of this study is to comprehensively assess their antimicrobial efficacy and mechanism of action as it would be of great advantage for a topical drug delivery platform to also possess antimicrobial properties against skin pathogens. Central to the formulation is the PAMAM dendrimer and this thesis will examine as to whether a PAMAM dendrimer skin pre-treatment and co-treatment increases the distribution and localisation of the model drug, CHX within the upper skin strata. Further, PAMAM dendrimers' interactions with CHG and the skin will also be investigated in an attempt to elucidate any enhancement effects.

The topical deposition of the CHG will be chemically mapped using a novel time-of-flight secondary ion mass spectrometry (ToF-SIMS) method. To improve the bioavailability of topically-applied formulations, the permeation pathway and distribution of a drug and its excipients throughout the skin strata must be understood. The method will reveal localisation of CHG to specific histological skin

compartments and to visualise any permeation enhancement effects elicited by the application of PAMAM dendrimers.

The final objective of this thesis is to develop a stable formulation that contains a clinically relevant concentration of CHG and a dendritic permeation enhancer. The formulation will be assessed to ensure increased antimicrobial efficacy against skin pathogens and to determine whether addition of the PAMAM dendrimer enhances the deposition of CHG within the upper skin strata.

2.0 A comprehensive study into the antimicrobial efficacy and mechanism of action of PAMAM dendrimers against opportunistic pathogens.

2.1 Introduction

2.1.1 Advantages of antimicrobial dendrimers

An increasing number of bacteria are evolving into antibiotic-resistant strains that are threatening our ability to treat infectious diseases within a primary, secondary and community care setting (Rice, 2009). This growing trend of resistance has depleted the armoury of available effective antibiotics. This is compounded by the fact that the development of novel antibiotics offers the second lowest return on investments (Walsh, 2000). The World Health Organisation (WHO) has declared antibiotic resistance one of the three greatest threats to human health (WHO, 2001).

In March 2013, the chief medical officer (CMO) for England released a second volume of her annual report into the state of public health in England, in which she focused specifically on the burden of infections and antimicrobial resistance (Davies, 2013(a)). The CMO stated the burden of infectious diseases was estimated to cost approximately £30 billion each year to the economy (Davies, 2012 (a)). In 2011, infectious diseases had accounted for 7 % of all deaths and accounted for 8 % of all hospital bed use in England (Davies, 2013 (b)).The same report showed that *Escherichia coli* accounted for around 36 % of all bloodstream infections (bacteraemia) and there was increasing emergence of multi-drug resistant strains. In cases of patient mortality, multi-drug resistant *E. coli* accounted for 30 % whereas susceptible *E. coli*

strains accounted for 15 % (Davies, 2013 (b)). Further, the report stated that many of the infections arise from the patient's own microbial flora with the most prominent pathogen being *Staphylococcus aureus*. *S. aureus* typically resides within the anterior nares and perineum (Davis *et al.* 2004) and those patients colonised on admission are at a greater risk of developing surgical site incision infections. It has also been shown to spread epidemically between patients and can be transferred from staff to patients (von Eiff *et al.*,2001).

The CMO calls for prevention strategies to stop colonisation from developing into infection and one of the recommendations from the report emphasises the need for further preventative strategies and that action is required at a national and local level to combat antibiotic resistance (Davies, 2013 (b)). With increasing resistance and little to combat complex infections, the availability of modern medical advancements such as major surgery, dialysis, organ transplantation and chemotherapy are in jeopardy (Cars *et al.* 2008).

To prevent a return to the pre-antibiotic era, design and delivery of antimicrobial drugs with improved efficacy and avoidance of drug resistance are of paramount importance. Innovative strategies as well as more efficient use of current antimicrobial compounds are mandatory. Efforts in synthetic chemistry have focussed on identifying orally bioavailable small-drug molecules utilising high throughput screening methods (McCarthy, 2005). This effort has not yet translated into the availability of novel antibiotics in the clinic. Biological targets, such as bacterial cell membranes, consist of macromolecules that rely on polyvalent interactions in their binding (Mammen *et al.* 1998). Most biological targets are of a nano-scale (1-100 nm) therefore polyvalent

macromolecules of a nano-size may have increased biological efficacy when compared to small-molecule drugs due to a match in scale and multivalent binding (McCarthy, 2005). Nanoparticles offer unique advantages in antimicrobial therapy such as a reduction in acute toxicity and avoidance of resistance *via* alternate mechanisms of action (Weir *et al.* 2008). Nanoparticles (silver) within a 1-10 nm size range (G3-PAMAM-NH_2 having a diameter of 3.6 nm) were shown to have a greater direct interaction with bacteria, suggesting a size dependency (Morones *et al.*2005). Polyamidoamine (PAMAM) dendrimers have become the most widely investigated dendrimers for a range of biomedical applications (Svenson, 2009, Esfand and Tomalia, 2001 and Sajja *et al.* 2009).

Due to the highly branched and globular nature of dendrimers, they possess unique properties enabling them to act as a multivalent biocide or a nano-platform for antimicrobial drug delivery (Meyers *et al.*,2008). The uniform branching of dendrimers provides a large surface area to volume ratio enabling high reactivity with micro-organisms *in vivo* (Zhang *et al*.,2010). The highly localized and dense functional groups on the dendrimer's surface can be tailored for antimicrobial efficacy or for the conjugation of targeting ligands to a variety of micro-organisms' receptors (Tomalia *et al.,*1990 and Gillies and Fréchet, 2005).

The strategies discussed in this chapter include the use of dendrimers as delivery platforms for conventional antibacterial drugs, (Cheng *et al.* 2007(a) and Kumar *et al.* 2006), competitive binding to bacteria and toxins to inhibit bacterial adhesion (Joosten *et al.* 2004) and biocidal dendrimers without complexation or

conjugation to conventional biocides (Wang *et al.* 2010, Calabretta *et al.* 2007 and Lopez *et al.* 2009).

2.1.2 Glycodendrimers

Glycodendrimers have been studied as to whether they prevent host-pathogen adhesion and thus toxin transport into the host cell. Glycodendrimers typically have saccharide residues on the surface though some may contain a sugar unit as a focal core with emanating carbohydrate branches (Cloninger, 2002). The multivalent nature of glycodendrimers has been exploited to improve their antimicrobial activity as the bacteria and their toxins can preferentially bind to the sugar group pendants on the surface of the glycodendrimer as opposed to the host cell *in vitro* (Mintzer *et al.* 2011).

Polypropylene imine (PPI) and PAMAM dendrimers have been modified by the covalent conjugation of oligosaccharides (phenylisothiocyanate derivatised (PITC) galb1-3galNAcb1-4[sialic acida2-3]-galb1-4glc residues) to the amine focal core. These were then shown *in vitro* to inhibit the binding of the heat labile enterotoxin of *E. coli* and require ~ 1000-fold lower concentration than that of the free oligosaccharide to achieve the same binding efficacy (Thompson and Schengrund, 1997). The same group also demonstrated that a PPI based glycodendrimer could beused to inhibit the binding of both cholera toxins and heat labile enterotoxins to a murine fibroblast cell line (Thompson and Schengrund, 1998). Since then, PPI and PAMAM dendrimers have been modified with various oligosaccharides to inhibit the binding of a range of pathogenic organisms or toxins (Joosten *et al.* 2004, Salminen *et al.* 2007 and Woller *et al*. 2003).

2.1.3Dendrimers as biocides andantimicrobial carriers

Dendrimers are emerging as novel topical antimicrobial macromolecules (Svenson and Tomalia, 2005). PAMAM dendrimers contain hydrophobic interior voids in which small non-polar drug molecules maybe encapsulated (Cheng *et al.* 2007(b)). PAMAM dendrimers also have a high density of surface functionalities allowing for the conjugation or complexation of antimicrobial agents (Patri *et al.* 2002). The use of dendrimers as antimicrobial drug delivery platforms offers a number of advantages over conventional antimicrobial drugs including increased bioavailability, decreased adverse side effects and increased deposition of the drug at target sites (Gardiner *et al.* 2008). Due to the hydrophilic exterior, PAMAM dendrimers can increase the solubility of hydrophobic drugs and this increase in solubility was shown to result in an enhanced antimicrobial effect *in vitro* when compared to the drug in free solution (Ma *et al.* 2007and Winnicka *et al.* 2011).

Silver ions have antimicrobial properties and is commonly utilised in the topical treatment of infected wounds. Silver ion complexes of PAMAM dendrimers and silver-PAMAM composites were shown to be effective antimicrobial compounds against, *S. aureus*, *E. coli* and *Pseudomonas aeruginosa in vitro* as shown by Balogh *et al.* (2001). Using a disc diffusion assay, they demonstrated that both compounds displayed antimicrobial activity that was either comparable to, or enhanced, when compared to standard silver nitrate solutions.

The aqueous solubility of sulfamethoxazole (SMZ), an antimicrobial sulfonamide, was increased, *in vitro*, when PAMAM dendrimers were used as a carrier

system. An enhancement in antimicrobial activity was observed against *E. coli*. with a four or eight-fold increase in the anti-bacterial activity of SMZ in a dendrimer solution compared to pure SMZ dissolved in dimethylsulfoxide (DMSO) or a 0.01M NaOH solution (Ma *et al.* 2007).

PAMAM dendrimers have been used to increase the aqueous solubility of both nadifloxacin and prulifloxacin however the increased solubility only resulted in an increase in the antimicrobial efficacy of prulifloxacin, as shown by Cheng *et al.* (2007a). The authors proposed the enhanced antibacterial efficacy of pruifloxacin was due to the PAMAM dendrimer's disruption of the bacterial cell membrane allowing the quinolone entry to the bacterial cytoplasm and as a result causing damage to DNA.PAMAM dendrimers have also been investigated to determine whether they increased solubility of the antimicrobial compound, triclosan. PAMAM dendrimer generation 3 (PAMAM G-3) and phenylalanine conjugated PAMAM G-3 dendrimer both failed to enhance the solubility of the antimicrobial compound (Gardiner *et al.* 2008). These studies suggest that PAMAM dendrimers may increase the solubility of antimicrobial drugs but that this does not directly translate into an increased efficacy in the case of nadifloxacin. In the case of triclosan the PAMAM dendrimer did not enhance the solubility therefore this effect may be dependent on the physiochemical interactions.

One strategy for producing dendrimer biocides is to synthesise them with antimicrobial monomers or tailor the dendrimer to terminate in antimicrobial surface groups.A single antimicrobial dendrimer offers the benefits of desirable cost of manufacture and an acceptable toxicity and biocompatibility profile (McCarthy *et al.*

2005). A PPI dendrimer was functionalized with dimethyl dodecyl ammonium groups for potent antimicrobial properties(Chen *et al.* 1999). The quaternary ammonium functionalised dendrimer exhibited an EC_{50} of 12 µg/mL against *E. coli*, whilst its small molecule counterpart displayed a MIC_{50} of 2000 µg/mL. The quaternary ammonium functionalised dendrimer was also found to display antimicrobial activity against *S. aureus* at 1 µg/mL for inhibition and 10 µg/mL for bactericidal effect.

Chen *et al.*(2000) used bioluminescence studies to determine the structure-activity effects of the functionalised dendrimers and they discovered that the generation number (G) affected the antimicrobial activity, in the decreasing potency of G5 > G4 > G1 > G2 > G3. The increased potency of the higher generations was attributed to the dense surface functionalisation with quaternary amines, but there was a concurrent decrease in permeability into the bacterial cell probably owing to the molecular weight and diameter of the dendrimers. G5 was found to achieve the highest antimicrobial effect, with 64 quaternary amines at its surface and with a molecular weight of 27578 Da. G1 was the third most potent, possessing only 4 surface quaternary amines and having a molecular weight of 1593 Da. This suggests that the number of surface groups and molecular weight influences the biocidal activity of dendrimers. When the antimicrobial activity was compared to that of a hyperbranched linear polymer with the same number of functionalities, the dendrimer exhibited a higher antimicrobial activity (Chen *et al.* 2000).Yang and Lopina (2003) designed the PAMAM to be an antimicrobial agent itself rather than a carrier. The group covalently conjugated penicillin V to G-2.5- and G-3-PEG-PAMAM dendrimers via amide and ester linkages. The results of the study showed that the ester-linked

conjugates had antimicrobial activity against *S. aureus* but no synergistic or enhanced antimicrobial effect was observed when compared to non-conjugated penicillin V (Yang and Lopina, 2003).

2.1.4 Antimicrobial properties of native PAMAM dendrimers

PAMAM dendrimers are the most studied class of dendrimers, being the first dendrimer structures to be synthesized (Tomalia *et al.* 1985). Despite extensive study in biomedical applications such as drug delivery and imaging, PAMAM dendrimers' antimicrobial effects without conjugation or complexation to a conventional antimicrobial compound have only recently been discovered. Calabretta and co-workers were the first to publish a study on unmodified PAMAM dendrimers' antimicrobial properties against ocular pathogens and the authors found that the amine terminated G-5 PAMAM dendrimer was extremely toxic to *P.aeruginosa* with anEC_{50} of 1.5 ± 0.1 µg/mL and less so for *S. aureus,* 20.8 ± 3.4 µg/mL. It was demonstrated that a partial coating of the amine groups with poly(ethyleneglycol)(PEG) reduced the toxicity of the G5-PAMAM against human corneal epithelial cells whilst retaining high toxicity against *P. aeruginosa* with a MIC_{50} of 0.9 ± 0.1 µg/mL. PEGylation of the G-5 PAMAM resulted in a further decrease in efficacy against the Gram positive *S. aureus* (Calabretta *et al.* 2007).

The same group also published further data comparing the antimicrobial properties of G-3 PAMAM-NH_2 and G-5 PAMAM-NH_2 and reported that even though G-5 PAMAM-NH_2 has a greater localization of amines at its surface compared to G-3 PAMAM, the potency was not increased. A microdilution broth assay measuring the

absorbance to calculate the MIC_{50} of G-3 PAMAM and G-5 PAMAM against *S. aureus* was found to be 12.5 µg/mL for both generations. The equipotent result is surprising as G-5 PAMAM has 96 more amine groups at its surface, theoretically. Again the authors found that PEGylation of G-3 PAMAM decreased the potency against the Gram negative *P. aeruginosa* and more markedly against Gram positive *S. aureus.* This is likely due to the PEG chains shielding the protons of the amines therefore reducing the cationic charge and thus limiting the antimicrobial effect (Lopez *et al.* 2009).

An *in vitro* and *in vivo* investigation of PAMAM dendrimers was conducted by Wang and co-workers (Wang *et al.* 2010)**.** G-4 PAMAM-OH, G-4 PAMAM-NH_2, and G-3.5 PAMAM-COOH were challenged against *E. coli* to determine the MIC_{50} using the method outlined in Lopez *et al.* (2009). It was found that the *in vitro* $MIC_{50}$for G-4 PAMAM-OH, G-4 PAMAM-NH_2, and G-3.5 PAMAM-COOH was 5.4 mg/mL, 22.0 mg/mL and 3.8 µg/mL, respectively. The study investigated the effect of the PAMAM dendrimers on the morphology of *E. coli* and the effects on the cell membrane including the inner and outer membrane using scanning electron microscopy (SEM). Whilst the preparation process for SEM may induce artifacts, the PAMAM treated bacteria were compared to untreated bacteria that had undergone the same preparative process. It was shown that G-4 PAMAM-NH_2 and G-3.5 PAMAM-COOH caused inner and outer membrane damage leading to lysis of the *E. coli,* whilst G-4 PAMAM-OH caused permeabilisation of the inner and outer membrane. Further, the *in vivo* study showed that when G-4 PAMAM-OH was applied to the cervix of a guinea pig, the intra-amniotic infection caused by contamination with *E. coli* was inhibited. The

amniotic fluid collected from different gestational sacs of infected guinea pigs post G-4 PAMAM-OH treatment failed to culture *E. coli* due to the antimicrobial effects of the PAMAM *in vivo* (Wang *et al.* 2010). It has been postulated that PAMAM dendrimers may act like antimicrobial peptides (AMPs) in that they disrupt the cell membranes leading to cell lysis (Calabretta *et al.* 2007). The reduced activity against Gram positive bacteria may be due to the different membrane composition as Gram positive bacteria have a thick peptidoglycan cell wall and no outer-membrane compared to Gram negative bacteria that have a phospholipid bilayer outer membrane. The studies conducted within this chapter also confirm this hypothesis.

Whilst there have been many studies investigating dendrimers as carriers of antimicrobial compounds or covalently conjugated antibiotics to a dendrimer, there are comparatively few studies that have investigated the antimicrobial effects and the mechanism of action of unmodified PAMAM dendrimers. The aforementioned studies (Wang *et al*. 2010, Calabretta *et al.* 2007, and Lopez *et al.* 2009), mainly focused on Gram negative bacteria and all selected to test only one or two PAMAM generations. The studies have also used different methods for determining the IC_{50} and none have used the antimicrobial susceptibility standard method or media. By utilising a standardised method such as the clinical and laboratory standards institute (CLSI) M162standard (Rennie, 2001),comparisons can be made between inter and intra laboratory experiments when calculating antimicrobial susceptibilities. For example, media deficient in magnesium or calcium cations may result in a much lower IC_{50} that is an underestimate of the bacteria count as bacteria require divalent cations for membrane stabilization (Reller *et al.* 1974 and Zimelis and Jackson, 1973). There is a

knowledge gap with regards to the antimicrobial efficacy and mode of action of a range of PAMAM generations. To determine whether the antimicrobial efficacy is indeed generation and thus size and charge related, a comprehensive study is required. There have also been limited studies into challenging the PAMAM dendrimers against Gram positive bacteria such as *S. aureus* and *Staphylococcus epidermidis* which are known skin pathogens.

2.1.5 Aims and objectives

The aim was to fully investigate a range of PAMAM dendrimer generations including amine and carboxyl terminated dendrimers against Gram positive and Gram negative skin pathogens. The study was designed to illustrate any differences in antimicrobial potency for different generations and thus differences in molecular weights and surface charges. The investigation into the PAMAM dendrimers' antimicrobial properties were achieved by using an adapted microdilution broth test with a viable count assay modified from Calabretta *et al.* (2007). Morphological changes to the cell membrane and cell wall due to the PAMAM dendrimers' interaction was observed using SEM. A cell membrane integrity study was conducted for a range of skin pathogens. An inner membrane permeabilisation study was also employed to determine generation and concentration effects on the PAMAM dendrimers' membrane disruption potential. By characterising the dendrimers' affect against skin pathogens it is hoped that ultimately they can be formulated into a topical antimicrobial drug delivery system.

2.2 Materials and methods

2.2.1 Microdilution broth with viable count assay to determine inhibitory concentration (IC_{50})

Bacterial culture grade petri dishes, universals and pipette tips were all purchased from Startstedt (Leicester, UK). Bacterial growth medium, Mueller-Hinton agar (MHA) and Mueller-Hinton broth (MHB) were obtained from Oxoid (Basingstoke, UK). The bacterial media MHA/MHB is a standardised growth media used for antimicrobial susceptibility testing. The cation content (Mg^{2+} and Ca^{2+}) was adjusted in line with recommendations from the CLSI (Rennie, 2001). All salts used in diluents or media were reagent grade and purchased from Fisher Scientific (Loughborough, UK).

S. aureus (ATCC 11832) and *E. coli* (ATCC 8277) were plated out on respective cation adjusted MHA using a streak plate method to ensure growth of single colonies. The inoculated MHA plates were inverted and incubated at 37°C ± 1°C for 18-24 hours in aerobic conditions. After incubation, 3-4 single colonies were swabbed with a sterile loop and used to inoculate 10 ml of cation adjusted MHB which was then incubated at 37°C ± 1°C for 18 hours. The dense overnight inoculum was then diluted to an absorbance of 0.140 using a UV-Vis spectrophotometer (Hitachi, U1-900, Berkshire, UK) to achieve an inoculum density of ~10^7 cells/mL. The bacterial cell density at an optical density of 0.140 was confirmed by diluting the bacteria and counting the cells using a haemocytometer. The inoculum was then further diluted in cation adjusted MHB to achieve a test inoculum of $1x10^5$ cells/mL.

PAMAM dendrimers of various generations (G2-G5) purchased from Sigma Aldrich (Dorset, UK) in varying concentrations in methanol were prepared at concentrations ranging from 1-500 µg/mL in ultrapure sterile water. After dilution of the stock in ultrapure sterile water the methanol content of the highest concentration of PAMAM tested was 0.125 % (v/v). To ensure the low concentrations of methanol present did not inhibit the bacteria a range of methanol concentrations higher than those used within this assay was analysed for antimicrobial effect (data not shown). The results showed that a concentration of up to 30 % methanol (v/v) in sterile ultrapure water did not inhibit bacteria. Each PAMAM dendrimer concentration was tested in triplicate and 50 µl of each solution was plated onto a sterile 96-well plate. 50 µl of the test bacteria inoculum was added to each well excluding 3 wells with cation adjusted MHB and sterile water only as a sterility control. The inoculum and PAMAM test solution of each well were then agitated 5 times with a pipette to mix thoroughly. A growth control was tested in parallel without the addition of PAMAM dendrimer and a positive control was included of gentamicin at 1 mg/mL. The 96-well plate was then incubated at 37°C ± 1°C for 2 hours and shaken at 200 rpm.

After a 2 hour incubation period, each well (excluding sterility control) was serially diluted 1:10 in cation adjusted MHB to achieve a range of dilutions down to 1:100,000. Each well was further agitated using a sterile pipette tip and 50 µL of each dilution was plated onto a petri dish using the pour plate method with the addition of 25 mL of molten cation adjusted MHA at ~45°C. The plates were then inverted and incubated for 18-24 h at 37°C ± 1°C in aerobic conditions. Post incubation, bacterial colonies on each plate were manually counted using a click counter. The dilutions

where 30-300 colony forming units (CFUs) had grown for each growth control or PAMAM test concentration were selected. Each test concentration was tested in triplicate and the inhibition percentage was calculated using Equation 2.1. The data was then plotted as a graph of log (inhibitor) versus normalized response to determine the IC_{50} (Equation 2.2) using GraphPad Prism® version 5 (San Diego, USA).

$$Inhibition\ \ percentage\ \% = (100 - \left(\frac{treated\ count}{growth\ control\ count}\right) \times 100)$$

Equation 2.1 Inhibition percentage calculation

$$Y = \frac{100}{(1 + 10^{((LogIC50 - X) \times Hillslope)})}$$

Equation 2.2 Calculation of IC_{50}concentration

The log (dose) response curve follows a sigmoidal curve and the data was normalized to the growth control as 100 %. The normalized model forces the curve from 0 % to 100 %. This is ideal for the calculation of the IC_{50} *i.e*. the concentration at 50 % growth inhibition. This model also does not assume a standard hill slope of 1.0 but fits the hill slope from the data therefore it is a variable slope model that is ideal when there are many data points. The broth microdilution assays to calculate the IC_{50} concentrations were ran as *n*=9 therefore this model was ideal.

2.2.2 Membrane integrity study

S. aureus (ATCC 11832),*S. epidermidis* (ATCC 12228) *E. coli* (ATCC 8277) were plated out on tryptone soya agar (TSA) plates using a streak plate method to ensure growth of single colonies. The inoculated TSA plates were inverted and incubated at 37°C ± 1°C for 18-24 hours in aerobic conditions. After the incubation period 2-3 single colonies were removed using a sterile loop and used to inoculate tryptone soya broth (TSB). The inoculated TSB was then incubated for 18 h at 37°C ± 1°C. Post incubation period the inoculated TSB was then centrifuged at 1000 x *g* for 10 mins to harvest the bacterial cells. The pellet was resuspended in1x phosphate-buffered saline (PBS) (pH 7.4). This was centrifuged (as above) and the supernatant discarded. The pellet was washed and resuspended in PBS and the absorbance was adjusted to 0.7 at 420 nm to dilute the cells to a final test suspension. A 3 mL aliquot of the final bacterial inoculum was added to a 3mL aliquot of the PAMAM dendrimer solution at a concentration of 10 x the calculated IC_{50} for each respective PAMAM dendrimer generation. The IC_{50} for PAMAM G=3 was calculated as 15.25µg/mL and this concentration was used to determine whether the PAMAM dendrimer could incite membrane damage.

At different time points (20, 40, 60, and 120 min) a 1.5 mL aliquot of the sample was removed and immediately syringe filtered using a 0.22 µm syringe filter (Millipore MCE sterile 33 mm filter, Watford, UK). Filtration removed the bacteria leaving a particulate free supernatant to be analysed for the release of materials absorbing at 260 nm that was assessed with a UV spectrometer (Hitachi, U1-900, Berkshire, UK).

The absorbance at 260 nm was plotted against each time point using GraphPad Prism® version 5 (San Diego, USA).

2.2.3 Inner membrane permeabilisation assay

Inner membrane permeabilisation was determined by the release of cytoplasmic β-galactosidase from *E. coli* into the culture medium. *E. coli* was cultured, harvested, and washed (as outlined previously) but re-suspended in 0.5 % NaCl as opposed to PBS (pH 7.4). *E. coli* was re-suspended at an absorbance of 0.6 at 420 nm and 100 µl of the test inoculum was transferred into each well of a 96-well plate. To each well 100 µl of PAMAM dendrimer (generation 2, 3, 3.5, 4 and 5 at concentrations of 0.1, 1, 5, 10, 25 and 50 µg/mL were added. Also 10 µl of a 30 mM *ortho*-nitrophenyl-β-galactoside (ONPG) (Sigma - Dorset, UK) solution was added to each well. A blank of *E. coli* with ONPG without PAMAM dendrimer was used as a negative control and a vehicle control was also run in parallel.

The production of *O*-nitrophenol was measured every 2 minutes for 12 minutes by monitoring the absorbance at 420 nm in a microplate reader (Biotek, Northstar, Bedfordshire, UK). The optimal time points and duration were determined by a preliminary assay. The study was repeated 3 times independently and the mean result including standard deviation of absorbance at 420nm was plotted against the different time points using GraphPad Prism® version 5 (San Diego, USA). Figure 2.1 illustrates the hydrolysis of ONPG by β-galactosidase found within the E. coli cytoplasm to form *ortho*-nitrophenol once the inner membrane has been permeabilised.

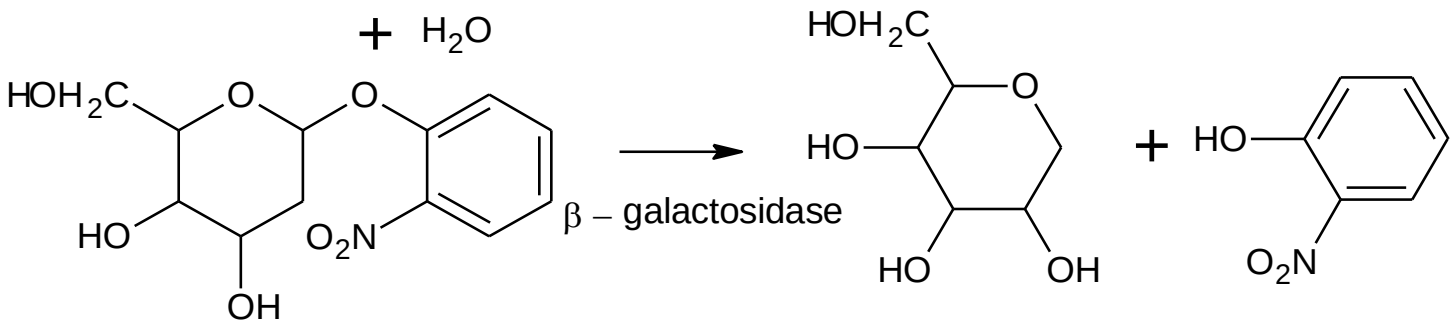

o - nitrophenyl - β - galactosidase
(colourless substrate)

β – galactose

o – nitrophenol
(yellow in colour)

Figure 2.1. A reaction schematic showing the formation of O- nitrophenol. *The scheme illustrates the hydrolysis of O-nitrophenyl-β-galactoside by cytoplasmic β-galactosidase into O- nitrophenol. The activity of β-galactosidase can be monitored by measuring the presence of the yellow compound O- nitrophenol at 420 nm using a spectrophotometer.*

2.2.4 Scanning electron microscopy

S. aureus (ATCC 11832) and *E. coli* (ATCC8277) were cultured, harvested and washed (as outlined above). The inoculum however was not resuspended at a lower density, instead an overnight culture of ~10^8 cells/mL was used for the study to ensure that bacterial cells were at a high enough density after the washes involved in electron microscopy preparation methods. A 200 µl aliquot of a range of concentrations of dendrimer from 1-200 µg/mL for G2, G3 and G4-PAMAM-NH_2 and 0.0025-12.5 µg/mL for G5-PAMAM-NH_2were constituted. For G3.5-PAMAM-COOH dendrimer the concentration range of solutions made were between 1-250 µg/mL. The PAMAM dendrimer solutions (200 µl) were added to 200 µl of the bacterial inoculum and

incubated at 37°C ± 1°C for 2 hours and shaken at 200 rpm. After the incubation period the bacteria were centrifuged at 10,000 x *g* for 10 mins, resuspended in PBS (pH 7.4), centrifuged as above and the supernatant discarded. This was repeated 3 times to wash the harvested bacteria. The bacteria were then fixed in 2.5 % glutaraldehyde in 0.1 M sodium cacodylate buffer (pH 7.4 containing 2mM $CaCl_2$) for 2 hours on a low speed rotator.

Fixative was washed from the bacteria (as described above) in sodium cacodylate buffer (pH 7.4 containing 2mM $CaCl_2$) 3 times. A 100 µl aliquot of each fixed sample was added to a poly-*L*-lysine coated cover slip. Various substrates were tested including scanning electron microscopy filters (Millipore, Watford, UK) and pelleted bacteria in sterile 1.5 mL tubes, but it was found that poly-*L*-lysine cover slips retained the bacteria most effectively. The bacteria on the poly-*L*-lysine coated cover slips were then post-fixed in a solution of 1 % osmium tetroxide in sodium cacodylate buffer. After a 1 hour contact time the osmium tetroxide was removed by washing the cover slips in sodium cacodylate buffer (pH 7.4 containing 2 mM $CaCl_2$). The cover slips were then submerged in 70 % ethanol and dehydrated at 4ºC for 6 days.

The samples were then further dehydrated for ten minutes each in 80 %, 90 % and 100 % ethanol. To remove the solvent from the samples they were critical-point dried to replace the 100 % ethanol with liquid CO_2 under pressure. This was repeated 3 times to ensure all of the ethanol had been displaced from the samples. The liquid CO_2 was subsequently removed by increasing the temperature to 40ºC and the pressure until the CO_2 vaporised. Samples were securedto a scanning electron microscope (SEM) stub mount using double-sided carbon tape. Samples were

carefully pressed down on to the stub to ensure efficient conductivity. Each sample was sputtered with gold to ensure an even coating and the samples were then placed in the high resolution (1.5 nm) field emission SEM (Hitachi, S4500).

2.2.5 Statistical analysis of results

All results within this section are reported as the mean ± SEM (standard error of the mean). All inner membrane permeabilisation data passed the D'Agostino and Pearson normality test ($\alpha = 0.05$) using GraphPad Prism® version 5 (San Diego, USA).The data obtained within the inner membrane permeabilisation assay was analysed using a nested mixed model analysis in SPSS® version 19 IBM corp®(Armonk, NY). The fixed effects were Time within concentration within dendrimer, dendrimer and then concentration within dendrimer. Firstly the analysis was applied to the four different generations of PAMAM dendrimer to establish any significant differences between the inner membrane permeabilisation of *E. coli* between the four tested PAMAM dendrimer generations. Then a least significant difference (LSD) posttest was utilised to establish pairwise comparisons between the PAMAM dendrimer generations. The output of the nested mixed model analysis also included the mean absorbance for each concentration across all time points and the corresponding 95 % confidence intervals. For the data displayed in Figure 2.8 a single final time point of 60 minutes was chosen therefore a two-way ANOVA with a Benferroni posttest was used to compare the two variables of dendrimer generation and dendrimer concentration at that specific time point.

2.3 Results

2.3.1 Microdilution broth with viable count assay to determine the inhibitory concentration (IC_{50}).

The antimicrobial activity of PAMAM dendrimers was evaluated against *S. aureus* and *E. coli*. The inhibitory effect of PAMAM dendrimers was determined by calculating the IC_{50} against Gram positive and Gram negative bacteria (Table 2.1). All of the PAMAM-NH_2 dendrimers tested inhibited both strains of bacteria at low concentrations (<27 µg/mL). Figure 2.2illustrates the percentage inhibition of *S. aureus* against 4 generations of PAMAM-NH_2 dendrimers at various dendrimer concentrations. The inhibition curves illustrated in Figure 2.2 were used to calculate the IC_{50} values (Figure 2.3). The IC_{50} values and physicochemical characteristics of PAMAM dendrimers that may be related to their antimicrobial activity are shown in Table 2.1. In order to inhibit 50 % of the *S. aureus,*G2-PAMAM-NH_2 dendrimer required >9 times the concentration that was required for G5-PAMAM-NH_2. With increasing PAMAM generation the concentration required to inhibit 50 % of *S. aureus* decreases dramatically (Figure 2.2 and Table 2.1). For the lowest concentrations of G2-PAMAM-NH_2 and G5-PAMAM-NH_2 tested, bacterial growth as opposed to inhibition was observed when compared to the untreated growth control.

Table 2.1: Calculated IC_{50} (µg/mL) with 95 % confidence intervals against *S. aureus* and *E. coli* including physicochemical characteristics of PAMAM dendrimer that determines their antimicrobial ability.

Bacteria	PAMAM generation	Molecular weight Da	No. of amine surface groups	IC_{50} (95 % CI) µg/mL
S. aureus	G2-PAMAM-NH2	3,256	16	26.77 (22.58-31.75)
	G3-PAMAM-NH2	6,909	32	9.374 (7.88- 11.15)
	G4-PAMAM-NH2	14,215	64	5.962 (5.375-6.614)
	G5-PAMAM-NH2	28,826	128	2.881 (2.473-3.355)
	G3.5-PAMAM-COOH	12,927	64	> 250
E. coli				
	G3-PAMAM-NH2	6,909	32	4.931 (4.28- 5.679)
	G3.5-PAMAM-COOH	12,927	64	>1000

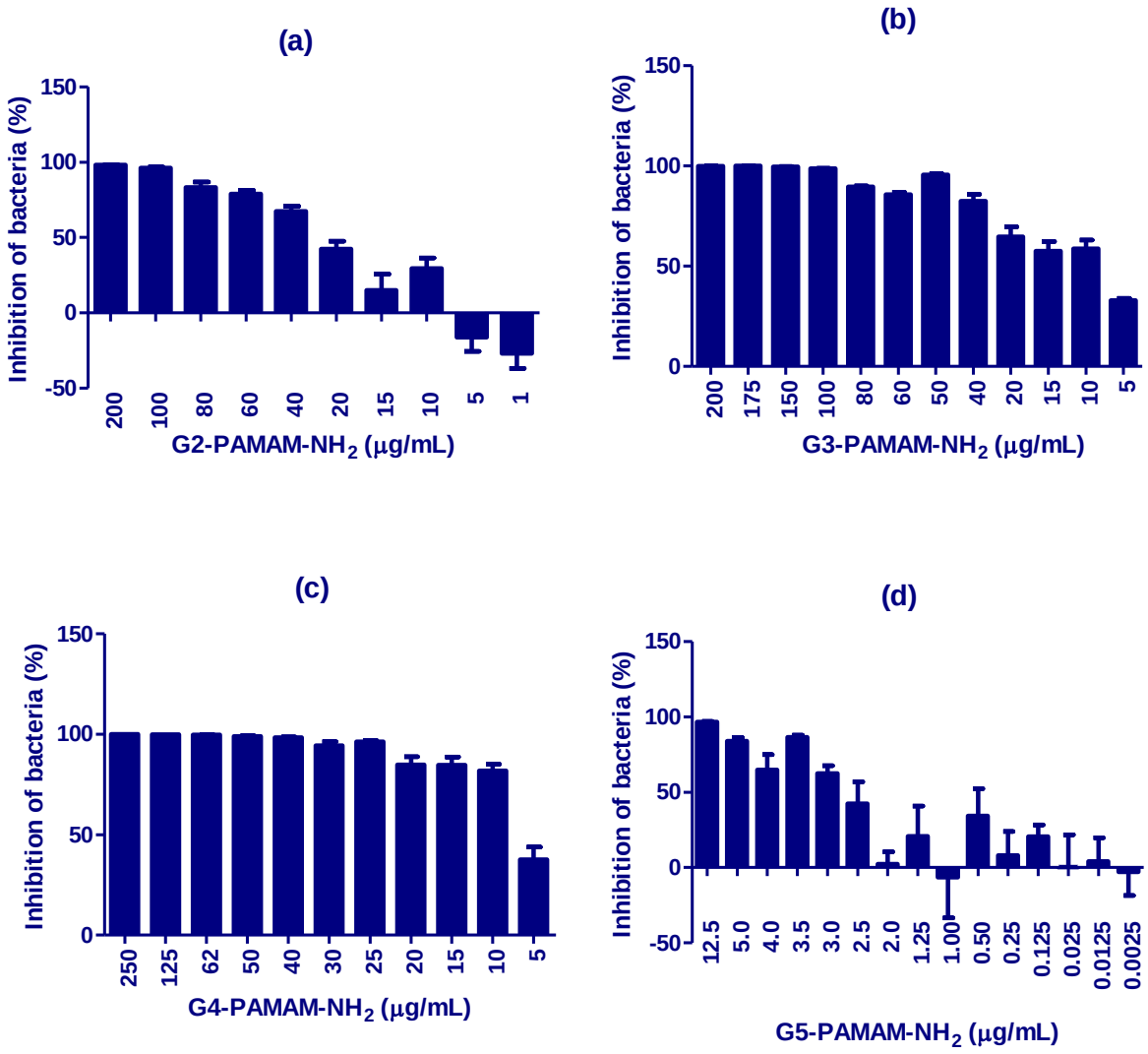

Figure 2.2 Inhibition of *S. aureus* against decreasing concentrations of PAMAM dendrimer (µg/mL). *(a) Corresponds to G2-PAMAM-NH_2 (b) G3-PAMAM-NH_2 (c) G4-PAMAM-NH_2 and (d) G5-PAMAM-NH_2. Results shown are the mean ± SEM (n=9).*

Figure 2.3 shows the IC_{50} (µg/mL) against *S. aureus* plotted against the number of surface amine groups on the corresponding PAMAM-NH_2 dendrimer. The IC_{50} (µg/mL) against *S. aureus* decreased with increasing numbers of surface amine groups on the PAMAM dendrimer. An inhibition curve was added to the graph showing an R^2 value of 0.9747. This trend related to the exponential increase in molecular weight and the number of amine surface groups with increasing PAMAM generation.

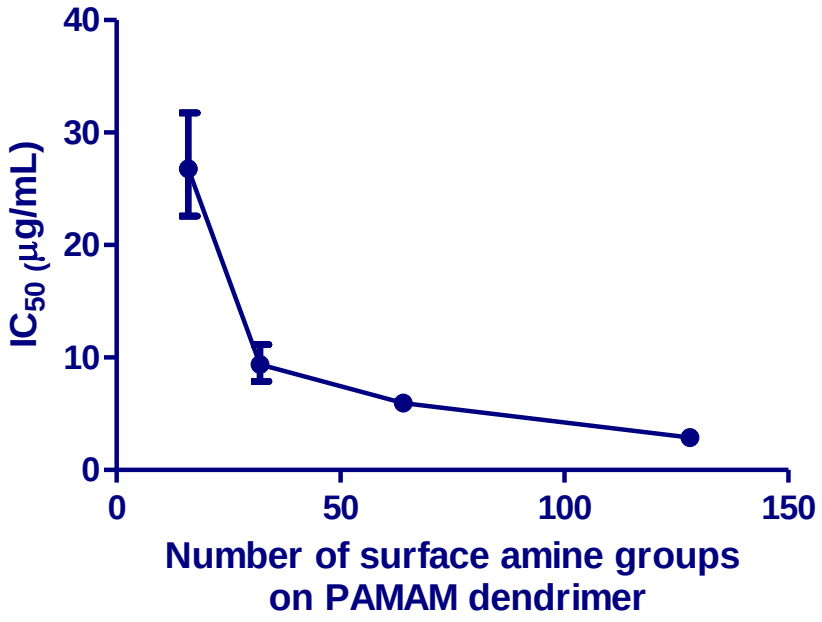

Figure 2.3.Graph illustrating the calculated IC_{50} (µg/mL) concentrations.*IC_{50} (µg/mL)with error bars representing 95% confidence intervals against* S. aureus *plotted against the theoretical number of surface amine groups corresponding to G2-PAMAM-NH_2, G3-PAMAM-NH_2, G4-PAMAM-NH_2 and G5-PAMAM-NH_2 dendrimers.*

The inhibitory concentrations for G3-PAMAM-NH_2 against *E. coli* were also determined (Table 1 and Figure 2.4). The IC_{50} required to inhibit 50 % of the *S. aureus*

was ~2 fold higher than the concentration required to inhibit 50 % of the *E. coli*. The G3-PAMAM-NH_2 antimicrobial activity suggests that it is much more effective against Gram negative bacteria than Gram positive bacteria in agreement with a previous paper (Calabretta *et al.* 2007).

The antimicrobial activity of G3.5-PAMAM-COOH was also determined for each bacteria, up to a concentration of 1000 µg/mL Figure 5 (a-b). When challenged with *S. aureus* the carboxyl-terminated dendrimer inhibited the bacteria but the IC_{50} could not be calculated. The inhibition varied from 10 % up to 40 % depending on the G3.5-PAMAM-COOH concentration; the results produced were highly variable. The results indicate that, to achieve an IC_{50} against *S. aureus* the concentration of G3.5-PAMAM-COOH would have to be in excess of 250 µg/mL. Figure 5 (b) shows the inhibition curve of G3.5-PAMAM-COOH challenged against *E. coli.*

At all concentrations tested the treated bacteria demonstrated growth as opposed to inhibition when compared to the untreated control. It is for this reason that the IC_{50} for G3.5-PAMAM-COOH challenged against *E. coli* could not be calculated as it exceeds the highest concentration tested,1mg/mL.

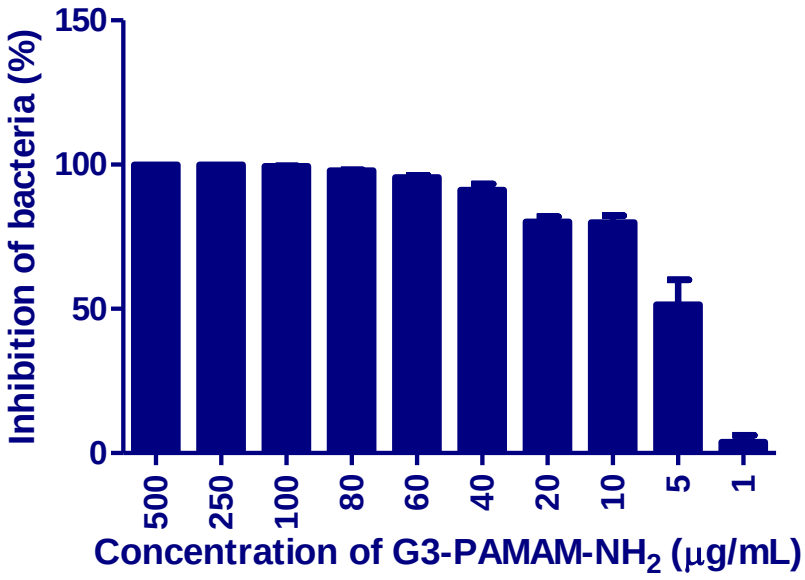

Figure 2.4.Inhibition of *E. coli* challenged against decreasing concentrations of G3-PAMAM-NH_2 dendrimer (μg/mL). *Results shown are the mean ± SEM (n=9).*

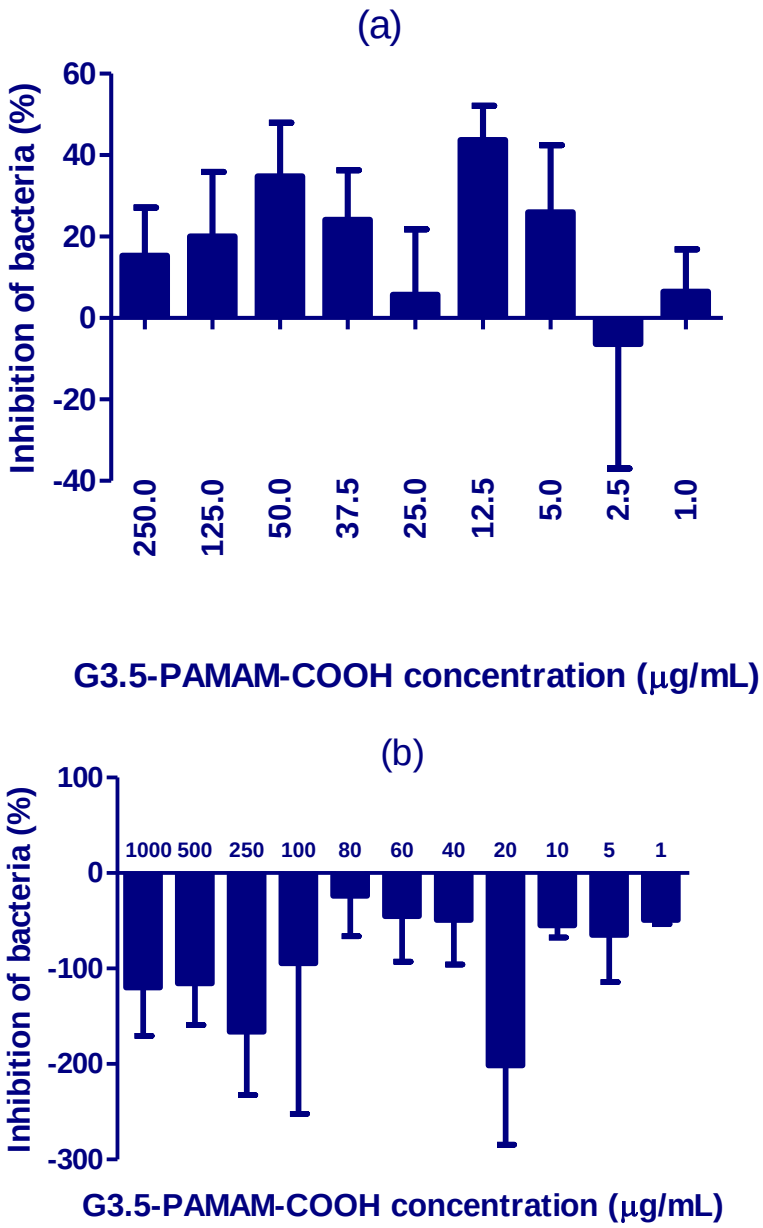

Figure 2.5.Inhibition of G3.5-PAMAM-COOH dendrimer (µg/mL) against *S. aureus* and *E. coli.* *(a) S. aureus against decreasing concentrations of G3.5-PAMAM-COOH dendrimer (µg/mL). Results shown are the mean ± SEM (n=9) as a consequence of three independent experiments. (b) E. coli challenged against decreasing concentrations of G3.5-PAMAM-COOH dendrimer (µg/mL). Results shown are the mean ± SEM (n=3).*

2.3.2 Membrane integrity study

The release of intracellular nuclear material was measured for two Gram-positive staphylococcal species including the resident skin microbe, *S. epidermidis* and the Gram negative gut microbe, *E. coli* after being challenged with 5 times the calculated IC_{50} of G3-PAMAM-NH_2 dendrimer. For all three bacterial strains, the absorbance at 260 nm increased with time with a plateau at 80 minutes for *S. aureus* (Figure 2.6 (a)) and 100 minutes for both *S. epidermidis* (Figure 2.6 (b)) and *E. coli* (Figure 2.6 (c)) respectively. The absorbance increase for *S. aureus* showed a sigmoidal relationship when plotted against time whereas with the absorbance for *S. epidermidis* increased monotonically up to a plateau at 100 minutes. *E. coli* showed a dramatic increase in absorbance over the first 60 minutes, a slight decrease in absorbance at 80 minutes but increased to the highest absorbance reading taken across all stains tested at 100 minutes.

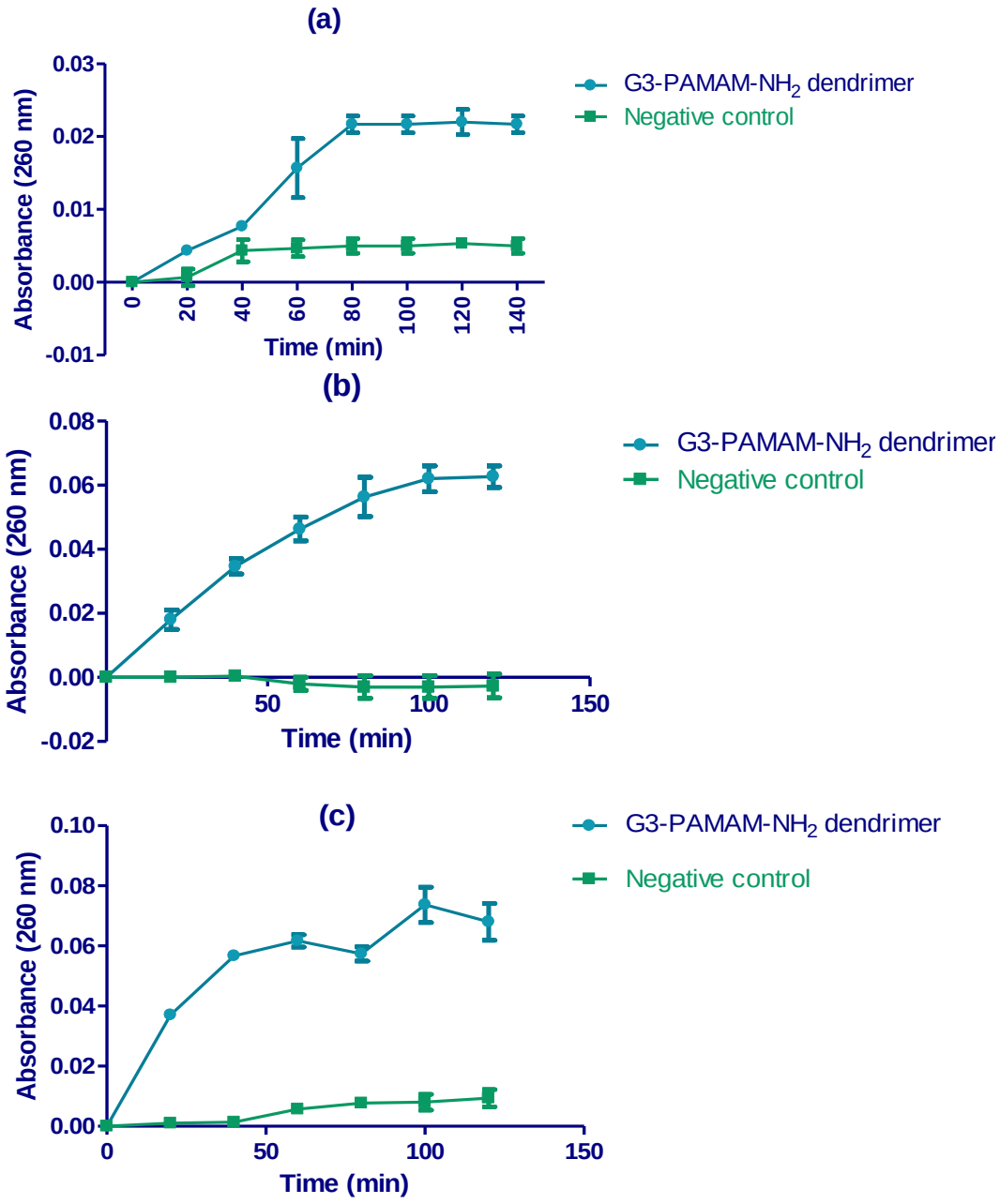

Figure 2.6.Graphs illustrating the release of nuclear material from *S.aureus, S. epidermidis* and *E. Coli*. *(a) Absorbance at 260 nm plotted against time for S. aureus challenged against G=3 x 5 IC_{50}. (b) Absorbance at 260 nm plotted against time for S. epidermidis challenged against G=3 x 5 IC_{50}. (c) Absorbance at 260 nm plotted against time for E. coli challenged against G=3 x 5 IC_{50}. All results are displayed as (n=3) mean ± standard deviation. Negative control was the absorbance at 260 nm for the untreated bacteria group.*

2.3.3 Inner membrane permeabilisation assay

The inner membrane integrity of *E. coli* was determined chromogenically. *E. coli* contains the enzyme β-galactosidase within the cytoplasm of the cell; if the integrity of the inner membrane is compromised the β-galactosidase would be released from the cytoplasm into the culture medium where it would hydrolyse the substrate β-galactosidase (ONPG) into *O*- nitrophenol (Figure 2.1). The *E. coli* was added to wells containing the chromogenic substrate ONPG and various concentrations of PAMAM dendrimer. The production of *O*- nitrophenol was determined by measuring the change in absorbance at 420 nm over time (Je and Kim, 2006). Due to the possibility of substrate depletion, the measurements were taken within the first 12 minutes of PAMAM-bacteria contact (Silvestro *et al.* 2000). It was found that the absorbance reached a plateau at around 20 minutes (data not shown).

A mixed model analysis of the data presented in Figure 2.7 illustrated a significant difference in the inner membrane of permeabilisation of *E. coli* overall between all four PAMAM-NH_2dendrimers tested (F=79.8 (3, 1708) p<0.001). The mean absorbance at 420 nm for G2-PAMAM-NH_2, G3-PAMAM-NH_2, G4-PAMAM-NH_2, and G5-PAMAM-NH_2 was 0.222 (95 % CI: 0.221-0.224) 0.228 (95 % CI: 0.227-0.230), 0.228 (95 % CI: 0.226-0.229) and 0.214 (95 % CI: 0.213-0.216) respectively. An *ad hoc* LSD test (pairwise comparisons of absorbance) revealed that there was a significant difference in absorbance and thus inner membrane permeability between all PAMAM dendrimers tested (df 1708, p<0.001) with the exception of G3-PAMAM-NH_2

when compared to G4-PAMAM-NH_2 in which no statistical significance was observed between the two.

For G2-PAMAM-NH_2 both concentration and time had an effect of the absorbance at 420 nm and thus the inner membrane permeability of *E. coli.* Time had a significant effect on the absorbance at 420 nm for all concentrations (df 427, for 1 µg/mL $p<0.05$ for concentrations 5-50 µg/mL $p<0.001$) with the exception of the vehicle control containing no PAMAM dendrimer and the lowest concentration tested, 0.1 µg/mL. A pairwise comparison of the absorbance for each concentration of G2-PAMAM-NH_2 dendrimer found that all concentrations were statistically different form the vehicle control (df 427, $p<0.001$) with the exception of 1 µg/mL. Further, all concentrations were different from each other (df 427, $p<0.001$). Interestingly, 0.1 µg/mL was significantly different from vehicle control but 1 µg/mL was not. This was because the mean absorbance of the vehicle control was 0.174 (95 % CI: 0.170-0.178) however the mean absorbance for 0.1 µg/mL G3-PAMAM-NH_2 dendrimer was much lower at 0.165 (95 % CI: 0.161-0.169). This trend of the vehicle control having a higher absorbance than 0.1 µg/mL of PAMAM dendrimer was observed across all generations tested.

For G3-PAMAM-NH_2 dendrimer again time and concentration had a significant effect on the absorbance at 420 nm. Time had a significant effect on the absorbance at all concentrations (df 427, $p<0.05$ for a concentration of 1 µg/mL and $p<0.001$for concentrations 5-50 µg/mL) with the exception of the vehicle control and again the lowest concentration of the G3-PAMAM-NH_2 dendrimer tested- 0.1 µg/mL. All G3-PAMAM-NH_2 concentrations were statistically different from one another and the

vehicle control (df 427, p<0.001) with the only exception being again, 1 µg/mL when compared to the vehicle control. For G4-PAMAM-NH_2 dendrimer, time had a significant effect (df 427, p<0.001) on concentrations 5-50 µg/mL only and not at the lower concentrations or the vehicle control. When comparing the concentration effects for G4-PAMAM-NH_2 dendrimer on the absorbance, all concentrations were significantly different from one another (df 427, p<0.001) with the exception of the vehicle control, 0.1 and 1 µg/mL when compared to each other. For the G5-PAMAM-NH_2 dendrimer time had a significant effect on the absorbance at all concentrations (df 427, p<0.05 for 1 µg/mL and p<0.001 for 5-50 µg/mL) with the exception of the vehicle control and the lowest concentration of 0.1 µg/mL.

After comparing the absorbance of all concentrations against each other and the vehicle control there was a definite concentration dependency on the inner membrane permeabilisation (df 427, p<0.05 when the vehicle control was compared to 1 µg/mL and p<0.001 for all other concentrations). The only exception was when the absorbance for the concentrations 0.1 and 1.0 µg/mL of G5-PAMAM-NH_2 dendrimer was compared where no statistical difference was observed.

The inner membrane permeabilisation and thus production of*O*-nitrophenol, increased with increasing concentrations of the PAMAM dendrimer and with time (Figure 2.7). For all four PAMAM-NH_2 dendrimer generations tested, a concentration as low as 5 µg/mL exhibited permeabilisation of the inner membrane at 12 minutes (Figure 2.7). The production of *O*-nitrophenol was significantly different (p<0.001) across the four PAMAM generations tested. The highest concentration tested (50 µg/mL) demonstrated the highest increase in absorbance therefore inducing the

highest degree of inner membrane permeabilisation. The exception to this was the G5-PAMAM-NH_2 dendrimer. At a particular time point of 4-10 minutes, 25 µg/mL solution of G5-PAMAM-NH_2 dendrimer showed a higher absorbance at 420 nm and thus *O*- nitrophenol production than at a 50 µg/mL concentration. G5-PAMAM-NH_2 dendrimer also demonstrated a longer lag period for absorbance increase at 420 nm.

The trend observed, with respect to decreasing absorbance (based on the mean across all time points for a specific concentration) was G2>G3>G5>G4 for PAMAM concentrations of 5 µg/mL. At a higher dendrimer concentration of 50 µg/mL the absorbance measurement trend in decreasing order was G3>G4>G2>G5. A measurement was taken at 60 minutes to determine a final measurement of*O*-nitrophenol production (Figure 2.8).A two-way ANOVA with a Bonferroni post-test was used to investigate the relationship between dendrimer generation and concentration in *O*-nitrophenol production at a 60 minute time point. There was a significant difference between the absorbance at 60 minutes for each dendrimer generation tested (F=460.8, df 4,p<0.001) and also between the different concentrations tested (F=1133, df 5,p<0.001). A Bonferroni posttest compared the different PAMAM dendrimer generations at different concentrations. It was established that even after 60 minutes there was no change in absorbance was observed for concentrations below 5 µg/mL (p>0.05). There was significant difference in absorbance when comparing all concentrations of each PAMAM generation to the vehicle control (p<0.001) with the exception of 0.1 and 1 µg/mL of PAMAM dendrimer. When the different PAMAM dendrimer generations were compared at various

concentrations there was no observed difference between generation 3 and generation 5 dendrimer at all concentrations.

A generation effect was also confirmed when comparing the absorbance at 420 nm of various PAMAM dendrimer generations over 12 minutes (Figure 2.9). At a dendrimer concentration of 10 µg/mL, the absorbance increase is very similar across all generations tested with the exception of G5-PAMAM-NH_2 showing a lag phase over the first 8 minutes of the assay (Figure 2.9 (a)). At the higher concentration of 50 µg/mL (Figure 2.9 (b)) the absorbance reading was spread and the lag time of G5-PAMAM-NH_2 was more pronounced.

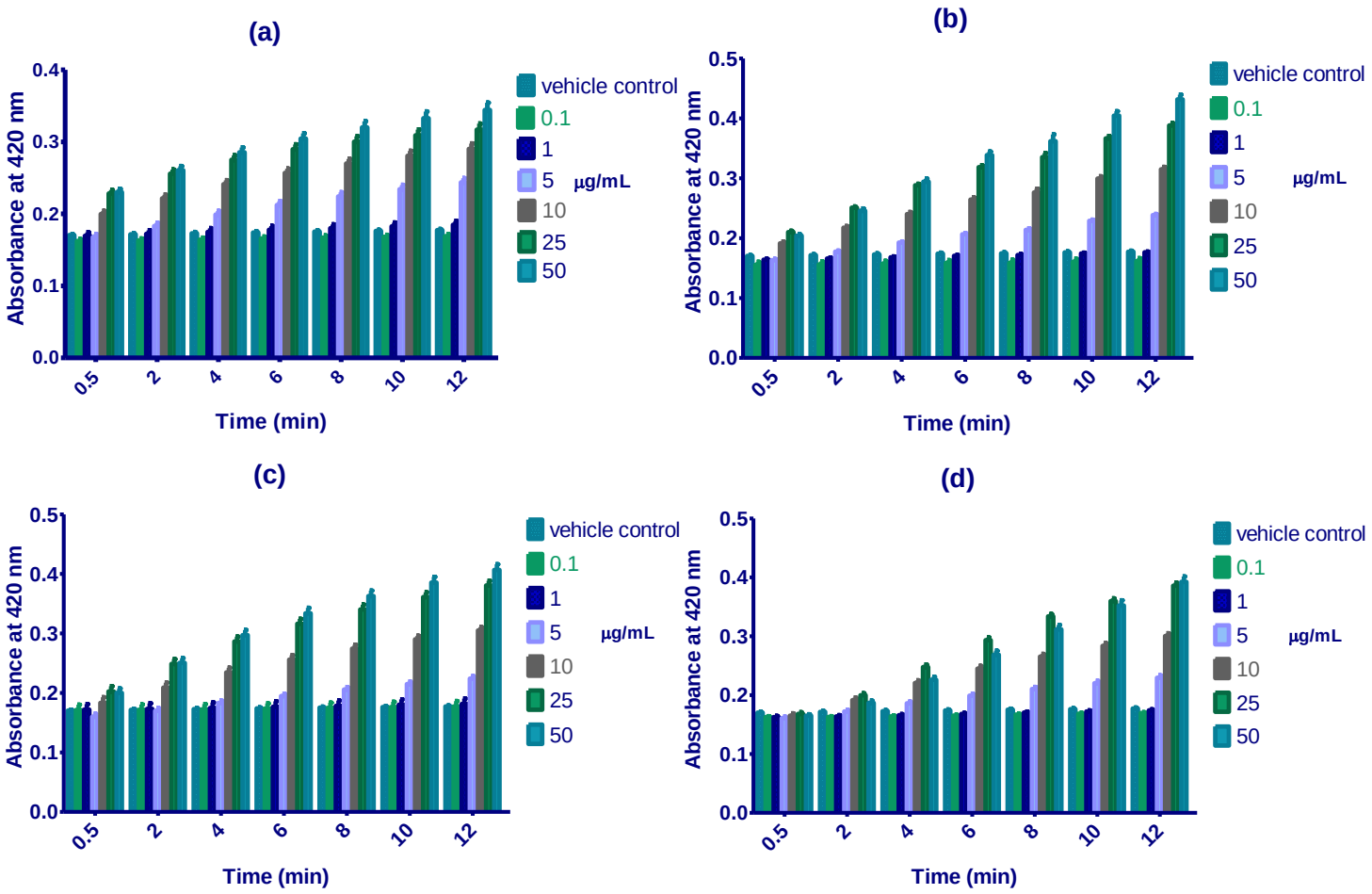

Figure 2.7.Graphs illustrating the relationship between concentration, time and dendrimer generation on the inner membrane permeabilisation of *E. coli*. *Absorbance at 420 nm plotted against time in minutes for a range of dendrimer concentrations (0.1- 50 µg/mL). (a) corresponds to G2-PAMAM-NH_2 treated E. coli, (b) G3-PAMAM-NH_2 treated E. coli, (c) G4-PAMAM-NH_2 treated E. coli and (d) G5-PAMAM-NH_2 treated E. coli. Vehicle control is displayed as the untreated control group. All results shown represent the mean ± SEM (n=9) as a result of 3 independent experiments.*

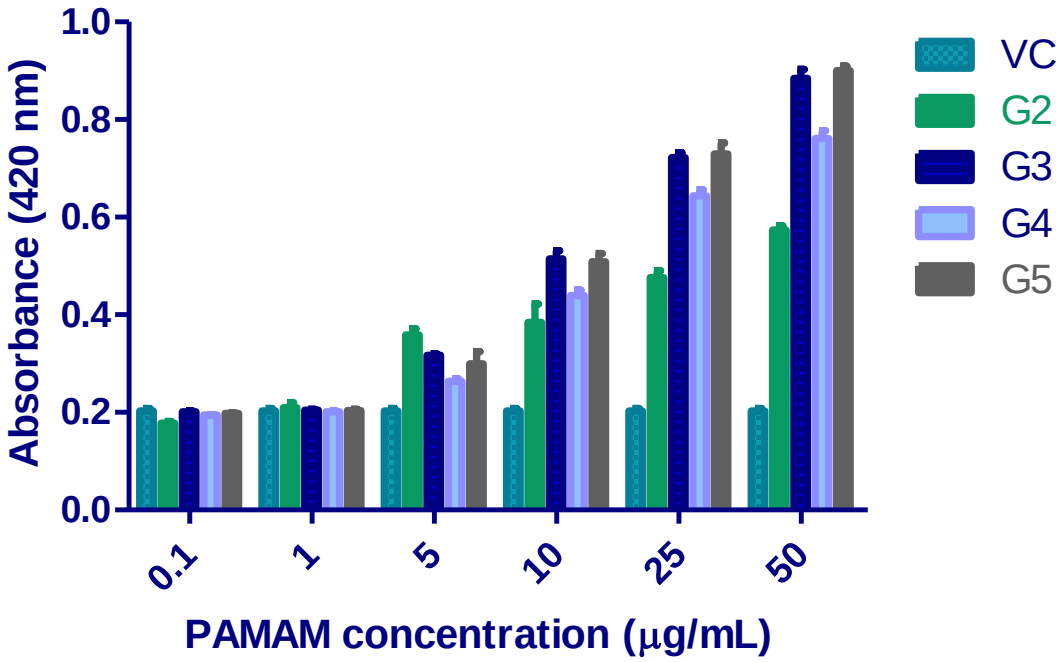

Figure 2.8. Graph illustrating the inner membrane permeabilisation of *E.* coli at 60 minutes for a range of dendrimer concentrations.*Absorbance at 420 nm plotted against a range of dendrimer concentrations (0.1- 50 µg/mL) at 60 minutes. G2 corresponds to G2-PAMAM-NH_2 treated E. coli, G3 G3-PAMAM-NH_2 treated E. coli, G4-PAMAM-NH_2 treated E. coli and (c) G5-PAMAM-NH_2 treated E. coli. VC corresponds to the vehicle control and is displayed as the untreated bacteria group control. All results shown represent the mean ± SEM (n=3).*

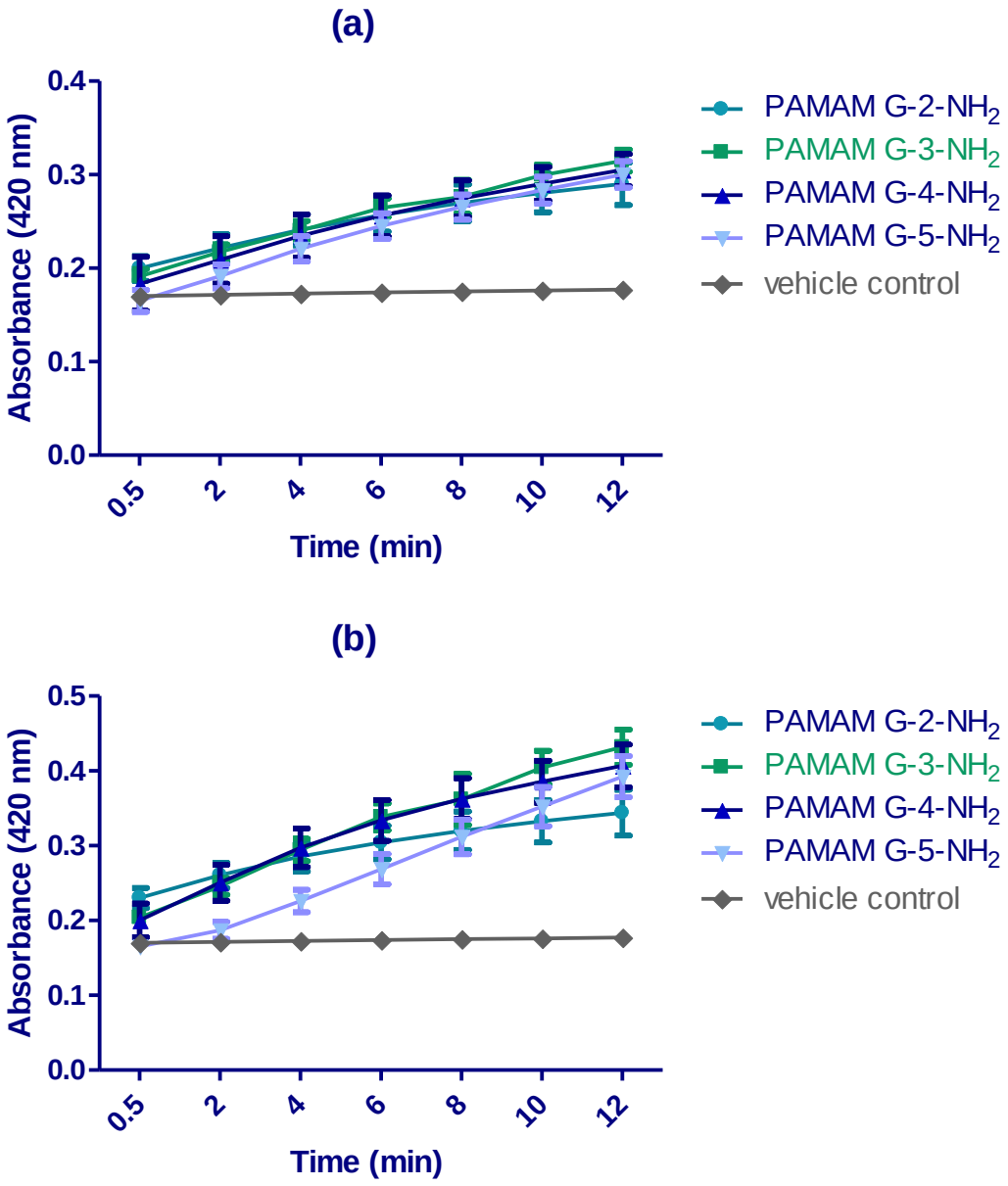

Figure 2.9.Graphs illustrating the effect of dendrimer generation and time at specific concentrations on the inner membrane permeabilisation of *E. coli.* *Absorbance at 420 nm plotted against time in minutes, (a) corresponds to each PAMAM generation at a concentration of 10 µg/mL challenged against E. coli, and (b) PAMAM generations at a concentration of 50 µg/mL challenged against E. coli. VC corresponds to the vehicle control and was displayed as the untreated bacteria group control. All results shown represent the mean ± SEM (n=9) as 3 independent experiments were conducted.*

2.3.4 Scanning electron microscopy

The SEM images (Figure 2.10) highlight the membrane effects of PAMAM dendrimers particularly with regards to the cocci-shaped *S. aureus*. Figure 2.10 (a-b) shows that there was cytoplasmic debris around the untreated control however this may have been a result of the SEM preparation process. When compared to the G3-PAMAM-NH_2 at a concentration of 5 times theIC_{50} (µg/mL) varying degrees of membrane damage was observed from minor blebbing through to total destruction of the cell membrane (Figure 2.10 (c-d)). This was also found to be the case with G2-PAMAM-NH_2 (Figure 2.10 (e-f)) and G5-PAMAM-NH_2 (Figure 2.10 (g-h)). The SEM images demonstrate the ability for G2-PAMAM-NH_2 and G5-PAMAM-NH_2 to cause severe bacterial cell membrane damage including blebbing of cytoplasmic contents from damaged cell membrane and complete cell lysis. Sheets of bacterial cell wall and cytoplasmic content debris can be observed in the PAMAM treated bacteria images (Figure 2.10 (a-h)). For G3.5-PAMAM-COOH at a concentration of 1 mg/mL (Figure 2.10(i-j)) there is no difference in bacterial cell morphology or changes to the integrity of the bacterial cell membrane when compared to the untreated *S. aureus* group. The damage to the *S. aureus* cell membrane and thus leakage of cytoplasmic contents observed in the collected SEM images further supports the results determined in the membrane integrity study see Section 2.3.2.

SEM images were also collected for the Gram negative, bacillus-shaped *E. coli* bacteria. Figure 2.11 (a-b) shows the intact PAMAM untreated group micrographs. Figure 2.11 (c-d) illustrates the G3-PAMAM-NH_2 treated group. Damage to the bacterial wall and cell membranes can be observed due to leakage and blebbing and

leakage of the cytoplasmic contents from the cell. The PAMAM dendrimer typically targeted the polar regions of the *E. coli* rods; this effect can also be observed elsewhere (Wang *et al.* 2010). Again, no changes in cell morphology were observed for the G3.5-PAMAM-COOH at a concentration of 1 mg/mL. The damage caused by the G3-PAMAM-NH_2 dendrimer to the *E. coli* is consistent with the results of the membrane integrity study in Sections 2.3.2 and the inner membrane permeabilisation results in 2.2.3.

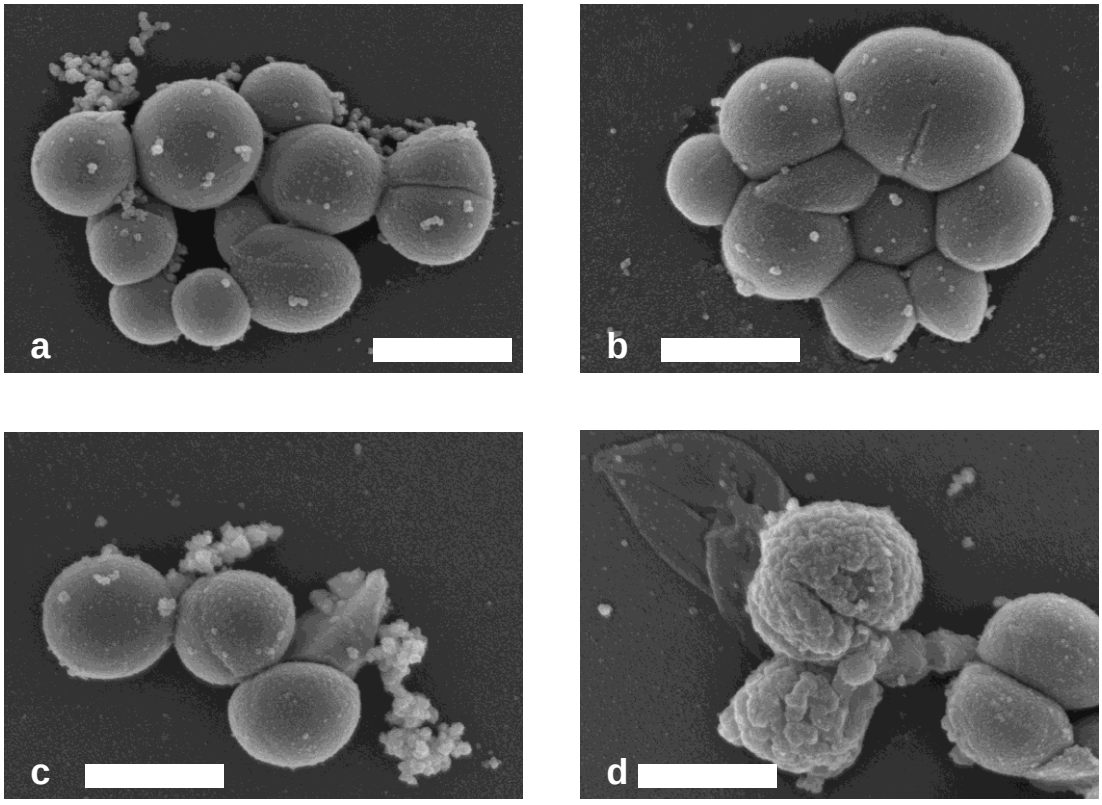

Figure 2.10.Scanning electron micrographs of *S. aureus* challenged with PAMAM dendrimer. *(a) Represents untreated S. aureus at a magnification of x25k, scale bar represents 1.2 µm. (b) illustrates untreated S. aureus at a magnification of x30k, scale bar represents 1 µm. (c) S. aureus treated with G3-PAMAM-NH2 at a concentration of 5x calculated IC_{50} from section 2.3.1. magnification x30k and scale bar represents 1 µm. (d) S. aureus treated with G3-PAMAM-NH_2 at a concentration of 5x calculated IC_{50} from section 2.3.1. magnification x30k and scale bar represents 1 µm.*

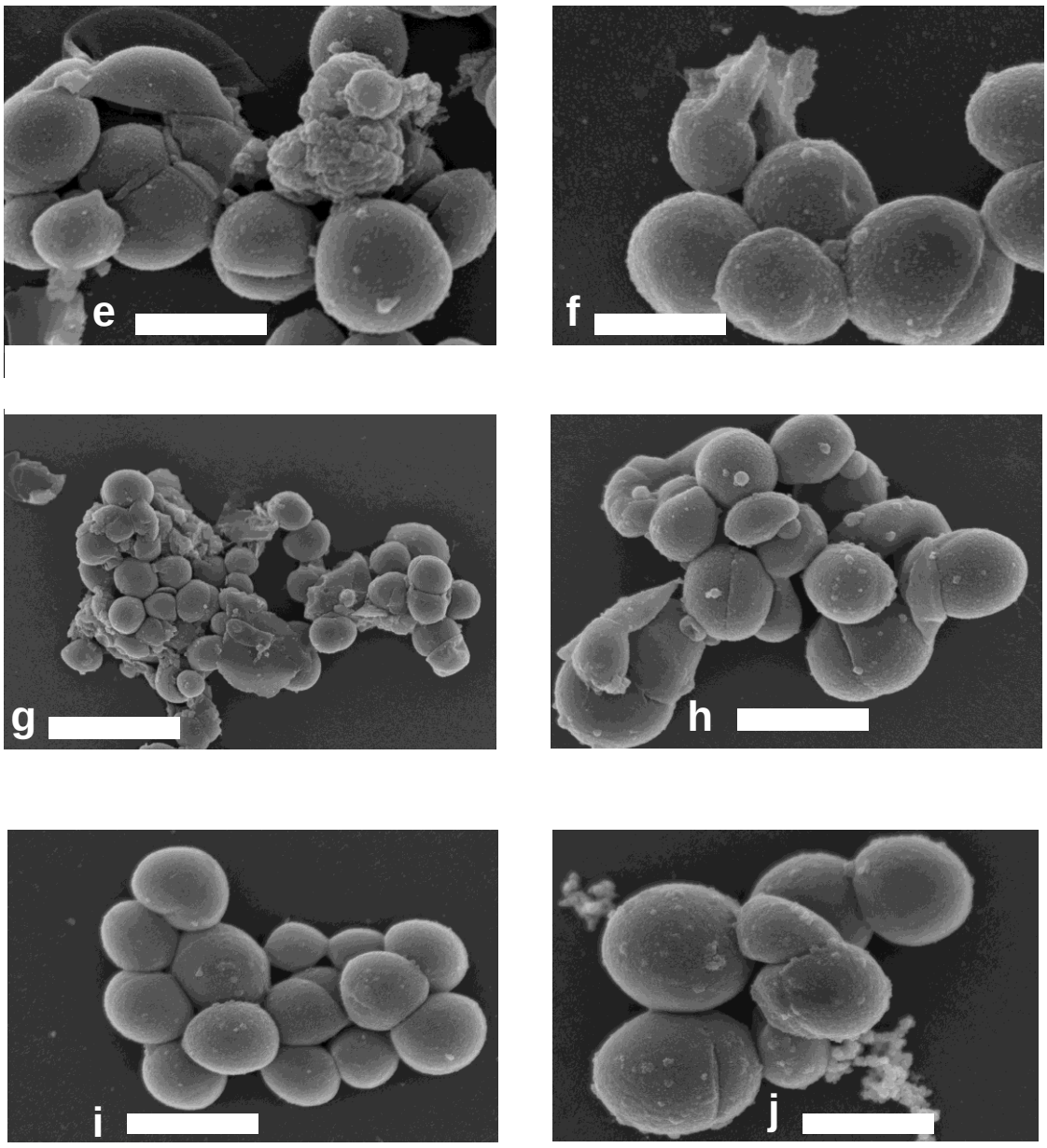

Figure 2.10. Cont. *(e) S. aureus treated with G2-PAMAM-NH2 at a concentration of 250 µg/mL, magnification x25k and scale bar represents 1.2 µm. (f) S.aureus treated with G2-PAMAM-NH_2 at a concentration of 250 µg/mL, magnification x 40 k and scale bar represents 750 nm. (g) S. aureus treated with G5-PAMAM-NH_2 at a concentration of 250 µg/mL, magnification x10k and scale bar represents 3 µm. (h) S. aureus treated with G5-PAMAM-NH_2 at a concentration of 250 µg/mL, magnification x20k and scale bar represents 1.5µm. (i) S. aureus treated with G3.5-PAMAM-COOH at a concentration of 1000 µg/mL, magnification x25k and scale bar represents 1.2µm. (j) S. aureus treated with G3.5-PAMAM-COOH at a concentration of 1000 µg/mL, magnification x30k and scale bar represents 1 µm.*

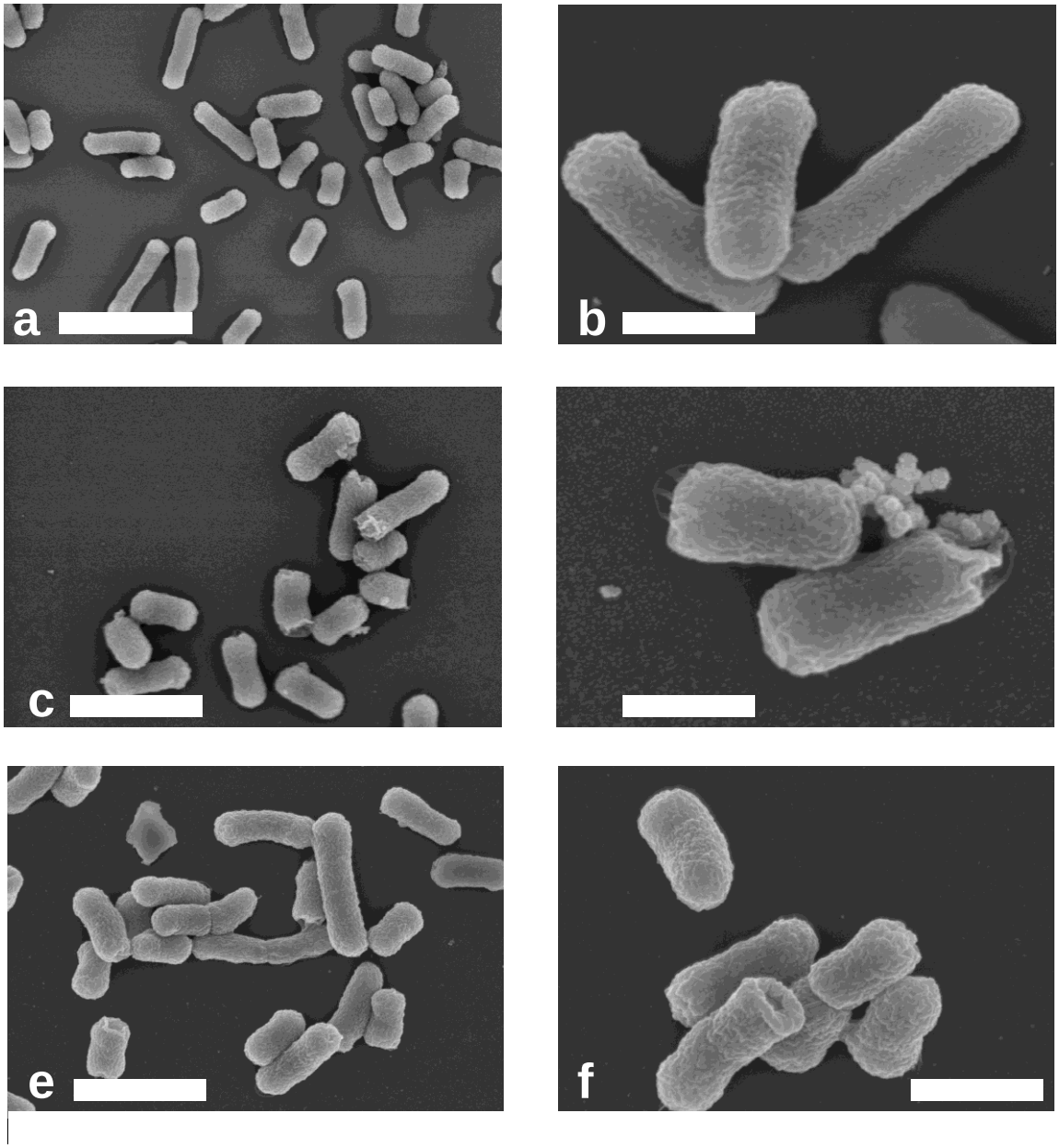

Figure 2.11.Scanning electron micrographs of *E. coli* challenged with PAMAM dendrimer.(a) *E. coli* untreated magnification x10 k scale bar scale bar represents 3 µm. (b) *E. coli* untreated magnification x40 k scale bar scale bar represents 750 nm. (c) *E. coli treated* G3-PAMAM-NH_2 at a concentration of 5x calculated IC_{50} as determined in Section 2.3.1, magnification x15 k and scale bar represents 2 µm. (d) *E. coli treated* G3-PAMAM-NH_2 at a concentration of 5x calculated IC_{50} as determined in Section 2.3.1, magnification x 50 k and scale bar represents 1 µm. (e) *E. coli* treated with 1000 µg/mL of G3.5-PAMAM-COOH magnification x15 k scale bar 2 µm. (f) *E. coli* treated with 1000 µg/mL of G3.5-PAMAM-COOH magnification x30 k scale bar 1. µm.

2.4 Discussion

Although PAMAM dendrimers are biocidal there have been very few PAMAM dendrimers that have been tested for antimicrobial activity hence the rationale for this study. In order to develop more efficacious antimicrobial dendrimers it is of paramount importance to determine the antimicrobial properties of a range of PAMAM dendrimers including lower and higher generations and amine and carboxyl terminated groups. A modified broth microdilution assay with a viable count was used to determine the surviving bacterial numbers (Calabretta *et al.* 2007) after exposure to a range of generations of PAMAM-NH_2 and PAMAM-COOH. A modification to the growth media was made to incorporate CLSI standardized growth media and a viable count assay was performed for an accurate measurement of surviving bacterial numbers (Rennie, 2001).

Typically the number of surviving bacteria is measured by reading the absorbance of each well (Zgoda and Porter, 2001), however the optical density depends on the shape, strain and growth stage of the bacteria; it also takes into account live and recently dead bacteria (Koch, 1994). After testing both methods it was decided that a viable count, though laborious, was much more accurate. It was found that after mixing the PAMAM dendrimer into the bacterial suspension a pellet formed on the bottom of each test well and therefore an accurate optical density measurement could not be taken.

Two skin pathogens, *S. aureus* and *E. coli* were tested against various concentrations of PAMAM dendrimers. *S. aureus* and particularly its meticillin-resistant

counterpart, is a well recognised nosocomial pathogen that causes skin and soft-tissue infections notably within immuno-compromised patients (Frazee *et al.* 2005, Leyden *et al.* 2006 and Miller *et al.* 2007). The skin pathogen *S. aureus* is known to release a number of pathogenic toxins including exfoliative toxin A that is the causative agent of bullous impetigo and scalded skin syndrome (Amagai *et al.* 2000). *E. coli* is a Gram-negative gut pathogen that can also be considered as a transient skin pathogen. The microorganism was utilised as it has been shown to be transmitted from skin to surfaces and *vice versa* resulting in the transmission of infections to immune-compromised patients (Fryklund*et al.* 1995).

The calculated IC_{50}values are shown in Table 2.1 along with the generation, molecular weight and number of theoretical amine surface groups. A clear, generation-dependent trend was observed when the IC_{50} of each PAMAM generation were plotted against their respective theoretical number of surface amine groups. The term 'theoretical' is used as the PAMAM dendrimers were used as purchased and occasionally structural defects can occur within the PAMAM dendrimer due to the incompletion of the Michaél reaction in the divergent synthesis process (Liuand Fréchet, 1999). Despite the possibility of structural defects, PAMAM dendrimers are widely accepted as being uniform, monodispersed polymers and have been characterized by a range of techniques including AFM (Li *et al.* 2000), MALDI-ToF mass spectrometry (Peterson *et al.* 2003) and zone capillary electrophoresis (Peterson *et al.* 2001).

There was an inverse correlation between the IC_{50} concentration and PAMAM dendrimer generation (as shown in Figure 2.3). G2-PAMAM-NH_2 that terminates in

18 amine groups required a ~10x higher concentration than G5-PAMAM-NH_2 with 128 surface amine groups to inhibit 50 % of the bacteria. It was found that by increasing the number of amine groups on the dendrimer surface the concentration required to inhibit 50 % of the bacteria dramatically decreased. Enhanced destabilization of bacterial membranes has been observed by increasing the number of amino groups on a polycation (Katsu *et al.* 2002).

This, generation-dependent, trend observed was contrary to the findings elsewhere in Lopez *et al.* 2009. The authors determined the minimum inhibitory concentration (MIC) using a broth microdilution assay and after re-suspension of the formed pellet in each well the optical density was used to determine the surviving bacterial numbers. They found that the MIC for G3-PAMAM-NH_2 and G5-PAMAM-NH_2 against *S. aureus* was identical at 12.5 µg/mL. A distinction in MIC value for two different PAMAM generations against *P.aeruginosa* as G3-PAMAM-NH_2 and G5-PAMAM-NH_2 exhibited a MIC of 6.3 µg/mL and 12.5 µg/mL respectively. The authors suggest the difference is due to the G3-PAMAM-NH_2 dendrimer's ability to penetrate the cell more easily due to a lower molecular weight compared to G5-PAMAM-NH_2. One would assume that if the molecular weight was preventing the penetration of the PAMAM dendrimer into the cell membrane of *E. coli* the same affect would be observed for the penetration into the cell membrane of *S. aureus*. The MIC values determined do not correlate to the calculated IC_{50} values determined in section 2.3.1 as MIC represents the lowest inhibitory concentration as exhibited by a sharp decrease in absorbance whilst IC_{50} determines the concentration required to kill 50 %

of the bacteria. The two different mechanisms of defining the antimicrobial effect of PAMAM dendrimers have shown opposing trends.

Another trend apparent from the results is that PAMAM dendrimers are more effective against Gram-negative bacteria such as *E. coli* as shown in Table 2.1 Section 2.3.1. This has been noted elsewhere asG4-PAMAM-NH_2 exhibited a higher biocidal affect against *P. aeruginosa* than against the Gram-positive *S. aureus* (Calabretta *et al.* 2007). *E. coli* is Gram-negative and has a very different cell wall structure and composition compared to Gram-positive *S. aureus*. The main barrier to the ingress of biocides is the outer membrane which for *E. coli* is exterior to a thin peptidoglycan layer and the outer cell membrane. The outer membrane consists of lipopolysaccharide (LPS), phospholipids and proteins (Nikaido, 1996). LPS carries a high anionic charge at physiological pH due to the ionisable phosphoryl and carboxyl groups (Beveridge, 1999). The polycationic nature of PAMAM dendrimers would ensure high reactivity and affinity for the outer membrane due to strong electrostatic forces. The high degree of interaction and disruption of the lipid bilayer of the outer membrane with the polycationic PAMAM dendrimer is one possible explanation for the enhanced antimicrobial efficacy observed for Gram negative bacteria in Section 2.3.1 and for G5-PAMAM-NH_2tested against *P. aeruginosa* in Calabretta *et al.* (2007).

Previously PAMAM dendrimers have been shown to form nano-holes within the lipid bilayer causing membrane permeabilisation and leakage of cytoplasmic contents however the effect was transient and the membrane integrity returned on removal of the G5-PAMAM-NH_2 dendrimer (Hong *et al*. 2004 and Hong *et al.* 2006). Further other polycationic compounds such as chitosan have been shown to disrupt and

permeabilise the outer membrane resulting in loss of barrier function (Helander *et al.* 2001).

Gram positive bacteria such as *S. aureus* do not have a protective outer membrane but rather a dense cross-linked peptidoglycan layer with threads of anionic teichoic acids consisting of repeating units of glycerol phosphate, glucosyl phosphate and ribitol phosphate (Silhavy *et al.* 2010). The peptidoglycan layer is a dense mesh network that is around 30 nm in thickness (Shockman and Barren, 1983). It regulates the ingress of nutrients, controls stabilizing cations and offers protection from antibiotics whilst maintaining osmotic pressure (Campbell *et al.* 2012).The sheer thickness and density of the polyanionic mesh would offer the microorganism a degree of protection from the penetration of PAMAM dendrimers. Though teichoic acids carry a lesser anionic charge than LPS (Beveridge, 1999) they still confer a continuum anionic charge across the bacterial cell wall resulting in an electrostatic attraction between the Gram positive bacteria and the polycationic PAMAM dendrimers. The difference in antimicrobial efficacy observed for Gram positive and Gram negative bacteria is explained by their distinctive cell wall compositions.

Surprisingly, at the lower concentrations tested for G2-PAMAM-NH_2 and G5-PAMAM-NH_2 PAMAM dendrimers, the number of bacteria was higher than in the growth control. This could be due to the polycationic PAMAM dendrimer displacing the membrane stabilizing cations (Ca^{2+} and Mg^{2+}) and replacing them ensuring stabilization of the cell membrane(Chen and Cooper, 2002). This replacement-stabilization effect has been observed for ethylenediamine and other polycations (Katsu *et al*. 2002). This is interesting as ethylenediamine is a key

component of PAMAM dendrimers and is even the compound at the focal core. For G3.5-PAMAM-COOH the IC_{50} values for each microorganism are of a higher concentration than those tested in section 2.3.1. The carboxyl terminated dendrimer did inhibit *S. aureus* at most concentrations but the dendrimer did not inhibit 50 % of the bacteria, even at a concentration of 250 µg/mL therefore it is likely that a much higher concentration is required (Figure 2.5). Against *E. coli* the carboxyl terminated dendrimer surprisingly enhanced the growth of bacteria when compared to the growth control. This may be due to the growth control being inhibited by some means during the experiment; further replicates would have to be conducted to confirm the observed effect. Wang *et al.* (2010) tested G3.5-PAMAM-COOH'santimicrobial affect against *E. coli* and found that very high concentrations of 6.25-100 mg/mL were required to inhibit *E. coli*.

It is imperative to establish the mechanism of action of novel antimicrobial compounds in order to fully exploit biocides, discover new bacterial targets, and develop innovative biocidal strategies and to give an insight into possible mechanisms of resistance. As the IC_{50} values calculated in Section 2.3.1 illustrate differing efficacies for various PAMAM generations against Gram positive and Gram negative bacteria, it was thought likely that the target for antimicrobial action is the cell membrane. The cytoplasmic membrane is the target for most polycationic biocides resulting in destabilization, leakage of cytoplasmic contents and precipitation of cytoplasm (Ikeda *et al.* 1986, Ioannou *et al.* 2007 and Liu *et al.* 2004). Moreover, cytoplasmic membrane disruption has been observed for quaternary ammonium functionalized poly(propylene imine) dendrimers against both Gram positive and Gram negative bacteria (Chen and

Cooper, 2002). With regards to establishing interactions with the cytoplasmic membrane, it appears that only G4-PAMAM-NH_2 has been analysed against one strain of bacteria, *E. coli* (Wang *et al.* 2010).

To assess as to whether PAMAM dendrimers impair the integrity of the cytoplasmic contents of Gram positive and Gram negative bacteria, the leakage of intracellular components was monitored over time. At bacteriostatic concentrations, destabilization of the cytoplasmic membrane causes the loss of small ions such as potassium and phosphate, and this affect is reversible. At bactericidal concentrations leakage of DNA, RNA and other cytoplasmic contents over time occurs resulting in either inhibition or cell death (Chen and cooper, 2002 and Joswick *et al.* 1971). The cytoplasmic material that is released into the supernatant over time absorbs at 260 nm and can therefore be measured to determine the membrane integrity. The results indicate that G3-PAMAM-NH_2 causes intracellular components to leak from *S. aureus*, *S. epidermidis* and *E. coli* within a very short time frame of 20 minutes. The integrity of the cytoplasmic membrane for all three bacterial strains is diminished with an increase in 260 nm absorbing material detected within the first 80 minutes of the assay. At 80 minutes for the *Staphylococci* species and 100 minutes for the *E. coli* a plateau was reached. This is indicative that precipitation and coagulation of nucleotides with the high concentration of PAMAM dendrimer had occurred that has been observed with other cations (Hugo and Longworth, 1964).

A differing profile of 260 nm absorbing material release was observed for each bacterial strain. *S. aureus* and *S. epidermidis* resulted in an immediate release of cytoplasmic material up to 80 minutes where a plateau was reached. For *E. coli* there

was a rapid release of cytoplasmic material up to 40 minutes and then a gradual release from 40-120 minutes. This trend is analogous to the intracellular contents release profile observed when *S. aureus* and *E.coli* was challenged with the polycation, chitosan acetate (Liu *et al.* 2004). *E. coli* resulted in the highest recorded absorbance that is in line with the increased antimicrobial efficacy of the G3-PAMAM-NH_2 against *E. coli* determined in Section 2.3.1. The differing release profiles for Gram negative and Gram positive bacteria is due to the dissimilarity in the cell wall structure and composition that the biocide must first penetrate before access to the cytoplasmic membrane. These distinctions have been outlined in Section 2.3.1.

The results of the membrane integrity test suggest that the biocidal activity of PAMAM dendrimers occurs over a very short time period of 80 minutes. The intracellular release profiles are indicative of an antimicrobial compound that targets bacterial cell membrane and its function, resulting in bacterial growth inhibition and cell death (Wang *et al.* 2010). Further analysis into the PAMAM dendrimer's interactions with the bacterial membrane were studied (see Section 2.3.3 and 2.3.4).

The permeabilisation of the inner membrane of *E. coli* was investigated by introducing a range of PAMAM dendrimer generations with a series of increasing concentrations. The inner membrane consists of a complex proteome within a lipid bilayer is formed principally from phosphatidyl ethanolamine, phosphatidyl glycerol and to a lesser extent cardiolipin. The latter of the two membrane lipids carries an anionic charge (Dowhan, 1997). The results in section 2.3.3 indicate that the polycation PAMAM dendrimers have a strong affinity for the anionic inner membrane of *E. coli*. The absorbance at 420 nm, corresponding to *o*-nitrophenol, rapidly increased within

30 seconds for concentrations >10 μg/mL for G2- PAMAM-NH_2, G3- PAMAM-NH_2 and G4- PAMAM-NH_2. A lag time of 2 minutes was observed for G5- PAMAM-NH_2 due to the slower diffusion of the high molecular weight PAMAM dendrimer. PAMAM dendrimers permeabilise and impair the inner membrane rapidly in a concentration dependent manner. A concentration as low as 5 μg/mL of all PAMAM dendrimers tested resulted in the production of *O*-nitrophenol and thus caused inner membrane permeabilisation.

It was found that there was also a generation-dependent effect of the inner membrane permeabilisation. Within the first 12 minutes the G3-PAMAM-NH_2 and G4-PAMAM-NH_2 resulted in the highest absorbance at 420 nm. This is likely due to a compromise between the number of surface amine groups and the molecular weight for diffusion through the outer membrane to reach the inner membrane. At 60 minutes however the absorbance at 420 nm for G3-PAMAM-NH_2 and G5-PAMAM-NH_2 was comparable after the lag time that G5-PAMAM-NH_2incurred due to its relative size and molecular weight. Furthermore, at a low concentration of 5 μg/mL of PAMAM dendrimer it was G2-PAMAM-NH_2 that displayed the highest absorbance after 60 minutes. The lower molecular weight PAMAM dendrimer incited the highest degree of inner membrane permeabilisation at the lower end of the concentration series tested. This may be an indication that PAMAM dendrimers aggregate at higher concentrations and for this reason diffusion throughout cell membrane and surface area are reduced. These novel results signify that there is an important time, concentration and generation dependent effect on the inner membrane permeabilisation of *E. coli.* Wang *et al.* reported a lag time of 20 minutes for the

release of *O*-nitrophenol when G4-PAMAM-NH_2 was tested at a single concentration. This result seems anomalous when they reported leakage of intracellular components within 20 minutes at the same PAMAM concentration (Wang *et al.* 2010). One would expect that the integrity of the inner membrane must first be impaired before the leakage of cytoplasmic contents can occur.

In order for the PAMAM dendrimer to contact the inner membrane the dendrimer must have first destabilized and traversed the outer membrane of *E. coli.* A number of cationic compounds have been reported to enhance the permeability of the outer membrane (Piers *et al.* 1994, Minnock *et al.* 2000, Domadia *et al.* 2010 and Katsu *et al.* 2002. The outer membrane is stabilized by Ca^{2+} and Mg^{2+} that have strong electrostatic binding affinities towards the anionic LPS. If polycations such as PAMAM dendrimers disturb or replace the stabilizing divalent cations, the integrity of the non-fluid continuum of LPS will be impaired and thus more permeable to biocides (Vaara, 1992 and Katsu *et al.* 1984). It has been observed that polycations with more than 4 amino groups were very affective at removing Ca^{2+} but to cause further membrane disruption bulky hydrophobic moieties were required (Katsu *et al.* 2002 and, Yasuda *et al.* 2004). PAMAM dendrimers have been shown to exhibit chelating behavior of metal ions in aqueous solutions due to their high density of nitrogen ligands along with amine terminal groups (Diallo *et al.* 2005 and Diallo *et al.* 2004). For PAMAM dendrimers to perturb the inner membrane of *E. coli*, shown in Section 2.2.3, the dendrimer must have first chelated, replaced and disturbed the stabilizing cations resulting in a disrupted and permeable outer membrane (Chen and Cooper, 2002 and Wang *et al.* 2010).

SEM is a method that has been used for decades to visualise the external features of bacteria shown in 3D form (Khalab *et al.* 2008). As such, electron microscopy has been used to study the structural and morphological changes induced by a range of antimicrobial agents including chlorhexidine (Tattawasart *et al.* 2000 and Khunkitti *et al.* 1998), silver nanoparticles (Kim *et al.* 2011) and tea tree oil (Carson *et al.* 2002). Cell wall damage caused by PAMAM dendrimers was visualised using SEM, supporting the membrane integrity and permeabilisation studies reported within previous sections of this chapter. With regards to the effects visualised, the untreated *S. aureus* illustrated blebbing of cytoplasmic material on the cell surface that had been extruded from damaged cell membrane. Leaked cytoplasmic material, severe membrane damage and even separation of the cell membrane from the cell was also exhibited due to the irreversible damage caused by the different generations of PAMAM dendrimers (Figure. 2.10). Unfortunately, there was also leaked cytoplasmic content clustered around the bacterial cells observed in the untreated *S. aureus* which is an artefact due to the SEM preparation procedure. It has been noted that morphological changes are likely to occur due to repeated centrifugation during the washing procedure (Kai *et al.* 1999). Though, the severity of membrane damage observed for treated *S. aureus* was not observed in the untreated control group. This degree and type of membrane damage has been observed in scanning electron micrographs of *S. aureus* challenged with cationic lens biocides, polyquaternium-1 and myristamidopropyl dimethylamine (Codling *et al.* 2005). Further, comparable cytoplasmic membrane damage was observed for *S. aureus* when challenged with the essential oil isolated from *O. Vulgare* (De Souza *et al.* 2010).

Marked release of cytoplasmic contents was also observed for *E. coli* due to membrane damage inflicted by the G3-PAMAM-NH_2 dendrimer (Figure. 2.11). Similar extracellular membrane blebbing was observed on *E. coli* when the bacteria were challenged with tea tree oil (Gustafson *et al.* 1998) and silver nanoparticles (Kai *et al.* 1999). Within the literature there was one instance where G4-PAMAM-NH_2 was challenged against *E. coli* and analysed by SEM after an eight hour contact time (Wang *et al.* 2010). The authors observed a range of detrimental morphological effects including ruptured cell walls, eroded cell membrane and shrinkage of bacterial cells (Wang *et al.* 2010). An incubation time of two hours was utilised in Section 2.3.4 therefore a lower extent of morphological damage was observed.

The membrane damage depicted in the scanning electron micrographs is consistent with the membrane integrity study that monitored the release of cytoplasmic material from the cell membrane (Section 2.3.2). Leakage of cytoplasmic contents that absorbs at 260 nm is a result of irreversible cell membrane damage that leads to cell death. Intracellular ion homeostasis is integral to all living cells as they are required for turgor pressure control, many metabolic processes and the divalent cations, Ca^{2+} and Mg^{2+} are of paramount importance for maintaining cell wall stabilisation (Shabala *et al.* 2001 and De Souza *et al.* 2010). As membrane damage is observed in the scanning electron micrographs, disruption of the stabilizing cations must have occurred. This destabilisation affect was also observed in the membrane permeabilisation assay (section 2.3.3). For both *E. coli* and *S. aureus* G3.5-PAMAM-COOH did not induce any morphological damage at a concentration of 1 mg/mL. It has been proposed that carboxyl terminated PAMAM dendrimers are antimicrobial, however only at very high

concentrations. The mechanism of action is conceivably due to the scavenging of the stabilizing divalent cations leading to permeabilisation of the cell wall. The SEM images provide supporting evidence that the mechanism of action of PAMAM dendrimers is to target and disrupt the bacterial cell membrane.

2.5 Conclusion

Though unmodified PAMAM dendrimers have been shown to possess antimicrobial properties (Calabretta *et al.* 2007, Lopez *et al.* 2009 and Wang *et al.* 2010) details on the antimicrobial properties of different generations, terminal functionalities and mechanism of action were lacking in the literature. Trends regarding PAMAM dendrimers' antimicrobial effects were based on the analysis of only two dendrimer generations. This gap in knowledge within the literature has been addressed in order to develop more efficacious dendrimer biocides or dendrimer-based formulations. The findings of the study indicate that unmodified amine-terminated PAMAM dendrimers exhibit high antimicrobial potency at low concentrations, but their potency is dependent on the generation of the PAMAM dendrimer. Contrary to what has been published within the literature it was found that the antimicrobial efficacy improved with increasing numbers of surface amines and molecular weight. This finding correlates well with the results observed in the inner membrane permeabilisation assay whereby, G5-PAMAM-NH_2incited the greatest membrane permeabilisation effect after 60 minutes possibly due to its high molecular weight a lag time was observed. The findings also suggest that carboxyl terminated PAMAM dendrimers are required in very high concentrations (> 1 mg/mL) in order to observe bacterial inhibition. The study has confirmed that the antimicrobial efficacy is

dependent on generation, concentration and terminal functionalities. There was a strong correlation between membrane disruption and the determined biocidal activity, thus making it a key contributing mechanism of action.

3.0 An investigation as to whether a PAMAM dendrimer skin pre-treatment enhances the permeation and deposition of CHG within porcine skin.

3.0 Introduction

3.1 Use of PAMAM dendrimers in transdermal and topical drug delivery systems

PAMAM dendrimers have previously been used as percutaneous absorption enhancers for a number of topically applied therapeutics. This is due to their unique physiochemical characteristics such as their monodispersed globular structure with interior voids and dense surface functionalities (Uppuluri *et al.* 1998). PAMAM dendrimers are ideal for therapeutic use due to their uniform size and structure allowing for pharmacological reproducibility unlike their linear polymeric counterparts. The interior voids within the PAMAM dendrimer may encapsulate low molecular weight hydrophobic drugs for drug delivery (Morgan *et al.* 2006, Milhem *et al.* 2000 and Gupta *et al.* 2006). PAMAM dendrimers also have dense surface functionalities; G4-PAMAM-NH_2 consists of 64 primary amine groups at the periphery, which can be utilised to electrostatically complex or to covalently conjugate a range of drugs to its surface (Wang *et al.* 2010 and Cheng *et al.* 2008). These physiochemical properties of PAMAM dendrimers allows for the protection of degradable drugs, increase the aqueous solubility of drugs, and can allow for modified drug release, i.e. through thermo or pH responsive properties (Sun *et al.* 2012, Zhao *et al.* 2011 and Criscione *et al.* 2009).

Dendrimers, particularly PAMAM dendrimers, have been used for the delivery of therapeutics across a range of biological membranes including Caco-2 cell monolayers (Elsayed *et al.* 2002), rat intestine (Wiwattanapatapee *et al.* 2000 and Ke *et al.* 2007), ocular drug delivery (Vandamme and Brobeck, 2005) and for the transfection of genetic material (Eichman *et al.* 2000 and Shakhabazau *et al.* 2010).

In recent years the ability of PAMAM dendrimers to enhance the permeation for the topical or transdermal delivery of therapeutics has been investigated. PAMAM dendrimers have the ability to act as drug carriers by facilitating drug transport and also by means of a physical perturbation of the skin barrier to enhance transdermal drug delivery (Venuganti and Perumal, 2008). Chauhan *et al* (2003) used G4-PAMAM-OH and G4-PAMAM-NH_2 to enhance the permeation of indomethacin across skin *in vitro*, a non-steroidal anti-inflammatory drug (NSAID) that permeates the skin poorly. PAMAM dendrimers form a complex with indomethacin through electrostatic and hydrophobic bonding. A solution of G4-PAMAM-NH_2 (0.2 % w/v) enhanced the *in vitro* permeation of indomethacin by a factor of 4.5, compared to the drug in free solution. The dendrimers were shown to be an effective penetration enhancer for the transdermal delivery of indomethacin.

The PAMAM dendrimer enhancement effect also translated well to *in vivo* conditions. In a carrageenan-induced rat paw oedema model, pharmacokinetic data highlighted a 1.6 and 1.5 fold increase for G4-PAMAM-NH_2 and G4-PAMAM-OH formulations respectively in % inhibition of paw volume. The authors proposed a cyclodextrin-like mechanism for the enhanced flux of drug across the rat skin in that

the dendrimer acts as a drug carrier. Though the dendrimer-indomethacin complex has a molecular weight too high to penetrate the *stratum corneum* (SC), the authors suggest the enhancement compared to the drug in free solution is a result of the dendrimer facilitating drug delivery to the SC in a solubilised form increasing the drug partitioning into the SC. Within the study it was shown that the PAMAM dendrimer enhanced the bioavailability of an NSAID by increasing the solubility and by enhancing the flux of the drug across the skin *in vitro* and *in vivo* (Chauhan *et al.* 2003).

Other non-steroidal anti-inflammatory drugs in the case of ketoprofen and diflusinal were also electrostatically complexed with PAMAM dendrimers to significantly enhance the steady-state flux of both drugs across *ex vivo* rat skin in a diffusion cell study (Chauhan *et al.* 2004). The solubility of both drugs was dramatically enhanced resulting in an increased flux across the skin when compared to the drugs in free solution. Again, this transdermal enhancement resulted in an increase in bioavailability *in vivo* using the acetic acid induced writhing model in mice. Blood-drug level studies were 2.73 times higher for ketoprofen-PAMAM complex and 2.48 times higher for diflusinal-PAMAM complex than the respective drug in free solution (Chauhan *et al.* 2004).

Wang *et al.* created a novel polymeric drug delivery matrix using G3-PAMAM-NH_2 dendrimers combined with polyhydroxyalkonoate (PHA). When placed in a patch design the model drug, tamsulosin hydrochloride, was successfully transdermally delivered at a rate of 24.0 µg/cm^2/day whilst the matrix without the presence of

PAMAM dendrimer has a delivery rate of only 15.7 µg/cm^2/day in an *in vitro* study using a snake skin membrane. Only the drug delivery system encompassing the G3-PAMAM-NH_2 dendrimer within the matrix achieved above the clinical aim of 20.0 µg/cm^2/day, transdermal delivery of tamsulosin hydrochloride. The authors also pre-dosed the skin with a G3-PAMAM-NH_2 preparation to investigate the effect of the dendrimer alone on the skin. It was found that the PAMAM dendrimer pre-dose weakly enhanced the permeation of tamsulosin hydrochloride over a 24 hour time frame. The same enhancement effect was not observed when the tamsulosin hydrochloride was added directly to the snake skin in a PAMAM dendrimer solution (G3-PAMAM-NH_2, 7.5 mM). The authors believe that the PAMAM dendrimer's interaction with the drug prevented the PAMAM dendrimer's interaction with the SC and thus prevented the modulation of the skin surface (Wang *et al.* 2003).

These studies have used rat or snake skin as the model membrane for the percutaneous absorption studies. Diffusion studies using *ex vivo* rat skin have repeatedly shown the membrane to be significantly more permeable to a vast range of drugs, particularly with regards to lipophilic drugs, when compared to human skin membranes (Takeuchi *et al.* 2011, Barber *et al.* 1992 and Scott *et al.* 1987). For this reason rodent models are considered a poor surrogate for human skin when investigating the percutaneous absorption of drugs (Catz and Friend, 1990). Previously shed snake skin has been shown to be unreliable and misleading for the investigation of penetration enhancement as the membrane has been shown to underestimate the enhancer's effect when compared to human skin *in vitro* (Rigg and Barry, 1990). Further, significant variability in the permeability of the model drug

progesterone was observed between the dorsal and ventral sites of snake skin (Haigh *et al.* 1998). Shed snake skin though ethical is not considered an acceptable model for human skin. It would be of interest to study the interactions of the previously mentioned PAMAM dendrimer-NSAID complexes upon an accepted membrane model such as *ex vivo* human or porcine skin. Though *ex vivo* human skin is considered the gold standard, porcine skin is regarded as the closest surrogate membrane for human skin in *in vitro* percutaneous absorption studies (Dick and Scott, 1992 and Chilcott *et al.* 2001). Pig flank skin has similar morphological properties and hair follicle density to human skin and using skin from pigs of the same age, sex, site of the body and gene pool ensures that the model is homogenous (Davies *et al.* 2004).

PAMAM dendrimers from G2.5-PAMAM-COOH up to G4-PAMAM-NH_2 have been utilised to enhance the solubility of 8-methoxypsoralene (8-MOP) after the drug was encapsulated within the interior voids of the PAMAM dendrimer. The drug-PAMAM complex formed with G3-PAMAM-NH_2 delivered a higher flux of the 8-methoxypsoralene into the skin and the receptor fluid in an *in vitro* model using commercial polyvinyldifluoride (PVDF) membrane and pig ear skin (PES) membrane (Borowska *et al.* 2010). The authors describe how the PAMAM dendrimer acts as a carrier to an increased localised delivery whilst reducing the diffusion across the skin compared to the 8-MOP in free solution. The increase in retention within the deeper layers of the skin would allow for enhanced therapeutic effect for diseases such as psoriasis and atopic eczema.

Venuganti and Perumal (2008), investigated PAMAM dendrimers as a permeation enhancer of 5-fluorouracil when dosed from a range of vehicles. The authors successfully increased the flux of 5-fluorouracil (5-FU) across *ex vivo* porcine skin using a Franz-type diffusion cell model. A formulation containing a saturated dispersion of a G4-PAMAM-NH_2 – 5-FU complex resulted in a 1.77-fold and 1.38-fold increase in flux for isopropyl myristate (IPM) and mineral oil, respectively when compared 5-FU alone dispersed in IPM and mineral oil. There was no significant increase in flux for the co-treatment applied in PBS when compared to the 5-FU dosed alone in PBS. To delineate the PAMAM dendrimer's interaction with the skin membrane the authors also conducted a pre-dose PAMAM treatment. A G4-PAMAM-NH_2 preparation (0.2 mL, 1 mM) was dosed onto the skin for a 2, 12 and 24 h contact period. Afterwards, the 5-FU was applied in an IPM formulation and a significant increase in flux was observed for 5-FU and was found to be proportional to the PAMAM dendrimer pre-treatment contact time. The pre-treatment of PAMAM dendrimer resulted in a higher flux than the co-treatment application (Venuganti and Perumal, 2008).

All of the vehicles were tested with PAMAM-5-FU and compared to 5-FU in the same vehicle. There was a significant enhancement in drug flux across the skin with the addition of PAMAM compared to the 5-FU in respective free solutions (with the exception of PBS). The PAMAM dendrimer pre-treatment results within this study that show ~ a tenfold increase in the penetration of CHG suggest that the PAMAM dendrimer has a physical effect on modulating the skin barrier as the drug flux across the skin was significantly higher for the pre-dose when compared to the co-dose

application. The enhancement in permeation was not due to the dendrimer-drug interactions but due to the dendrimer-skin interactions.

PAMAM dendrimers were also shown to enhance the permeation of riboflavin in an oil-in-water (o/w) emulsion two to three-fold across porcine ear epidermis and polyvinyldifluoride membrane. The authors established that the G2-PAMAM-NH_2 dendrimer was the most effective at enhancing the penetration of riboflavin. The penetration enhancement was shown to be generation dependent and in decreasing order of penetration enhancement was, G2 **>** G3 ≫ G2.5 **>** G3.5 **>** G4 across the porcine epidermis (Filipowicz and Wolowiec, 2011). The authors believe that the enhancement is due to the solubilisation of the poorly soluble drug and due to the absorption of the PAMAM dendrimer. No mechanism or evidence for PAMAM penetration was offered or eluded to. The assumption that PAMAM dendrimers, that are large macromolecules, diffused 'faster' within the skin compared to the low molecular weight riboflavin was based on the detection of a fluorophore and not the native dendrimer. Fluorescein isothiocyanate was detected throughout the skin strata however there was no evidence to suggest that the fluorophore was still attached to the PAMAM dendrimer. Riboflavin has a molecular mass of 376.36 Da that is ~10 times smaller than G2-PAMAM-NH_2 that has a molecular mass of 3256 Da.

The passive diffusion of a compound across the SC is governed by Fick's second law of diffusion that contains the diffusion coefficient of a compound (Williams and Barry, 2012). The diffusion coefficient is dependent on the molecular size therefore it is unlikely that macromolecule as large as a PAMAM dendrimer would

diffuse through a membrane that is approximately 2500 µm in thickness (Meyer and Zschemisch, 2002) within a ten hour time frame. Therefore it is likely that it is the free fluorophore that has readily penetrated the skin rather than the dendrimer with a fluorophore attached, particularly in light of the 500 Da cut off for skin penetrants (Bos and Meinardi, 2000).

As to whether the dendrimer itself permeates the skin remains a controversial subject with very few investigations published in the literature. A recent study established that generation 4 PAMAM dendrimers with various terminal functionalities were limited to the superficial layers of the SC once topically applied (Venuganti *et al.* 2011). The authors found that -NH_2 terminated PAMAM dendrimers penetrated further within the SC than –COOH or -OH terminated PAMAM dendrimers. This may be a result of the cationic PAMAM dendrimers causing perturbation of the intercellular lipids through a range of mechanisms such as lipid extraction and/or fluidization (Barry, 2004). Neutral surface engineered dendrimers were found not to penetrate the SC of porcine skin (Küchler *et al.* 2009).

The degree of SC penetration of a dendrimer is severely limited due to the dense surface charge, hydrophilicity and the excessive molecular weight (typically >5000 Da) (Chauhan *et al.* 2003). The bulkiness of the macromolecule would significantly impair the ability for a PAMAM dendrimer to diffuse through the SC. The routes of drug penetration across the skin were discussed in detail within the general introduction but it should be noted that the tortuous intercellular lipid channels are between 0.5-40 nm wide (Cevc and Vierl, 2010 and Van der Merwe *et al.* 2006).

PAMAM dendrimers are hydrophilic and therefore diffusion across the SC along the tortuous intercellular lipid pathway would be unlikely. With the possible aggregation and coalescence of PAMAM dendrimers it is highly unlikely without a driving force that PAMAM dendrimers (ranging from 1- 10 nm) would be able to passively penetrate the SC past the superficial layers. There is a lack of free space for the diffusion for large macromolecules due to the restrictive nature of the densely organized intercellular lipids (Sun *et al.* 2012).

The advantage of high molecular weight, skin-surface modulating enhancers is that they are less likely to generate irritation or an immuno-response unlike conventional small molecular weight chemical enhancers that easily penetrate the skin and cause irritation (Aoyagi *et al.* 1990). The mechanistic aspect of the PAMAM dendrimer's modulation of the skin surface will be discussed in the following chapter.

3.1.2 Rationale for the investigation of a PAMAM dendrimer skin pre-treatment to enhance the topical delivery of a model antiseptic, chlorhexidine digluconate.

The poor permeability of CHG within the skin has been discussed in detail in Chapter 1. Increasing the deposition and permeation of CHG within the upper skin (i.e. SC, viable epidermis and follicles) to increase biocide contact with the resident bacteria would increase the efficacy. To increase the efficacy of CHG as an antiseptic, a novel permeation enhancement strategy is required. PAMAM dendrimers have been utilised as novel polymeric drug delivery systems for a variety of drugs discussed in Section 3.0.1. Though PAMAM dendrimers have been shown to

enhance the solubility of antimicrobial compounds (Cheng *et al.* 2007a), until this study an investigation into the potential use of PAMAM dendrimers as permeation enhancers of a topically applied antiseptic had not been conducted. This chapter investigates whether there is a permeation enhancement effect after a PAMAM dendrimer pre-treatment for the model antiseptic, CHG.

3.1.3 Aims and objectives

The aim of this Chapter is to investigate as to whether a PAMAM dendrimer pre-treatment enhances the permeation of CHG within porcine skin.

To achieve this aim a number of objectives were necessary:

(i) To conduct studies to determine whether a pre-treatment of G3-PAMAM-NH_2 enhanced the percutaneous absorption of CHG within porcine heat-separated epidermis.

(ii) To determine whether any enhancement effect is proportional to the PAMAM concentration of the pre-treatment application.

(iii) To characterise the enhanced permeation profile after a PAMAM dendrimer pre-treatment within the SC by conducting a gravimetric tape strip assay on dermatomed porcine skin.

3.2 Materials and methods

All in vitro percutaneous absorption studies within this Chapter were conducted using the following regulatory protocols as a guide;

(i) OECD Test Guideline 428 (2004)- Skin absorption: In vitro method.

(ii) OECD Guidance Document No. 28 (2004)

The above method is accepted as a reliable standard for percutaneous absorption studies and permits the use of porcine skin as a surrogate for human skin. In addition to measuring the dermal absorption of CHG, a mass balance recovery of the drug in the various compartments of the skin was determined at 24h.

3.2.1 Preparation of porcine ear epidermis and dermatomed porcine flank

The pig ears were obtained from a local abattoir prior to any steam cleaning treatment. The skin was washed with distilled water and carefully shaved using clippers so as not to damage the tissue. The ears were secured firmly by being pinned down on a cork board. An incision around the outer edge of the pig ear was made using a scalpel and, using tweezers to pull the skin taut, the scalpel was slowly moved along the underside of the skin above the cartilage. The skin was slowly separated from the cartilage and removed. It was then placed on foil and the cartilage was disposed of. The skin was then placed in a beaker of stirring water at a temperature of 60ºC for 60 seconds. After the 60 seconds the skin was pinned securely to a cork board. The epidermis was removed from the dermis by gentle scraping using the side of a spoon whilst keeping the skin taut with a pair of tweezers. The epidermis was gently separated from the dermis and rolled up as it was removed (Bhatti *et al.* 1988, Dick and Scott, 1992 and Scott and Clowes, 1992). At the end of the pig ear, the epidermis was lifted from the dermis noting which side is the SC and was floated on a tray of deep water. The epidermis was then captured on to a piece of foil with the SC facing upwards and with the skin stretched out and with air bubbles

removed. The skin was then hung to dry at room temperature and once dried, labeled and placed in a -20 ºC freezer until use (Davies *et al.* 2004).

Dermatomed skin was prepared from the flank of six week old pigs obtained from a local abattoir prior to any steam cleaning treatment. The skin was washed with distilled water and secured on to a wooden block. The skin was carefully shaved using clippers and care was taken to not damage the tissue. The subcutaneous fat was carefully removed using a scalpel and then the skin was dermatomed to a thickness of 400 µm with an electric dermatome. It was then wrapped in aluminum foil and frozen at -20°C until required.

Heat-separated porcine ear epidermis has been shown to be an excellent surrogate for human epidermis for skin permeation studies as it has similar morphological and permeability characteristics that are closer to that of a human compared to a rodent model (Benech-Kieffer *et al.* 2000 and Schmook *et al.* 2001). For studies using a tape stripping method to determine the drug permeation profile within the different histological skin compartments (SC, epidermis and dermis), dermatomed porcine flank has been shown to be an ideal surrogate for human skin. Pig flank skin has similar morphological properties and hair follicle density to human skin and also by using skin from pigs of the same age, sex and gene pool ensures that the model is homogenous and therefore suitable for dermal absorption studies and formulation optimisation (Davies *et al.* 2004).

3.2.2 Skin integrity check

The dermatomed or pig ear epidermis was punched out with a 3 cm diameter punch and placed upon a stainless steel mesh support grid within a Franz cell, with the SC facing upwards. The application site of the Franz cell was an area of 2.54 cm^2. To check the integrity of the skin, 4.5 mL of physiological saline (0.9 % w/w NaCl) was added to the receptor chamber and 2 mL of physiological saline was added to the donor chamber and placed in a circulating water bath on a submersible magnetic stirrer at 32°C for 30 minutes. After the cells had equilibrated, the transepithelial electrical resistance (TEER) was measured to check the integrity of the porcine skin. Prior to readings being taken, the instrument was calibrated using a resistor. It has been established that normal porcine skin in the Franz cells used should have an electrical resistance reading of ≥ 3 KΩ to pass the integrity check (Davies *et al.* 2004). Any diffusion cells that did not meet the integrity threshold were not included within the studies. TEER was used as opposed to trans-epidermal water loss (TEWL) due to the method being quicker whilst still correlating well with membrane integrity.

3.2.3 The effect of PAMAM dendrimer pre-treatment on the *in vitro* permeation on CHG using porcine epidermis.

The diffusion cells that had passed the integrity check were removed from the water bath and the skin surface was allowed to air dry for 2 h at ambient temperature. 4.5 mL of physiological saline was added to the receptor chamber of each Franz cell. The Franz cells were placed in the water bath (32°C ± 1°C) on a submersible stirring plate for 30 minutes and allowed to equilibrate. Both a G3-PAMAM-NH_2

(0.5 mM-10 mM) and a 2 % (w/v) solution of CHG were prepared in distilled water from a 20 % (w/v) solution of G3-PAMAM-NH_2 and a 20 % (w/v) solution of CHG respectively. Once the Franz cells had equilibrated, a 0.2 mL of G3-PAMAM-NH_2 (0.5 mM-10 mM) was applied to the skin surface for a 24 h contact time or in the case of the controls the vehicle was dosed without the presence of PAMAM dendrimer. After a 24 h time period the PAMAM dendrimer layer was removed from the skin surface by rinsing 2 mL aliquots of distilled water (10 mL in total) over the surface of the dosed skin, taking care not to damage the skin. The vehicle control was treated in an identical way and was also washed at 24 h. The skin surface was then blotted dry with adsorbent paper and dosed with an infinite dose (1 mL) of the CHG solution (2 % w/v). This was applied to the skin surface and left for a contact time of 24 h. At various time points a 500 µL aliquot of receptor fluid was removed and replaced with fresh physiological saline. After 24 h, excess CHG was removed from the skin surface of each diffusion cell by rinsing with 2 mL aliquots of distilled water (10 mL in total) over the surface of the dosed skin. The washings were placed in a labelled 25 mL volumetric and made up to volume.

The pig ear epidermis was immediately placed into HPLC mobile phase (see Section 3.2.5 for HPLC methodology section) for CHG extraction. The CHG from the donor cells was also extracted in 10 mL of HPLC mobile phase overnight. The following day the skin samples were agitated using a vortex mixer for 15 minutes and sonicated for 15 minutes. An aliquot of the sample was syringe-filtered (0.2 µm, 15 mm diameter polypropylene filters, Fisher Scientific, Loughbrough, UK) and diluted appropriately. The aliquots taken over the 24 h period were also filtered but not

diluted to prevent dilution below the limits of quantification. The samples were placed in 2 mL HPLC vials with a soft septum and analysed by HPLC for the CHG content. Only diffusion cells that had leaked upon dosing were not incorporated within the results.

3.2.4 Franz diffusion cell studies using porcine dermatomed skin for tape stripping.

The Franz cells were dosed as above in section 3.2.3 but the dermatomed skin was also tape stripped at the end of the experiment. Gravimetric analysis of SC content on the tape strips was conducted for each tape strip. Each tape strip was pre-cut and allowed to sit at room temperature for 2 h to allow volatile adhesive components to evaporate from the tape strip (Lademann *et al.* 2009). This is due to the volatile components skewing the gravimetric analysis of the tape strips. The weight of each tape strip was measured to 4 decimal places on a balance (Precisa, 262 SMA-FR, Milton Keynes, UK) before and after the tape strip was taken. A thin plastic mask was placed around the dosed area (2.54 cm^2) so that only SC material that was treated would be removed on to the tape strip. Between each tape strip the mask was cleansed in water and ethanol as to not contaminate the skin layers below. Once 21 tape strips were taken they were pooled together; tape strips 1-3 were analysed separately, tape strips 4-6, 7-10, 11-16 and strips 17-21 were pooled together and CHG was extracted in 10 mL of HPLC mobile phase. The tape stripped skin and donor chambers were also extracted in 10 mL of HPLC mobile phase. The samples were left overnight and the following morning the time point aliquots were

syringe filtered and transferred into 2 mL HPLC vials (Trebilcock *et al.* 1994). The skin, washings, donor chamber and tape strip samples were first vortex mixed for 15 minutes and sonicated for 15 minutes before being syringe filtered, diluted if appropriate and placed into 2 mL HPLC vials. The samples were analysed by HPLC for the detection of CHG.

Equation 3.1 was used to normalise the concentration of drug on the tape strip to the amount of SC material removed was taken from Reddy *et al.* (2002).

$$C_n = m_n \rho_{sc} / m_{sc,n}$$

Equation 3.1 used to normalise the concentration of drug on each tape strip to the amount of SC on the corresponding tape. *C_n is the concentration of the drug of the nth tape strip accounting for the mass of SC material (deduced gravimetrically), m_n is the mass of drug in the nth tape strip, ρ_{sc} is the density of the SC assumed to be 1 g/cm^3 (Pirot et al. 1997) and $m_{sc,n}$ is the mass of SC on the tape strip determined gravimetrically.*

3.2.5 HPLC method and validation for the detection of CHG

HPLC analysis of the samples was conducted on a Shimadzu UCFC modula system with an SPD M20 diode array detector using an isocratic mobile phase consisting of a methanol: water mixture (75:25) with 0.005 M sodium octane-1-sulphonate and 0.1 % (v/v) triethylamine. The pH was adjusted with glacial acetic acid to pH 4. The flow rate was 1.5 mL per minute on a MetLab ODS-H reverse phase column (150 × 4.6 mm, 5µm) that was set for 40ºC. Mobile phase was used as the solvent for all CHG extractions and this method was adapted from (Karpanen *et al.* 2008). The HPLC method was validated on the Shimadzu system. The limit of

detection (LOD) was calculated to be 0.050 µg/mL and the limit of quantification (LOQ) was calculated as 0.167 µg/mL. The relative standard deviation (RSD) % was calculated for 6 repeats of the 10 µg/mL standard and was found to be 0.40 %. For the skin assays conducted in this chapter the RSD % for each standard was <5 % and the R^2 value was 0.9999.

3.2.6 Statistical data analysis

All data is presented as the mean ± SEM unless otherwise stated and were analysed using GraphPad Prism® version 5 (San Diego, USA). Prior to statistical analysis all data were placed in to a histogram to check for normality. To compare the mean total concentration of CHG detected within the porcine epidermis after various skin pre-treatments (various PAMAM dendrimer concentrations and phys. saline), a Kruskal Wallis ANOVA test (data was non-parametric) was conducted with $p<0.05$ representing significance (Section 3.3.0, Figure 3.2). A Kruskal Wallis ANOVA with a Dunn's post test to compare treatment groups was also performed to determine if there was a different in total CHG concentration within the receptor fluid at 24 h for the different skin pre-treatment groups (Section 3.3.0, Figure 3.3). In Section 3.3.1 A Kruskal Wallis ANOVA was utilised to determine whether there was a significant difference between the total CHG concentration extracted from the tape strips after various skin pre-treatments with $p<0.05$ signifying statistical significance (Figure 3.7a). In Figure 3.7b a Kruskal Wallis test with a Dunn's post test was employed to determine whether there was a significant difference in CHG concentration within the epidermis and dermis after various skin pre-treatments.

3.3 Results

3.3.0 *In vitro* Franz diffusion cell study investigating the effect of a PAMAM dendrimer pre-treatment on the permeation on CHG using porcine epidermis.

CHG is known to adsorb on to a variety of surfaces including glass, cotton wool and skin (Denton, 1991). *In vitro* Franz diffusion cell studies are often used to provide mass balance data to determine the % recovery of a drug from the various diffusion cell compartments. With the knowledge that CHG adsorbs strongly on to a range of materials, a 100 µL aliquot of three different concentrations of CHG was spiked onto the compartments of a Franz cell (Table 3.1). The % of recovered CHG from each Franz cell compartment was very similar across the three concentrations tested. The average coefficient of variance for each Franz cell compartment (*n*=3) for the three CHG concentrations was 2.41 % suggesting that the adsorption of CHG onto the surfaces is not concentration dependent but more likely surface area dependent. The lowest % recovery was exhibited after spiking (a dose area of 2.54 cm^2) porcine epidermis in which across the three CHG concentrations (1, 5 and 10 % w/v) was 84.78 ± 1.336, thus resulting in around a 15 % loss of CHG. Typically, 6.3 % of the total amount of CHG dosed on to a strip of adhesive tape (20 mm in length) was not recovered. The percentage of dosed CHG that was not recovered from the glass donor chamber was ~9 %. A provisional study was conducted whereby silanised glass (silanised within the laboratory) was used in parallel to glassware that had not undergone silanisation. Surprisingly, it was found that the silanisation process of the glass did not enhance the recovery of the dosed CHG (data not shown). A

published silanisation protocol was used (Seed, 2001) though it is possible that the chlorotrimethylsilane had not covered the whole surface area of the glassware. Further, a range of adhesive tapes manufactured by different companies, in addition to the conventional Scotch 3M tape, were investigated and a range of extraction processes including length of time, solvent, agitation processes and temperature were investigated (data not shown). The optimal extraction process that was determined is outlined in section 3.2.3 and was found to be extraction in mobile phase for 24 h at room temperature followed by 15 minutes of high speed vortex mixing and 15 minutes of sonication.

Table 3.1 Percentage recovery of three concentrations of aqueous chlorhexidine digluconate after 100 µl was spiked on to each compartment of a Franz cell.

CHG concentration	% Recovered of dose spiked onto Franz cell compartments after 24 h		
	Epidermis	Adhesive tape strip	Donor chamber
1 % (w/v) CHG dosed	88	94	93
	84	92	91
	86	94	91
Mean ± SEM	86.00 ± 1.16	93.33 ± 0.67	91.67 ± 0.67
5 % (w/v) CHG dosed	88	91	91
	82	94	88
	81	91	93
Mean ± SEM	83.67 ± 2.19	92 ± 1.00	90.67 ± 1.45
10 % (w/v) CHG dosed	84	92	88
	86	97	94
	84	94	91
Mean ± SEM	84.67 ± 0.67	94.33 ± 1.45	91.00 ±1.73

The *in vitro* dermal delivery and absorption of CHG applied after a range of G3-PAMAM-NH_2 skin pre-treatments can be found within this section. The data within this section presents the distribution of CHG extracted from the diffusion cell compartments (including the epidermis) and also the rate of the absorption within the skin over 24 h. The data is illustrated as the concentration (μg/cm^2) but also as the percentage of applied dose for ease of interpretation. Table 3.2 shows the absorption and distribution of CHG within the Franz cell system after a skin pre-treatment of physiological saline (0.9 %) for 24 h (to act as a control for G3-PAMAM-NH_2 dendrimer pre-treated skin). It was found that a mean concentration (815.13 ± 154.94 μg/cm^2) of CHG applied to the skin was extracted from the glass donor chamber. Therefore, ~10 % of the dosed CHG was possibly adsorbed onto the glass of the donor chamber of the Franz cell. Over 50 % of the dosed CHG was removed on washing the skin at 24 h leaving ~13 % of the dosed CHG absorbed. A very low concentration of absorbed CHG was located within the receptor fluid (3.226 ± 1.622 μg/cm^2, ~0.04 % of applied dose) and a mean concentration of 1030.668 ± 130.917 μg/cm^2 that is ~13 % of the applied CHG was extracted from the porcine epidermis. A mean total CHG recovery of 75.299 ± 8.715 % of the applied dose was obtained therefore around 25 % of the dosed CHG is unaccounted for within the data shown. Potential explanations for the loss of CHG and comparison of the total recoveries compared to the spiking assay are outlined within the discussion.

Table 3.2. Compartmental diffusion cell data of CHG concentration for the control skin pre-treatment. *Percutaneous absorption (mass balance) of CHG within porcine epidermis after a 24 h pre-treatment of physiological saline (NaCl 0.9 %). Mean ± SEM (n=15) is shown.*

Sample (*n*=15)	CHG (µg/cm^2)		% of applied dose	
	Mean	SEM	Mean	SEM
Donor chamber	815.13	154.94	10.35	1.97
Skin wash	4080.06	398.89	51.82	5.07
Epidermis	1030.67	130.92	13.09	1.66
Receptor fluid	3.23	1.62	0.041	0.02
Total recovered	5929.09	686.37	75.30	8.72

The rate of absorption of CHG was calculated after a physiological saline pre-treatment in substitute of G3-PAMAM-NH_2 dendrimer as a control. The mean rate of CHG absorption was particularly slow over the 0-24h time period at 0.10 ± 0.02 µg/cm^2/h. A 12 h lag phase was observed and the mean rate of absorption from 15-24 h was calculated to be 0.22 ± 0.10 µg/cm^2/h. As observed within Table 3.2 & 3.3, CHG applied to skin alone has a slow rate of absorption and CHG was demonstrated to permeate the epidermis poorly. In order to reduce the lag time and increase the rate of absorption a PAMAM dendrimer pre-treatment was utilised in the following studies within this Section.

Table 3.3 Rate of absorption of CHG over 24 h after a control skin pre-treatment. *Rate of absorption (µg/cm^2/h) after application of CHG (2 % w/v, 1 mL, 24 h) within porcine epidermis.*

Cell number (n=15)	Absorption rate (µg/cm^2/h)		
	0-12 h	15-24 h	0-24 h
113	0.00	0.00	0.00
118	0.00	0.00	0.00
120	0.18	0.94	0.48
124	0.00	0.00	0.00
117	0.00	0.45	0.22
128	0.00	0.76	0.38
114	0.00	0.00	0.00
137	0.00	0.00	0.00
144	0.00	0.00	0.00
156	0.00	0.00	0.00
138	0.00	0.00	0.00
139	0.00	0.00	0.00
136	0.06	1.13	0.37
151	0.00	0.00	0.00
134	0.00	0.00	0.00
Mean	0.016	0.22	0.10
SEM	0.013	0.10	0.05

Table 3.4 exhibits the percutaneous absorption of CHG after the skin has been pre-treated with a 0.5 mM G3-PAMAM-NH_2 solution for 24 h. As expected, around 57 % of CHG was recovered from the skin wash after 24 h after CHG application. It was found that ~4 % of the total CHG applied was recovered from the glass donor chamber and was therefore unlikely to be available for skin absorption. The total percentage of applied drug that was considered to be absorbed was ~16.5 % with 15.3 % (1202.76 ± 177.21 µg/cm^2) absorbed within the porcine epidermis and 0.4 % (92.01 ± 34.49 µg/cm^2) absorbed within the receptor fluid over a 24 h time period. There was a mean total CHG recovery of 77.7 % from the applied dose which is

considered acceptable for cold studies under OECD 428 guidelines, but does leave ~20 % of the applied CHG dose unaccounted for within this data set.

Table 3.4. Compartmental diffusion cell data of CHG concentration after a skin pre-treatment of G3-PAMAM-NH_2 dendrimer (0.5 mM). *Percutaneous absorption (mass balance) of CHG (2 % w/v, 1 mL, 24 h) within porcine epidermis after a 24 h skin pre-treatment of G3-PAMAM-NH_2 (0.5 mM, 0.2 mL).*

Sample (n=19)*	CHG (µg/cm^2)		% of applied dose	
	Mean	SEM	Mean	SEM
Donor chamber	307.79	59.48	3.91	0.76
Skin wash	4515.08	301.08	57.34	3.82
Epidermis	1202.76	177.21	15.28	2.25
Receptor fluid	92.01	34.49	1.17	0.44
Total recovered	6117.64	572.26	77.69	7.27

***Cell 140 and 150 was excluded due to skin membrane damage. No lag phase was observed in the CHG absorption as the barrier integrity was impaired.

CHG was detected within the receptor fluid at various time points over a 24 h period after a pre-treatment of 0.5 mM G3-PAMAM-NH_2 dendrimer. Table 3.5 highlights the rate of absorption (µg/cm^2/h) that was calculated from 0-9 h and 12-24 h (absorption time intervals were determined from steady state portion of the mean CHG concentration absorption profile). For the majority of the Franz cells there was a 9 h lag time in the permeation of CHG with a mean absorption rate of 0.340 ± 0.25 µg/cm^2/h. The rate of absorption of CHG increased over the 12 to 24 h time period with a mean absorption rate of 1.62 ± 0.40 µg/cm^2/h. The mean rate of absorption of CHG within the receptor fluid from 0-24 h after a 0.5 mM

G3-PAMAM-NH_2 dendrimer treatment was calculated to be 0.89 ± 0.21 µg/cm^2/h. At the lowest concentration of PAMAM dendrimer pre-treatment the absorption rate over 24 h was increased from 0.10± 0.05 µg/cm^2/h without a PAMAM pre-treatment to a mean 0.89 ± 0.21 µg/cm^2/h;an ~10 fold increase.

Table 3.5. **Rate of absorption of CHG over 24 h after a skin pre-treatment of G3-PAMAM-NH_2 dendrimer (0.5 mM).** *Rate of absorption (µg/cm^2/h) after application of CHG (2 % w/v, 1 mL, 24 h) within porcine epidermis after a 24 h skin pre-treatment of G3-PAMAM-NH_2 (0.5 mM, 0.2 mL). Data is displayed as the mean n=19.*

Cell number (*n*=19)	Absorption rate (µg/cm^2/h)		
	0-9 h	12-24 h	0-24 h
144	0.00	0.01	0.003
150	2.74	0.71	0.96
157	0.00	0.00	0.00
153	0.11	6.17	3.00
140*	7.212	2.04*	-2.58*
151	3.57	1.80	2.43
150**	5.02	-0.92	1.53
144	0.00	1.99	0.81
153	0.17	1.91	0.86
161	0.00	1.76	0.75
151	0.03	2.24	0.10
157	0.00	2.97	1.30
115	0.00	0.00	0.00
113	0.00	1.91	0.79
125	0.08	3.78	2.15
118	0.02	2.06	1.020
111	0.00	0.006	0.002
119	0.00	0.02	0.01
137	0.00	0.17	0.07
Mean	0.40	1.62	0.89
SEM	0.25	0.40	0.22

*Cell excluded from the calculation of the mean as no lag phase (i.e. very high CHG concentration detected at 3 h) is observed in the CHG absorption profile which is indicative of skin membrane damage.

Table 3.6 illustrates the mean absorption and distribution of CHG within the Franz diffusion cell system after a 1 mM pre-treatment of G3-PAMAM-NH_2 dendrimer. There was approximately a 2 fold increase in the concentration of CHG extracted from the glass donor chamber compared to the 0.5 mM G3-PAMAM-NH_2 dendrimer

treatment after 24 h. A mean total of ~50 % of the applied CHG dose was washed from the skin surface at 24 h. The mean total percentage of CHG absorbed was ~13 % (1033.55 ± 130.31 µg/cm^2) of the applied dose, with 0.60 ± 0.15 % detected within the receptor fluid and 12.53 ± 1.50 % of the applied dose was extracted from the epidermis. The mean total % of CHG recovered was ~72 %. This is comparable to the recovery of CHG from the PAMAM untreated control in Table 3.2.

Table 3.6. Compartmental diffusion cell data of CHG concentration after a skin pre-treatment of G3-PAMAM-NH$_2$ dendrimer (1 mM). *Percutaneous absorption (mass balance) of CHG (2 % w/v, 1 mL, 24 h) within porcine epidermis after a 24 h skin pre-treatment of G3-PAMAM-NH$_2$ (1 mM, 0.2 mL). Data is represented at the mean ± SEM (n=24).*

Sample (n=24)*	CHG (µg/cm^2)		% of applied dose	
	Mean	SEM	Mean	SEM
Donor chamber	700.35	96.38	8.89	1.22
Skin wash	3924.29	291.12	49.84	3.70
Epidermis	986.23	118.16	12.53	1.50
Receptor fluid	47.32	12.15	0.60	0.15
Total recovered	5658.19	517.81	71.86	6.58

* Cell 149 excluded from the calculation of the mean.

The CHG absorption rate after a 1 mM G3-PAMAM-NH$_2$ dendrimer skin pre-treatment is presented within Table 3.7. As with the 0.5 mM dendrimer concentration the first 12 h rate of CHG absorption is relatively slow due to the lag time having a mean absorption rate of 0.17 ± 0.06 µg/cm^2/h. The absorption rate increases over the 15-24 h time period with a mean absorption rate of 1.10 ± 0.25

µg/cm^2/h. An overall absorption rate over the 24 h time period was calculated to be 0.61 ± 0.14 µg/cm^2/h. This absorption rate over 24 h is a similar value to the rates obtained for the other PAMAM concentrations tested for this time range and it is ~6.5 times higher than the physiological saline pre-treated control skin.

Table 3.7. Rate of absorption of CHG over 24 h after a skin pre-treatment of G3-PAMAM-NH_2 dendrimer (1 mM). *Rate of absorption (µg/cm^2/h) after application of CHG (2 % w/v, 1 mL, 24 h) within porcine epidermis after a 24 h skin pre-treatment of G3-PAMAM-NH_2 (1 mM, 0.2 mL).*

Cell number (n=24)	Absorption rate (µg/cm^2/h)		
	0-12 h	15-24 h	0-24 h
157	0.00	0.18	0.07
135	0.00	1.35	0.61
126	0.00	4.19	1.58
105	0.79	1.90	2.05
107	0.17	0.14	0.21
149*	30.48*	4.73*	15.98*
152	0.14	2.34	0.62
145	0.18	0.98	0.51
141	0.10	0.99	0.50
146	0.02	0.06	0.04
153	0.00	0.008	0.002
154	0.00	0.00	0.00
153	0.034	0.89	0.35
140	0.032	0.87	0.36
153	0.13	2.54	1.24
118	0.40	3.95	1.99
129	0.96	1.004	0.81
102	0.11	0.73	0.37
112	0.00	0.23	0.07
155	0.95	1.04	0.867
151	0.00	0.03	0.009
102	0.00	0.08	0.02
110	0.00	1.60	1.73
111	0.00	0.22	0.07
Mean	0.17	1.10	0.61
SEM	0.06	0.25	0.14

* Cell 149 excluded from the calculation of the mean as no lag phase (i.e. very high CHG concentration detected at 3 h) is observed in the CHG absorption profile which is indicative of skin membrane damage.

The absorption and distribution of CHG after treatment with the highest concentration of PAMAM dendrimer pre-treatment (10 mM) tested is shown in Table 3.8. As with the 1 mM G3-PAMAM-NH_2 pre-treatment, a mean of 7.836 ± 1.735 % of the applied dose was recovered from the glass donor chamber. Expectedly, > 50 % of the dosed CHG was recovered within the 24 h wash (4419.766 ± 285.820 µg/cm^2). The total percentage of CHG absorbed after a 10 mM PAMAM pre-treatment was ~19.1 % (1504.587 ± 203.750 µg/cm^2) with ~18.1 % absorbed within the epidermis (1421.675 ± 187.069 µg/cm^2) and ~1.1 % absorbed within the receptor fluid (82.912 ± 16.681 µg/cm^2).

Table 3.8. Compartmental diffusion cell data of CHG concentration after a skin pre-treatment of G3-PAMAM-NH_2 dendrimer (10 mM). *Percutaneous absorption (mass balance) of CHG within porcine epidermis after a 24 h pre-treatment of G3-PAMAM-NH_2 (10 mM). Data is represented at the mean ± SEM (n=24).*

Sample (*n*=24)*	CHG (µg/cm^2)		% of applied dose	
	Mean	SEM	Mean	SEM
Donor chamber	617.04	136.62	7.84	1.74
Skin wash	4419.77	285.82	56.13	3.63
Epidermis	1421.68	187.07	18.06	2.38
Receptor fluid	82.91	16.68	1.05	0.21
Total recovered	6541.39	626.19	83.07	7.95

*With one diffusion cell (99) excluded.

The absorption rate for CHG after a 10 mM G3-PAMAM-NH_2 dendrimer skin pre-treatment can be observed in Table 3.9. The first 0-12 h time period had a mean observable absorption rate of 0.48 ± 0.14 μg/cm^2/h which increased to 1.53 ± 0.32 μg/cm^2/h at a time period of 15-24 h. Over a 24 h time period the CHG absorption rate was calculated as 0.98 ± 0.19 μg/cm^2/h. The CHG 0-24 h absorption rate for 10 mM PAMAM dendrimer was ~10 fold higher than for physiological saline pre-treated skin. All PAMAM dendrimer skin pre-treatments exhibited a similar 0-24 h CHG absorption profile with 0.5 mM, 1 mM and 10 mM exhibiting absorption rates of 0.89 ± 0.22, 0.61 ± 0.14 and 0.91 ± 0.19 μg/cm^2/h respectively. Without a PAMAM dendrimer pre-treatment the absorption of CHG over 24 h was only 0.10 ± 0.05 μg/cm^2/h.

Table 3.9 Rate of absorption of CHG over 24 h after a skin pre-treatment of G3-PAMAM-NH_2 dendrimer (10 mM). *Rate of absorption (µg/cm^2/h) after application of CHG (2 % w/v, 1 mL, 24 h) within porcine epidermis after a 24 h skin pre-treatment of G3-PAMAM-NH_2 (10 mM, 0.2 mL).*

Cell number (n=24)	Absorption rate (µg/cm^2/h)		
	0-12 h	15-24 h	0-24 h
87	0.00	0.00	0.00
109	0.00	0.00	0.00
86	0.83	0.59	0.65
83	0.00	0.07	0.05
99*	14.81*	0.84*	5.41*
72	2.64	1.55	1.79
94	0.00	0.13	0.03
83	0.00	0.41	0.11
109	0.00	0.30	0.19
86	0.00	0.77	0.24
99	0.88	4.15	2.85
85	1.66	0.74	1.20
92	0.00	2.99	1.29
93	0.83	4.71	2.95
60	0.36	3.51	2.01
64	0.21	1.41	0.83
55	0.60	3.31	2.12
91	0.00	1.98	0.69
117	0.54	0.26	0.49
124	0.16	0.59	0.33
119	1.13	4.21	2.06
111	0.73	0.71	0.96
130	0.007	0.70	0.28
115	0.40	1.98	1.40
Mean	0.48	1.53	0.98
SEM	0.14	0.32	0.19

*Cell 99 excluded from the calculation of the mean as no lag phase is observed in the CHG absorption profile which is indicative of skin membrane damage.

A graph plotting the permeation profiles of CHG within the receptor fluid over a 24 h time period after all pre-treatment conditions is illustrated in Figure 3.1. When CHG was dosed after a pre-treatment of physiological saline only 3.23 ± 1.62 µg/cm^2 of CHG had permeated into the receptor fluid at 24 h and a 9 h lag time was

observed. The highest total concentration of CHG detected within the receptor fluid was observed for 0.5mM G3-PAMAM-NH_2 dendrimer pre-treated skin at 24 h (92.01 ± 34.49 µg/cm^2) compared 1 mM G3-PAMAM-NH_2 dendrimer pre-treated skin that yielded the lowest concentration of CHG permeation within the receptor fluid (47.32 ± 12.15 µg/cm^2). The concentration profile of CHG within the receptor fluid was very similar across all PAMAM dendrimer concentrations tested up to a time period of 9 h. There was a steady increase in the concentration of CHG up to 6 h where there is a slight plateau until 12 h. The largest concentration increase was observed from the 12 to 24 h time period. Figure 3.2 illustrates the concentration of CHG extracted from the epidermis after 24 h for all four skin pre-treatments. Though the 10 mM G3-PAMAM-NH_2 dendrimer skin pre-treatment yielded the highest CHG deposition within the epidermis no significant difference was observed between the CHG concentrations (µg/cm^2) extracted from the epidermis for the four skin pre-treatment groups (Kruskal Wallis ANOVA, p>0.05).

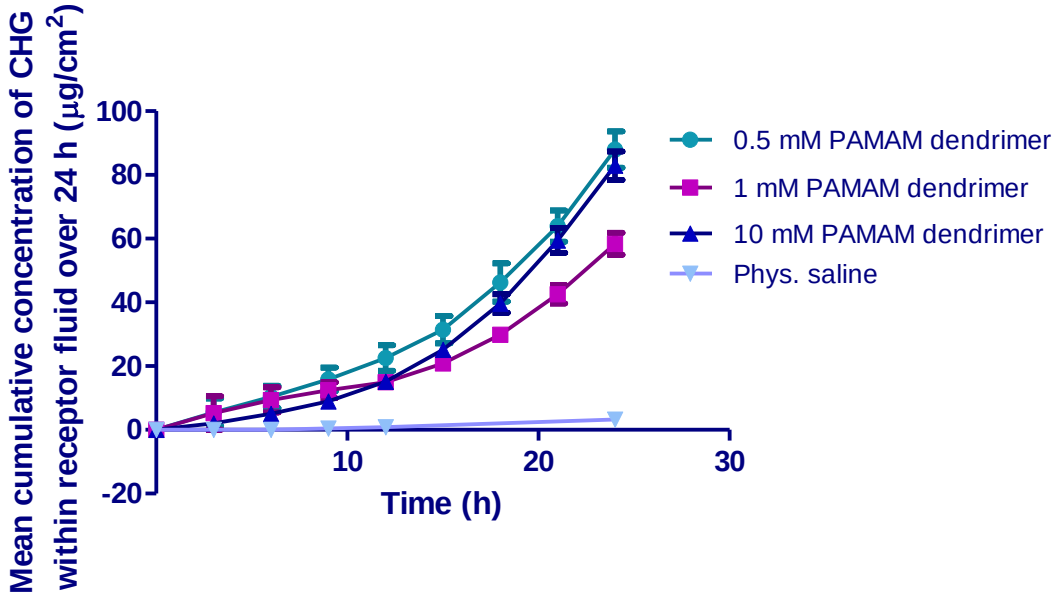

Figure 3.1 Mean concentration of CHG detected within the receptor fluid over a 24 h time period after a range of skin pre-treatments. *Profile of amount of CHG absorbed (Mean ± SEM) over a 24 h time period after application of CHG (2 % w/v, 1 mL, 24 h) within porcine epidermis after a 24 h skin pre-treatment of Phys. saline (0.9 % NaCl, 0.2 mL) represented by turquoise circles, G3-PAMAM-NH_2 (10 mM, 0.2 mL) represented by purple squares, G3-PAMAM-NH_2 (1 mM, 0.2 mL) represented by dark blue triangles and G3-PAMAM-NH_2 (0.5 mM, 0.2 mL) is represented by light blue inverted triangles.*

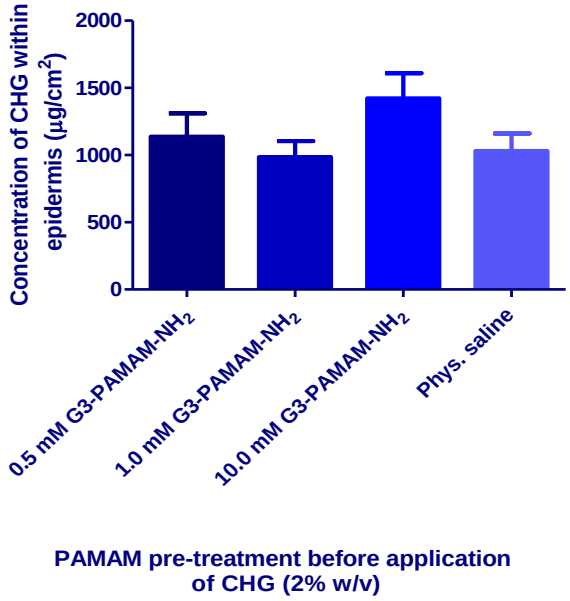

Figure 3.2. Concentration of CHG within the epidermis at 24 h after a range of skin pre-treatments. *Data is represented as the mean ± SEM. CHG was dosed in the same volume and concentration as the PAMAM treated groups after a 24 h pre-treatment of phys. saline. No statistical significance was observed between groups or treated and untreated (p>0.05).*

The total concentration of CHG (mean ± SEM) detected within the receptor fluid at 24 h for a range of PAMAM dendrimer pre-treatments is displayed in graphical form in Figure 3.3. The data was plotted as a histogram which revealed that the data was not normally distributed. A Kruskal Wallis ANOVA with a Dunn's post test confirmed that for all three concentrations of G3-PAMAM-NH_2 dendrimer skin pre-treatment tested, the total concentrations of CHG absorbed within the receptor fluids at 24 h were statistically different (p< 0.0001) from the physiological saline pre-treated skin. No significant difference in the absorption of CHG at 24 h was observed between the different PAMAM dendrimer concentrations tested (p>0.05)

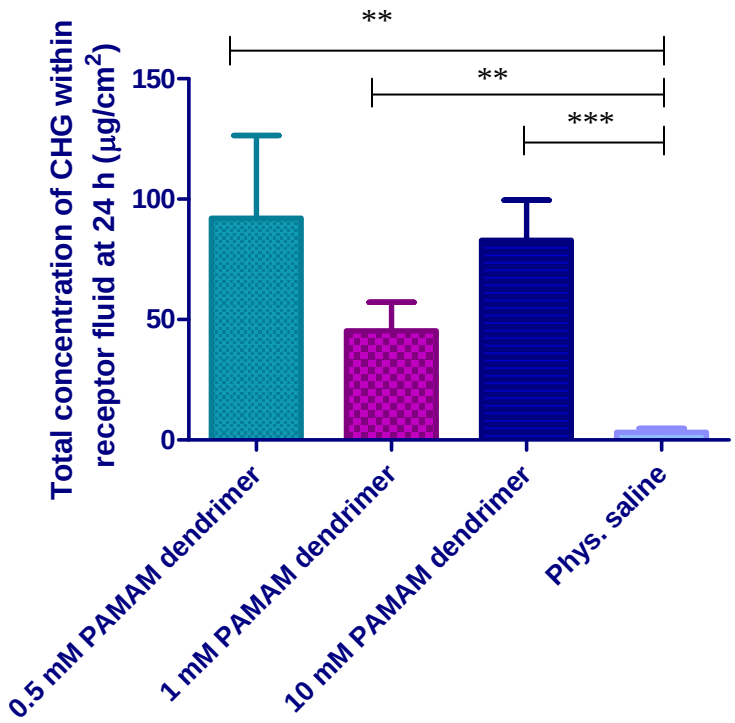

Figure 3.3 Concentration of CHG absorbed within the receptor fluid at 24 h after various skin pre-treatments. *Illustration of the (mean ± SEM) concentration of CHG permeated into the receptor fluid at 24 h (µg/cm^2) against the PAMAM dendrimer pre-treatment post application of a 2 % CHG (w/v) solution. PAMAM dendrimer pre-treated skin was significantly different from the phys. saline pre-treated skin (p<0.0001).*

After application of a PAMAM dendrimer solution to the skin it was noted that a thin film formed once the vehicle had evaporated. The PAMAM dendrimer film was tacky, transparent and viscous. Figure 3.4 illustrates the difference in appearance of the skin surface of a vehicle control compared to that of PAMAM dendrimer dosed skin. The PAMAM dendrimer film was found to be water soluble and was removed from the skin surface by agitating water across the skin surface. Due to the hygroscopic nature of PAMAM dendrimers it was not possible to determine the transepidermal water loss (TEWL) of the layer to determine whether it could be considered 'breathable' i.e. allows for TEWL.

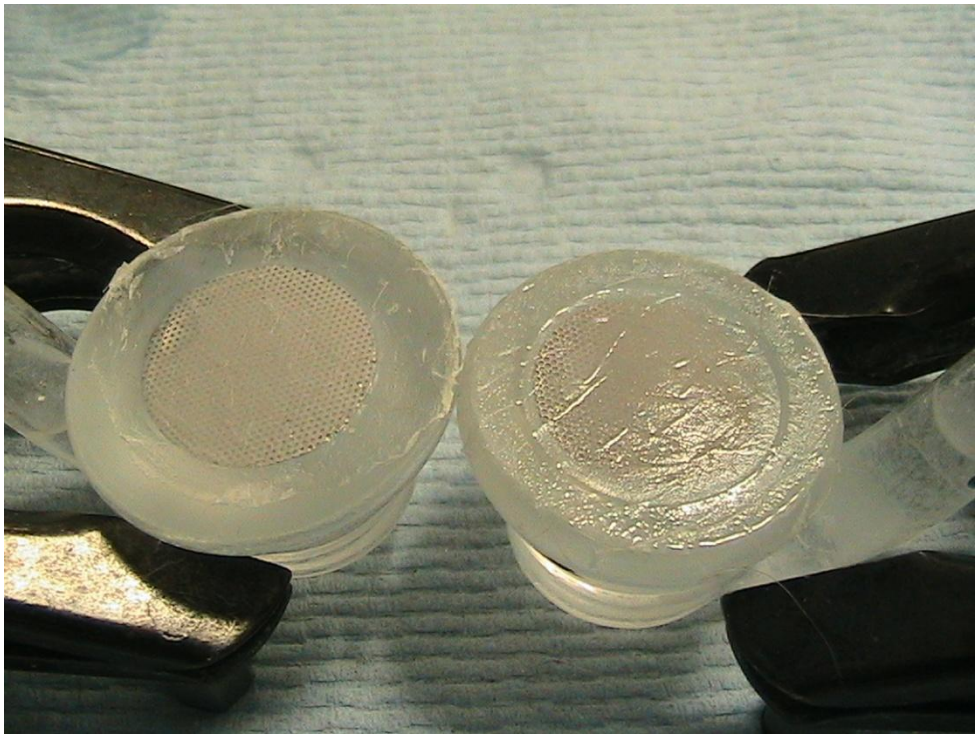

Figure 3.4. Photograph of the skin surface comparing the control to skin dosed with PAMAM dendrimer. *Franz cells with the donor chamber removed to reveal the epidermis. The Franz cell on the left was dosed with a vehicle control (H_2O:MeOH) and the Franz cell on the right was dosed with a G3-PAMAM-NH_2 dendrimer solution (10 mM, 0.2 mL). A dendrimer film across the skin surface is clearly visible on the right-hand-side.*

3.3.1 Franz diffusion cell studies using tape stripping to profile CHG within porcine dermatomed skin

The percutaneous absorption studies using porcine epidermis were used as a screening approach to determine whether a PAMAM dendrimer pre-treatment would enhance the permeation of chlorhexidine into the skin and which concentration would be most effective. The concentration chosen to be taken forward to tape stripping studies was the mid-range 1 mM solution of G3-PAMAM-NH_2 dendrimer. The tape stripping method is the gold standard in determining the distribution of a compound within the SC (OECD, 2004). To fully remove the SC, 21 tape strips were removed from each dosed Franz cell (Trebilcock *et al.* 1994) but were weighed before and after so that gravimetric analysis could be used to determine the amount of SC removed on each tape strip. The difference in weight of each tape strip was calculated to determine the mass of SC material on each tape strip which was then plotted against the tape strip number. A number of observations during this procedure are worthy of note. At around tape strip 6 the skin became very moist therefore interstitial fluid was being removed as well as SC on the tape strips and recorded within the mass data. The moisture attributed to interstitial fluid also caused the epidermis to tear during the tape stripping process, typically after the template had been placed over the dose area and pressure applied to the tape strip. It is for this reason why 21 tape strips were not obtained from the skin in every case.

Figure 3.5 illustrates the mean cumulative amount of SC material plotted against the tape strip number. The skin that was dosed with a physiological saline pre-treatment then dosed with CHG (2 % w/v) had a mean cumulative amount of SC material of 12.24 ± 2.62 mg at tape strip 20. This was comparable to the dendrimer solution vehicle control (H_2O: MeOH) that had a cumulative total amount of 14.08 ± 3.27 mg at tape strip 19. The highest mass of SC material removed was after the skin was pre-treated with the PAMAM dendrimer and a mean cumulative mass of 23.64 ± 8.11 mg was removed at tape strip 15. Also, it was noted that fewer tape strips were taken from the PAMAM dendrimer pre-treated skin as the skin was prone to tear during the procedure.

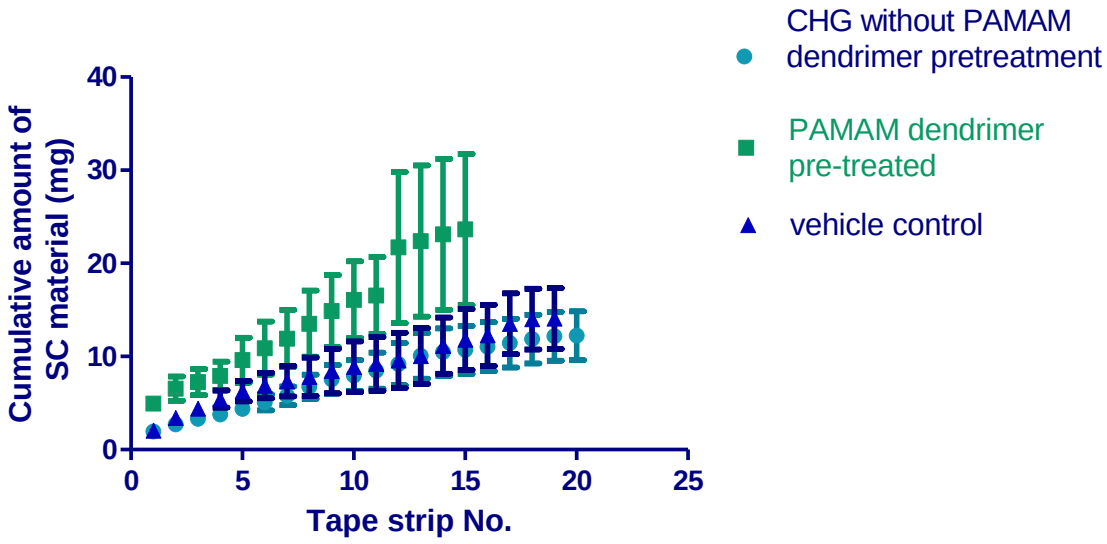

Figure 3.5. Graph illustrating the cumulative mass of SC material on individual tape strips for various skin pre-treatments. *Cumulative mass of SC material (mg) plotted against tape strip number. Light blue circles represents dermatomed (400 µm) porcine skin dosed for 24 h with CHG (2 % w/v), green squares corresponds to skin pre-treated with a 1 mM solution of G3-PAMAM-NH_2 dendrimer for 24 h before dosing with CHG (2 % w/v for 24 h). Dark blue triangles corresponds to the vehicle control (H_2O:MeOH). The data points are presented as mean ± SEM (CHG n=21, PAMAM n= 13 and vehicle control n=3).*

Figure 3.6. (a) illustrates the mean concentration of CHG extracted from the corresponding tape strips resulting in a profile of the CHG distribution. The superficial layers of the SC considered to be removed by tape strips 1-3 exhibited the highest concentration of CHG after a PAMAM dendrimer pre-treatment. The first tape strip (that is considered as having adsorbed CHG rather than having absorbed it) exhibited an average CHG concentration of 4012.91 ± 919.34 µg/mL, 2339.76 ± 1131.10 µg/mL and 1635.24 ± 296.84 (mean ± SEM) for PAMAM pretreated, vehicle control and physiological saline pretreated respectively. The higher the tape strip number (and thus the deeper within the SC) the lower the concentration of CHG was detected across all treatment groups. For example, for tape strips 7-10 the mean concentration of CHG extracted from the tape strips was 179.18 ± 63.06 µg/mL, 132.02 ± 6.35 µg/mL and 99.87 ± 23.29 µg/mL for PAMAM dendrimer pretreated, vehicle control and physiological saline pretreated skin respectively. That is approximately a 20 fold decrease in CHG concentration when compared to tape strip 1, but would still be considered a high biocidal concentration of CHG. As with tape strip 1 the PAMAM dendrimer pretreated skin demonstrated the highest concentration of CHG for tape strips 7-10, however a high variability was observed between each Franz cell. With each successive tape strip removed from the skin (after ~tape strip 6) the moisture content increased resulting in tearing of the epidermis. After the epidermis has torn the remaining skin is removed from the Franz cell and the CHG is extracted from the skin and the last tape strip which tore the epidermis is included with the skin compartment. Comparisons between the CHG concentrations at the higher tape strip

numbers were not feasible due to the low sample number of the higher tape strips due to tearing of the epidermis.

Figure 3.6 (b) illustrates the concentration of CHG calculated per mg of SC material removed on the corresponding tape strip(s). The calculation used to account for the weight of SC material can be found in section 3.2.4, Equation 3.1. If the gravimetric analysis is taken into account a different CHG distribution profile is observed within the SC (Figure 3.6 (b)). The profile appears rather irregular which may be due to the issue of the moisture that was observed on tapes strips 6 and upwards.

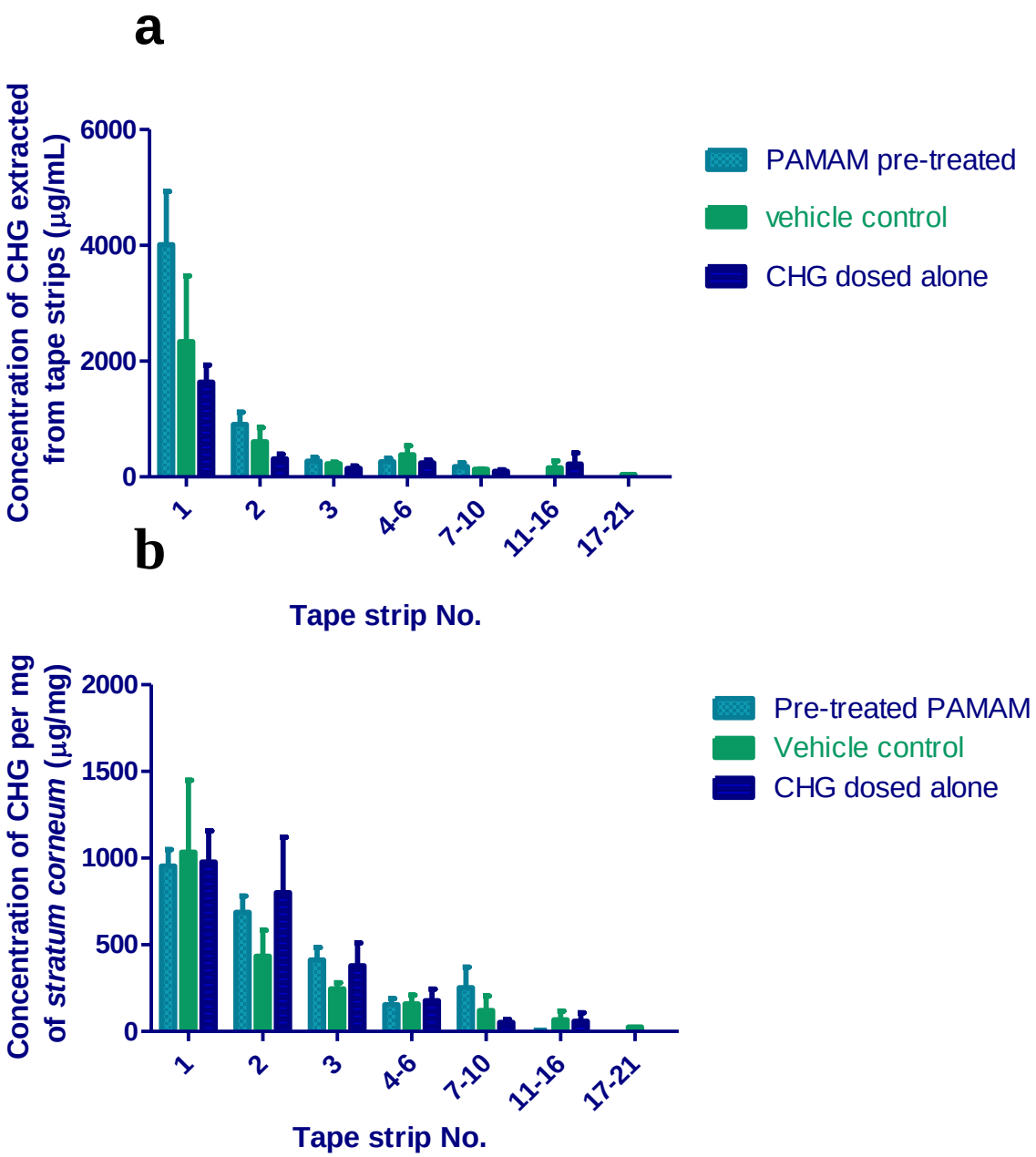

Figure 3.6. Concentration profile of CHG detected on each tape strips. *(a) Concentration of CHG (µg/mg) extracted from tapes into a fixed volume of solvent. Extraction occurred after stripping 400 µm dermatomed skin after a pre-treatment for 24 h with a 1 mM PAMAM solution of G3-PAMAM-NH_2 dendrimer, vehicle control and Phys. saline. (b) Concentration of CHG per mg of SC material weighed gravimetrically (µg/mg) after stripping 400 µm dermatomed skin after a pre-treatment for 24 h with a 1 mM PAMAM solution of G3-PAMAM-NH_2 dendrimer, vehicle control and Phys. saline Data is represented at the mean ± SEM (CHG n=21, PAMAM n= 13 and vehicle control n=3).*

Table 3.10 illustrates the mean absorption and distribution of CHG within the Franz cell system after a pre-treatment of physiological saline (0.9 % NaCl, 0.2 mL). After the excess unabsorbed CHG was removed within the wash, in this case a mean of 56.09 ± 6.56 % of applied dose (4416.09 ± 516.50 µg/cm^2), the skin surface was allowed to dry at ambient temperature. The skin was then tape stripped up to 21 times to remove the SC and assuming that the tape strips have removed the SC the mean percentage of applied dose of CHG distributed throughout the SC was found to be 16.49 ± 3.29 % (1298.03 ± 259.40 µg/cm^2). The mean percentage of applied dose considered to be absorbed at 24 h including tapes strips (SC), the remaining epidermis/dermis and the concentration detected within the receptor fluid was calculated to be 6.39 ± 1.18 % (503.10 ± 92.87 µg/cm^2). Again ~5.5 % of the dosed CHG was extracted from the glass donor chamber which is comparable to the CHG adsorbed on to the donor chambers across the studies mentioned previously within this section. A total recovery of ~85 % was achieved which is considered a good recovery when using non radio-labeled drugs. This is a CHG recovery increase of~10 % when compared to the epidermis study. This is due to an increased recovery of CHG from the skin due to extraction of CHG using tape strips from the SC.

Table 3.10. Compartmental diffusion cell data (including tape strips) of CHG concentration for the control skin pre-treatment. *Percutaneous absorption (mass balance) of CHG (2 % w/v, 1 mL, 24 h) within porcine dermatomed skin (400 µm thick) after a 24 h skin pre-treatment of phys. saline (0.9 % NaCl, 0.2 mL). Data is represented at the mean ± SEM (n=21).*

Sample (*n*=21)	CHG (µg/cm^2)		% of applied dose	
	Mean	SEM	Mean	SEM
Donor chamber	434.41	85.97	5.52	1.09
Skin wash	4416.09	516.50	56.08	6.56
Tape strips	1298.03	259.40	16.48	3.29
Epidermis/ dermis	503.10	92.85	6.39	1.18
Receptor fluid	0.02	0.02	0.0002	0.0002
Total recovered	6651.65	954.74	84.47	12.13

The percutaneous absorption and distribution of CHG within the Franz diffusion cell after a pre-treatment for 24 h of the vehicle solution without PAMAM dendrimer can be observed in Table 3.11. The concentration of CHG extracted from the glass donor chamber is again typical of the previous studies and of the recovery when the donor chamber was spiked. Also typical is the mean 48.41 ± 2.59 % recovery of CHG within the skin wash at 24 h. The mean percentage of applied dose recovered from the tape strips which are assumed to have removed the SC was 18.83 ± 6.87 % (1483.08 ± 540.78 µg/cm^2). The mean percentage of applied dose of CHG recovered from the tape strips (SC), epidermis/dermis, and receptor fluid for the vehicle control was 27.95 ± 8.98 % (2200.4 ± 707.49 µg/cm^2). This is a higher value

than the physiological saline control but still within the error range therefore the increase in absorbed CHG after being dosed with the vehicle solution is not significant (p>0.05).

Table 3.11. Compartmental diffusion cell data (including tape strips) of CHG concentration after a vehicle control skin pre-treatment. *Percutaneous absorption (mass balance) of CHG (2 % w/v, 1 mL, 24 h) within porcine dermatomed skin (400 µm thick) after a 24 h skin pre-treatment of the vehicle solution without PAMAM dendrimer (H_2O: MeOH, 82.5:17.5). Data is represented at the mean ± SEM (n=4).*

Sample (n=4)	CHG (µg/cm^2)		% of applied dose	
	Mean	SEM	Mean	SEM
Donor chamber	495.60	166.61	6.29	2.12
Skin wash	3812.01	204.40	48.41	2.59
Tape strips	1483.08	540.78	18.84	6.87
Epidermis/dermis	716.70	166.35	9.10	2.11
Receptor fluid	0.67	0.35	0.009	0.005
Total recovered	6508.07	1078.50	82.65	13.70

Table 3.12 presents the percutaneous absorption and distribution data corresponding to the Franz cells dosed with a 1 mM G3-PAMAM-NH_2 dendrimer solution pre-treatment before dosing with CHG (2 % w/v). There was an increase in the percentage of applied dose of CHG extracted from the tape strips and thus SC when compared to the physiological saline and the vehicle control. The mean percentage of applied dose recovered from the tape strips and thus the SC was 25.95 ± 5.35 % (2043.10 ± 421.68 µg/cm^2). This is the highest concentration of CHG recovered from the SC within the dermatomed study. The mean concentration of

CHG absorbed within the SC (tape strips), remaining epidermis/dermis and CHG recovered from receptor fluid was 39.64 ± 7.25 % (3121.53 ± 570.88 µg/cm^2). A mean recovery of ~85 % of the total CHG applied to the skin was recovered.

Table 3.12 Compartmental diffusion cell data (including tape strips) of CHG concentration after a G3-PAMAM-NH$_2$ dendrimer (1 mM) skin pre-treatment. *Percutaneous absorption (mass balance) of CHG (2 % w/v, 1 mL, 24 h) within porcine dermatomed skin (400 µm thick) after a 24 h skin pre-treatment of G3-PAMAM-NH$_2$ dendrimer (1 mM, 0.2 mL). Data is represented at the mean ± SEM (n=18).*

Sample (*n*=18)	CHG (µg/cm^2)		% of applied dose	
	Mean	SEM	Mean	SEM
Donor chamber	460.31	86.63	5.85	1.10
Skin wash	3142.01	401.61	39.90	5.10
Tape strips	2043.10	421.68	25.95	5.36
Epidermis/dermis	1077.50	148.99	13.68	1.89
Receptor fluid	0.94	0.21	0.012	0.002
Total recovered	6723.85	1059.11	85.39	13.45

When the skin was pre-treated with a 1 mM solution of G3-PAMAM-NH$_2$ a higher concentration of CHG was extracted from the total number of tape strips that is assumed to represent the SC. A mean concentration of 2043.10 ± 421.61 µg/cm^2 of CHG was extracted from the tapes after a PAMAM dendrimer pre-treatment, 1483.08 ± 540.78 µg/cm^2 after a vehicle solution pre-treatment and 1298.03 ± 259.40 µg/cm^2 was the mean CHG total extracted from all tape strips for physiological saline skin pre-treatment (Figure 3.7 (a)). The PAMAM dendrimer pre-treatment yielded the highest concentration of CHG from the total number of tape strips corresponding to

the SC compared to the treatment groups without the presence of the PAMAM dendrimer. This enhancement effect is not statistically significant due to the high inherent variability observed within this study.

Figure 3.7 (b) shows the mean concentration of CHG within the rest of the epidermis and dermis after the tape stripping procedure. The CHG concentration within the epidermis and dermis illustrates the same trend as Figure 3.7 (a) with regards to the CHG concentration within the SC. After a PAMAM dendrimer pre-treatment the concentration of CHG within the skin was statistically higher than that of the skin that had been pre-treated with physiological saline. No statistical difference was observed between the vehicle control and the negative physiological saline control (p>0.05).

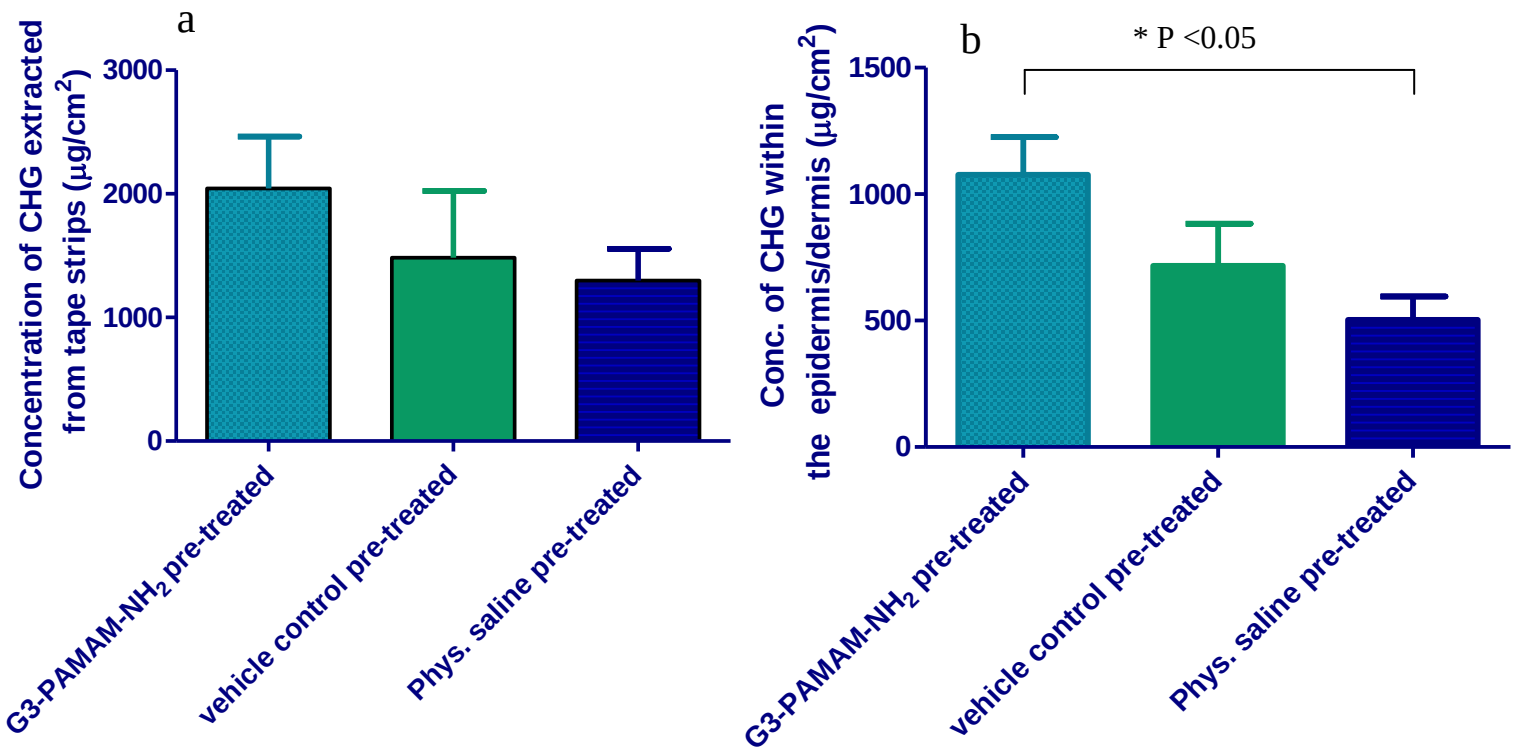

Figure 3.7 CHG concentrations extracted from tape strips and the remaining skin after various skin pre-treatments. *(a) Graph plotting the mean total CHG extracted from the tape strips (µg/cm^2) for each of the dermatomed skin (400 µm thick) pre-dose treatments. (b) Graph illustrating the mean total concentration (µg/cm^2) of CHG extracted from the remaining epidermis and dermis after the SC had been removed by tape stripping. A non parametric Kruskal-Wallis test was conducted with a Dunn's post-test. The median for all 3 groups differed significantly (p<0.05) and the Dunn's multiple comparison post-test highlighted a statistically significant difference between the G3-PAMAM-NH$_2$ skin pre-treatment with a phys. saline skin pre-treatment (p<0.05). Data represented as mean ± SEM.*

3.4 Discussion

The penetration enhancement effect of the PAMAM dendrimer was not concentration-dependent. The data displayed within this chapter exhibited similar activity over the concentration range of 1-10 mM of G3-PAMAM-NH_2 dendrimer used within the studies (Figure 3.3 showed no significant different between the PAMAM dendrimer concentrations in penetration enhancement $p>0.05$). It was shown that a PAMAM dendrimer pre-treatment (0.5 and10 mM) resulted in significant (~30 fold) increase ($p<0.0001$) in the concentration of CHG within the receptor fluid at 24 h (Figure 3.3). For a 1 mM G3-PAMAM-NH_2 dendrimer skin pre-treatment ~16 fold increase in CHG within the receptor fluid was observed though a high variability for the study was observed also. This is likely due to inherent donor-donor skin variability as 5 skin donors were utilised for the epidermis studies. Further, after a PAMAM dendrimer pre-treatment the rate of CHG absorption over 24 h increased by ~6.5-10 fold. Increasing the concentration of the PAMAM dendrimer did not proportionally increase the skin permeation of CHG. This effect was also reported for the hydrophilic drug 5-fluorouracil after a G4-PAMAM-NH_2 skin pre-treatment (Venuganti and Perumal, 2009). This may be due to aggregation of the PAMAM dendrimers at high concentrations (Klajnert and Epand, 2005).

It has been reported that a PAMAM dendrimer skin pre-treatment (24 h, unoccluded) enhanced the permeation of the hydrophobic NSAID, tamsulosin hydrochloride. A 7.5 mM solution of G3-PAMAM-NH_2 in a chloroform vehicle resulted in ~4 fold increase in the amount of Tamsulosin permeated across a snake skin

membrane when compared to the control (Wang *et al.* 2003). Further; a 1 mM solution of G4-PAMAM-NH_2 enhanced the permeation of the anti-cancer drug, 5-fluorouracil, into the skin with an increase in the permeability coefficient of the hydrophilic drug by 4-fold in a mineral oil vehicle, 2.5 fold in isopropyl myristate vehicle but decreased by half in phosphate buffered saline (Venuganti and Perumal, 2008). The permeability coefficient of the 5-fluorouracil increased after a PAMAM dendrimer pre-treatment but only from a lipophilic vehicle. Within the study outlined in Section 3.3.0 it was demonstrated that a PAMAM dendrimer pre-treatment (1-10 mM) enhanced the permeation of CHG, a hydrophilic antiseptic, across porcine epidermis from a hydrophilic vehicle. A comparison between the different species' membrane models used and their suitability for permeation are discussed in further detail in chapters 4 and 6. Previously, PAMAM dendrimers had only been shown to enhance the topical or transdermal delivery of hydrophobic drugs or hydrophilic drugs within a hydrophobic vehicle. Further, this is the first study to investigate PAMAM dendrimers as a topical penetration enhancer of an antiseptic to increase the exposure between the biocide and resident bacteria.

A PAMAM dendrimer pre-treatment reduced the lag time required for CHG to permeate the skin. Within the first 6 h it was the 10 mM PAMAM dendrimer solution pre-treatment that exhibited the highest CHG absorption. At 9-24 h it was 0.5 mM PAMAM dendrimer closely followed by 10 mM PAMAM dendrimer skin pre-treatment concentrations that resulted in the highest absorbance of CHG within the receptor fluid (Figure 3.1). This is also reflected in the calculated absorption rates of CHG dosed alone in aqueous solution in which the rate over 15-24 h time period is

considerably higher than for the 0-12 h absorption rate. The lag time for CHG permeation for the vehicle control was 12 h therefore the PAMAM dendrimer significantly reduced the lag time and would therefore have a much quicker antisepsis action. An efficacious antiseptic has been described by the Food and Drug Administration (FDA) for healthcare antiseptic drug products as-

> "a fast-acting [rapidly kills microorganisms], broad spectrum [kills a wide variety of microorganism species], persistent [suppresses regrowth of remaining microorganisms], antiseptic containing preparation that significantly reduces the number of microorganisms on intact skin" (Federal Register, 1994 and Art, 2005).

Chlorhexidine digluconate possesses these attributes but has been shown to permeate the skin very slowly with a 12 h lag time therefore by decreasing the lag time with a PAMAM dendrimer pre-treatment the antisepsis of the deeper skin layers would occur within a shorter time frame. This capability therefore fulfills the first requirement of the FDA monograph more effectively and would result in an increased efficacy. The pre-treatment of PAMAM dendrimer on porcine epidermis surprisingly did not enhance the deposition of CHG significantly within the dermatological layer. Figure 3.2 illustrates that a 10 mM PAMAM dendrimer skin pre-treatment did increase the concentration of CHG within the epidermis but it was not statistically significant when compared to the vehicle control. It appears that the PAMAM dendrimer skin pre-treatment significantly enhanced the concentration of CHG across the skin

It was observed throughout the experiments that once the vehicle had evaporated (*ca.* 3-6 h) a viscous and adhesive layer of G3-PAMAM-NH_2 dendrimer was deposited across the skin surface (Figure 3.4). This is due to the highly hygroscopic nature of PAMAM dendrimers (Uppuluri *et al.* 1998) that extract water

from the surrounding environment to exist in a gel-like state. A dense PAMAM dendrimer layer distributed across the skin surface may reduce the TEWL from the skin causing skin hydration thus acting as a possible mechanism of enhancement for the skin permeation of CHG.

Occlusion of the skin leading to increased hydration has been a known mechanism of skin penetration for many years (Wester and Maibach, 1995 and Roberts and Walker, 1993). The water content of the SC is typically 15-20 % dry weight of tissue but can increase up to 400 % of the dry weight of tissue under occlusion and increased humidity (Williams and Barry, 2012). Occlusion has been utilised as a permeation enhancer for a range of therapeutics and biomolecules including fluorescein isothiocyanate conjugated bovine serum albumin (Tan *et al.* 2009) and C^{14} acetylsalicylic acid (Fritsch *et al*. 1963). The mechanism that results in the penetration enhancement of hydrated skin is not yet fully understood as no evidence of swelling within the lipids has been found but pools of water altering the micro-structure have been observed within the intercellular lipids using freeze fracture electron microscopy (Van Hal *et al.* 1996). On hydration of the skin, corneocytes within the centre of the SC become highly swollen increasing the cell volume (Bouwstra *et al.* 2003). Hydrating the skin for permeation enhancement of a wide range of therapeutics has been used for many years with regards to ointments and occlusion, but it does not enhance the skin permeation of all compounds (Bucks and Maibach, 1999). Further mechanisms of penetration enhancement by PAMAM dendrimers are explored in the following chapter.

A tape stripping assay on porcine dermatomed skin established an increase in the deposition of CHG within the SC (tape strips) and the remaining epidermis and dermis. Gravimetric analysis was used to quantify the amount of SC material removed with each tape strip. A template was used when tape stripping in order to remove only SC material from the 2.54 cm^2 dosed region. During the experiment it was observed that at tape strip 6 and upwards a considerable portion of the weight was moisture; possibly interstitial fluid from the viable epidermis or remaining receptor fluid from underneath the skin. It has been shown that the SC hydration increases from the outer SC towards the inner *stratum granulosum* interface (Bommannan *et al.* 1990) however it is unlikely that this would account for the degree of moisture observed upon the later sequential tape strips. The cumulative amount of SC material was calculated for the PAMAM dendrimer treated skin (G3-PAMAM-NH_2, 1 mM), vehicle control and for skin pre-dosed with physiological saline. The cumulative weight of each tape strip for the vehicle control and the physiological saline pre-treated skin were very similar with overlapping error bars (Figure 5). A considerable increase in the cumulative weight of SC material removed with each tape strip was observed after a PAMAM dendrimer skin pre-treatment. Also the number of tape strips that were removed before the epidermis was torn decreased after application of PAMAM dendrimer. This suggests that the PAMAM dendrimer caused a physical effect upon the skin which resulted in the increased removal of SC material.

There are a number of reasons why the amount of SC material removed on a single tape strip can vary. Inherent experimental conditions such as anatomical site, age (Myer *et al.* 2006 and Lademann *et al.* 2009) and season of the skin donors were

accounted for as the skin was collected and prepared in parallel. Other extrinsic variables include the amount of pressure applied to remove each tape strip, duration of pressure applied and speed of tape strip removal (Löffler *et al.* 2004). These variables were reduced as all the tape stripping was conducted by the author using the same adhesive tape throughout and the same thumb to apply pressure to the skin for an equal time period of 5 seconds. The increase in SC material removed from each sequential tape strip for the PAMAM dendrimer pre-treatment is likely due to the PAMAM dendrimer itself as the applied formulation can have a marked effect on the tape stripping procedure (Schwarb *et al.* 1999 and Weighmann *et al.* 1999). PAMAM dendrimers have been shown to interact with skin lipids (Venuganti *et al.* 2009) and within chapter 4 G3-PAMAM-NH_2 was shown to cause peak shifts of the amide I and II bands indicating alteration of the protein-lipid organisation within the SC. This physical effect upon the skin caused by the PAMAM dendrimer could explain the increased mass of SC material observed upon each sequential tape strip.

Figure 3.6 (a) reports the concentration of CHG as a function of the tape strip number. The concentration of CHG within the first 3 tape strips was highest in the order of PAMAM dendrimer > vehicle control > physiological saline pre-treated skin. The CHG concentration was slightly higher for the vehicle control for tape strips 4-6 but for tape strips 7-10 the PAMAM dendrimer pre-treated skin revealed a higher concentration of CHG. The amount of SC material removed with increasing tape strip number decreases as observed in Figure 3.5. Figure 3.6 (b) illustrates the same data but normalises (Equation 3.1) the drug concentration to the weight of the SC removed. The resulting permeation profile is irregular in nature which is likely due to

the inclusion of moisture within the gravimetric analysis, skewing the profile plot of CHG within the SC. It is for this reason that further analysis such as calculation of drug concentration as a function of SC depth was not pursued.

The results of the tape strip study (Tables 3.10-12) show that after a 1 mM PAMAM dendrimer skin pre-treatment a higher concentration of CHG was extracted from the tape strips (SC) and from the remaining epidermis and dermis (2043.095 ± 421.683 μg/cm^2 and 1077.502 ± 148.991 μg/cm^2 respectively). The CHG concentration in decreasing order was PAMAM dendrimer > vehicle control > physiological saline pre-treated skin for both tape strips (and thus SC) and for the remaining epidermis and dermis (Figure 3.7). There was a statistically significant increase in CHG concentration (p<0.05) within the epidermis and dermis when the PAMAM pre-treated skin was compared to the physiological saline pre-treated skin. The results indicate that the PAMAM dendrimer pre-treatment increases the deposition of CHG within not only the superficial layers of the SC but also the epidermis and dermis. The aim of this study was to increase the penetration and retention of CHG within the skin and this has been demonstrated within the epidermis and dermatomed percutaneous absorption studies within this section. An increase in the deposition of CHG within the skin may improve antisepsis efficacy by increasing the exposure of opportunistic pathogens to CHG (Karpanen *et al.* 2010).

3.5 Conclusion

The aim of this chapter was to determine whether a PAMAM dendrimer skin pre-treatment would enhance the permeation and distribution of CHG within the layers of porcine skin. This study was conducted to confirm that the PAMAM dendrimer without the presence of CHG does have a physical interaction with the skin resulting in a penetration enhancement effect. As PAMAM dendrimer pre-treatment studies were conducted any dendrimer-CHG interactions resulting in an increased permeation are shown not to be the only contributing factor to the increased skin delivery of CHG observed. PAMAM dendrimers have previously been utilised as a novel dendritic penetration enhancer of the hydrophilic compound 5-fluorouracil (Venuganti and Perumal, 2008). There was a gap in the literature regarding their application to other hydrophilic compounds such as CHG and their mechanism of action. This chapter has established for the first time that a G3-PAMAM-NH_2 dendrimer pre-treatment does indeed enhance the permeation of CHG through porcine epidermis and also increases the concentration of CHG localized within the upper skin strata.

This Chapter in its entirety illustrates how PAMAM dendrimers enhance the distribution of CHG within the skin thus increasing the interaction of the conventional biocide with opportunistic skin pathogens. This enhanced antisepsis could potentially have significant benefits to the health care sector by means of reducing the occurrence of nosocomial infectious diseases.

4.0. Elucidation of the interaction between PAMAM dendrimers and porcine skin.

4.0 Introduction

4.0.1 Interaction between PAMAM dendrimers and the skin

The exact mechanism of enhanced topical and transdermal drug delivery is still unknown but is suggested to be in varying degrees the following; a) action as a drug release modifier thus increasing drug dissolution, b) preferential accumulation within the appendages of the skin and c) impairing the barrier function of the SC (Chapter 3 and Sun *et al.* 2012). PAMAM dendrimers have been suggested as a drug release modifier that has a cyclodextrin like mechanism in that they act as a carrier system for indomethacin (log P 4.3) (Wang *et al.* 2003). As with PAMAM dendrimers, lipophilic drugs form an electrostatic or hydrophobic complex with cyclodextrins that then increases the solubility of a drug within an aqueous vehicle. This then results in an increase in the concentration of drug that partition into the SC (Legendre *et al.* 1995). The drug that is encapsulated within or complexed to nanoparticles such as PAMAM dendrimers and cyclodextrins are in a solubilized form but are only poorly soluble within the aqueous vehicle. This forms a high thermodynamic driving force once the nanoparticle has carried the drug to the SC surface; on release the lipophilic drug partitions into the lipophilic SC as opposed to dissolving within the aqueous vehicle.

The carrier mechanism for facilitating drug delivery to the SC would account for the enhanced permeation of lipophilic drugs within the skin but not for hydrophilic drugs therefore there must be other mechanisms at work. Another

example of this possible mechanism was given by Küchler *et al.* (2009) where it was demonstrated that PAMAM dendrimers did not penetrate the SC but did enhance the topical delivery of the lipophilic nile red (log P 3.8) by 8 fold within the SC and 13 fold within the viable epidermis (Küchler *et al*. 2009).

A vehicle-dependent mechanism was proposed by Venuganti and co-workers, who used potent vehicles such as IPM and mineral oil in conjunction with lower generation PAMAM dendrimers to enhance the permeation of a hydrophilic drug (Venuganti *et al.* 2008). Using potent solvents that impair the barrier nature of the SC via fluidisation or extraction of skin components may aid the ingress of lower generation PAMAM dendrimers within the SC. The synergism between potent solvent and the dendrimers resulted in an increase in the partitioning of the hydrophilic 5-Fluorouracil (log P -0.89) within the SC. The same group demonstrated that the surface groups of the PAMAM dendrimer affected the permeability coefficient of the 5-Fluorouracil in decreasing order of G4-PAMAM-NH_2 > G4-PAMAM-OH > G4-PAMAM-OH. They also revealed that the enhancement in the drug permeability coefficient was inversely proportional to the molecular weight of the PAMAM dendrimer. Further, structure-activity relationship studies showed that increasing the concentration of the PAMAM dendrimer did not proportionally increase the skin permeation of the 5-Fluorouracil (Venuganti *et al.* 2009). This was also observed in Chapter Three, in that increasing the concentration of G3-PAMAM-NH_2 within the pre-treatment and co-treatment does not result in a proportional increase in the permeation of CHG.

Cationic dendrimers have been shown to have a physical effect on the skin, decreasing the barriers resistance. Cationic PAMAM dendrimers are protonated at

the pH of the skin surface which has a pH of 5 (Liu *et al.* 2009). It was previously demonstrated using differential scanning calorimetry (DSC) and Raman spectroscopy that the charged G4-PAMAM-NH_2 dendrimers interact with the hydrophilic head groups of phospholipids and can incorporate themselves within the lipid bilayers, altering its structure and fluidity (Gardikis *et al.* 2006). This interaction of cationic dendrimers with the hydrophilic and anionic components of membranes can result in an increase in permeability (Hong *et al.* 2004 and Hong *et al.* 2006). Shcharbin *et al.* (2006) also noted that PAMAM dendrimers can cause alteration in the lipid architecture; the importance of the intercellular lipid organisation as a property of the skin's barrier was discussed in detail within the general introduction. Cationic dendrimers were shown to interact with the hydrophilic head groups of ceramides and fatty acids resulting in an increase in the trans-epidermal water loss (TEWL) as a result of barrier disruption (Venuganti *et al.* 2009). In mind of the PAMAM dendrimer skin pre-treatment as well as physical perturbation of the skin components it should also be noted that the cationic PAMAM dendrimers retained within the superficial layers of the SC may alter the ionic charge and possibly hydrophobicity of the SC. The cationic PAMAM dendrimers may act as a depot within the superficial layers of the SC for the enhanced partitioning of hydrophilic or charged drugs within the SC.

Nanoparticles have been reported to preferentially accumulate within the hair follicles of the skin. It was shown that due to the follicular penetration of polystyrene nanoparticles, the topical delivery of nile red was enhanced when compared to the dye in free solution (Alvarez-Roman *et al.* 2004(a) and Alvarez-Roman *et al.* 2004(b). PAMAM dendrimers labeled with a fluorescein isothiocyanate fluorophore were found to preferentially accumulate within follicles

found within the porcine skin. The follicular route may therefore heavily contribute to the enhanced skin permeation of a drug complexed or encapsulated within a nanoparticle including PAMAM dendrimers. It is possible that the cationic PAMAM dendrimer acts as a depot within the follicles and aids penetration of large polar molecules that would typically find it difficult to penetrate the intact SC.

Other mechanisms that may contribute to the penetration enhancement effect include the extraction of skin components. Cyclodextrins have been shown to remove SC lipids and proteins that would decrease the barrier nature of the skin (Bentley *et al.* 1997). This mechanism of skin barrier impairment has not yet been investigated for PAMAM dendrimers and will therefore be covered within this Chapter. Hydration caused by the occlusion of the SC surface by viscous PAMAM dendrimers and an increase in wettability and reduction of surface tension due to the presence of PAMAM dendrimers should also be considered as a possible contributing penetration enhancing effect.

4.0.2 Rationale for the investigation of a PAMAM dendrimer skin pre-treatment interaction with the skin.

In the previous Chapter it was ascertained that PAMAM dendrimers act as a penetration enhancer for CHG after a pre-treatment on the skin. This chapter aims to assess the interactions that occur between the PAMAM dendrimer and the skin using a range of techniques. It may be possible to design optimized PAMAM dendrimers and formulations for topical or transdermal delivery of therapeutics once the mechanism of penetration enhancement has been elucidated. This chapter addresses whether a cationic PAMAM dendrimer skin treatment impairs the SC barrier nature by increasing TEWL and decreasing the TEER. Further, a

number of novel strategies employed within this chapter include optical coherence tomography (OCT) that is a non-destructive and non-invasive imaging system capable of revealing structural changes within optical cross-sections of opaque tissue with a thickness of up to 2 mm. This chapter undertakes an OCT investigation in order to delineate the mechanisms of the interactions of PAMAM dendrimers with the porcine skin surface.

A biochemical test for the determination of protein concentration was conducted to determine whether PAMAM dendrimers extract skin components to reduce the resistance for enhanced drug delivery. Moreover, the concentration of cholesterol extracted from the SC by PAMAM dendrimers was determined through solvent extraction and HPLC methods. To investigate the direct interactions between the PAMAM dendrimer and the components of the SC, it is necessary to first isolate the SC using proteolytic enzymes (Haigh and Smith, 1994). This then allowed for the elucidation of the interactions between the dendrimer and SC using attenuated total reflectance Fourier transform infra-red spectroscopy (ATR-FTIR).

4.0.3 Aims and objectives

The aim of this Chapter is to explore the skin modulation effects, i.e. possible barrier alterations, after application of PAMAM dendrimer to porcine skin that may aid the penetration of drugs within the skin.

To delineate the interactions between PAMAM dendrimer and porcine skin a number of objectives to be addressed:

(i) A skin barrier integrity study before and after a PAMAM application utilising both TEER and TEWL.

(ii) Non-invasive visualisation of the PAMAM dendrimer on the skin surface by optical coherence tomography (OCT).

(iii) Classical histological analysis of cryo-sectioned dermatomed skin sections after PAMAM dendrimer treatment.

(iv) Attenuated total reflectance Fourier transform infrared spectroscopy (ATR-FTIR) analysis of the PAMAM-skin interactions

(v) To determine whether PAMAM dendrimers extract skin components, i.e. cholesterol and skin lipids.

4.1 Materials and methods

4.1.0 Measurement of Transepidermal Water Loss (TEWL) and Transepithelial Resistance (TEER) after a PAMAM dendrimer treatment

The barrier integrity was measured after dosing porcine skin with PAMAM dendrimer for a 24 h contact time. The Franz cells were set-up as outlined in Sections 3.1.1 and 3.1.2. The treated Franz cells were dosed with G3-PAMAM-NH_2 (10 mM) and the controls were dosed with the vehicle control (water:methanol, 35:65) and sodium dodecyl sulphate (SDS) (5 % w/v, 0.2 mL) as a positive control and were left for a 24 h contact time. After which, the G3 PAMAM-NH_2 was removed by rinsing with 2 mL aliquots of distilled water (10 mL in total) over the surface of the dosed skin. When measuring the TEWL, the Franz cells were left to dry at ambient temperature until the skin surface was dry, typically around 3 h. The Franz cells were then placed in a humidity chamber (Stuart Scientific incubator SI60, Bibby Scientific, Stone) where the relative

humidity (RH%) was controlled between 40-45% measured using a precision hygrometer (Diplex, Meinheim, Germany) and at skin temperature of 32ºC (Chilcott *et al.* 2002). The RH% was controlled by placing a 50 mL beaker of a saturated solution of K_2CO_3 in distilled water within the humidity chamber (O'Brien, 1947). The Franz cells were left to equilibriate within the humidity chamber for a minimum of 3 hours before the TEWL measurements were taken. TEWL was measured on an Evaporimeter EP2 (Servo-med, Varburg, Sweden) within an environmental chamber maintained at 32ºC and 40-45 % RH as the holding humidity chamber. The sensor was placed over the skin so that it gently contacted the skin surface for 45 seconds and then for a final 15 seconds an average TEWL in $g/m^2/h$ was recorded with the standard deviation.

To measure the TEER after the G3-PAMAM-NH_2 dose preparation had been washed from the skin surface, 2 mL of physiological saline (0.9 % w/v) was added to the donor compartment and the electrical resistance across the porcine skin was measured as previously outlined in Section 3.2.1.

4.1.1 Optical Coherence Tomography (OCT) analysis of the skin surface after dosing with PAMAM dendrimers

The diffusion cells that had passed the integrity check were removed from the water bath and the skin surface was allowed to air dry for 2 h at ambient temperature. 4.5 mL of physiological saline was added to the receptor chamber of each Franz cell. The Franz cells were placed in the water bath (32°C ± 1°C) on a submersible stirring plate for 30 minutes and allowed to equilibrate. Two generations of PAMAM dendrimers, G3-PAMAM-NH_2 and G3.5-PAMAM-COOH

(Sigma Aldrich, UK) in two concentrations, 5 mM and 10 mM, were applied in this study. The vehicle solutions, the mixture of water and methanol in the ratio of 65:35 for G3-PAMAM-NH_2, and 82.5:17.5 for G3.5-PAMAM-COOH have been used as the control. 0.2 ml solution was placed on to the skin surface and incubated for a given contact time before taking OCT images. Anhydrous glycerol was applied to the skin surface as a positive control (0.2 mL). To determine whether the PAMAM dendrimer reaction with the skin is reversible, the applied PAMAM dendrimer layer was removed from the skin surface by rinsing 2 mL aliquots of distilled water (10 mL in total) across the skin surface. Care was taken not to impair the barrier of the skin. The skin surface was then blotted dry with adsorbent paper.

To visualise the interaction of PAMAM dendrimers with the skin surface, a custom built polarization sensitive OCT was used. A laboratory built bench-top optic fibre-based time-domain polarization sensitive-OCT (PS-OCT) system was used in this study which employed a 1300 nm superluminescence diode with a bandwidth of 52 nm. The beam from the diode is sent through a polarizer, a polarizer modulator and then split 50/50 by a 2x2 all-fibre beam splitter into a sample and reference arm. After recombination, the polarized light is sent through a polarization beam splitter. The interference fringes are detected with two balanced detectors, for horizontal and vertical polarization. The system has an axial resolution of 14 μm in free space and a penetration depth up to 2 mm. The PS-OCT images were scanned at 100 Hz.(Bagnaninchi *et al.* 2007).

4.1.2 Histological analysis of PAMAM dendrimer dosed porcine skin

Haematoxylin and eosin are classical stains which have been used to visualise morphological features of a vast range of biological tissue and cells. Haematoxylin is used to stain the nuclei of cells dark blue whilst the counter-stain, eosin stains the cytoplasm pink offering a great contrast. This staining technique was used to visualise any morphological changes apparent within the SC after dosing with G3-PAMAM-NH_2 dendrimer for 24 h. G3-PAMAM-NH_2 (10 mM, 0.2 mL), vehicle control (water:methanol, 65:35) and a SDS (5 % w/v, 0.2 mL) positive control were dosed on to dermatomed skin mounted on Franz cells as outlined in Section 3.2.3. The samples were cryo-sectioned as opposed to tape stripped. The flank of the porcine skin was removed using a scalpel, leaving only the dosed skin area. The samples were snap frozen in liquid nitrogen and then embedded in optimal cutting temperature embedding material. They were placed in the cryostat chamber set to a temperature of -28ºC before being sectioned in to 8 µm thick sections using a Leica CM1850 cryostat. Occasionally cryospray (Cellpath, UK) was used to reduce the temperature of the anti-roll plate to prevent the porcine skin slices from curling. The skin sections were then captured onto poly-L-lysine covered microscope slides and rested in a trough of 3 % glacial acetic acid in methanol (v/v) to fix the samples to the slide.

The skin sections were placed in a tray of haematoxylin and were left for 60 s. To remove excess haematoxylin, the samples were placed under a gentle flow of warm tap water to act as a weak alkali to oxidise the hematoxylin to form an insoluble blue aluminium haematin complex that stains the nuclei of the cells dark blue (Cooksey, 2010). The sections were then differentiated in a 0.3 %

HCL/ethanol solution until the background tissue that was unstained appeared colourless. The sections were then rinsed under tap water and placed in an eosin solution made up in water. To remove excess eosin the samples were rinsed in 50 % ethanol (v/v). The sections were tapped dry and dehydrated in a series of ethanol solutions. The sections were placed in a 50 %, 70 %, 80 % and 100 % series of ethanol/ water solutions for 3 minutes at each ethanol concentration. The sections were cleared using histoclear to improve the contrast of the staining and mounted using dibutyl phthalate in xylene (DPX) mountant (Khitam, 2011). The skin sections were visualized on a Nikon Eclipse E200 microscope and the images were captured on a Nikon DS-Fi 1 with a Nikon digital sight at various magnifications (x10-x40).

4.1.3 Isolation of porcine SC

The porcine SC was isolated by floating porcine epidermis prepared as outlined in Section 3.2.1 onto a trypsin solution (0.01 % w/v made up in PBS). The samples were then placed in a shaking incubator (150 RPM) at 37ºC for 6 h. The digested epidermis was carefully washed from the SC with distilled water and the SC was floated on distilled water and captured on aluminium foil. The SC was gently refloated until the membrane was stretched out without any air bubbles on to the foil. The SC was then washed with ice cold acetone for 10 s and placed in a dessicator over zeolite for 72 h. This method was adapted from Yamane *et al.* 1995.

4.1.4 ATR-FTIR analysis of the interaction between PAMAM dendrimer and porcine SC

To determine whether there are any conformational changes through direct interactions between PAMAM dendrimers and isolated SC, ATR-FTIR spectra were obtained and analysed for differences in PAMAM treated and untreated samples. SC was isolated as previously outlined in section 4.1.3. After the drying process a hole punch was used to punch out 5 mm disks of SC and the foil backing was removed. Each sample was incubated at 32ºC in 200 µL of 10 and 5 mM solutions of G3-PAMAM-NH_2, a 5 mM G3.5-PAMAM-COOH, respective vehicle controls (water:methanol), and a PBS negative control. After a 24 h contact time the SC was removed from the solutions and blotted dry on filter paper. Each sample was placed on the diamond of the ATR attachment (GladiATR, Pike Technologies, Wisconsin, USA) on a Thermo Scientific Nicolet iS10 (Hemel Hempstead, UK). 32 scans were taken with an 8 cm^{-1} resolution. The spectra were analysed using OMNIC software suite (Thermo Scientific, Hemel Hempstead, UK).

4.1.5 Determination of skin cholesterol extraction by PAMAM dendrimers

PAMAM dendrimers were incubated on the skin surface of porcine dermatomed skin (400 µm thick) to determine whether skin cholesterol or skin lipids were extracted during a 24 h time frame. Franz cells were set-up as outlined in Sections 3.2.1-3.2.3 and 200 µL of a positive control (cholesterol: methanol, 3:2), a vehicle control (water:methanol, 65:35) and a 10 mM solution of G3-PAMAM-NH_2 dendrimer were applied to the skin. The Franz cells were kept under occluded conditions with Vaseline rubbed around the top of the donor chambers so that the taut parafilm was secure as to not leave gaps for the dosed

vehicle to evaporate. After a 24 h contact time at 32ºC ± 1ºC, 4 mL of physiological saline (0.9 % w/v) was added to each of the donor chambers in 2 mL aliquots and agitated over the skin surface with a Pasteur pipette. The 4 mL of physiological saline was added to a vial that contained 4 mL of diethyl ether. The vials were vortex mixed to agitate the solvent extraction and were left for a 4 h period. After this, the 4 mL aqueous phase was decanted into a labeled vial and placed into the fridge (4ºC ± 1ºC) until required.

The diethyl ether phase was centrifuged at 5000 RPM for 5 minutes and the supernatant was decanted into a solvent cleansed vial. This was then blown down under a stream of nitrogen until the ether had evaporated and reconstituted in 1 mL of isopropanol. The samples were then transferred into a clean and labeled 2 mL HPLC vial for HPLC analysis. This method was modified from an outlined method found in Legendre *et al.* 1995. The HPLC method used to determine total cholesterol content was an isocratic acetonitrile: isopropanol 50:50 mobile phase at a flow rate 1 mL per min, the column oven temperature was set to 25°C (Duncan *et al.* 1979). The injection volume was 50 µL and detector channel wavelength used was set to 200 nm.

A cholesterol standard (Sigma Aldrich, Loughborough, UK) was used as purchased and a series of standard solutions made up in isopropanol ranging from 1-100 µg/mL were used to validate the method on the Shimadzu HPLC described previously in Section 3.2.5. The results of the validation assay can be found in appendix 2. The standards were found to be linear over the concentration range chosen (1-100 µg/mL) as shown by an R^2 value of 0.9992 and were also found to be reproducible with an RSD% of 1.15% for 6 replicate injections of the cholesterol

standard 25 µg/mL. The limit of quantification was calculated to be 1.186 µg/mL using Equation 4.1 and the limit of detection was calculated to be 0.356 µg/mL using Equation 4.2 (*n*=6).

$$\mathrm{LOQ} = 10\ x\ \left(\frac{SD}{m}\right)$$

Equation 4.1 Calculation of the limit of quantification. *SD corresponds to the standard deviation and m corresponds to the gradient of the slope.*

$$\mathrm{LOD} = 3\ x\ \left(\frac{SD}{m}\right)$$

Equation 4.2 Calculation of the limit of detection. *SD corresponds to the standard deviation and m corresponds to the gradient of the slope.*

4.1.6 Determination of skin protein extraction by PAMAM dendrimers

The aqueous phases of the solvent extractions from section 4.19 were used to determine the concentration of soluble proteins extracted from the skin by PAMAM dendrimers. All chemicals used within the protein quantification assay were used as purchased from Sigma Aldrich (Dorset, UK). A micro Lowry assay with Peterson's modification was used; the Lowry solution contains sodium dodecylsulphate (SDS) which enables solubilisation of lipo-proteins (Lowry *et al.* 1951). Peterson's modification was used to overcome interference from other biomolecules such as amino acids, EDTA, sucrose by precipitating the protein in deoxycholate (DOC) and trichloroacetic acid (TCA) (Peterson, 1977). The protein quantification occured as a result of two chemical reactions; (i) biuret reaction, in which alkaline cupric tartrate reagent forms complexes with the peptide bonds of the protein and (ii) reduction of the Folin and Ciocalteu's phenol reagent which generates a deep purple colour. This colour change was monitored by measuring

the absorbance at a wavelength of 700 nm. Firstly, 1 mL protein standard (bovine serum albumin) solutions were prepared in distilled water at a protein concentration range of 50-400 µg/mL. 1 mL of each of the aqueous phase dendrimer-skin extraction samples was transferred into a 2 mL snap cap tube. Also, a blank of 1 mL of distilled water was also placed in a labeled 2 mL snap cap tube. To the standards, blank and samples, 0.1 mL of a 0.15% DOC solution (w/v aqueous solution) was added. The 2 mL snap cap tubes were then vortex mixed and left to stand for 10 minutes. After a 10 minute contact time, 0.1 mL of a 72 % (w/v) solution of TCA was added to each 2 mL snap cap tube and then each sample was again vortex mixed and left for 10 minutes. After the protein had precipitated the supernatant was decanted and removed.

The protein pellets were dissolved in 1 mL of Lowry reagent (5 % w/v aqueous solution) and were then transferred into a test tube. 1 mL of distilled water was used to wash the 2 mL snap cap tube and transferred into the respective test tube. The samples were left to stand for 20 minutes to allow the protein to dissolve. Then, 0.5 mL of Folin and Ciocalteu's phenol reagent were rapidly mixed into each test tube and the purple colouration was allowed to develop for 30 minutes. Immediately after a 30 minute time point, 1 mL of the standards, blank and samples were transferred to a quartz cuvette and the absorbance at a wavelength of 700 nm was recorded. The BSA protein standards were used to construct a calibration curve used to calculate the protein quantification of the unknown dendrimer-skin extraction solutions. The R^2 value of the calibration curve was 0.9900.

4.1.7 Statistical data analysis

All data is presented as the mean ± SEM unless otherwise stated and were analysed using GraphPad Prism® version 5 (San Diego, USA). Prior to statistical analysis all data were placed in to a histogram to check for normality. To determine whether the difference in TEER was significant, when comparing the PAMAM dendrimer treated skin with the vehicle control treated skin, a Mann Whitney test was conducted as the data was not normally distributed. The same statistical analysis was also applied to determine if there was a significant difference in TEWL comparing the PAMAM dendrimer treated skin with the vehicle control treated skin (see section 4.2.0). In section 4.2.6 a Kruskal Wallis test was conducted to determine whether a peak shift after application of 10 mM and 5 mM G3-PAMAM-NH_2 dendrimer to isolated SC is significantly different from the vehicle control dosed SC (Figure 4.15). Further in section 4.2.6 a Mann Whitney test was applied to the data in Figure 4.19. This was to determine whether the shift in peak corresponding to the CH_3 asymmetric stretch was significantly different between the G3.5-PAMAM-COOH dendrimer treated SC and the vehicle control treated SC (p<0.05).

4.2 Results section

4.2.0 Measurement of Transepidermal Water Loss (TEWL) and Transepithelial Resistance (TEER) after application and removal of G3-PAMAM-NH_2 dendrimer.

The previous chapter showed that by pre-treating the skin with a PAMAM dendrimer application, a significant increase in the CHG concentration can be achieved within the skin. This section was conducted to establish a mechanism of enhancement. TEWL and TEER are commonly used methods to determine any changes to the integrity of the skin barrier. Both methods were utilised to illustrate the change in TEWL or TEER after a 24 h contact time with the highest PAMAM dendrimer solution tested (G3-PAMAM-NH_2, 10 mM). Figure 4.1 shows the change in TEWL and TEER that occurred after dosing the skin with a G3-PAMAM-NH_2 solution (10 mM, 0.2 mL) for 24 h and the vehicle solution (water: methanol, 65:35, 0.2 mL) after a 24 h contact time. The mean change in TEER when comparing pre-dose integrity to post dose integrity was 2.55 ± 0.53 kΩ for G3-PAMAM-NH_2 dendrimer (10 mM, 0.2 mL) compared to 2.45 ± 0.47 kΩ for the vehicle control treated skin (mean ± SEM, *n*=18). A Mann Whitney test (U=162.0, *n*=18, *p*>0.05 two-tailed) showed that there was no significant difference in TEER (non-parametric data) between the PAMAM treated skin (median-2.23 kΩ) and the vehicle control treated skin (2.04 kΩ). The mean change in TEWL when comparing pre-dose integrity to post dose integrity was 2.76 ± 1.47 g/m^2h for G3-PAMAM-NH_2 (10 mM, 0.2 mL) compared to 3.08 ± 1.31 g/m^2h for the vehicle control treated skin (mean ± SEM, *n*=18). A Mann Whitney test (U=129.0, *n*=18, *p*>0.05, two-tailed) showed that there was no significant difference in TEWL (non-

parametric data) between the PAMAM treated skin (median-2.25 g/m^{2}h) and the vehicle control treated skin (median- 3.73 g/m^{2}h).

The highest change in TEER and TEWL in the PAMAM dendrimer treatment group corresponds to the same skin donor. A 5% SDS (w/v) solution was also applied to Franz cells (*n*=3) as a positive control to indicate severe damage to the skins barrier integrity. The positive control yielded a decrease in TEER of 5.34 ± 0.82 kΩ and an increase in TEWL of 48.74 ± 4.32 g/m^{2}h that indicates the surfactant had caused an extensive reduction in skin barrier integrity as anticipated.

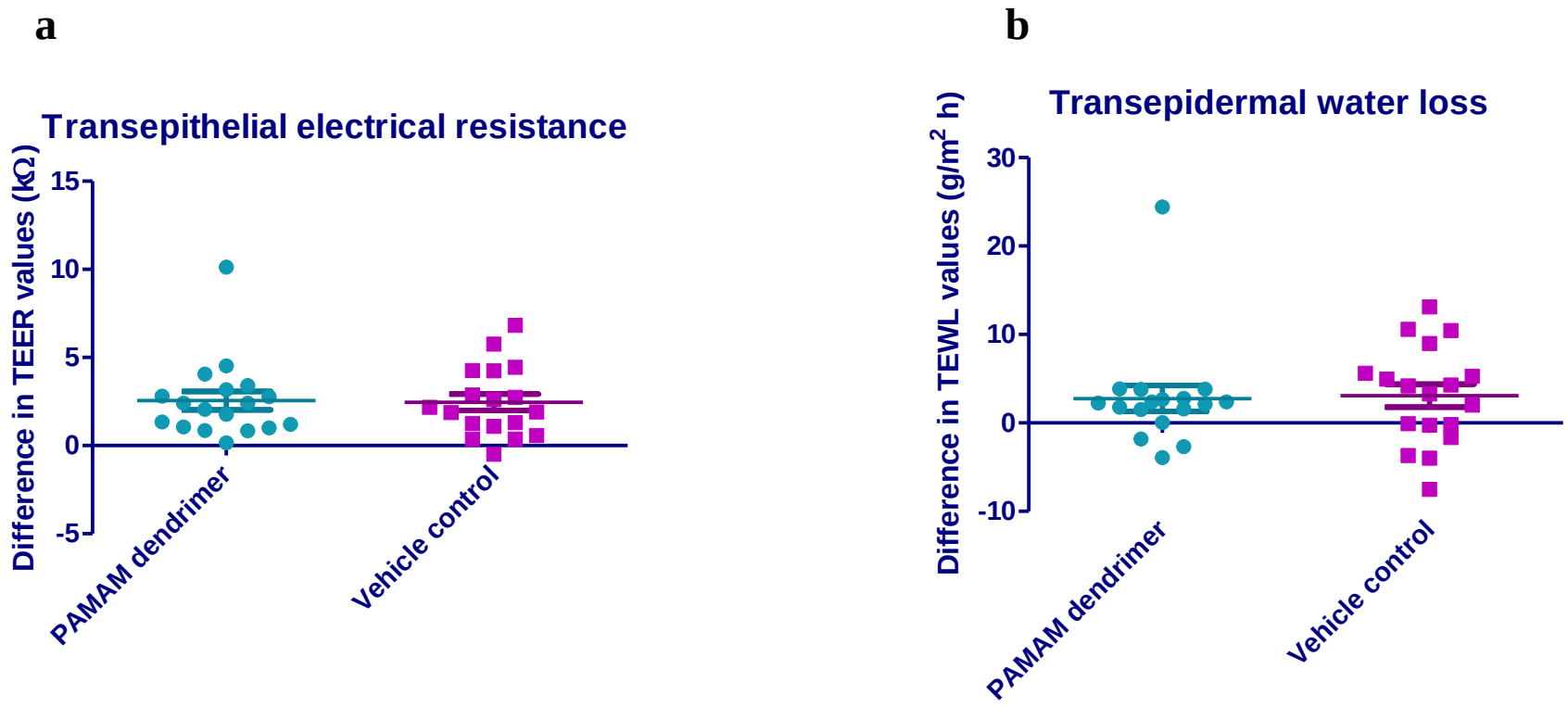

Figure 4.1. Measurement of the barrier integrity of the skin before and after dosing with PAMAM dendrimer *(a) Difference in TEER before and after dosing with G3-PAMAM-NH_2 dendrimer (10 mM, 0.2 mL) for 24 h (mean – 2.55 ± 0.53 kΩ) and the difference in TEER before and after dosing the skin with a vehicle control solution (2.45 ± 0.47 kΩ mean ± SEM). (b) corresponds to the difference in TEWL before and after dosing with PAMAM dendrimer (10 mM, 0.2 mL) for 24 h (2.76 ± 1.46 g/m^2h) and the difference in TEWL before and after dosing the skin with a vehicle control solution (water: methanol, 65:35) for 24 h (3.08 ± 1.31 g/m^2h) (n=18 ± SEM)*

4.2.1 Optical Coherence Tomography (OCT) to delineate the interactions of PAMAM dendrimers with the porcine skin surface.

4.2.1.0 The effect of amine functionality of the PAMAM dendrimer on the porcine skin surface

The OCT images shown in Figure 4.2 illustrate non-invasive imaging of porcine dermatomed skin (400 µm in thickness). The plane of polarized light forms a hyper-reflective entrance signal on the skin surface where the polarized light reflects off the keratin of the corneocytes. In Figure 4.2 the untreated sample shows this hyper-reflective band on the skin surface and also a reflective band on the bottom of the dermatomed skin corresponding to the stainless steel support grid of the Franz cell. The skin had been dosed with a 10 mM solution of G3-PAMAM-NH_2 (0.2 mL) and a 5 mM G3-PAMAM-NH_2 (0.2 mL) shown in Figure 4.2 (a) and (b) respectively. After 30 minutes the constant entrance signal observed in the untreated skin surface had sporadically disappeared. The distribution of the entrance signal across the skin surface had significantly altered as a consequence of a change in the refractive index (RI) due to the presence of the PAMAM dendrimer. After a 20 hour contact time the water/methanol vehicle had evaporated leaving a viscous G3-PAMAM-NH_2 film. The distribution of the entrance signal was sporadic as opposed to the constant entrance signal observed for the untreated control image. Figure 4.2 (a) & (b) demonstrates the skin surface at different time points and up to 6 h appears to be increasingly undulated with a disrupted and dense entrance signal. Though, at 20 hours the entrance signal disruption seems to recover. The distribution of the entrance signal was altered at all PAMAM concentrations tested.

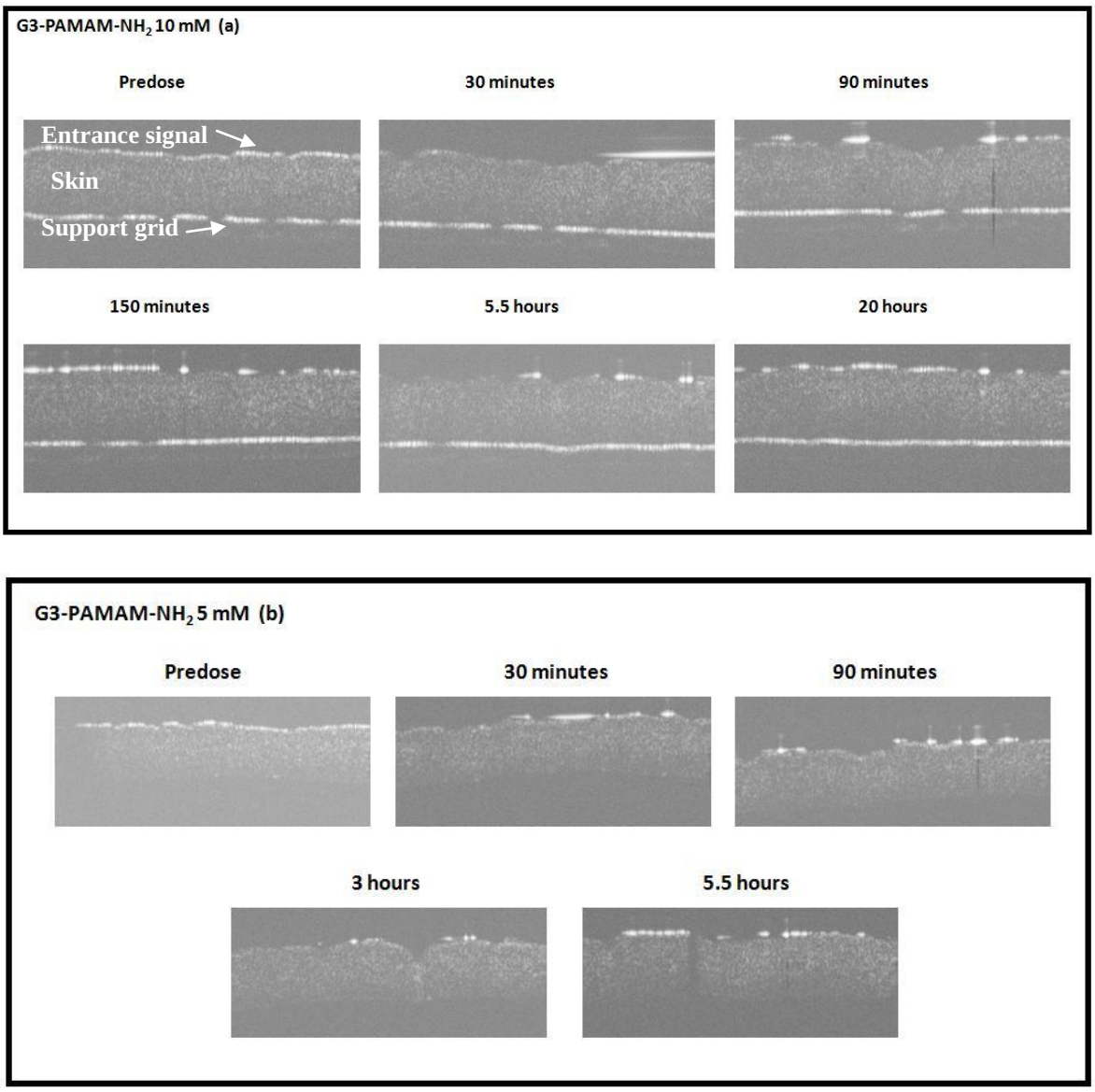

Figure 4.2 OCT images of porcine skin dosed with various concentrations of G3-PAMAM-NH_2 dendrimer taken at various time points. *(a) OCT images of G3-PAMAM-NH_2 (0.2 mL, 10 mM) dosed porcine dermatomed skin (400 µm) imaged at different time points. A typical example illustrated is Franz cell sample 127 which is representative of the replicate samples (n=3) (b) OCT images of G3-PAMAM-NH_2 (0.2 mL, 5 mM) dosed porcine dermatomed skin (400 µm) imaged at different time points. A typical example illustrated is Franz cell sample 153 which is representative of the replicate samples (n=3)*

The skin dosed with a water:methanol vehicle that was equivalent to the prepared PAMAM dendrimer solution did not alter the entrance signal on the skin surface in comparison to untreated skin specimens. The intensity and distribution of the entrance signal of the vehicle control treated skin samples typically remained constant as shown in Figure 4.3, particularly at a 2 hour time period as at this point the water:methanol vehicle had evaporated. This was due to the skin samples being mounted on Franz cells that were incubated at a skin temperature of 32ºC ± 1ºC between the imaging times. At the 6 hour and 20 hour time points the 'white layer' of the entrance signal resembled that of the pre-dose image.

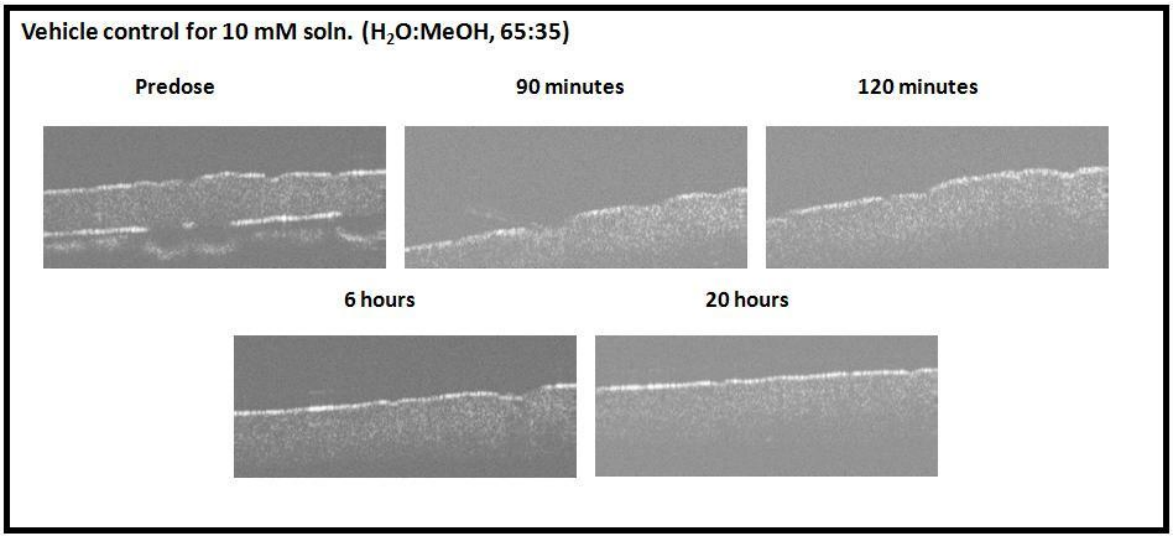

Figure 4.3. OCT images of porcine skin dosed with the vehicle control taken at various time points. *Vehicle control (water: methanol, 65:35) dosed porcine dermatomed skin (400 µm) imaged at a range of time points. A typical example illustrated is Franz cell sample 150 which is representative of the replicate samples (n=3).*

4.2.1.1 The effect of carboxyl functionality of the PAMAM dendrimer on the porcine skin surface

Half generation 3.5 PAMAM dendrimers (G3.5-PAMAM-COOH) terminate in carboxyl groups. G3.5-PAMAM-COOH dendrimers were also dosed on to the skin to observe any changes after the alteration of the surface groups on the optical characteristics of the skin. Figure 4.4 demonstrates the OCT images taken after dosing the skin with 5 mM G3.5-PAMAM-COOH dendrimer at various time points. The distribution of the entrance signal was disrupted after 30 minutes but not to the extent that was observed for the amine terminated PAMAM dendrimers. The entrance signal was very sporadic in distribution at 5.5 h after dosing with G3.5-PAMAM-COOH. Figure 4.4 (b) illustrates the skin dosed with the vehicle control and the hyper-reflective signal can be observed intact and remained the same as the pre-dose sample.

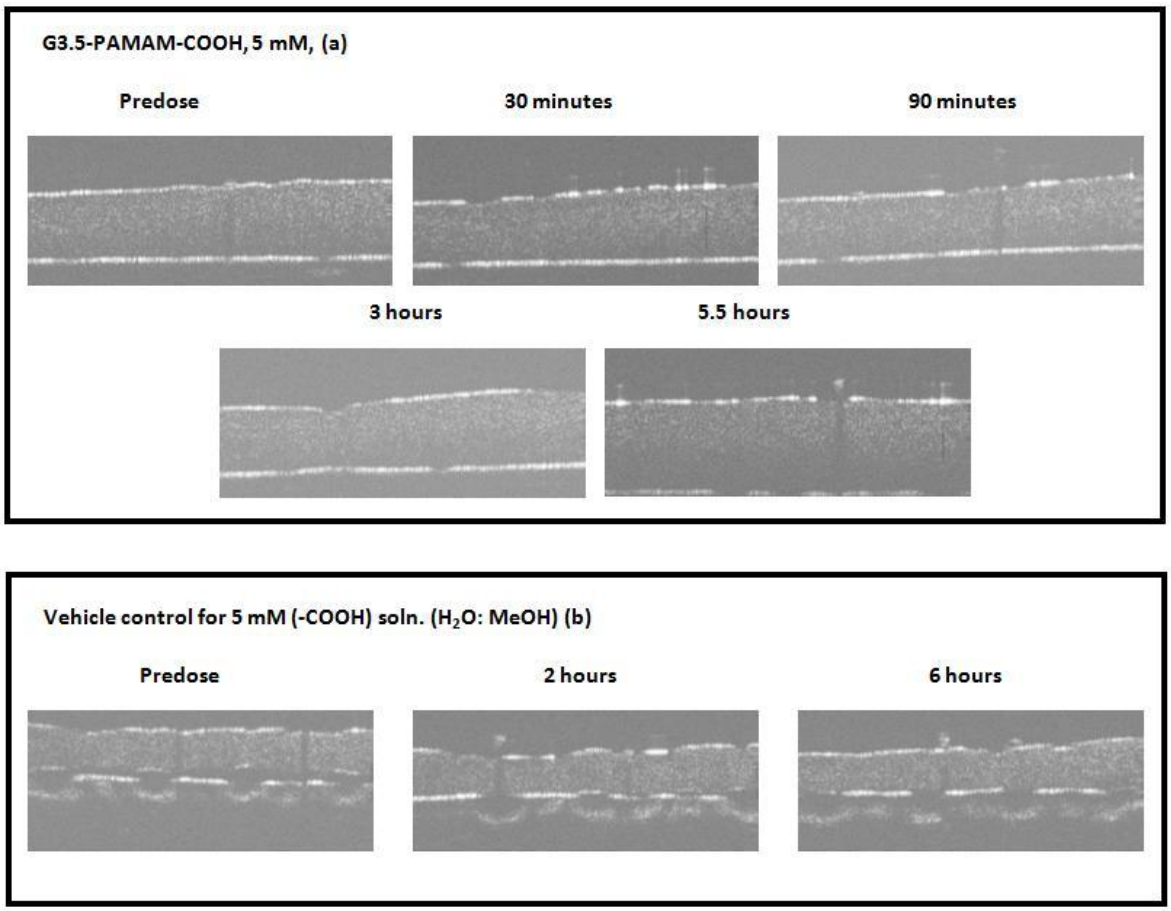

Figure 4.4 OCT images of porcine skin dosed with the G3.5-PAMAM-COOH dendrimer and corresponding vehicle control taken at various time points. *(a) OCT of G3.5-PAMAM-COOH (0.2 mL, 5 mM) dosed porcine dermatomed skin (400 µm) imaged at different time points. A typical example illustrated is Franz cell sample 156 which is representative of the replicate samples (n=3). Figure 4.4 (b) OCT images of the vehicle control (water: methanol, 82.5:17.5) dosed porcine dermatomed skin (400 µm) imaged at a range of time points. A typical example illustrated is Franz cell sample 152 which is representative of sample replicates (n=3).*

4.2.1.2 The effect of the known tissue clearing agent glycerol on the porcine skin surface

Glycerol was dosed on to the porcine skin surface using the same experimental parameters as for the PAMAM dendrimer treatment and the skin was imaged using the OCT at a range of different time points. Figure 4.5 illustrates the OCT skin images after application of glycerol at various time points. The entrance

signal disappeared from the skin surface after application of glycerol. The alteration of the OCT image is clearly observed in the comparison of the untreated skin with the skin treated with glycerol for a 15 minute contact time in Figure 4.6.

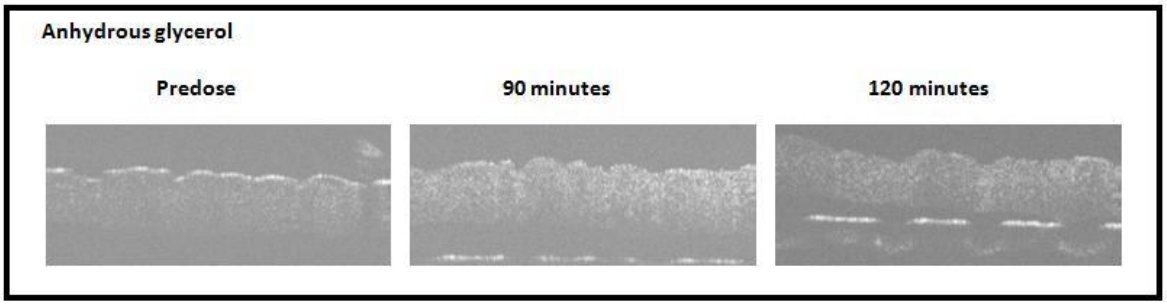

Figure 4.5 OCT images of porcine skin dosed with glycerol at various time points. *Anhydrous glycerol (0.2 mL) dosed porcine dermatomed skin (400 µm) imaged at three time points. A typical example illustrated is Franz cell sample 112 which is representative of the replicate samples (n=3).*

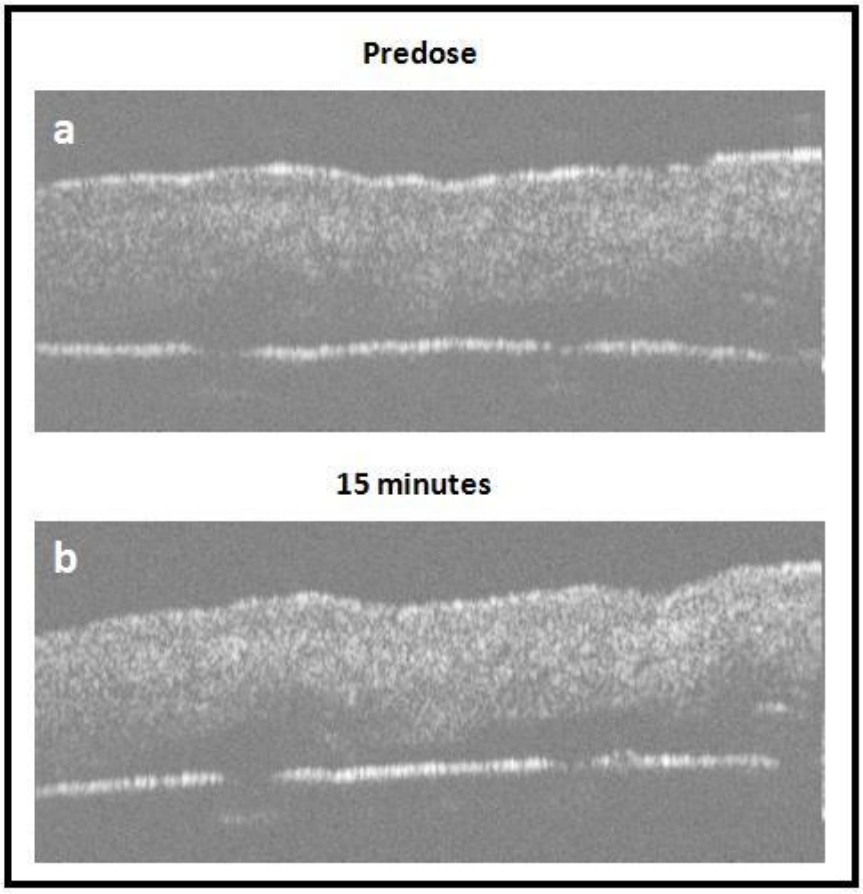

Figure 4.6. In situ OCT images of porcine skin dosed with glycerol. *OCT images that correspond to (a) porcine dermatomed skin (400 µm) dosed with 0.2 mL of anhydrous glycerol and (b) image taken in situ after 15 minutes illustrating the 'clearing' of the tissue.*

4.2.2 The transient nature of the PAMAM dendrimer's effect on the skin

To determine whether the optical changes that occur due to the interaction of the PAMAM dendrimer with the skin are reversible, the skin was imaged using the OCT on removal of the PAMAM dendrimer layer. Figure 4.7a displays OCT images of untreated skin, skin dosed with 10 mM G3-PAMAM-NH_2 *in situ* for 1 h and the skin post wash after the PAMAM application. The re-appearance of the hyper-reflective entrance signal after removal of the PAMAM dendrimer is clearly visible. The OCT image returns to a state that was observed before treatment. Figure 4.7b illustrates OCT images taken post removal of the G3-PAMAM-NH_2 PAMAM dendrimer layer with increasing incubation time. Again, the hyper-reflective entrance signal returns to resemble that of the pre-dose image.

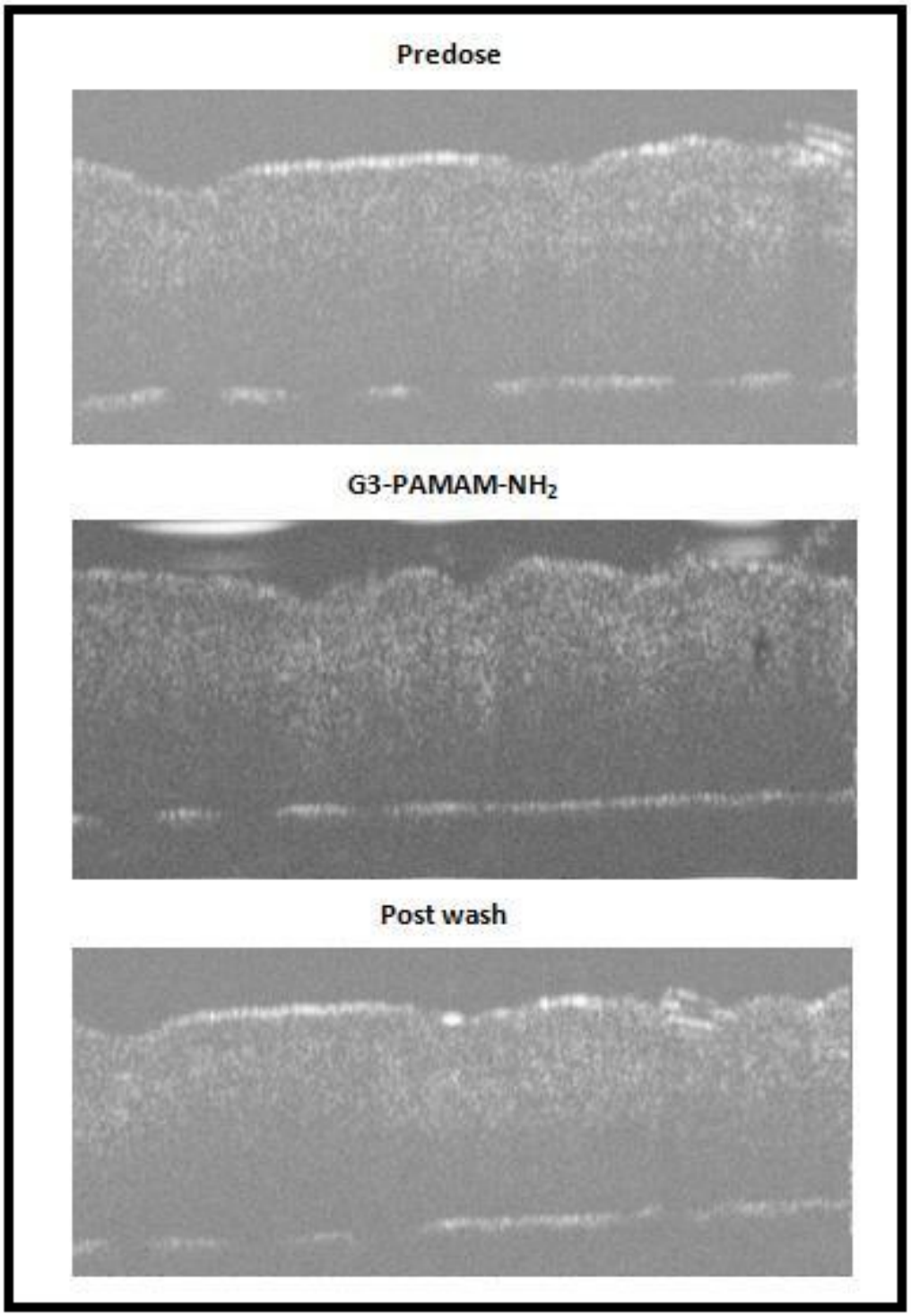

Figure 4.7a OCT images showing porcine skin before, during and after application of G3-PAMAM-NH_2 dendrimer. *Images displaying porcine dermatomed skin prior to G3-PAMAM-NH_2 treatment, after dosing with G3-PAMAM-NH_2 (10 mM, 0.2 mL) for a ten minute contact time (PAMAM in situ) and after removal of G3-PAMAM-NH_2 layer with a 10 mL wash (2 mL aliquots agitated over skin surface) of ultrapure water (n=2). N.B the recovery of the hyper-reflective entrance signal post PAMAM removal.*

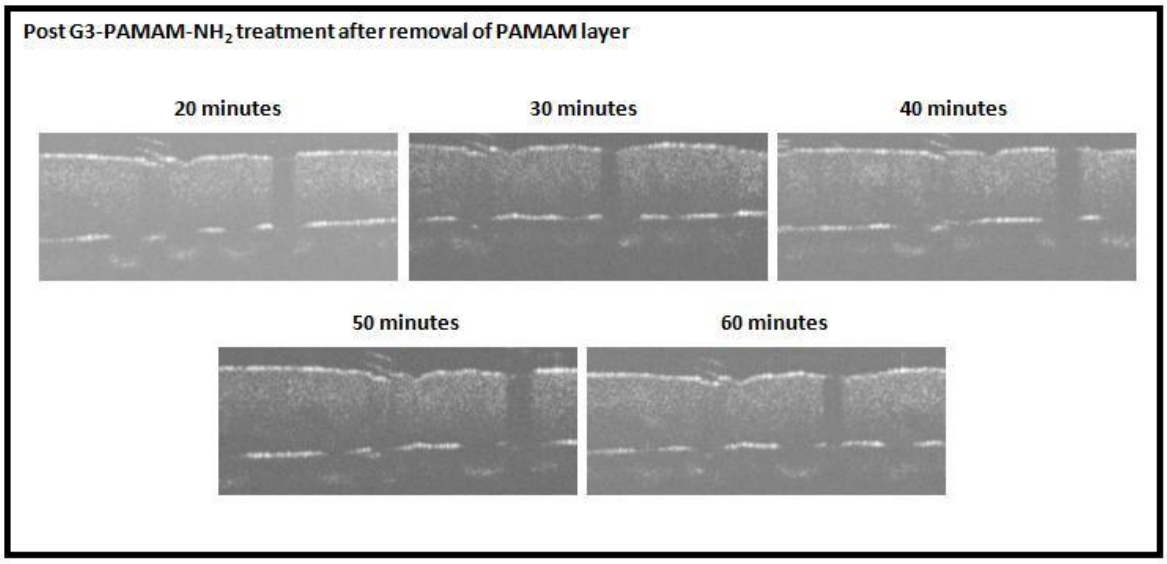

Figure 4.7b OCT images showing porcine skin after removal of applied G3-PAMAM-NH_2 dendrimer. *Images displaying porcine dermatomed skin prior to G3-PAMAM-NH_2 treatment, after dosing with G3-PAMAM-NH_2 (10 mM, 0.2 mL) for a range of time points after removal of G3-PAMAM-NH_2 layer with a 10 mL wash (2 mL aliquots agitated over skin surface) of ultrapure water (n=2). N.B the recovery of the hyper-reflective entrance signal post PAMAM removal.*

The reduction in the pixel grey value (pixel intensity) was used to investigate the optical changes to the skin caused by the application of the PAMAM dendrimer solution. A Yellow line was placed at the same representative co-ordinates (x=158, y=0) on both images and each had the contrast enhanced to an equal degree of 0.4 % saturation of pixels. A grey value plot profile was conducted along the yellow line to determine and changes to the intensity of the skin tissue. The entrance signal can be observed where the light propagates the skin at a depth of around 0.16 mm on the plots of Figure 4.8. This signal decreases on dosing the skin with 0.2 mL of a 10 mM solution of G3-PAMAM-NH_2 which is consistent across the whole PAMAM dosed data set. Figure 4.9 represents a plot of the pixel grey value at the depth of where the hyper-reflective entrance signal is observed. It was found that there was a reduction in the pixel grey value and profile after dosing the skin with PAMAM dendrimer when

compared to the pre-dose skin pixel grey values at the same depth. A grey scale line plot could be a valuable method to semi-quantify the optical changes that occur after application of a novel penetration enhancer such as PAMAM dendrimers or a drug.

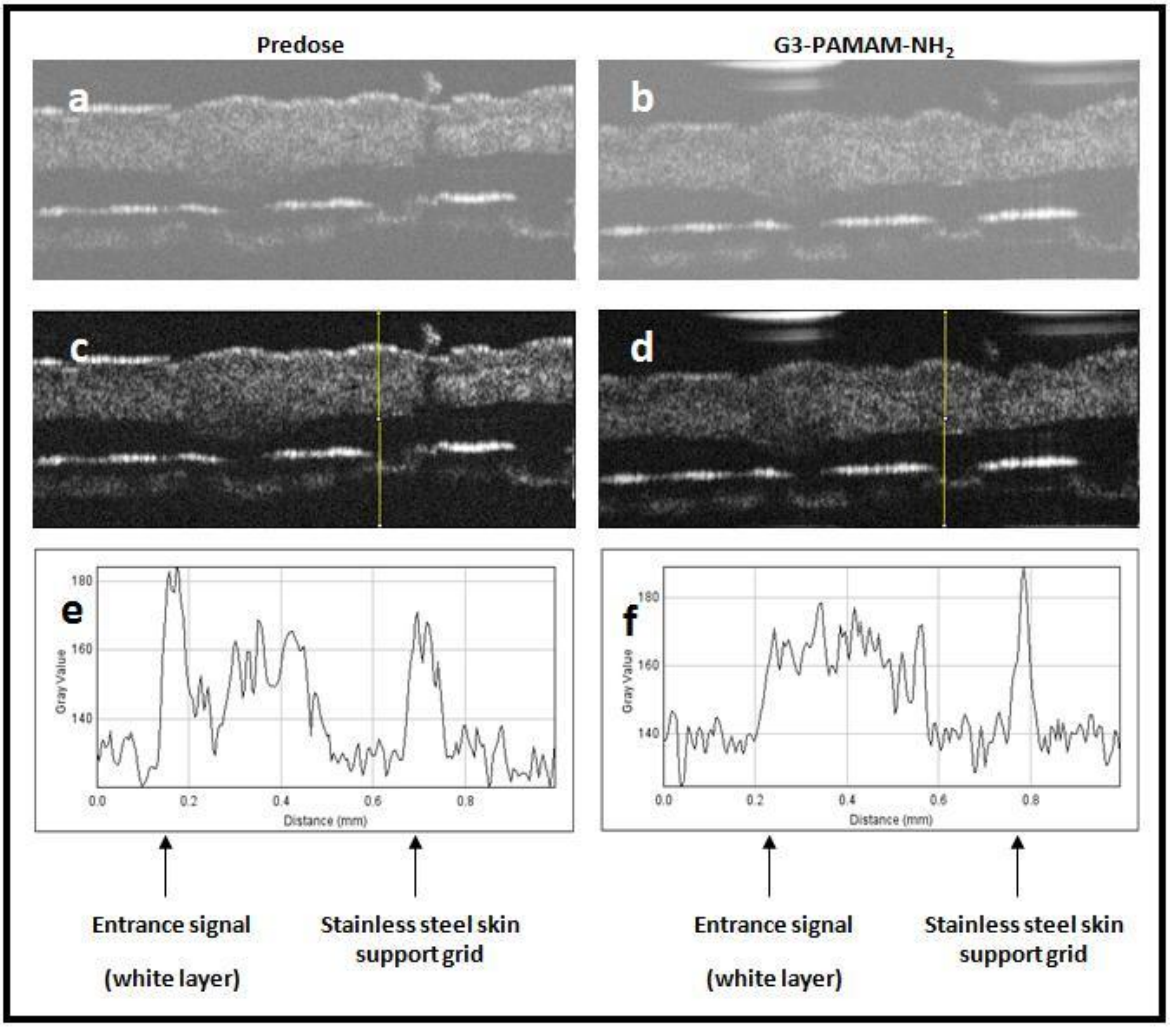

Figure 4.8. OCT image analysis of porcine dermatomed skin prior and post G3-PAMAM-NH_2 treatment. *(a) Corresponds to untreated porcine skin (b) after dosing with G3-PAMAM-NH_2 (10 mM, 0.2 mL) for a contact time of 15 minutes. Image (c) corresponds to (a) and image (d) corresponds to image (b) with the contrast enhanced to an equal degree of 0.4% saturation of pixels (e) is a gray scale line plot of the untreated skin and (f) corresponds to a gray scale line plot of the G3-PAMAM-NH_2 dosed skin. The yellow line was placed at co-ordinates x=158 and y=0 that was the location used to take a gray scale line plot on both (c) and (d).*

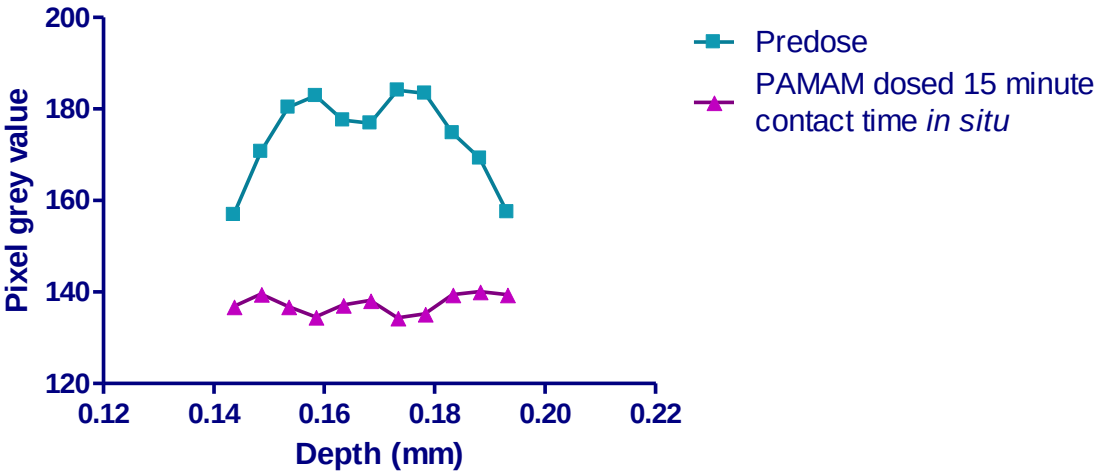

Figure 4.9. Graph showing pixel gray value against depth illustrating a change in the gray values after application of G3-PAMAM-NH_2 dendrimer (10 mM, 0.2 mL) compared to skin before treatment.

4.2.3 Histological analysis of PAMAM dendrimer dosed porcine skin

The haematoxylin and eosin stained the anucleate corneocytes of the SC pink in contrast to the dark blue nuclei found within the viable epidermis and the dermis. The micrographs of the stained skin sections illustrate slight morphological differences in the structure of the SC. In Figure 4.10 (a-b) that was dosed with the vehicle control, the SC appears intact. This is not observed for the G3-PAMAM-NH_2 dendrimer dosed skin (Figure 4.10 (c-d)) where the SC appears thin and dense compared to that of the vehicle control. The SC of the PAMAM dendrimer dosed skin sections again appears dissimilar to the surfactant damaged SC (Figure 4.10 (e-f)). As expected the positive damage control in Figure 4.10 (e-f) illustrates severe structural damage to the SC that would result in a significantly impaired barrier. The SDS application had caused the layers of the SC to detach from the viable epidermis (Figure 4.10 (f)).

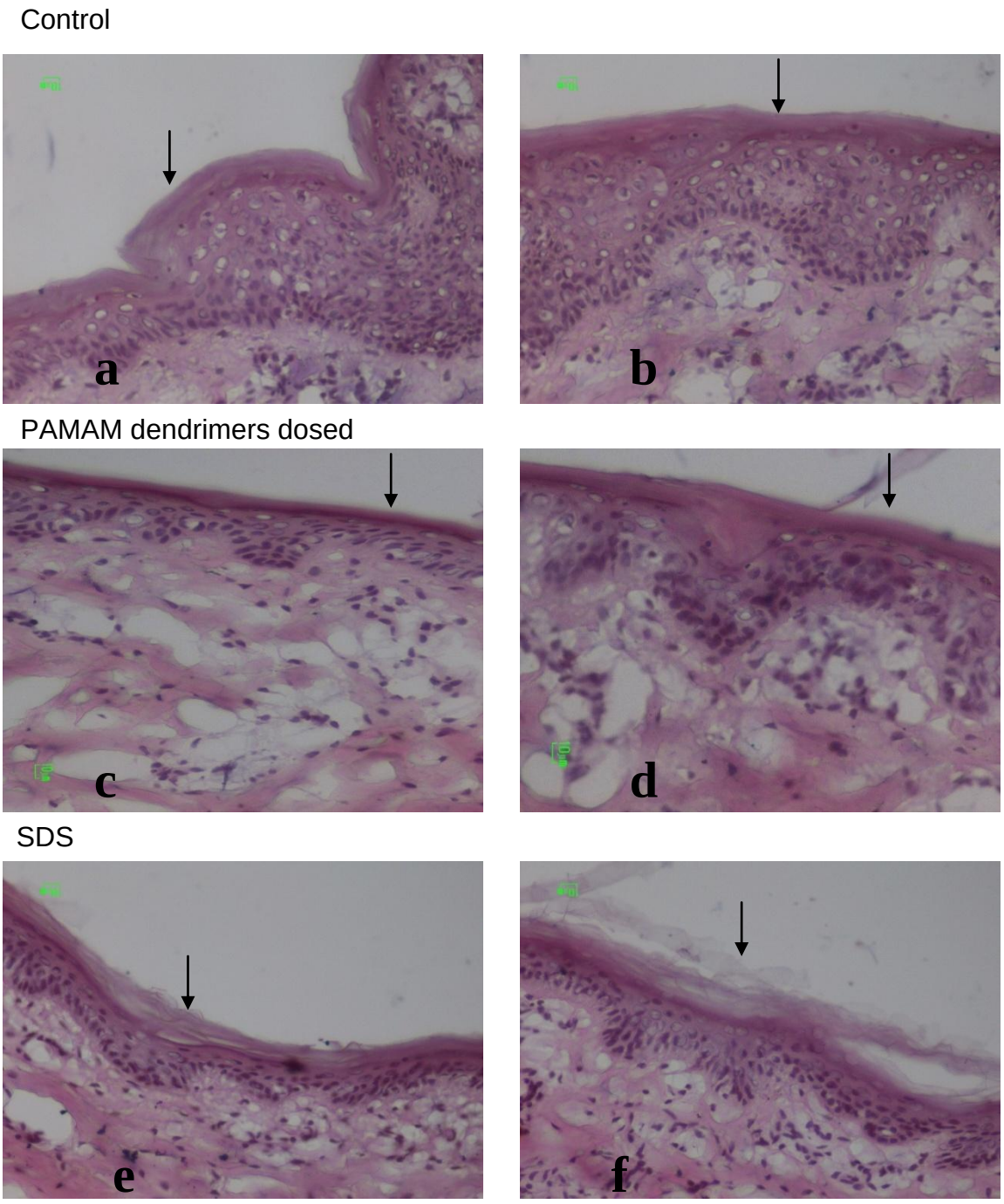

Figure 4.10. Haematoxylin and eosin stained porcine dermatomed skin cryo-sections after application of PAMAM dendrimer, vehicle control and an SDS positive control. *Images of the skin cryo-sections (400 µm depth, 8 µm thickness) were taken at a magnification of x 40. The skin was dosed for 24 h at 32ºC with (a-b) vehicle control (water: methanol, 65:35), (c-d) G3-PAMAM-NH_2 (10 mM, 0.2 mL) and a positive control (e-f) SDS (5 % w/v, 0.2 mL).*

4.2.4 Determination of total cholesterol concentration extracted by PAMAM dendrimer from porcine dermatomed skin.

In Section 3.2.0 it was shown that there was no significant reduction to the barrier integrity of the skin. It was then considered that perhaps the effect of the PAMAM on the skin was more subtle or temporary as shown in Section 4.2.1 with regards to the optical changes conferred by the PAMAM dendrimer on the skin surface. These solutions were analysed for the presence of cholesterol (Figure 4.11). The mean concentration of cholesterol extracted from the skin was 1.486 ± 0.280 µg/mL (mean ± SEM, *n*=3) and 0.293 ± 0.142 µg/mL (mean ± SEM, *n*=10) for the positive control and the G3-PAMAM-NH_2 dendrimer solution respectively. No cholesterol was detected within the vehicle solution. The cholesterol concentrations for all treatment groups however are below the calculated LOQ (1.186 µg/mL) therefore the results are only tentative (and as such no statistical analysis was applied).

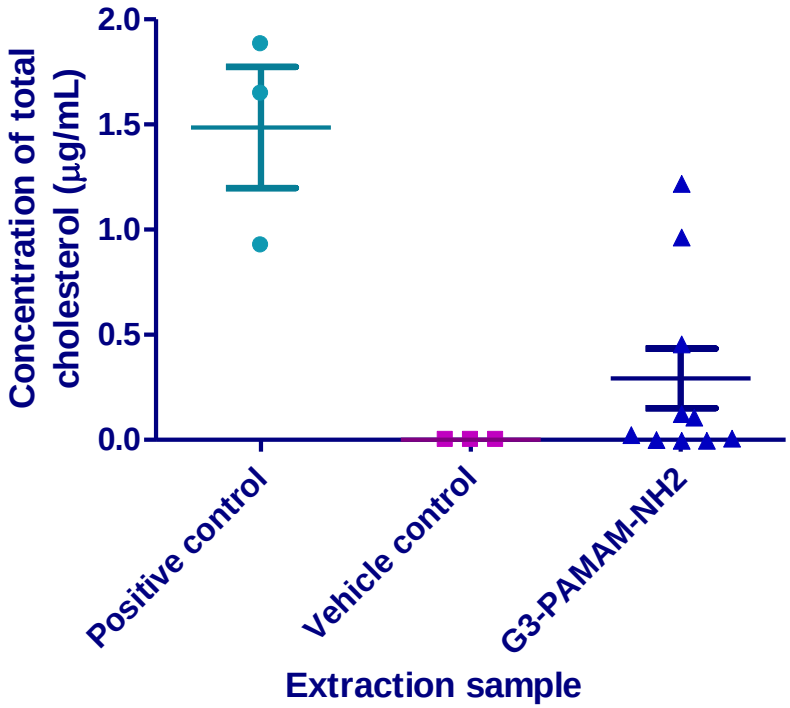

Figure 4.11 Concentration of total cholesterol (µg/mL) extracted from the dermatomed porcine skin (400 µm) after a 24 h contact time under occluded conditions. *(a) positive control- (chloroform: methanol, 3:2) which extracted an average concentration of 1.486 ± 0.280 µg/mL of cholesterol (n=3 mean ± SEM) (b) vehicle control- (water: methanol, 65:35) from which no cholesterol was detected (n=3 mean ± SEM) and (c) G3-PAMAM-NH_2 (10 mM, 0.2 mL) that extracted on average 0.293 ± 0.142 µg/mL of cholesterol (n=10 mean ± SEM). No cholesterol was detected for the negative control (0.2 mL distilled water, n=3). The concentrations of cholesterol extracted from the skin by all treatment groups are however below the calculated LOQ.*

4.2.5 Determination of skin protein concentration extracted by PAMAM dendrimer from porcine dermatomed skin.

To establish whether a PAMAM dendrimer extracts protein from the skin after application of a 10 mM G3-PAMAM-NH_2 solution a Lowry assay with a Peterson's modification was conducted (Legendre *et al.* 1995). The Peterson's modification is a protein precipitation step (addition of DOC and TCA) that removes the protein from all interfering substances such as ammonium sulphate, guanine, urea, sucrose, detergents and also EDTA (Ethylenediaminetetraacetic

acid) (Peterson, 1977). One of the monomers of the PAMAM dendrimer is ethylenediamine and it is likely that it would act as an interfering substance within the biuret reaction that forms the colouration for the protein determination. The assay has a working detection sensitivity range of 1-1500 µg/mL therefore the results are on the border of the LOD of the assay (according to the kit's specification (Anon, 2012). Only a very low concentration of protein was extracted from the skin with regards to the positive control. The positive control was a solution of chloroform:methanol (3:2) which under occlusive conditions extracted a mean protein concentration of 0.741 µg/mL (<LOD) in one Franz cell and no protein was extracted within the other two Franz cells. Therefore the positive control failed and did not extract a detectable concentration of protein from the skin. The vehicle control again extracted a minute concentration of protein, 0.136 µg/mL (<LOD) from a single cell and no protein was extracted from the other two Franz cells. The PAMAM dendrimer extracted a mean concentration of 1.979 ± 0.756 µg/mL of protein from the skin which is more than 2.5 times that of the positive control (Figure 4.12). The protein concentration extracted by the PAMAM dendrimer solution was however only 0.979 µg/mL over the LOD therefore again the results displayed in Figure 4.12 should be considered tentative.

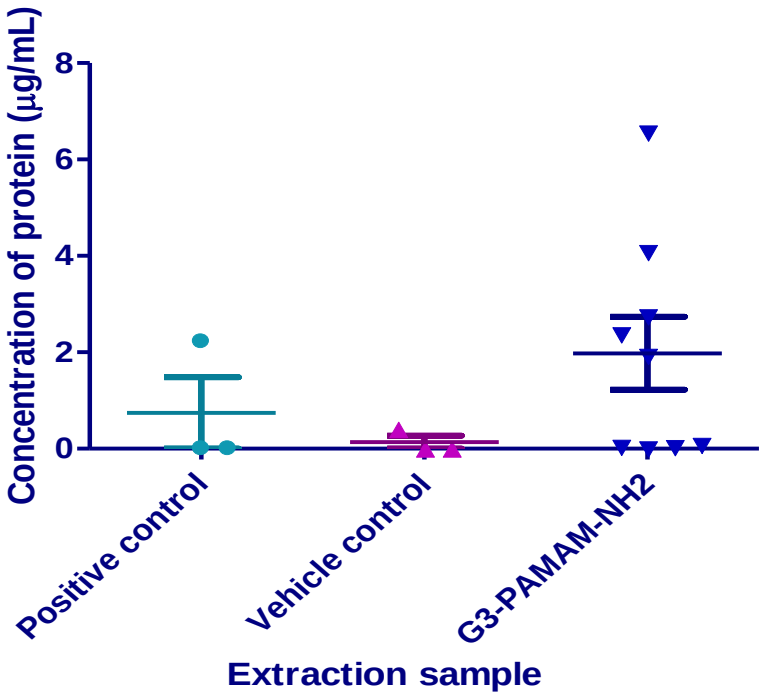

Figure 4.12. Concentration of protein (µg/mL) extracted from the dermatomed porcine skin (400 µm) after a 24 h contact time under occluded conditions. *(a) positive control- (chloroform:methanol, 3:2) which extracted an average concentration of 0.741 ± 0.741 µg/mL of protein (n=3 ± SEM) (b) vehicle control- (water: methanol, 65:35) that extracted 0.1358 ± 0.1358 µg/mL (n=3 ± SEM) and (c) G3-PAMAM-NH_2 (10 mM, 0.2 mL) that extracted 1.979 ± 0.756 µg/mL (n=9 ± SEM). No protein was detected for the negative control (0.2 mL distilled water, n=3). N.B LOD for the assay is 1 µg/mL.*

4.2.6 ATR-FTIR analysis of the interaction between PAMAM dendrimers and porcine SC

Figure 4.13 exhibits the stacked spectra of the PAMAM in aqueous solution, the isolated SC alone and dosed with the vehicle control and the PAMAM dendrimer solution. General peak changes to the spectra can be observed but also the similarities between the aqueous PAMAM dendrimer spectrum and the untreated isolated SC spectrum. The overall spectra have been utilised to focus on specific peak shifts that are explained further in the Chapter. The peak assignments for the PAMAM dendrimer spectrum (Figure 4.13 (a)) are 3250 & 3050 cm^{-1} corresponding to –NH-, 1450 cm^{-1} corresponding to $–CH_2$- and 1650 &

1550 cm^{-1} corresponding to the –HN-CO-. It was found that the –C(O)NH- peak of the G3-PAMAM-NH_2 PAMAM dendrimer overlaps with the amide I peak of the SC.

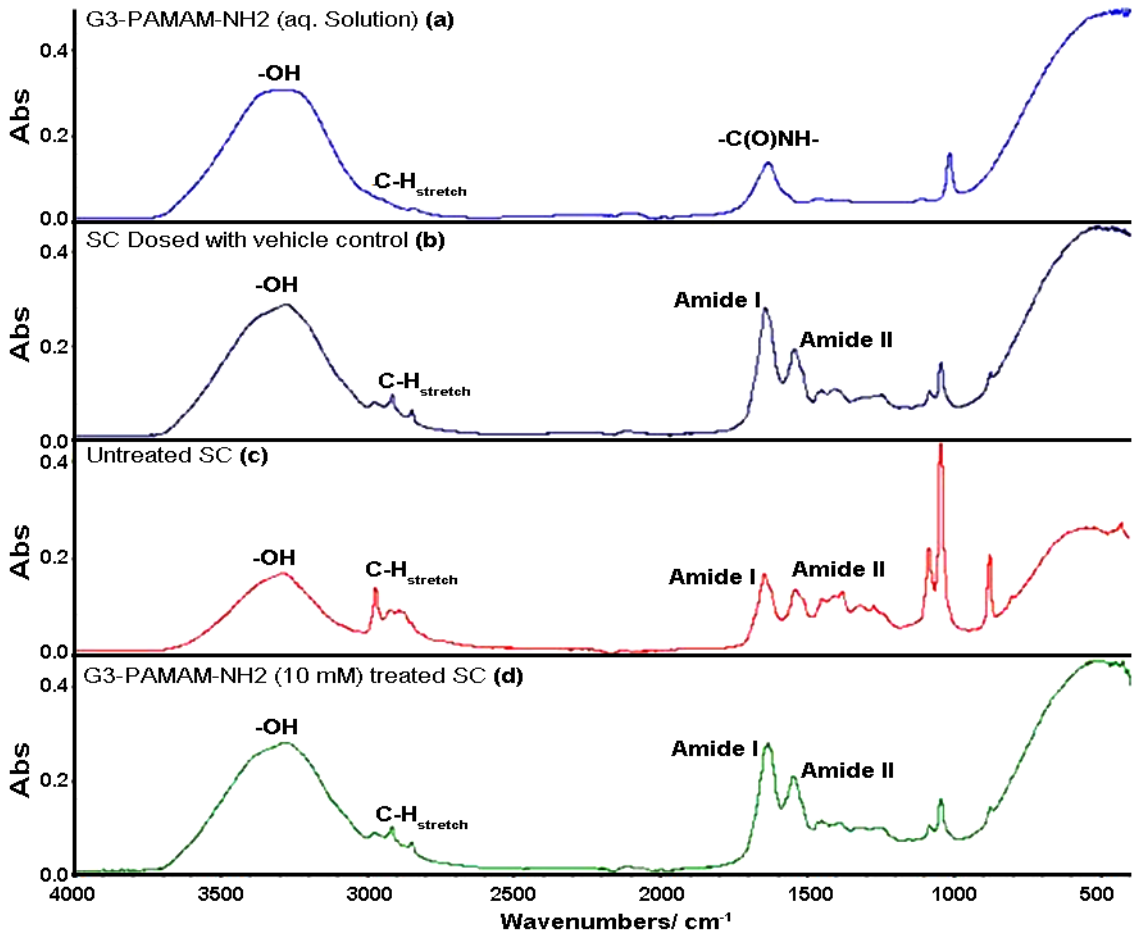

Figure 4.13 ATR-FTIR spectra of isolated native SC and isolated SC dosed with PAMAM dendrimer and the corresponding vehicle control. *(a) Corresponds to an aqueous solution of G3-PAMAM-NH_2 dendrimer (10 mM, 0.2 mL) (b) SC dosed with the vehicle control (water: methanol, 65:35, 0.2 mL), (c) untreated SC and (d) SC dosed with 10 mM G3-PAMAM-NH_2.*

2

Figure 4.14 represents three replicate spectra corresponding to G3-PAMAM-NH_2 dendrimer dosed SC and the red spectrum which corresponds to the vehicle control. The spectra highlight a shift in amide I graph and amide II which is possibly due to changes in the β-sheet (~1629 cm^{-1}) structure of keratin (Lin et al. 1996). There are no observable changes in the scissoring mode at 1454

cm^{-1} suggesting no alterations in the lateral chain packing. There is a peak shift in the CH_2 wagging mode with the PAMAM dendrimer dosed SC. The peak is at 1150 cm^{-1} but the vehicle control peak shifts to 1175 cm^{-1}. A peak at 1410 cm^{-1}equates to CH_2 bending present in the vehicle control SC (red) but not in the SC that was dosed with PAMAM dendrimer.

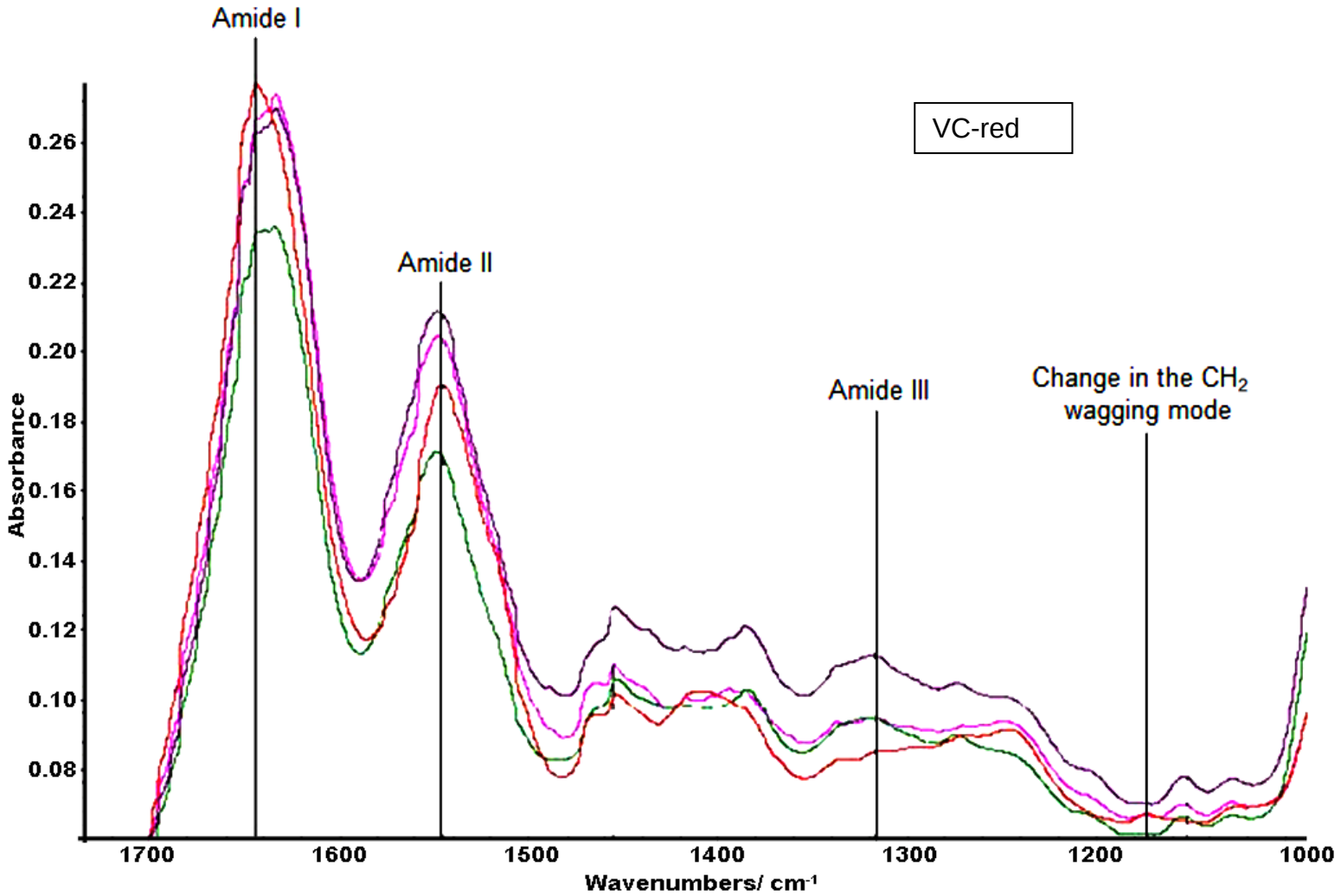

Figure 4.14. ATR-FTIR spectra of isolated SC dosed with 10 mM G3-PAMAM-NH_2 dendrimer overlaid with the vehicle control spectrum. *Overlaid spectra of G3-PAMAM-NH_2 dendrimer dosed SC replicates (purple, pink and green). The red spectrum corresponds to the vehicle control (water:methanol, 65:35). Differences in wavenumber or peak shape between PAMAM dendrimer treated and the vehicle control treated SC are marked on the spectra.*

The wavenumber of the amide bond corresponding to the protein within the SC was plotted against each treatment group to determine whether there was a significant peak shift. Figure 4.15 demonstrates the shift in wavenumber from the vehicle control for 5 mM and 10 mM G3-PAMAM-NH_2 dendrimer treated SC. A 5 mM PAMAM dendrimer solution resulted in a shift of the amide band for two (out of four replicates) of the SC samples as high variability within the 5 mM replicates was observed. This may possibly be due to the 5 mM concentration being on the cusp of the concentration that induces a shift in the amide I band. The SC was isolated from a range of pig donors therefore possible donor or regional variations in the SC may account for the split in amide I band shift observed for the 5 mM PAMAM dendrimer concentration. Differences in the contact between the SC and the diamond or possibly due to differences between the wavenumber or depths of penetration (Grdadolnik, 2002) may account for variability observed between the replicate samples. There was no statistically significant difference between the peak shifts for 10 mM and 5 mM PAMAM dendrimer treated SC and the vehicle control treated SC (Kruskal Wallis ANOVA, $p>0.05$).

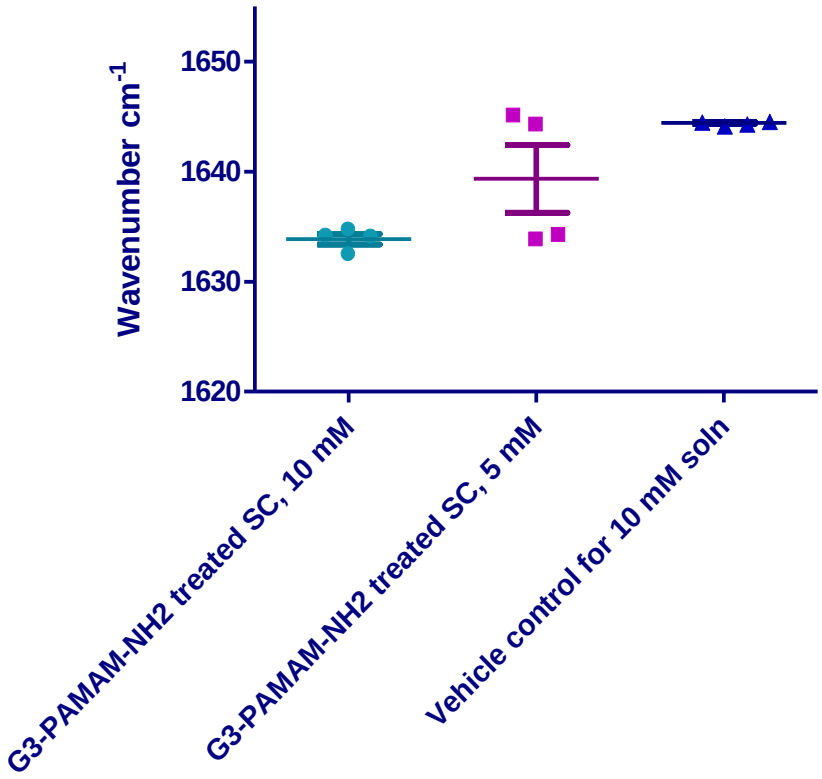

Figure 4.15 Graph illustrating the peak shift of the amide I band for 10 mM and 5 mM G3-PAMAM-NH_2 dendrimer treated SC and for the vehicle control treated SC. *The data is presented as the mean ± SEM (n=4), a Kruskal Wallis ANOVA found no statistical significance (p>0.05).*

The amine II band also saw a shift in wavenumber after treatment with a 10 mM G3-PAMAM-NH_2 dendrimer solution when compared to that of the vehicle solution treated (Figure 4.16). No shift in peak was observed for the 5 mM G3-PAMAM-NH_2 dendrimer solution. The amide II band is due to the N-H bending vibration of the protein within the SC and C-N stretching vibration. This may be evidence of a change in conformation.

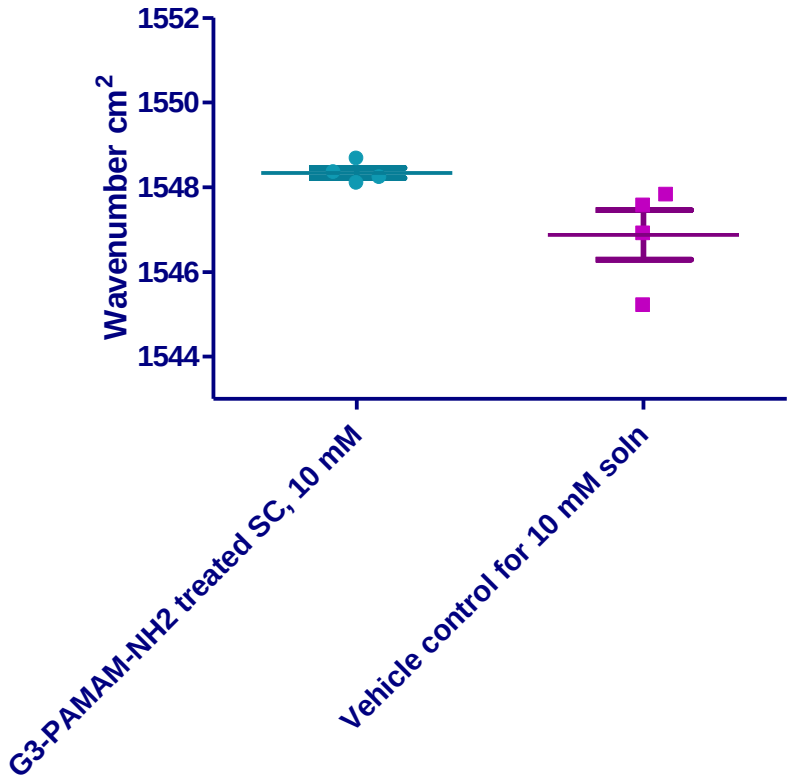

Figure 4.16. Graph illustrating the peak shift of the amide II band for 10 mM G3-PAMAM-NH_2 dendrimer treated SC and for the vehicle control treated SC. *(n=4)*

Carboxyl terminated PAMAM dendrimers (G3.5-PAMAM-COOH) were dosed onto SC and analysed by ATR-FTIR also. Figure 4.17 illustrates the differences to the peak shape and frequency shifts that correspond to the G3.5-PAMAM-COOH dendrimer dosed SC. There is a peak shift of the CH_2 scissoring peak at 1410 cm^{-1} where it alters when the SC was dosed with the carboxyl terminated PAMAM dendrimer. A magnification of the peak shift at 2979 cm^{-1} illustrating G3.5-PAMAM-COOH dendrimer (5 mM, 0.2 mL) compared to the vehicle control (Figure 4.18).

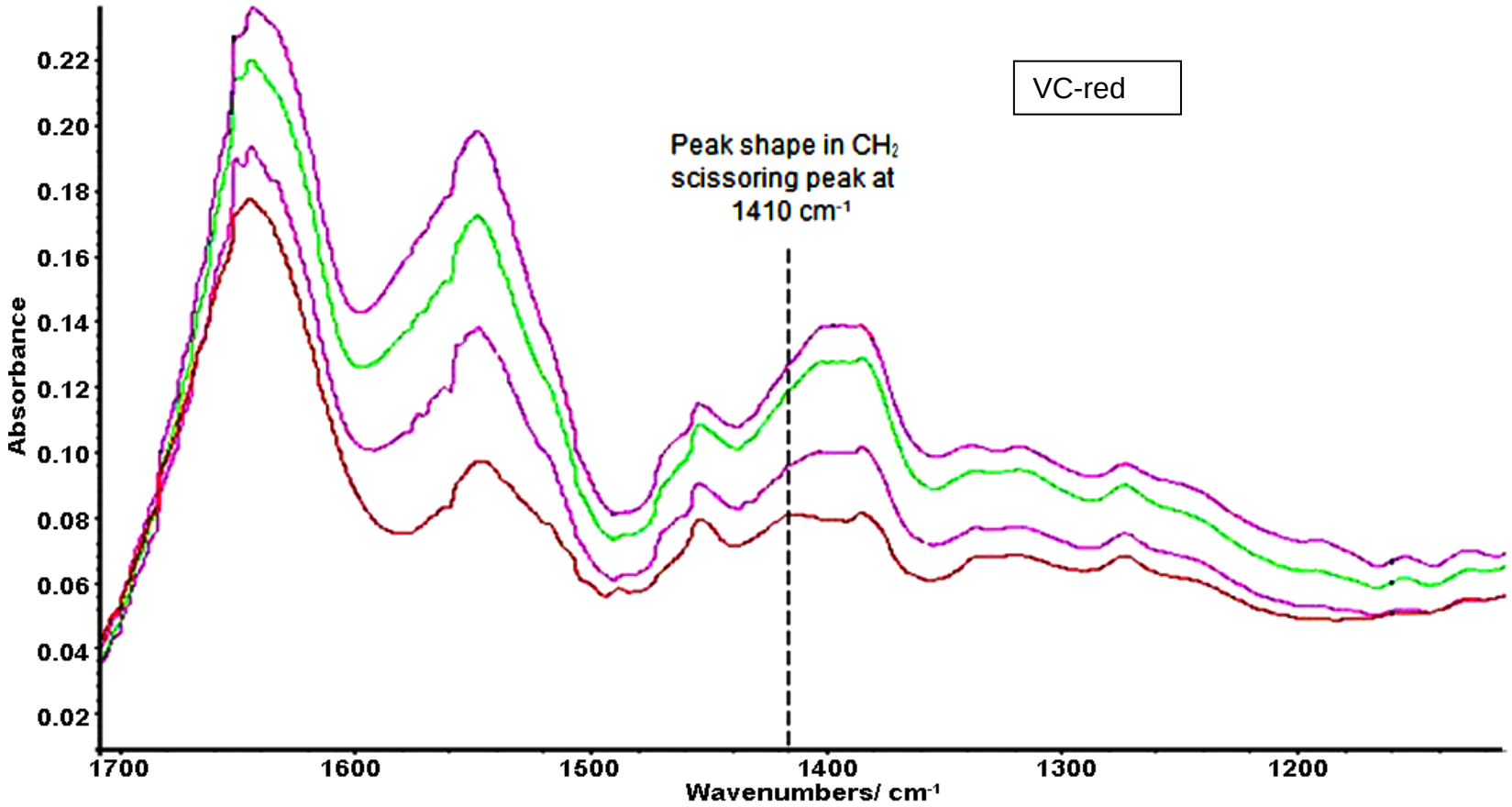

Figure 4.17 ATR-FTIR spectra corresponding to G3.5-PAMAM-COOH (5 mM solution) and corresponding vehicle control applied to the SC. *The PAMAM treated spectra is displayed as pink, purple and green and a spectrum corresponding to the vehicle control solution is red. The changes in peak shape and frequency are marked on the spectra.*

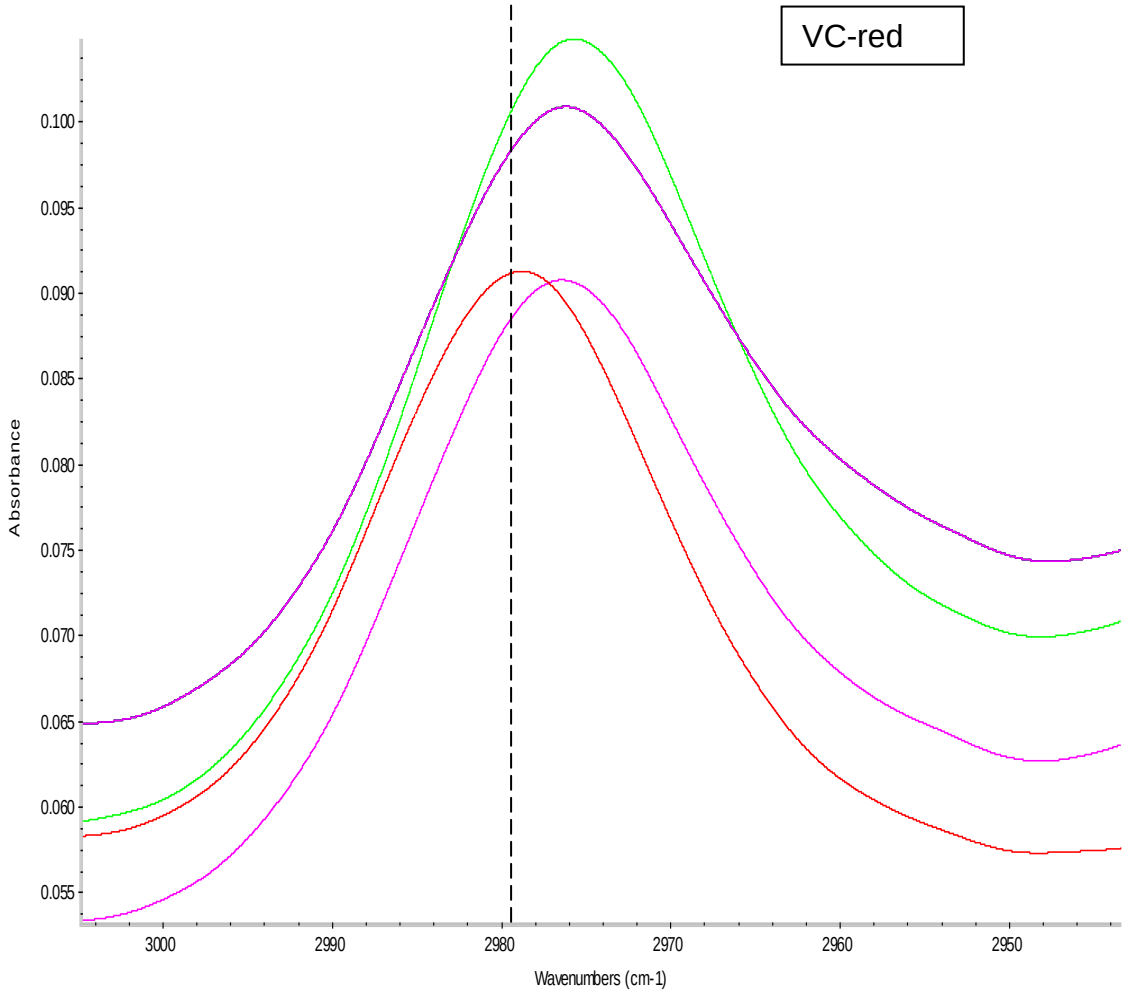

Figure 4.18. Magnification of ATR-FTIR spectra demonstrating peak shift after application of G3.5-PAMAM-COOH dendrimer to isolated SC compared to vehicle controlled dosed SC. *G3.5-PAMAM-COOH dendrimer (5 mM, 0.2 mL) dosed SC corresponds to the pink, purple and green spectra and a spectrum corresponding to the vehicle control solution dosed SC is displayed in red.*

The wavenumber of the CH_3 asymmetric stretch was plotted against the SC treatment. Figure 4.19 demonstrates the shift in frequency of the CH_3 asymmetric stretch for the vehicle control treated SC compared to the G-3.5-PAMAM-COOH dendrimer treated SC though this was not significantly different (Mann Whitney test $p>0.05$).

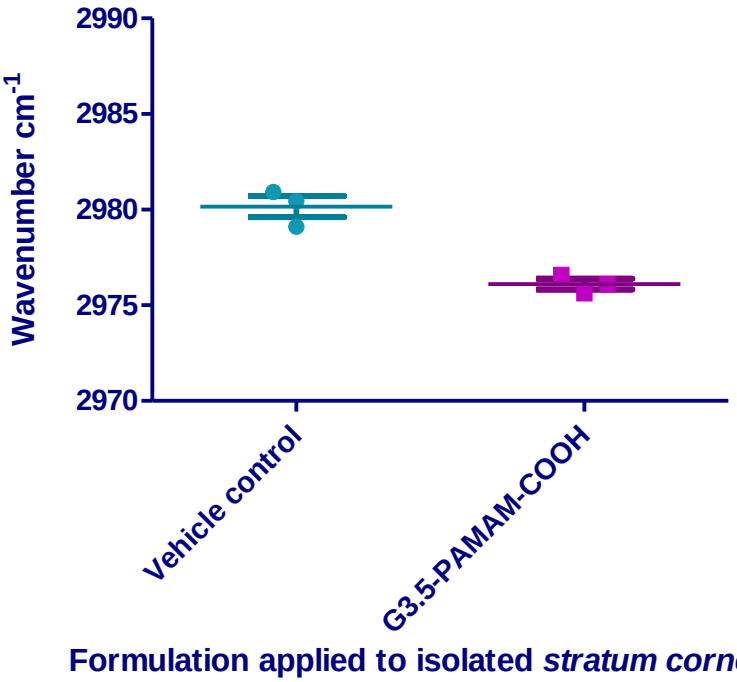

Figure 4.19 Graph illustrating the peak position of C-H stretch at 2981 cm^{-1} after application of G3.5-PAMAM-COOH dendrimer to SC compared to the vehicle control treated SC. *The data is presented as the mean ± SEM (n=3).*

4.3 Discussion

The studies within this section showed that a PAMAM dendrimer skin pre-treatment enhanced the permeation and distribution of CHG within porcine skin. The mechanism of action behind the PAMAM dendrimer's effect upon the skin is unknown. To determine whether PAMAM dendrimers impair the integrity of the barrier of the skin the TEER and TEWL was measured. The TEER was used to measure the electrical resistance across the skin to determine whether there was a significant decrease in the resistance caused by the PAMAM dendrimer's application to the skin. No significant difference was observed between the TEER determined before application and after application of PAMAM dendrimer (Figure 4.1 (a)). This suggests that no significant damage to the barrier nature of the skin was sustained due to a contact time of 24 h with the highest concentration of G3-PAMAM-NH_2 dendrimer tested (10 mM).

Further to this, TEWL was also measured which has been utilised to measure the damage incited by a range of skin penetration enhancers including micro-needles (Badran *et al.* 2009), ethanol/propylene glycol solutions (Levang *et al.* 1999), surfactants (Elmahjoubi, 2009) and terpenes (Gao and Singh, 1997). Macroscopic damage to the skin would result in a sharp increase in the TEWL measurements however damage to the skin's barrier integrity on a micro scale may not be detected by TEWL measurements (Netzlaff *et al.* 2006). Figure 4.1 (b) illustrates the TEWL measurements recorded. It was found that the data was spread around the mean. G3-PAMAM-NH_2 dendrimer (10 mM) treated skin had a mean measurement (mean ± SEM, n=18) of 2.71 ± 1.46 g/m^2h and the untreated skin control skin had a mean result of 3.08 ± 1.31 g/m^2h. There was no statistically

significant difference between PAMAM treated skin and the control. There was greater variability found within the TEWL data when compared to the TEER data. The increase in variability for the TEWL measurements may be due to the increase in variables such as temperature, humidity or due to interference from residual (not removed after wash procedure) hygroscopic PAMAM dendrimer bound to the superficial layers of the SC.

The results within this section from both TEER and TEWL studies are in very good agreement in that the PAMAM dendrimer pre-treatment does not incite significant macroscopic skin barrier impairment, however to the contrary Venuganti and Perumal (2008 and 2009) reported a significant increase in TEWL and a decrease in TEER. The authors reported a 40 % reduction in skin resistance after application of cationic and neutral PAMAM dendrimers and a significant increase in TEWL measurements (ratio mean ± SEM) of 2.9 ± 0.7 for G4-PAMAM-NH_2 10 mM when normalized to pre-dendrimer value). However it is worth noting that the study had a very low sample number of n=3 and the temperature of the laboratory fluctuated by 6°C during the measurements. An increase of 7- 8°C in temperature doubles the rate of TEWL in normal skin (Grice *et al.* 1971) and TEER measurements are also significantly affected by changes in temperature (Blume *et al.* 2010). A 40 % decrease in electrical resistance across the skin is a substantial decrease in the barrier nature of the skin and was only observed in this study for the SDS 5 % (w/v) positive control.

For the positive SDS control, visually it was apparent that the surfactant had extensively damaged and permeabilised the skin lipids and protein. This was not observed for the PAMAM dendrimer pre-treated skin which appeared intact

therefore a 40 % reduction in electrical resistance appears to be a very high value. The authors do not mention whether the PAMAM dendrimer is still present on the skin surface during the TEWL and TEER measurement or as to whether it has been removed. As PAMAM dendrimers are strongly cationic and extremely hygroscopic, measurement of the skins barrier integrity using TEER and TEWL in the presence of the PAMAM dendrimer may give inaccurate results. This may account for the opposing findings between the two studies.

The OCT images throughout this Chapter consistently demonstrate that the PAMAM dendrimers have caused an interaction with the skin resulting in the alteration of the hyper-reflective entrance signal on the skin surface. Two hypotheses may explain the mechanism behind this. Firstly, it could be due to a refractive index (RI) match (or close approximation the RI) that reduces the random back scattering of light from the skin surface (Vargas *et al.* 1999). When focusing a plane of light on to the skin surface to record the images, photons travel within different media; from air across an interface into skin tissue which contains interstitial fluid and a range of proteins and lipids. These skin components possess significantly different refractive indices for example hydrated collagen found within the dermis has an RI of around 1.43 (Wang *et al.* 1996). The major contributor to the random scattering of photons is due to the filamentous keratin found within the corneocytes of the epidermis and it has an RI of approximately 1.62 (Xu *et al.* 2003). Air has a RI of 1.000, and skin has an approximate average RI of 1.440 (Tearney *et al.* 1995), hence the strong reflective entrance signal at the skin-air interface. PAMAM dendrimers (G3-PAMAM-NH_2) have a RI of 1.367 at 20ºC (compounds specification, Sigma-Aldrich). One possibility is that the PAMAM dendrimer reduces the back-scattering of light and thus the mismatching of the RI

at the air-skin interface. This would result in a significant reduction to the hyper-reflective entrance signal at the skin-air interface that has been observed throughout the OCT studies. After application of the vehicle control to the skin, there was no change in the hyper-reflective entrance signal. The vehicle control was a water/methanol solution that has a RI of around 1.328 (Phillips, 2013). This indicates that it is the PAMAM dendrimer that is influencing the optical changes observed at the skin-air interface.

The second mechanism proposed by the author is that the changes occur due to the hydration effect that the PAMAM dendrimers exert upon the skin. The G3-PAMAM-NH_2 dendrimer, could hydrate the skin for prolonged periods of time because PAMAM dendrimers are very hygroscopic (Uppuluri *et al.* 1998) and are known to adsorb moisture from the atmosphere (Topp et al. 1999). PAMAM dendrimers may absorb water from the atmosphere and make it freely available at the SC surface. Occlusion is another possible mechanism of skin hydration as a result of the viscous PAMAM dendrimer layer distributed across the skin surface. Either one or both of these hydration mechanisms would result in an increase in SC hydration. Typically SC hydration results in an increase in the topical or transdermal penetration of both hydrophilic and lipophilic drugs (Williams and Barry, 2012). Previously, aqueous colloidal layers including films and hydrogels have been utilised to enhance the topical delivery of drugs (Das *et al.* 2006 and Luo *et al.* 2000). There is the possibility that the PAMAM dendrimer adsorbs moisture from the SC. This would reduce the size of the corneocytes and result in a lower permeation of topically applied drugs in particular hydrophilic drugs (Barry, 1987). This mechanism is unlikely however as the PAMAM dendrimers have

enhanced the deposition and penetration of CHG within the skin as discussed in chapter three and five.

After a 20 hour contact time of PAMAM dendrimer dosed on to the skin surface the water/methanol vehicle had evaporated leaving a viscous G3-PAMAM-NH_2 dendrimer layer. The strong reflective entrance signal was sporadic in appearance at the air-skin interface. The sporadic disruption of the entrance signal caused by the PAMAM dendrimer may be a result of preferential accumulation of the PAMAM dendrimer within the skin furrows and undulations. After application to the skin, polymeric nanoparticles were reported to be localised within the furrows and pores of the skin with preferential accumulation detected within the hair follicles (Alvarez-Román *et al* 2004a). Accumulation of amine terminated PAMAM dendrimers within hair follicles was also shown using confocal microscopy (Venuganti *et al.* 2011). The sporadic alteration to the optical characteristics of the SC may be due to an uneven distribution of the dendrimers across the skin surface. Another possible explanation for the intermittent entrance signal is that PAMAM dendrimers self-aggregate when applied to the skin. PAMAM dendrimer aggregation was observed using DSC when applied to model membrane lipids (Klajnert and Epand, 2005).

The immediate surface reflection reduction effect has been observed elsewhere for topically applied ointments and glycerol (Welzel, 2001). These hyper-osmotic compounds such as paraffin oil, glycerol and petroleum have been shown to be tissue clearing agents (Welzel *et al.* 2004). A clearing agent is a compound that matches the refractive index of the tissue. Glycerol has an RI of 1.48 (Diaspro *et al.* 2002) and the refractive index of the skin was calculated to be

approximately 1.44 (Tearney, 1995). The clearing agent enhances the delineation of the epidermis and the dermis and allows for a more detailed image of skin appendages to be collected. It also allows for a deeper depth profile to be obtained due to the reduction of random scattering. A white, hyper-reflective entrance signal was not observed in the OCT images when dosed with glycerol with the exception of the pre-dosed images. At the 90 minute contact time the underlying viable epidermis becomes clearer and the structures of the skin become more pronounced. This is due to the anhydrous glycerol matching the refractive index of the viable epidermis, allowing enhanced visualisation of the skin. This effect of reducing the random scattering has been noted elsewhere for glycerol and occurs shortly after skin application (Vargas *et al.* 1999).

Azone, a known chemical skin-penetration enhancer, has also been shown to act as a skin-clearing agent and reduces the back scattering of light within skin tissue (Xu and Zhu, 2007). The PAMAM dendrimers may also partially act as a clearing agent as the PAMAM dendrimer has a similar RI to that of glycerol and the skin. After application of a PAMAM dendrimer solution to the skin surface, it was apparent that the underlying morphology or microstructures of the epidermis and dermis did not become clearer or more defined. This is expected as the PAMAM dendrimers are large macromolecules (>2500 Da) and are not expected to traverse the SC due to their high molecular weight and strong ionic charge. PAMAM dendrimers have been shown to act as a penetration enhancer (chapter three, Venuganti and Perumal, 2008, Chauhan *et al.* 2003 and Wang *et al.* 2003) as has glycerol (Bettinger, 1998) for a range of topically applied drugs. The PAMAM dendrimers' (Topp *et al.* 1999) and glycerol's (Hara and Verkman, 2003) hygroscopic nature may result in skin tissue hydration. It has been noted that

hydration of skin tissue can reduce the refractive index (Knuttel and Boehlau-Godau, 2000 and Sand *et al.* 2006). This study has also demonstrated a further commonality between glycerol and PAMAM dendrimers in their ability to reduce the light attenuation of the SC after topical application (Welzel, 2001).

The optical effect that the PAMAM dendrimer exerts upon the skin surface appears to be temporary in nature and this is an important characteristic in a topical penetration enhancer (Idson, 1971). After rinsing off the applied PAMAM dendrimer, the strong reflective entrance signal on the interface of the skin re-appeared on OCT images. A PAMAM dendrimer is a large macromolecule with limited permeation capacity and is confined to the superficial layers of the SC. This allows for a transient and reversible effect as shown throughout the OCT images. This section provides further evidence that dendrimers are of benefit in the dermal delivery of topical pharmaceuticals.

Light microscopy after haematoxylin and eosin (H&E) staining revealed no major morphological changes to the SC (Figure 4.10). The only difference visible between the vehicle control and the PAMAM dendrimer dosed skin was that the SC appeared to be more compact. After PAMAM dendrimer application the SC appears compact and dense which has been observed in clinical trials after microdermabrasion (Shim *et al.* 2001) and after tretinoin treatment (Ellis *et al.* 1990). These studies however, were conducted *in vivo* over many weeks and therefore the compaction is due to metabolic activity. As the dermatomed porcine skin is *ex vivo* and is not metabolically active the compaction is due to an extrinsic physical affect. That could be an artifact of the cryo-sectioning process though cryo-sectioning compared to other sectioning techniques has been shown to result

in minimal tissue compression in the z axis (Gardella *et al.* 2003). Another possibility is that the dense, aqueous and cationic PAMAM dendrimer layer causes compaction of the SC and thus reduction of the path-length for the permeation of CHG. This hypothesis would support the percutaneous absorption data in which PAMAM dendrimers were shown to enhance the localization of CHG throughout the dermatological layers of the skin. Further studies would be required to confirm this hypothesis. After application of a 5 % SDS solution (w/w) the damage to the SC was significant with disruption and severe disintegration to the SC layers. This degree of alteration to the SC barrier was not observed after application of the PAMAM dendrimer solution.

The barrier integrity, OCT and histology studies suggested that the PAMAM dendrimer's effect on the skin was not on a macro scale. Cyclodextrins are large macromolecules that demonstrated to have a permeation enhancement effect upon the skin. It has been reported that cyclodextrins can extract skin components which may be a contributing mechanism of action to their drug penetration enhancement effect (Legendre *et al.* 1995). Whilst the PAMAM dendrimer solution did extract cholesterol (over 24 h) from the skin (0.293 ± 0.142 µg/mL), the positive control extracted more than five times the concentration of cholesterol. The vehicle control did not extract any detectable levels of cholesterol; this was expected as lipid loss from the skin does not occur due to water: methanol solutions (Abrams *et al.* 1993). Under all test concentrations only very low concentrations of cholesterol below the calculated LOQ were detected; particularly when compared to the cyclodextrin 2-hydroxypropyl β-cyclodextrin that extracted a concentration of 7 µg/cm^2 of cholesterol from rat skin (Legendre *et al.* 1995). The total cholesterol content of the SC is 38.8 % (w/w) (Walters and Roberts, 2005) therefore a minimal

concentration of cholesterol was extracted by the PAMAM dendrimer. Cholesterol extraction due to the PAMAM dendrimer may be an almost insignificant contributing factor to their drug penetration enhancement effect upon the skin. As the positive control failed to extract a concentration of cholesterol above the LOQ, extraction over a larger skin area (this study used 2.54 cm^2 skin area) should be examined in future work. Other possibilities include increasing the sensitivity of the detection system or replacing the positive control with a more effective cholesterol extractor.

To further investigate the skin's modification as a result of contact with PAMAM dendrimers a Lowry protein assay with a Peterson's modification was used to detect and quantify extracted protein from the skin. The concentrations detected were again very low, the positive control yielded a protein concentration below the LOD of the assay (1 µg/mL) of 0.741 µg/mL in only one Franz cell (*n*=3). One would expect a higher concentration of protein extraction from the skin after a 24 h contact time with chloroform:methanol solution. The PAMAM dendrimer solution yielded a concentration of protein >2.5 times that of the positive control. The low concentrations of protein extracted are at the LOD which for bovine serum albumin was calculated to be 3 µg/mL (Sözgen *et al.* 2006). This assay is however sensitive to different protein compositions therefore diverse proteins result in different absorbance values (Winters and Minchin, 2005). The results suggest that the PAMAM dendrimer solution may extract a higher concentration of protein from the skin than the positive control but as the results are at the LOD further studies would have to be conducted for confirmation. Again the positive control failed to yield a concentration of protein above the LOD and the PAMAM dendrimer extracted protein only marginally over the LOD. For future assays a larger surface

area of skin should be utilised for the extraction procedure to ensure any protein extracted is above the LOD.

ATR-FTIR was utilised in an attempt to elucidate the interactions between the amine and carboxyl terminated PAMAM dendrimers and isolated SC. The ATR-FTIR spectra did show some evidence of interaction between the PAMAM dendrimer and the isolated SC. The amide I band arises from the C=O stretching vibration and the amide II band arises from the C-N stretching and the N-H bending (Shakeel *et al.* 2008). These correlate to the proteins of the SC. Shifts in the amide bands are related to changes in the hydrogen bonding of the proteins to the heads of the ceramides. It is this hydrogen bonding that affords support to the bilayers of the intercellular lipids and thus plays an integral part of the skin's barrier properties (Panchagnula *et al.* 2005 and Moore *et al.* 2001). The polycationic PAMAM dendrimers may have disrupted the network through competitive hydrogen bonding with the amide head groups of the ceramides causing a shift in the amide I and amide II bands. Terpenes which are also penetration enhancers are thought to disrupt the hydrogen bonding due to competitive bonding between the terpene and ceramide which results in lower activation energy required for diffusing drug molecules (Jain *et al.* 2008). This mechanism may explain the increase in permeation of CHG within the skin after a G3-PAMAM-NH_2 dendrimer pre-treatment.

Further, a peak shift was observed in the conformation sensitive CH_2 wagging and scissoring modes after G3-PAMAM-NH_2 dendrimer treatment. CH_2 wagging modes are very sensitive to alterations in the chain and packing order of lipids (Mendelsohn *et al.* 2000). This suggests that the G3-PAMAM-NH_2 dendrimer

alters the packing and organisation of the intercellular lipids. Perturbation of the skin lipids would result in an impaired SC and would thus result in an enhanced topical drug delivery as observed for CHG within Chapter 3. A different change in spectra was observed when the isolated SC was incubated with G3.5-PAMAM-COOH dendrimer. For the amide I band it appears that there is a shoulder peak resulting from the overlap of the amide I band with the -OH- peak resulting from water within the sample. There was a change in the wavenumber of the CH_2 scissoring peak which corresponds to conformation changes to the densely packed lipids (Bouwstra *et al.* 2003).

There was no difference in the wavenumber of the symmetric and asymmetric methylene stretching modes at around 2850 and 2920 cm^{-1} for G3-PAMAM-NH_2 (when compared to the vehicle control) but a peak shift did occur after application of G3.5-PAMAM-COOH (Figure 4.18) (Moore and Rerek, 2000). There were frequency shifts when the native SC was compared to the G3-PAMAM-NH_2 vehicle control so that it is the water:methanol solution that disorders the fatty acid and ceramide chains and not the cationic G3-PAMAM-NH_2 dendrimer in this case. Figures 4.18 and 4.19 do however show that the carboxyl terminated PAMAM dendrimer causes a shift in wavenumber (when compared to the vehicle control) corresponding to disorder of the fatty acid and ceramide chains (though this was not shown to be significant).

The ATR-FTIR spectra confirms that both amine and carboxyl terminated PAMAM dendrimers exhibit a disordering effect of the intercellular lipid packing and the hydrogen bonding of the SC proteins to the ceramide head groups. This

perturbation of the SC barrier may explain the enhanced drug deposition observed in Chapter 3.

4.4 Conclusion

This Chapter addresses a number of gaps in the literature about the mechanism of action of PAMAM dendrimers and their properties as penetration enhancers. In the present work there was no observed PAMAM dendrimer induced damage to the skin on a macro scale as illustrated by barrier integrity studies including TEER, TEWL and histological analysis of haematoxylin and eosin stained cryo-sectioned skin. It was determined that PAMAM dendrimers extract negligible concentrations of cholesterol and protein from the skin. Though the results obtained were below the LOQ extraction of skin components by the dendrimer should not yet be ruled out may still be a minor contributing cause of enhanced topical drug delivery. Disruption of the packing and organisation of the SC lipids, hydrogen bonding between SC proteins and ceramide head groups was made evident by the collected ATR-FTIR spectra. Further, the OCT images suggest that the PAMAM dendrimers accumulate within the follicles and undulations of the skin. The OCT images also allude to a transient PAMAM dendrimer affect as the alterations to the optical characteristics of the SC recovered after the PAMAM dendrimer was washed from the SC surface. This Chapter has illustrated that it is likely there are a range of contributing factors that allow for PAMAM dendrimers to act as topical and transdermal penetration enhancers. This new information may aid the optimisation and design of future dendritic architectures as a platform for efficacious topical and transdermal drug delivery.

5.0 The use of time-of-flight secondary ion mass spectrometry to map the distribution of CHG within tissue.

5.0 Introduction

5.0.1 Techniques available for imaging drug-skin deposition

In order to develop more efficacious strategies towards effective topical antisepsis it is imperative to first understand the localization and distribution of the antimicrobial compound throughout the skin strata, following its application to the skin, in order to determine whether the compound reaches the microbial reservoir. This also stands for all topically applied compounds including antiperspirants, antifungals, cosmetics that are applied to the skin intentionally, in addition to pesticides and industrial chemicals that may come in contact with the skin during normal use. Mapping the location of a compound *in situ* within a biological tissue as complex as the skin, may also aid in elucidating the permeation pathway and mechanism of action. Conventional diffusion studies, such as those conducted using Franz-type skin diffusion cells, combined with tape stripping can yield informative dermatopharmacokinetic data (N'Dri-Stempfer *et al.* 2009 and Alberti *et al.* 2001) for topically applied drugs.

The existing gold standard is a tape stripping technique that was described in Chapter 3. Whilst it is a widely accepted method for investigating the dermatopharmacokinetics of topically applied drugs and chemicals where the method has been validated in human volunteer studies (Trebilcock *et al*, 1994) there are

some methodological flaws leaving scope to develop alternative novel methods. There is great inter-laboratory variability with regards to tape stripping methods and the methods are also laborious and time-consuming (Marttin *et al.* 1996). There are also difficulties in standardizing the tape stripping to determine the amount of a compound in different layers of the epidermis due to the removal of varying amounts of the *stratum corneum* (SC) (Van der Molan *et al.* 1997, Lademann *et al.* 2009 and Dreher, 2007). Whilst there have been advances in quantifying SC material on each tape strip, in a purely comparative sense, some tape stripping approaches are still laborious and time consuming. Gravimetric analysis (Higo *et al.* 1993) and others require destructive techniques, for example: a modified protein Lowry assay (Dreher *et al.* 2005). Other protein quantification techniques require further analytical equipment such as a microscope (Lindemann *et al.* 2003), spectroscopic equipment (Weighmann *et al.* 2003) and an infra-red densitometer (Voegeli *et al.* 2007 and Hahn *et al.* 2010). The ToF-SIMS technique is rapid in comparison and as well as detecting the drug or biomolecules of interest, it also has means of only including SC material in the analysis.

Imaging techniques that have been applied to mapping percutaneous absorption include Confocal Laser Scanning Microscopy (CLSM) (Alvarez-Roman *et al.* 2004), Infra Red (IR) imaging (Mendelsohn *et al.* 2006), Confocal Raman Microscopy (Zhang *et al.* 2007), Stimulated Raman Scattering Microscopy (Saar *et al.* 2011) and Matrix-Assisted Laser Desorption/Ionisation - Time of Flight mass spectrometry (MALDI-ToF) analysis. Confocal studies have the advantage of being able to capture 3D optical images of the skin but the information obtained is based

upon a fluorophore, that may limit the application of the technique, particularly as species often require fluorescent “tagging”. This restricts the number of compounds that can be analyzed by confocal microscopy; fluorescently tagging a compound may yield localization information within tissue that does not necessarily reflect that of the native compound. IR and Raman microscopes have an achievable spatial resolution (pixel size) of around 4-10 µm (Kazarian and Chan, 2013) and ~1 µm (Krafft *et al.* 2009), respectively.

Recently with the advent of stimulated Raman scattering microscopy, low sensitivity and interference signals from the coherent non-resident background have been overcome, therefore it now offers label-free, non-invasive and real-time skin imaging (Freudiger *et al.* 2008). Stimulated Raman scattering microscopy is a relatively new and non-destructive skin-imaging technique that has been used to image skin drug delivery of retinoic acid, the distribution of DMSO (Freudiger *et al.* 2008) and the chemical distribution of ibuprofen and ketoprofen throughout mammalian skin (Saar *et al.* 2011). Raman spectroscopy techniques offer the advantages of being a non-invasive, 3D high resolution imaging technique (Lademann *et al.* 2012). Mass spectral imaging techniques offer unparalleled sensitivity. MALDI-ToF has been employed successfully to characterize the deposition of pharmaceutical compounds within skin but again lacks the desired spatial resolution (each pixel corresponds to 0.2 mm × 0.2 mm) (Bunch *et al.* 2004). Within the Bunch *et al.* paper the mass spectrum obtained had to be overlaid onto a haematoxylin and eosin stained skin Section, which may be considered somewhat subjective. Whilst there is advanced MALDI software available to superimpose MALDI

spectra over an optical image, it is not possible to distinguish morphological features only the tissue outline (Walch *et al.* 2008). Therefore typically the tissue Section would have to be histologically stained to correlate the tissue with the MALDI IMS spectra (Chaurand *et al.* 2006). There are nevertheless advancements being made and commercially available imaging MALDI instruments that have achieved a 20 µm spatial resolution when analyzing biological samples (Lagarrigue *et al.* 2011).

5.0.2 Time-of-flight Secondary Ion Mass Spectrometry

Time-of-Flight Secondary Ion Mass Spectrometry (ToF-SIMS) is a highly sensitive surface analytical technique that characterises the surface chemistry of a sample accompanied by the spatial distribution. It was initially predominantly used for the analysis of inorganic samples such as semiconductors (Zanderigo *et al.* 2000 and Douglas and Chen, 1998), polymers (Wien, 1997, Briggs, 1998) and Urquhart *et al.* 2008) and solid state therapeutics (Prestidge *et al.* 2010). With the advent of liquid metal cluster ion sources such as Bi_n^+ and polyatomic cluster ion sources such as C_{60}^+ and Ar superclusters it became possible for improved data analysis of higher mass biomolecules. This advancement meant that more efficient primary ions could be produced resulting in an increased yield of secondary ions and thus an increase in sensitivity when analysing large biomolecules. The incorporation of a flood gun ensuring charge neutralisation allowed for the analysis of organic material. The use of a cryostage enabled hydrated biological tissue to be kept frozen at a temperature < 70°C whilst under ultra high vacuum to maintain the morphology of the tissue Sections.

ToF-SIMS analysis involves rastering a pulsed primary ion beam onto the sample surface that is supported by a cryostage *in vacuo* (Figure 5.1). This bombardment of ions results in a collision cascade on the sample surface (~1 - 2 nm of the outermost surface) resulting in the liberation of secondary ions (Figure 5.2). These secondary ions are made up of monatomic and polyatomic particles, whole molecules and fragment ions, some of which will carry a positive or negative charge and many will remain neutral (Barnes *et al.* 2011). They occur due to a range of processes including fragmentation, gaining of protons, loss of protons or less frequently due to molecular re-arrangement. The charge of the ion is dependent on the species' ionisation efficiencies (Grams, 2007). The liberated secondary ions of the same polarity and thus kinetic energy are then accelerated into the drift field of the time-of-flight analyzer (Schueler, 1992). The secondary ions are separated according to their mass-to-charge ratio, which is dependent on the time taken for the ion to reach the detector. With the sputtering of charged species from the sample surface an electron flood gun is used to then neutralise the sample (Barnes *et al.* 2011).

A significant benefit of utilising a ToF-analyser is that it can simultaneously detect all secondary ions of the same polarity resulting in each pixel of the spatial map representing a full mass spectrum (Belazi, 2009). As a result, ToF-SIMS has the ability to characterise the spatial distribution of a compound within the surface of complex tissue; this can yield information on the distribution of the drug within the tissue and may allow elucidation of the mechanism of action (Benninghoven, 1994).

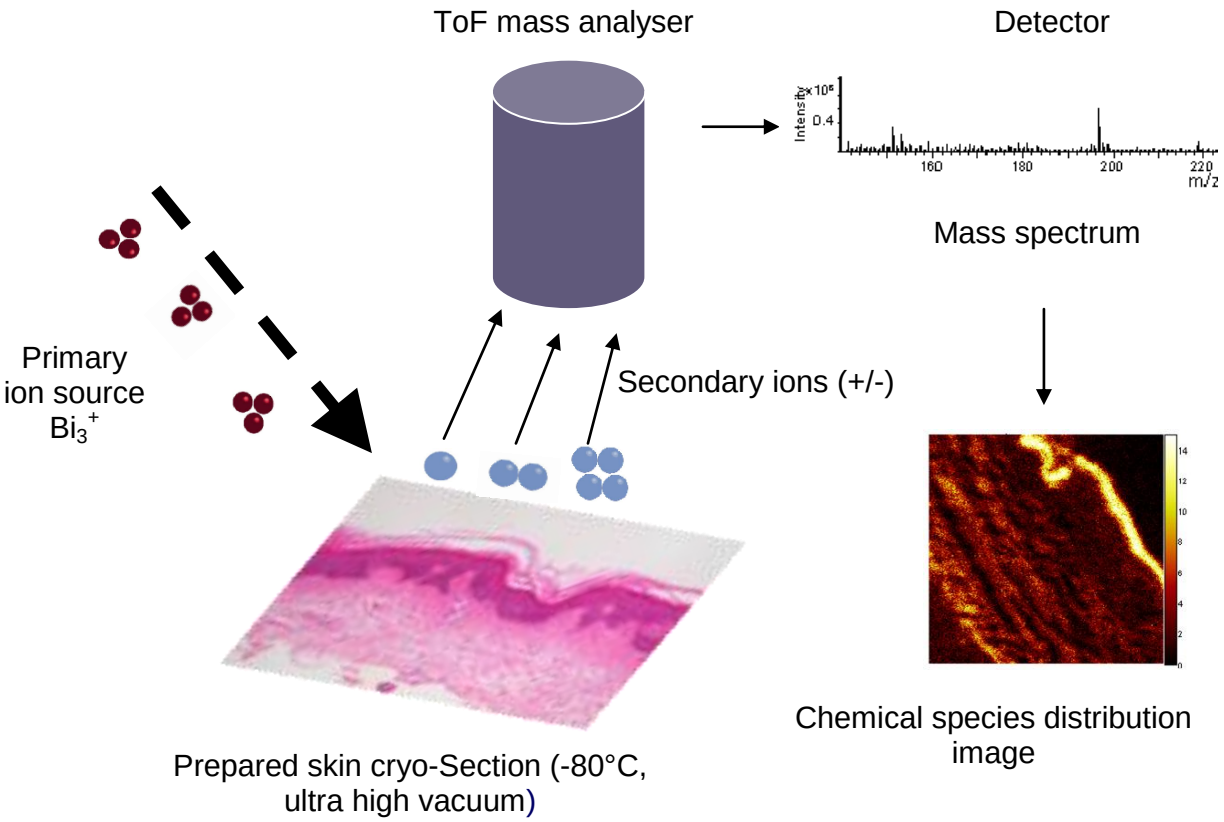

Figure 5.1 Schematic of the analysis of a skin cryo-Section by ToF-SIMS. *Primary ions from a Bi_3^+ are rastered onto the frozen skin Section surface and after a collision cascade, secondary ions are emitted. Those of the selected polarity are accelerated by an electric field into the flight path of a time-of-flight mass spectrometer in which the ion's mass to charge ratio is determined. The detector receives chemical and spatial information therefore a chemical distribution image can be retrospectively built.*

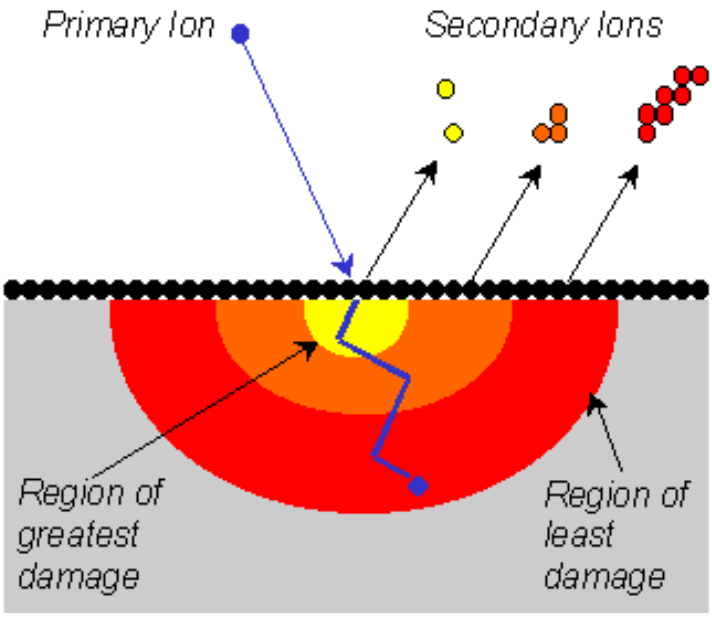

Figure 5.2. Schematic of the SIMS process taken from: http://www.phi.com/surface-analysis-techniques/tof-sims.html [Accessed on 11/3/13].

5.0.3 Characteristics of ToF-SIMS

The advantages of ToF-SIMS include high mass resolution (>7,000), a wide mass range, from the detection of elements up to the detection of macromolecules, excellent spatial resolution (in the burst alignment mode) and an ability to simultaneously detect fragment ions over a wide mass range that can be analysed retrospectively (Chabala *et al.* 1995). These capabilities are unsurpassed by spectroscopy techniques or other imaging mass spectral methods such as MALDI-ToF. Chemical images of selected secondary ions can be retrospectively reconstructed for the analysed areas or a selected region of interest (Figure 5.1). Each pixel within the chemical image corresponds to a full mass spectrum, yielding

substantial chemical and spatial information for each sample. The ability to analyse the data retrospectively reduces the number of samples that would need to be tested, particularly in light of new information. For example, if the ToF-SIMS analysis reveals that a drug has a particular affinity for a specific biomolecule, previously obtained data can be re-analysed incorporating that biomolecule. This capability would be ideal in drug development and toxicology. Furthermore, as the ToF analyser detects all secondary ions liberated of the same polarity, the technique has the potential for analysing the localisation of not only the active therapeutic but also many other components of a complex dose formulation. This has the potential for analysis of excipients in parallel, e.g. in topical preparations the preservatives that may act as a skin irritant, or visualisation of the distribution of silicones across the skin surface.

ToF-SIMS chemical distribution maps not only highlight the localization of an exogenous compound within the tissue but can also profile the organic components of the different histological compartments of the tissue sample, allowing the depth of permeability to be estimated. The localization of the therapeutic agent within a particular tissue layer or the binding to a particular biomolecule may elucidate a drug's permeation or any drug depot effects (Andanson *et al.* 2009 and Teichman *et al.* 2005). This effect has been observed within this Chapter where CHG was shown to be highly associated with the SC in both cryo-Sections of skin tissue and on tape strips. Another benefit of the technique is that it is not dependent on the penetration of a reagent or probe reactivity and is not adversely affected by background staining (Malmberg *et al.* 2011). ToF-SIMS is the analysis of native molecules such as

un-labelled exogenous chemicals or endogenous biomolecules within un-fixed organic tissue.

The limitations of ToF-SIMS include its inherent inability for quantification due to matrix effects (Benninghoven, 1994). The yield of secondary ions is dependent on the ionization energies of the various species analysed, i.e. the secondary ion yield for a particular species is dependent on the strength of the bonding to the matrix (Piantadosi and Smart, 2002). If the matrix is kept consistent then the secondary ion yield should be proportional from sample to sample over a specific area for comparison. When analysing samples as complex as biological tissue, only semi-quantitative analysis is possible due to these matrix effects. ToF-SIMS is an analytical technique and as such the system may incur instrumental drift (Thompson, 1991). One limitation to the analysis of biological material is that ultra-high vacuum conditions must be maintained throughout the analysis. To maintain morphology cryo-preparation such as those techniques used in electron microscopy must be utilised. Confirmation of the tissue structure integrity and cell morphology is however possible by using conventional histological analysis after ToF-SIMS analysis (as conducted within this Chapter).

Though ToF-SIMS analysis of biological samples is in its infancy, a broad range of biologics have been analysed to date including; mouse adrenal gland cortex (Malmberg *et al.* 2011), *xenopus leavis* oocytes (Fletcher *et al.* 2007), He La cells (cervical cancer cell line) (Fletcher *et al.* 2008) and Sections of rat brain (Benabdellah *et al.* 2010 and Nygren *et al.* 2005). Previous studies have been limited regarding

ToF-SIMS and skin tissue analysis. Previous studies included the analysis of the incorporation of pseudo-ceramides into the *SC* delivered from a cosmetic formulation (Okamoto, *et al.* 2006) and (Tanji *et al.* 2008). These studies used high resolution chemical images of the skin surface to which the pseudo-ceramides had been applied in order to demonstrate that synthetic pseudo-ceramides can effectively partition into the SC. The analysis of the cosmetic formulation treated skin samples resulted in two unique ion peaks that were unique to the pseudo-ceramides and were not present in untreated samples. The unique fragment ions giving rise to the two additional ion peaks were clearly attributed to the pseudo-ceramides as the peaks were not present in the analysis of native ceramides. The difference in mass spectra between the native and pseudo-ceramide was exploited by the authors to investigate the incorporation of pseudo-ceramides within the SC. This study showed that ToF-SIMS can provide valuable information regarding the distribution of cosmetic components within the skin.

The application of ToF-SIMS to biomedical and biophysical applications has been shown previously. For example, photo-ageing effects on skin, before and after UV irradiation, were determined and changes in the ToF-SIMS chemical images of key skin components such as collagen and lipid molecules within a cross Section of human skin were reported (Lee *et al.* 2008). A ToF-SIMS study into the analysis of human skin lipids has previously been conducted, where the authors characterised the chemical distribution profile of skin lipids and vitamin E within normal human skin (Belazi *et al* 2009). Despite these studies having produced novel and biomedically relevant chemical distribution data for human skin, no subsequent follow up ToF-

SIMS studies have since been published. This Chapter outlines the use of analyzing the localization of a common topically applied antiseptic and investigates a novel permeation enhancer. There is great scope to further develop the ToF-SIMS method from both an efficacy and toxicology point of view with wide ranging biomedical applications discussed further in the Chapter.

Whilst CHG has been used extensively in topical antimicrobial formulations, it has been shown in Franz cell diffusion studies to permeate into and across the skin poorly (Lafforgue *et al.* 1997) and (Karpanen *et al.* 2008), leaving potential pathogens viable within the deeper layers of the skin. To develop novel and efficacious antisepsis strategies it is imperative to first understand the drugs deposition on the skin surface and within the epidermis as little is understood about its distribution post topical application. There is increasing interest in the development of suitable protocols and applications for imaging techniques that do not require radiolabelling or laborious sample preparation. ToF-SIMS has the potential to determine the distribution of CHG and other topically applied antimicrobials to fully elucidate a biocide's permeation pathway. At the time of writing there are no published studies investigating the application of ToF-SIMS to skin permeation and distribution of therapeutic agents. Thus, this is the first time ToF-SIMS has been utilised to visualize the distribution of a topical antiseptic applied to the skin.

5.0.4 Aims and objectives

The primary aim of this study was to use ToF-SIMS to map the distribution and localization of a clinically relevant, topical dose of chlorhexidine digluconate (2 % w/v) once applied to dermatomed porcine skin. In order to validate the results and ensure no artifacts due to the cryo-preparation are involved, a tape stripping study was undertaken in parallel with using cryo-Sectioned skin. These tape strips were also analysed by ToF-SIMS to determine the potential application of combining conventional tape stripping skin studies with a novel ToF-SIMS detection system.

The aims of this Chapter are as follows-

(i) To develop a simple and rapid method for dosing *ex vivo* porcine skin for ToF-SIMS analysis.

(ii) To determine whether CHG can be distinguished from endogenous skin components and whether unique fragment ions for the drug can be detected.

(iii) To use the developed novel method to map the distribution and permeation of CHG once topically applied to *ex vivo* porcine skin. Further, to establish whether it is possible to make semi-quantitative measurements of CHG ingress into the skin.

(iv) To combine the novel ToF-SIMS method with the widely accepted tape strip method to determine whether a permeation profile could be created from the ToF-SIMS analysis of individual tape strips. This may also be

developed further to allow for the measurement of ingress of exogenous chemicals within the skin.

PAMAM dendrimers were shown to enhance the permeation of chlorhexidine in Chapter 3. An additional aim of this Chapter was to visualize the permeation enhancement effect of a PAMAM dendrimer pre-dose on the model antiseptic, CHG. The ToF-SIMS method developed in this Chapter may be applied in the analysis of the efficacy and localization of permeation enhancers.

5.1.0 Materials and Methodology

5.1.1 Materials

Chlorhexidine digluconate (CHG) 20 % (w/v) and NaCl for physiological saline (0.9 % w/w) were purchased from Sigma Aldrich, UK. Tape stripping was performed using Scotch tape, 3M, UK. Analytical grade methanol, chloroform and hexane were obtained from Fisher, UK and were used to solvent-clean glass cover-slips prior to sample mounting. De-gassed ultra pure water was used for the preparation of receptor fluid and for skin surface washings. Skin integrity was measured using Trans-Epithelial Electrical Resistance (TEER) LCR Databridge, Tansley, UK. Skin Sectioning was conducted using a cryostat (Leica, CM1850). The temperature of the cryostat chamber was found to be optimal for cryo-Sectioning skin Sections at -28°C. Samples were embedded within OCT embedding material, supplied by Fisher scientific, UK. OCT is an inert mounting medium containing 10.24 % (w/w) polyvinyl alcohol 4.26 % (w/w) polyethylene glycol 85.5 % (w/w) non-reactive ingredients. As

the OCT embedding material is frozen on contact with the skin sample at -28°C there should be minimal interaction between the mounting agent and tissue and is widely considered inert.

5.1.2 Skin preparation

Skin was prepared from the flank of six week old pigs obtained from a local abattoir prior to any steam cleaning treatment. The skin was washed with distilled water and carefully shaved using clippers so as to not damage the integrity of the tissue. The subcutaneous fat was carefully removed using a scalpel and then the skin was dermatomed to a thickness of 400 μm with an electric dermatome. It was then wrapped in aluminum foil and frozen at -20°C until required. The dermatomed skin was then punched out with a 3 cm diameter punch and placed upon a stainless steel mesh support grid within a Franz cell, with the SC facing upwards. To check the integrity of the skin, 4.5 mL of physiological saline was added to the receptor chamber and 2 mL of physiological saline was added to the donor chamber and placed in a circulating water bath on a submersible magnetic stirrer at 32°C for 30 minutes. After the cells had equilibrated, the TEER was measured to check the integrity of the porcine skin. Prior to readings being taken, the instrument was calibrated using a resistor. It has been established that healthy and intact porcine skin in Franz-type cells used should have an electrical resistance reading of ≥ 3 KΩ to pass the integrity check (Davies *et al.* 2004).

5.1.3 Diffusion (Franz-type) cell study

The diffusion cells that had passed the integrity check were removed and the skin was allowed to air dry for 2 h at ambient temperature. 4.5 mL of physiological saline was added to the receptor chamber of each Franz cell. The Franz cells were placed in the water bath (32°C) on a submersible stirring plate for 30 minutes and allowed to equilibrate. A 2 % (w/v) solution of CHG and a 10 mM solution of G3-PAMAM-NH_2 were prepared in distilled water from a 20 % (w/v) solution of CHG and a 20 % (w/v) solution of G3-PAMAM-NH_2 stock. Once the Franz-type cells had equilibrated, the G3-PAMAM-NH_2 (0.2 mL, 10 mM) was dosed for a 24 h contact period. After 24 h the G3-PAMAM-NH_2 was washed from the skin surface of each diffusion cell by rinsing with 2 mL aliquots of distilled water (10 mL in total) over the surface of the dosed skin. Once the skin surface was dry (left at ambient temperature to dry for 2-3 h) an infinite dose (1 mL) of the CHG solution was applied to the skin surface and left for a contact time of 24 h. Excess CHG was removed from the skin surface of each diffusion cell by rinsing with 2 mL aliquots of distilled water (10 mL in total) over the surface of the dosed skin, taking care not to damage the skin. The skin was then allowed to air dry at ambient temperature, after which the Franz-type cells were dismantled and the skin destined for the cryo-Section experiment was snap frozen in liquid nitrogen. Skin samples intended for the tape stripping study were stripped immediately after as described in Section 3.2.4 and as outlined elsewhere (Trebilcock *et al.* 1994) and (OECD, 2004). Samples were then transported to the cryostat and the ToF-SIMS instrument on dry ice.

5.1.4 Sample preparation for ToF-SIMS analysis

The frozen skin samples were mounted on a cryostat using Optimal Cutting Temperature (OCT) embedding material. Vertical cross Sections of skin of an 8 µm thickness were cut and placed on to a clean glass cover-slip (1 cm × 1 cm). The cover slips were first rinsed in ultra-pure water followed by methanol, chloroform and lastly hexane before the skin sample was loaded. For the tape strip experiment, 21 tape strips were taken to remove the SC. The strips were then freeze-dried and placed on a solvent-cleaned microscope slide ready for analysis.

5.1.5 ToF-SIMS analysis

Full credit for the ToF-SIMS analysis must go to Dr David Scurr at the Laboratory of Biophysics and Surface Analysis at the School of Pharmacy, University of Nottingham. ToF-SIMS was performed on a ToF-SIMS IV instrument (IONTOF, GmbH, Münster, Germany) using a Bi_3^+ cluster primary ion source and a single-stage reflectron analyzer. ToF-SIMS data was analysed using SufaceLab 6 software. The cover-slip containing the samples was mounted onto a cryo-stage with a cold-finger mechanism and frozen to -80°C using a liquid nitrogen cooling system. The mounted skin samples were then exposed to an ultra high vacuum. A primary ion energy of 25 kV along with a pulsed target current of approximately 1 pA and post-acceleration energy of 10 kV were employed throughout the analysis (Mains *et al.* 2011). The primary ion dose density was maintained at less than 1×10^{12} ions per cm^2 throughout to ensure static conditions. Spectra were acquired in both the positive and negative modes at a resolution of 256 × 256 pixels by scanning a primary beam over

the sample area. Charge compensation of the sample was performed by irradiating the sample with a pulsed beam of electrons using an electron flood gun. Samples were analysed using both bunched and burst alignment modes thereby providing both high mass and spatial resolution data, respectively. A reference sample of OCT was analysed whereby a small amount of the OCT embedding material was applied to a solvent cleaned cover slip.

Data processing was performed using SurfaceLab 6, IONTOF (Münster, Germany) for both spectroscopy and image analysis. Although data was collected in both positive and negative polarity, only the negative ion data will be presented as the positive ion data, though supportive, is much less informative. A scheme of the sample preparation and analysis can be observed in Figure 5.1.

5.1.6 Statistical analysis of data

All data shown within this Chapter are displayed as the mean ± SEM/ SD (as stated) followed by the sample number. To determine whether there was statistical significance between the data presented in Figure 5.18 (the measured CHG ingress (µm) within the skin, with and without a PAMAM dendrimer pre-treatment) a two way T test was conducted after confirming the data was normally distributed in a histogram using the software GraphPad Prism® version 5 (San Diego, USA).

5.2.0 Results

5.2.1 Method Development

5.2.1.1 Identification and analysis of fragment ions characteristic of chlorhexidine digluconate (CHG).

To discover fragment ions that are unique or characteristic of CHG, dermatomed porcine skin (400 µm in thickness) was dosed with a 2 % solution of CHG (w/v) overnight and unabsorbed CHG was washed from the skin surface. Once analysed in the negative polarity an overview spectra corresponding to treated and untreated skin was obtained (Figures 5.3 and 5.4). The overview spectra with an equivalent scale were used to indicate characteristic ion peaks in the CHG treated spectra that were more intense or were not present in the untreated spectra. The peak corresponding to chlorine was highly prominent in the CHG treated skin compared to the untreated skin. A peak at 151 atomic mass units (amu) was documented within the overview spectrum (Figure 5.3 (a)) and was calculated to be $C_7H_4N_2Cl^-$ (m/z = 151). The structure of this fragment ion was determined (Figure 5.3 (b)) and it corresponded to a fragment of one of the aromatic branches of chlorhexidine. This peak is not present for the untreated skin as observed in the spectrum magnification (Figure 5.3 (c)). Survey spectra illustrating the ion peaks of a higher mass (160-550 amu) contained the molecular ion ($[M-H]^-$) for chlorhexidine (Figure 5.4 (a)). At 505 amu a peak corresponding to the $[M-H]^-$ can be observed for CHG treated skin but no ion peaks are observed for the untreated skin at this mass (Figure 5.4 (b-c)). These characteristic element and fragment ions have been used as a marker for CHG within this study.

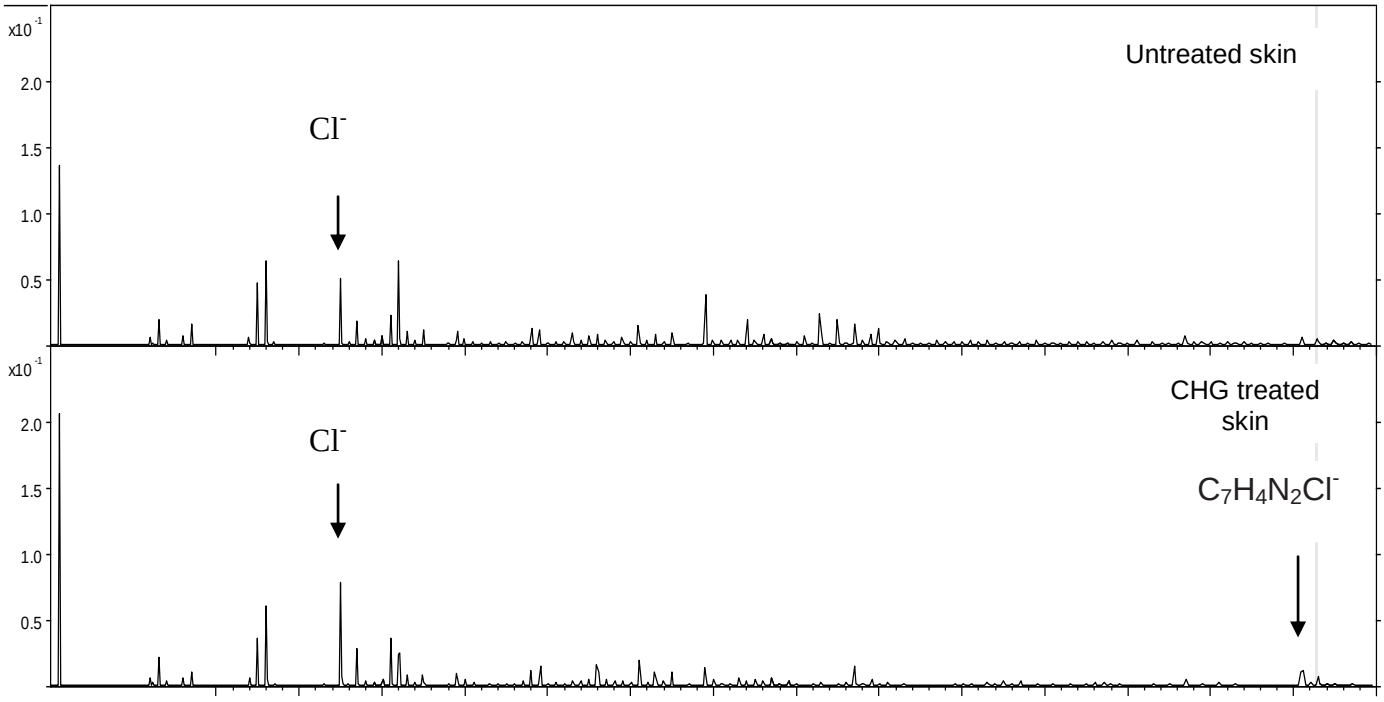

Figure 5.3 (a) Identification of characteristic CHG markers. *ToF-SIMS overview spectrum detected in the negative polarity of un-dosed porcine skin and skin dosed with a 2 % CHG (w/v) solution after a 24h contact time and wash. CHG markers, chlorine and $C_7H_4N_2Cl^-$ fragment ion can be observed.*

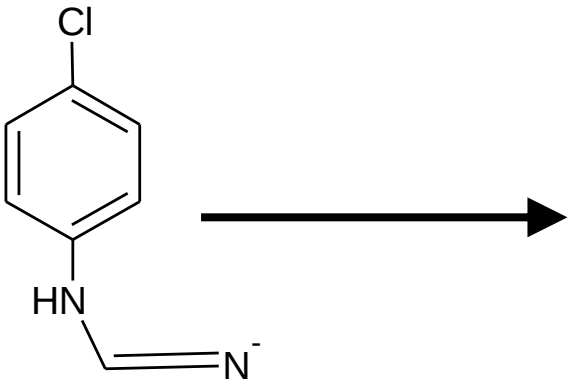

Figure 5.3 (b) *Structure of fragment ion unique to CHG identified from negative polarity overview spectra of CHG treated porcine skin.*

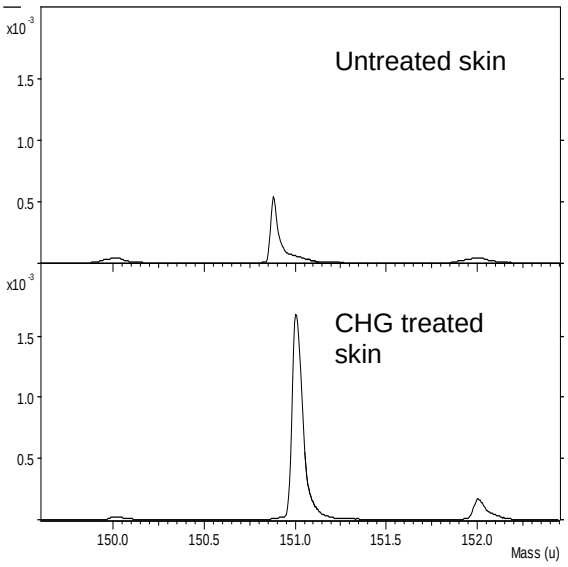

Figure 5.3 (c) *Magnification of CHG unique fragment ion within ToF-SIMS overview spectrum for un-dosed porcine skin and skin dosed with a 2 % CHG (w/v) solution after a 24 h contact time and wash.*

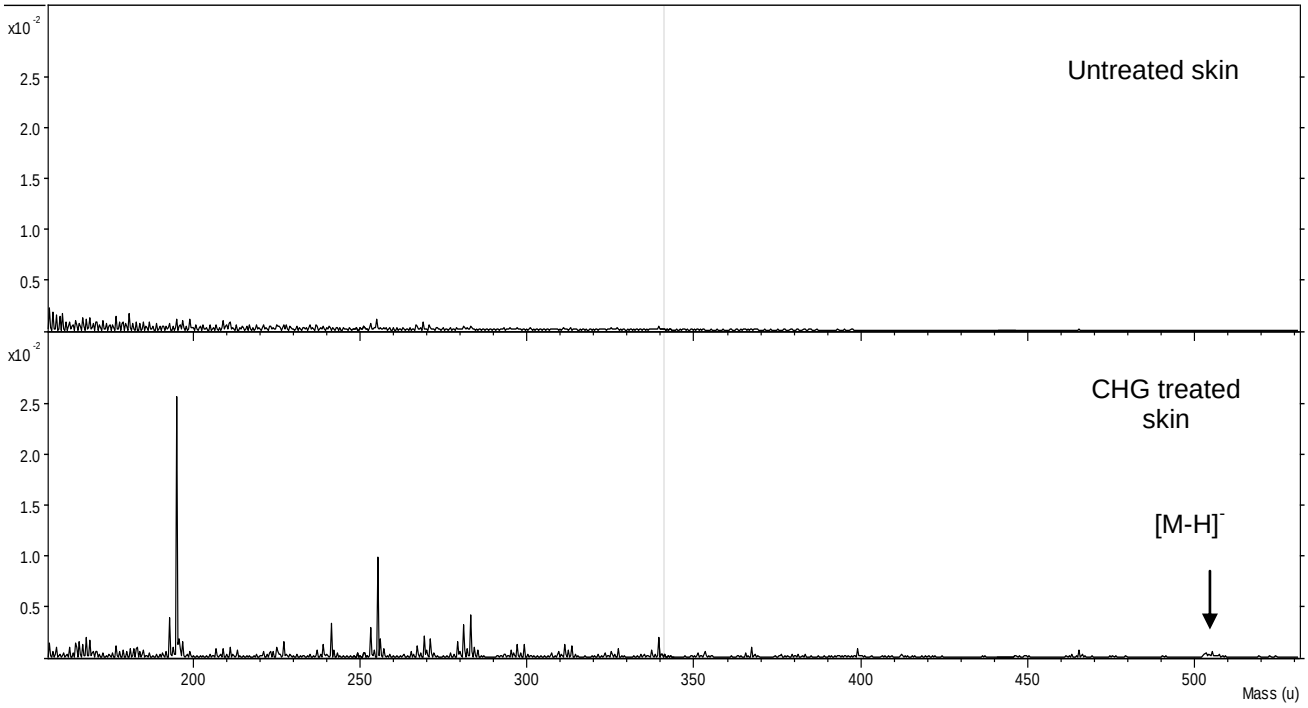

Figure 5.4 (a) Identification of the molecular ion for CHG. *ToF-SIMS overview spectrum detected in the negative polarity of un-dosed porcine skin and skin dosed with a 2 % CHG (w/v) solution after a 24h contact time and wash. CHG markers, chlorine and $C_7H_4N_2Cl^-$ fragment ion can be observed.*

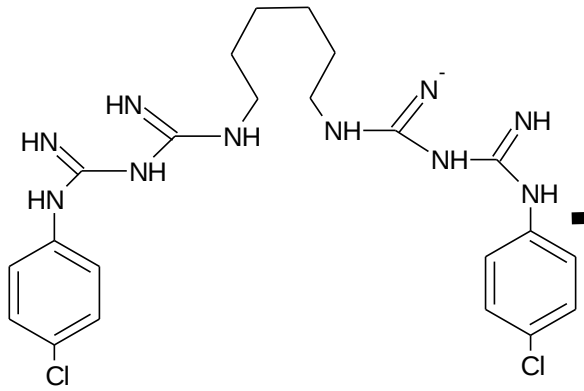

Figure 5.4 (b) *Molecular ion of chlorhexidine $[M-H]^-$ identified within the overview spectra of the porcine skin dosed with a 2 % CHG (w/v) solution.*

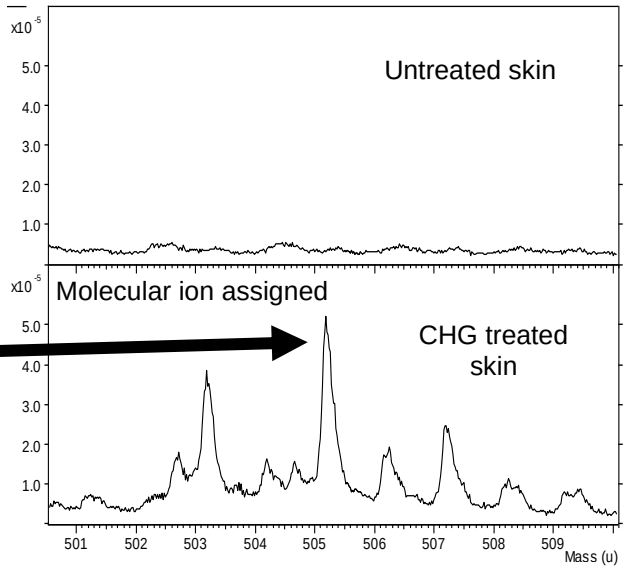

Figure 5.4 (c) *Magnification of chlorhexidine $[M-H]^-$ within the ToF-SIMS overview spectrum for un-dosed porcine skin and skin dosed with a 2 % CHG (w/v) solution after a 24h contact time and wash.*

To visualise the chosen markers from Figures 5.3 and 5.4, the chemical distribution map of the selected markers were obtained from the surface of 2 % CHG (w/v) dosed porcine skin. The justification for the use of porcine skin as a surrogate for human skin was discussed previously in Chapter 3. It was observed that though the ion intensity of chlorine was higher for the CHG treated skin it was still readily observed on the surface of the untreated skin (Figure 5.5). The two markers, $C_7H_4N_2Cl^-$ (m/z = 151) and the $[M-H]^-$ $C_{22}N_{10}H_{30}Cl_2$ (m/z = 505) were visualized clearly and were found to be distributed evenly across the skin surface. At the lower left hand corner of the chemical distribution maps there is a shadow, even in the total ion intensity chemical distribution maps. This is likely due to the uneven topography of the skin surface and therefore may be out of the range of the pulsing primary ion beam.

The difference in mass resolution for the two operating modes is evident using the $^{37}Cl^-$ ion when shown in Figure 5.6. A compromise between high spatial resolution and high mass resolution must be made by either analyzing the sample in the burst alignment mode (high spatial resolution, low mass resolution) or the bunched mode (high mass resolution, low spatial resolution). The ions indicative of the drug should therefore be selected in the bunched mode to achieve the highest mass resolution for fragment ion identification and assignment. All CHG markers were chosen from spectra that were operated in the bunched mode.

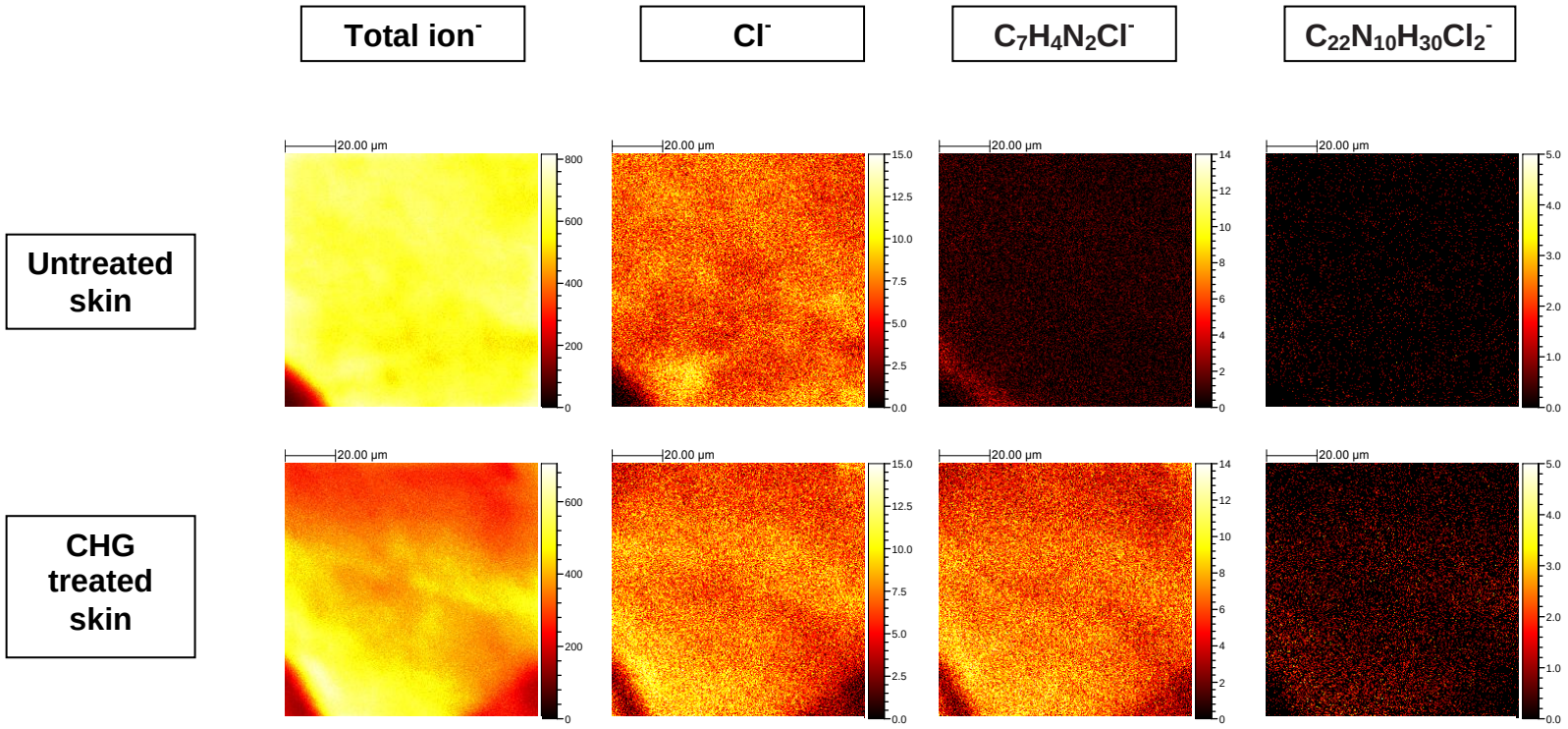

Figure. 5.5 ToF-SIMS images of various secondary ions chosen as markers for CHG. *ToF-SIMS images of Cl^-, $C_7H_4N_2Cl^-$ and $[M-H]^-$ of the negative control and 2 % CHG (w/v) dosed porcine dermatomed skin (400 µm thick). Data taken from skin surface after washing negative control and dosed skin surface with 10 mL of ultrapure water. Scale bar equates to 20 µm, TC represents the total ion count for the specific ion of interest.*

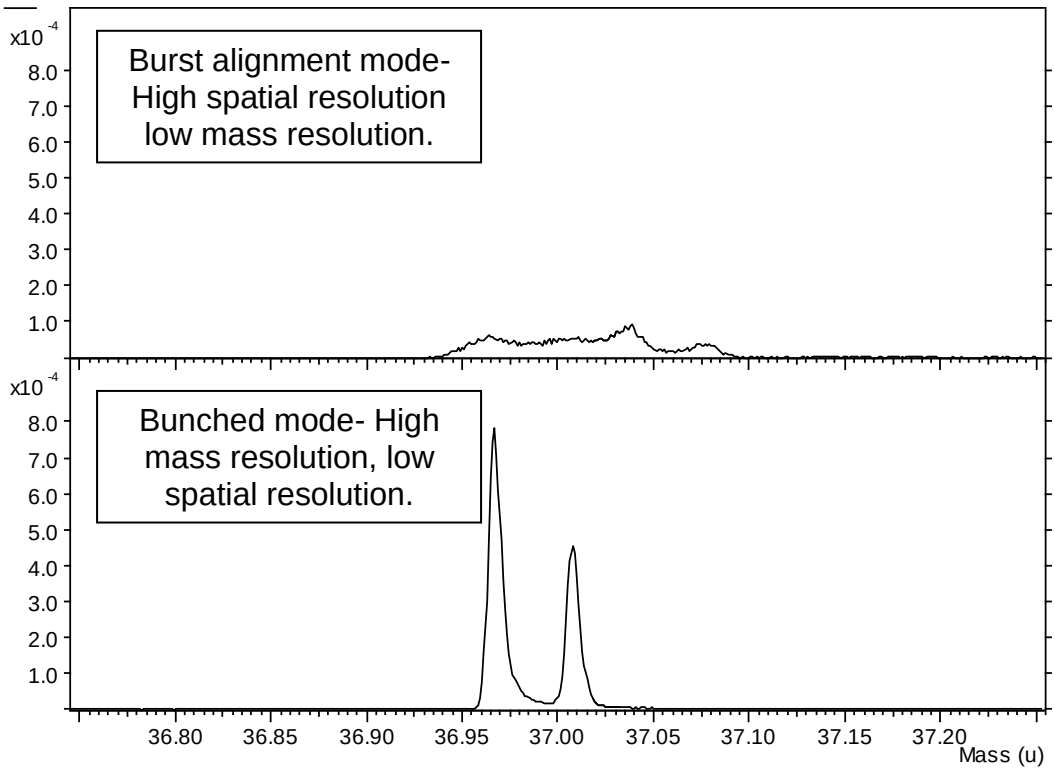

Figure 5.6. Mass spectra illustrating the difference in mass resolution between the two ToF-SIMS operating modes. *ToF-SIMS spectra of $^{37}Cl^-$ present in cryo-Sections (8 µm thick) of untreated control dermatomed porcine skin (400 µm) and skin dosed with 2 % CHG (w/v). The spectra were obtained in negative polarity using burst alignment and bunched mode to demonstrate the difference in observed mass resolution. The bunched mode can resolve $^{37}Cl^-$ and C_3H^- ion peaks unlike the burst alignment mode.*

To observe differences in the spatial resolution of the two operating modes, a proof of concept study was conducted on a CHG-treated skin cryo-Section. It was found that the integrity of the skin tissue was impaired due to the cryo-preparation process and the SC had folded on to the dermis (Figure 5.7). In the bunched mode the chemical distribution maps illustrate a high ion intensity for all CHG markers. The high molecular weight $[M-H]^-$ ion also exhibited a strong ion intensity within the displaced SC layer. Though the ion intensities of the CHG markers are prevalent, the spatial resolution in the bunched mode is clearly lacking. The spatial resolution achieved in the burst alignment mode is excellent as the morphology of the differing histological skin layers can be observed (Figure 5.7). The high spatial resolution is particularly distinguishable when compared to images obtained in the bunched mode (Figure 5.7). The ion intensities of the CHG markers in the burst alignment mode are not as high. The lack of mass resolution is exhibited by the difficulty in visualisation of the $[M-H]^-$ ion in the burst alignment mode.

The chemical distribution images show that the skin Section was not intact. Haematoxylin and eosin was used to stain the skin cryo-Section and a light microscope with an attached camera was used to image the cryo-Sectioned skin. Figure 5.8 illustrates the folding of the SC on to the dermis which is due to the preparation process. This displacement of the SC was clearly identifiable in the chemical distribution maps (Figure 5.7) and the haematoxylin and eosin staining was found to be an easy technique to confirm the skin integrity.

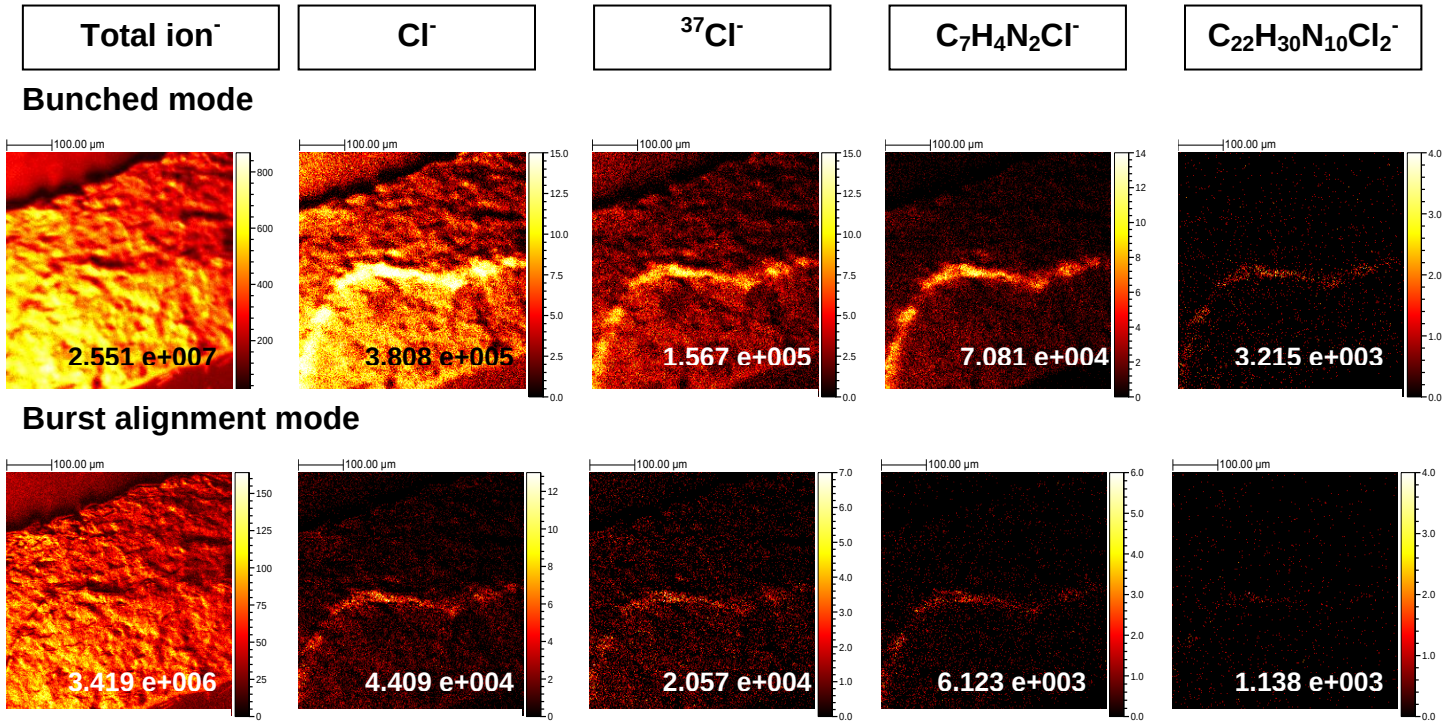

Figure 5.7. Imaging of selected CHG marker ions within the skin. *Various CHG ion marker chemical images of 2 % CHG (w/v) dosed porcine dermatomed skin (400 µm thick) vertically cryo-Sectioned into 8 µm thick Sections. Curling of the sample occurred when adsorbing the Section onto solvent cleaned coverslip (10 mm x 10 mm). Scale bar equates to 100 µm, TC is the total ion count for the specific ions of interest.*

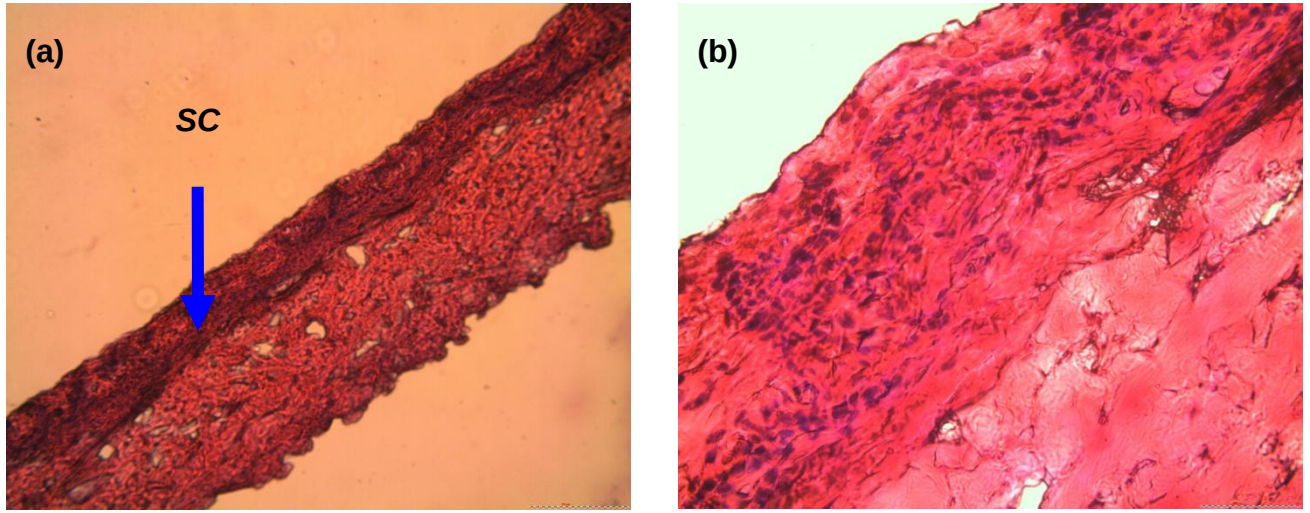

Figure 5.8. Histological analysis of skin sample after ToF-SIMS analysis. *Haematoxylin and eosin stained cryo-Section of dermatomed porcine skin (400 µm) post dosing with 2 % CHG, illustrating the folding of the SC and viable epidermis onto the dermis. (a) ×10 magnification (b) ×40 magnification.*

5.2.2. ToF-SIMS analysis of chlorhexidine digluconate treated porcine skin cryo-Sections.

After identification and assignment of secondary ions indicative of CHG, cryo-Sections of CHG treated skin and untreated skin were analysed by ToF-SIMS. Figure 5.9 shows an example of the magnified mass spectra for the selected CHG markers within dermatomed porcine skin. OCT that was used as an embedding material for the cryo-Sectioning was also analysed in parallel as a reference material to determine any peak overlap. Baseline noise can be observed for the OCT and the untreated skin, however unsaturated ion peaks exhibiting high signal to noise intensities for $^{37}Cl^-$, $C_7H_4N_2Cl^-$ (*m/z* = 151) and $C_{22}H_{30}N_{10}Cl_2^-$ (*m/z* = 505) were detected for the CHG treated skin.

The chemical distribution images of three replicates and the untreated skin cryo-Sections are shown in Figure 5.10. The two drug ion markers for CHG, $^{37}Cl^-$ and $C_7H_4N_2Cl^-$ (*m/z* = 151), can be observed within the SC. The highest ion intensity for the drug markers was found to be in the superficial layers of the skin and the SC. No significant signal intensity was detected for the drug markers within the lower epidermis or the dermis. No ion intensity for either of the drug markers were observed for the untreated skin Section. Figure 5.10 also illustrates the PO_2^- (*m/z* = 61) distribution images that were utilised as a marker for the viable epidermis. The ion PO_2^- (*m/z* = 61) was typically found distributed throughout the upper viable epidermis and the ion intensity for the CHG markers were localised within the SC layers above the ion intensity corresponding to the PO_2^- (*m/z* = 61) and thus the viable epidermis.

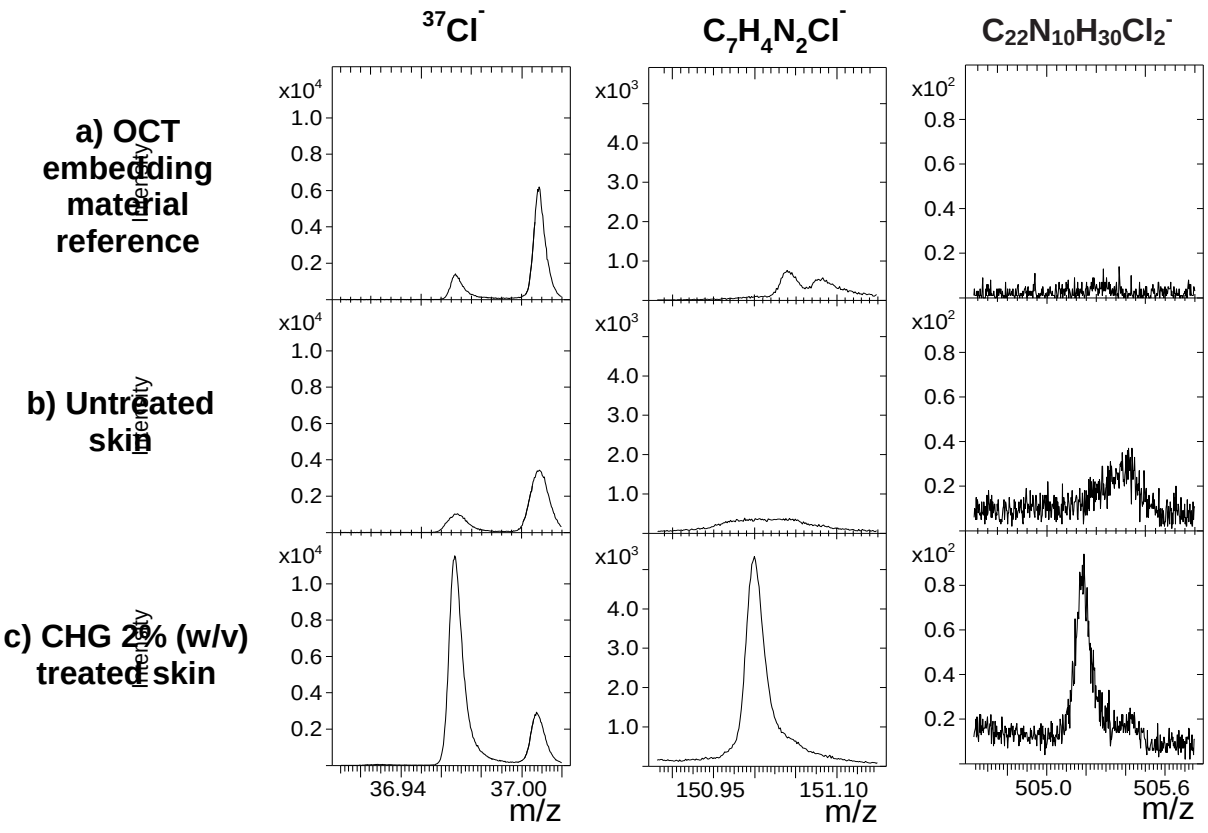

Figure 5.9 Magnified mass spectra of CHG marker ions within skin tissue. *ToF-SIMS mass spectra of various fragment ions ($^{37}Cl^-$, $C_7H_4N_2Cl^-$ and $[M-H]^-$ - $C_{22}N_{10}H_{30}Cl_2^-$) present in OCT embedding material, untreated control skin and skin dosed with 2 % CHG (w/v). The spectra were obtained in the negative ion mode.*

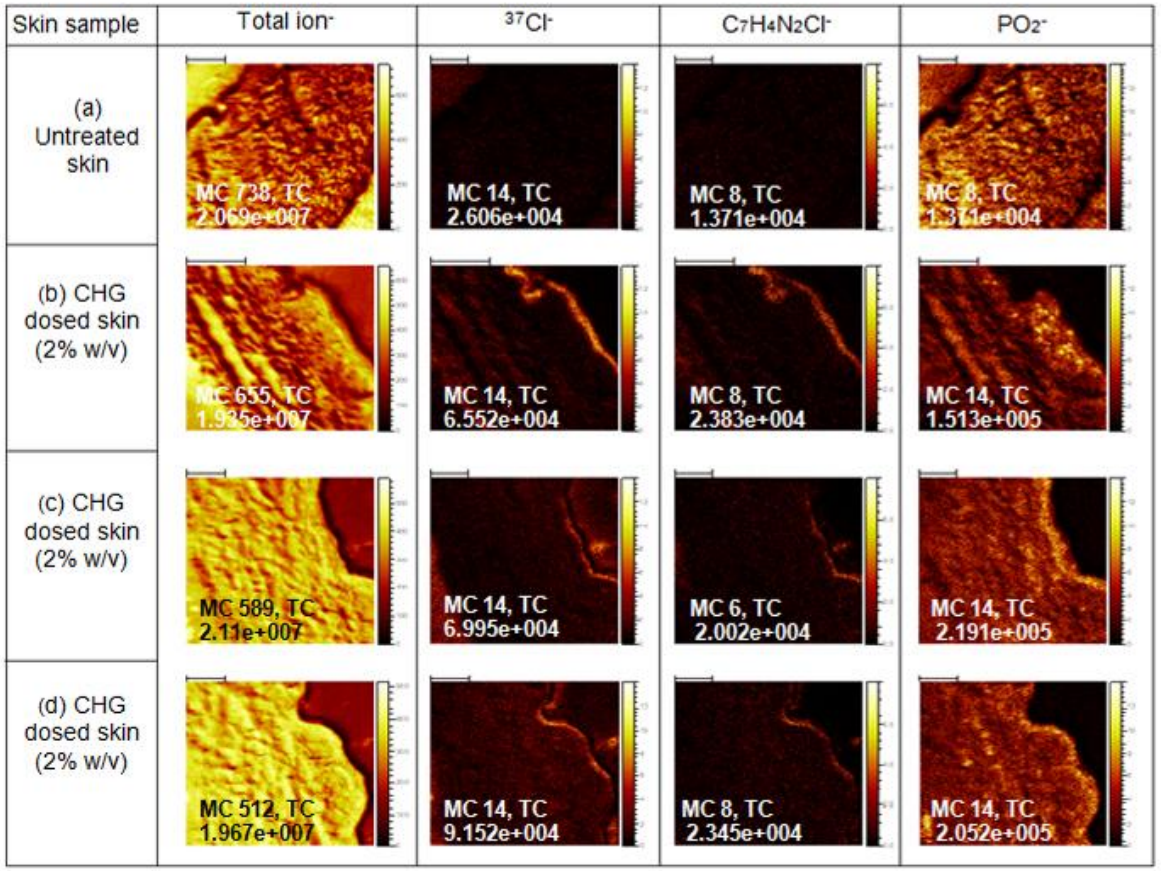

Figure 5.10. ToF-SIMS images of various CHG marker ions distributed within the skin. *ToF-SIMS images of various CHG markers of the negative control and 2 % CHG (w/v) dosed porcine dermatomed skin (400 µm thick), where the scale bar represents 100 µm, MC = maximum ion count per pixel and TC = total ion count for the specific ion of interest.*

The ToF-SIMS instrument is also capable of selecting a region of interest (ROI) by changing the area that is rastered and also the pixel density can be altered thereby changing the resolution of the resulting image. An area of SC was selected as an ROI to clearly identify the distribution of CHG within the skin (Figure 5.11). The ion CNO^- (m/z = 41) is indicative of biological tissue and was used to determine the tissue-glass interface of the magnified skin cryo-Section.

Chlorine was used as a CHG marker that is characteristic of CHG and was found to be distributed within the outer layers of the SC. Again, the ion PO_2^- (m/z = 61) was found to be distributed throughout the viable epidermis. In order to achieve a high enough spatial resolution for the magnification the analysis must be operated in the burst alignment mode. In this mode, longer timed pulses of primary ions are focussed on to the skin sample surface. This allows for a higher spatial resolution as observed in Figure 5.11. Due to a compromise in the mass resolution the ion intensity for the more discriminatory CHG markers were too low to observe. It was established that burst alignment and bunched mode are highly complementary for the analysis of exogenous and endogenous compounds within the skin. For a complete ToF-SIMS chemical analysis of skin tissue it is necessary to analyse the samples in both modes (Figures 5.10 and 5.11).

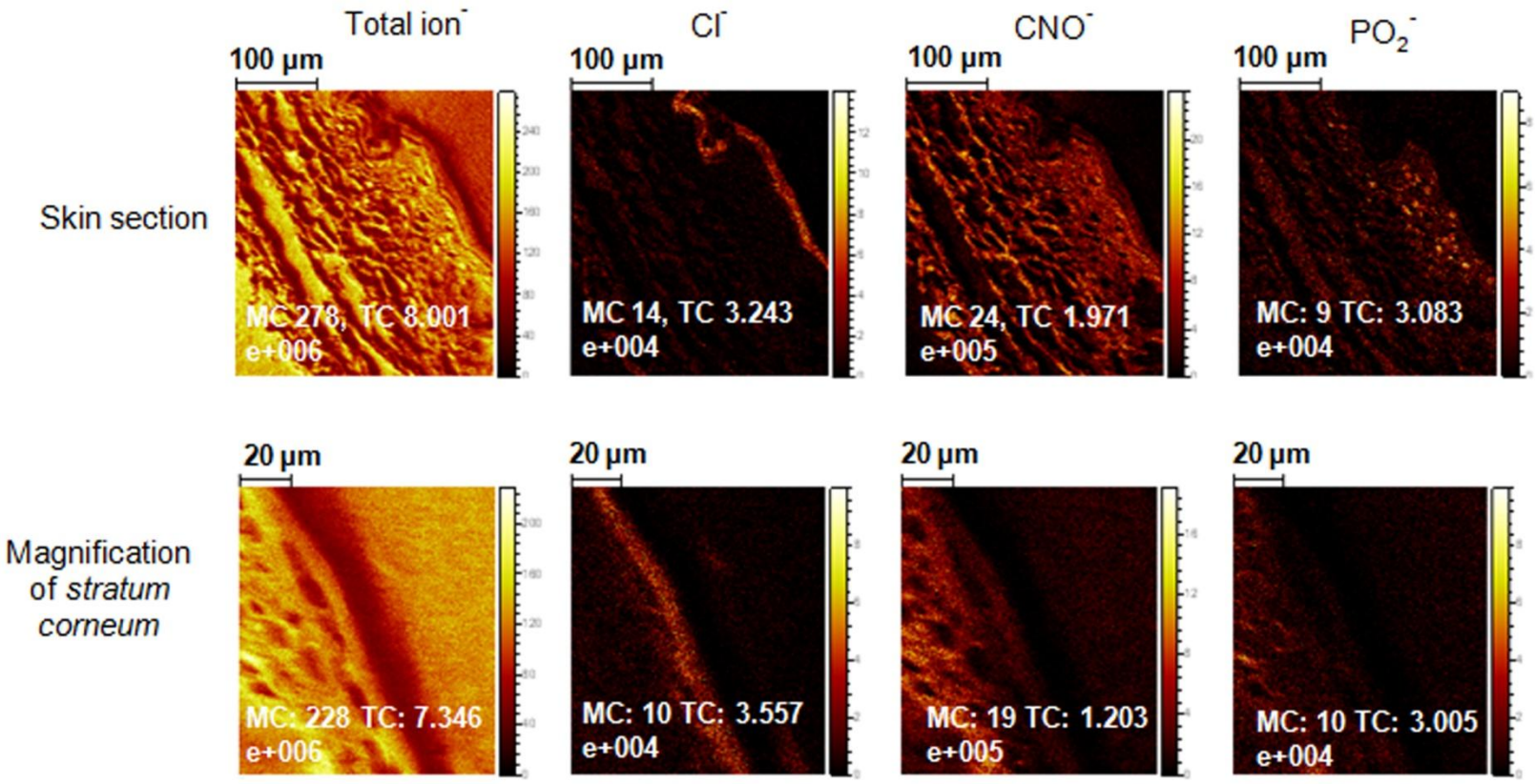

Figure. 5.11 ToF-SIMS images of CHG markers within the skin taken in the burst alignment operating mode. *ToF-SIMS images taken in burst alignment of various CHG markers liberated from the skin sample of 2 % CHG (w/v) dosed porcine dermatomed skin (400 µm thick). The SC was magnified to enhance the visualisation of the ion distribution. MC = maximum ion count per pixel and TC = total ion count for the specific ion of interest.*

5.2.3 ToF-SIMS analysis of chlorhexidine digluconate treated porcine skin tape strips.

To characterise the ingress of CHG into the skin, a tape-stripping study was conducted in parallel to the cryo-Section study. Once the unabsorbed CHG (2 % w/v) was washed from the skin surface after a 24 h contact time, 21 tape strips were removed from the skin. Each tape strip was analysed in series in the bunched mode after being freeze dried to remove water from the SC material. To determine as to whether there are any overlap ion peaks with regards to the tape strip adhesive and the CHG ion markers an untreated control was analysed in parallel. Figure 5.12 illustrates the ion distribution maps for tape strips 1 to 21.

The control tapes at the top of the table show no intensity for the chosen CHG ion markers with the exception of natural noise for $^{37}Cl^-$. The intensity for the ion PO_2^- is more marked for the control tape strips 1 and 2 than for the treated tape strips 1 and 2. All 21 tapes strips from the CHG treated skin sample show high ion intensity for $^{37}Cl^-$ even at tape strip 21. The distribution of the ion intensity of $C_7H_4N_2Cl^-$ (*m/z* = 151) is evenly distributed up to tapes strip 11 -14 where the distribution becomes uneven but a higher signal intensity is observed. This sporadic but intense distribution of $C_7H_4N_2Cl^-$ (*m/z* = 151) on the tape strips then continues until the final tape strip. Interestingly, from tape strip 14 and onwards the PO_2^- ion intensity signal increases as the viable epidermis is approached (Figure 5.12). It can also be observed that there is a general decrease of SC coverage on the tape strips with increasing tape strip number.

Figure 5.13 exhibits the magnified mass spectra of the CHG ion markers for the untreated tape strip, tape strip 2 and tape strip 20. Only baseline noise was observed in the mass spectra for the untreated sample therefore no difficulties with interfering ion peaks were encountered. Tape strip 2 showed the most intense peak for the CHG ion markers- $^{37}Cl^-$, $C_7H_4N_2Cl^-$ (*m/z* = 151) and $C_{22}H_{30}N_{10}Cl_2^-$ (*m/z* = 505). For tape strip 20 a reduction in peak intensity and broadening of peak shape was observed. The peak for $[M-H]^-$ ($C_{22}H_{30}N_{10}Cl_2^-$) (*m/z* = 505) cannot be distinguished from the noise of the baseline. A decreasing ion intensity signal was observed from tape strip 1 to tape strip 21 for all CHG markers.

The chemical distribution images corresponding to the mass spectra discussed above can be found in Figure 5.14. Great coverage of SC material on the adhesive tape was observed for the untreated sample in the total ion distribution image (Figure 5.14). There was low level distribution of $^{37}Cl^-$ across the SC material on the tape strip for the untreated sample and low level baseline noise for $C_7H_4N_2Cl^-$ (*m/z* = 151) and the $[M-H]^-$ (*m/z* = 505). For tape strip 2, full coverage of SC material was observed in the total ion distribution image and the ion intensity for both $^{37}Cl^-$ and $C_7H_4N_2Cl^-$ (*m/z* = 151) was found to be high and localised to the SC material. For the $[M-H]^-$ (*m/z* = 505) the intensity was low but evenly distributed across the SC material for tape strip 2. For tape strip 20, only moderate SC coverage was observed and therefore the intensity of the CHG markers was dramatically decreased. Though the distribution of the ion intensity for $^{37}Cl^-$, $C_7H_4N_2Cl^-$ (*m/z* = 151) and to a certain extent $[M-H]^-$ (*m/z* = 505) can still be clearly observed on tape strip 20 that was found to be localised to the SC coverage.

As the SC coverage decreases and becomes sporadic in distribution the signal intensity for CHG markers also significantly decreases. To obtain an accurate distribution profile within the skin it was necessary to determine whether the CHG markers' ion intensity was decreasing due to a reduction of SC material being recovered or whether it is a correct CHG distribution profile within the skin.

Using the SurfaceLab 6 software mass spectra and ion images can be acquired for selected ROIs. This application was applied to the selection of SC material (ROI) and to discount the tape strip background. The ROI selection was accomplished by thresholding the very different chemical compositions of biological tissue contrasting to the tape adhesive. Once an ROI had been selected the mass spectra and distribution images were rebuilt for the total ion and CHG markers. The ion intensity of the highly discriminatory CHG marker, $C_7H_4N_2Cl^-$ was normalised to the total ion within the ROI to obtain a representative ion intensity. This allowed for the determination of an accurate permeation profile as the decrease of SC removal with increasing tape strip number was accounted for.

Tape strip sample	Total ion $^-$	$^{37}Cl^-$	$C_7H_4N_2Cl^-$	$[M\text{-}H]^-$	PO_2^-
Control Tape strip	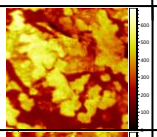	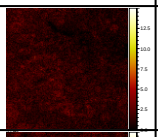	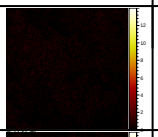	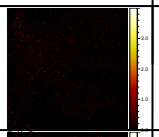	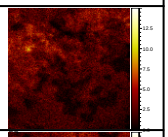
Control Tape strip	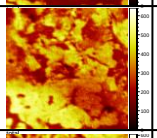	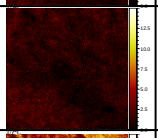	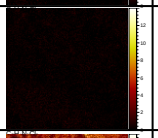	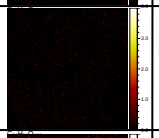	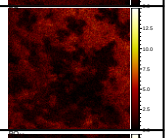
Tape strip 1	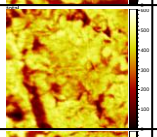	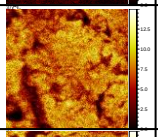	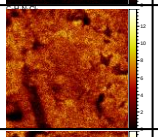	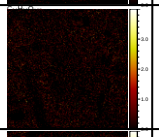	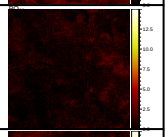
Tape strip 2	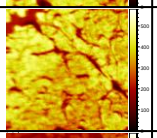	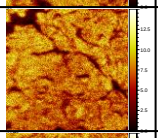	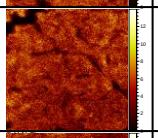	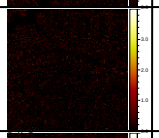	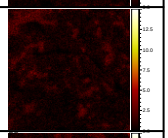
Tape strip 3	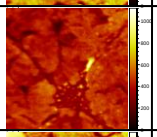	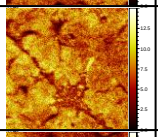	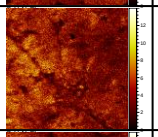	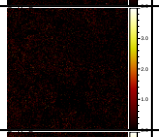	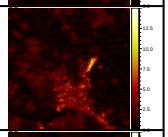
Tape strip 4	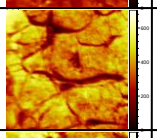	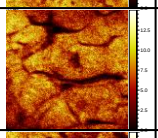	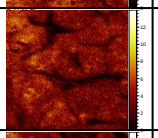	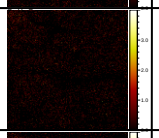	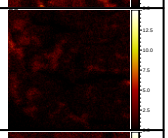
Tape strip 5	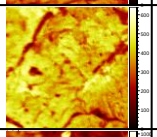	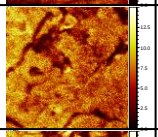	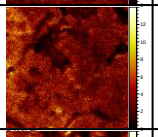	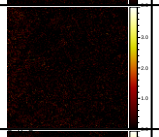	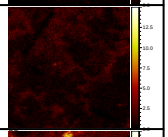
Tape strip 6	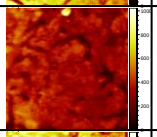	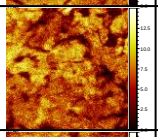	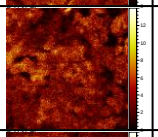	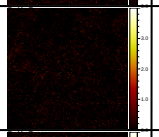	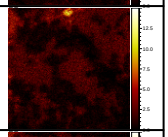
Tape strip 7					
Tape strip 8					
Tape strip 9					
Tape strip 10					
Tape strip 11					
Tape strip 12					

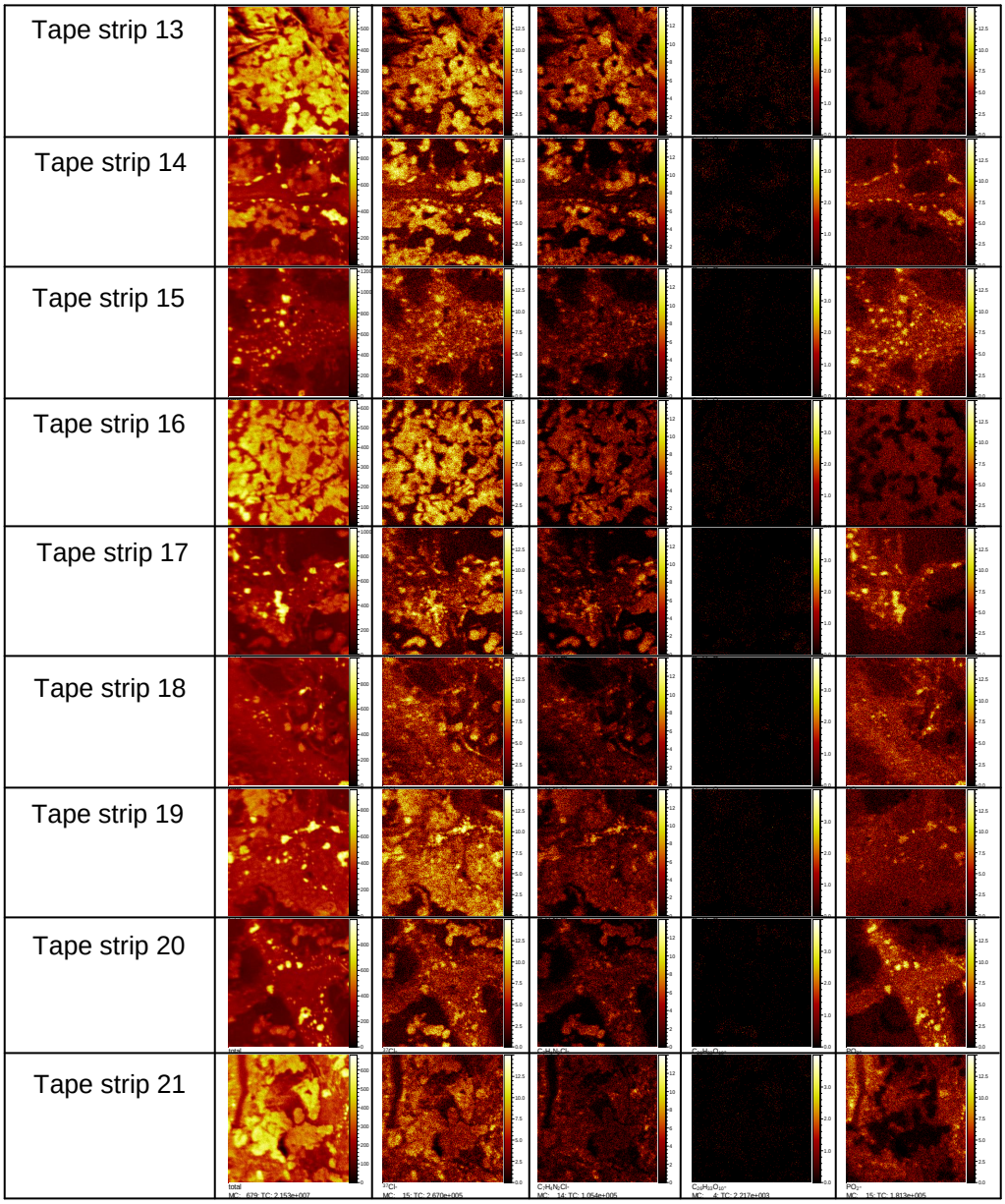

Figure 5.12 ToF-SIMS images of CHG marker ions and biomolecules for 21 consecutive tape strips. *ToF-SIMS images of various CHG specific ions and PO_2^- of the negative control and tape strips 1-21 taken from 2 % CHG (w/v) dosed porcine dermatomed skin (400 µm thick), MC = maximum ion count per pixel and TC = total ion count for the specific ion of interest.*

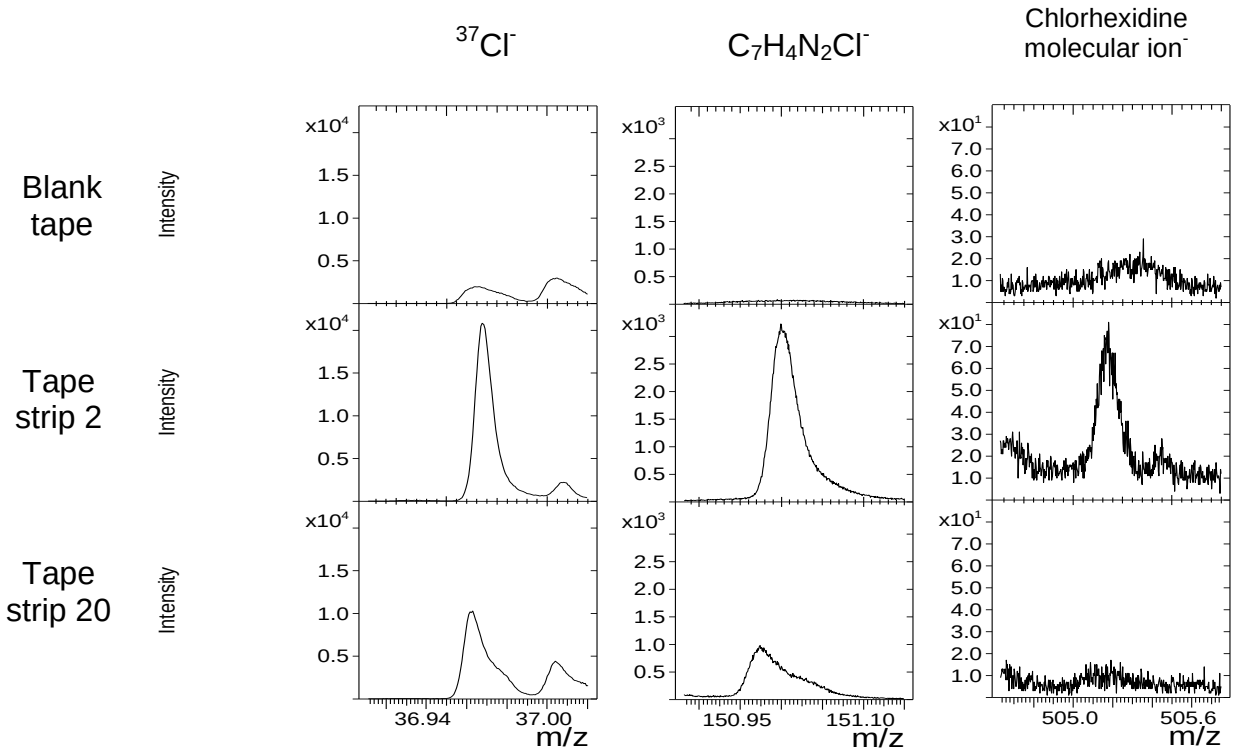

Figure 5.13. ToF-SIMS mass spectra of various CHG ion markers distributed across the surface of various tape strips. *$^{37}Cl^-$, $C_7H_4N_2Cl^-$ and CHG molecular ion$^-$ present on the surface of control tape, tape strip 2 and tape strip 20 from skin dosed with 2 % CHG (w/v). The spectra were obtained in the negative ion mode.*

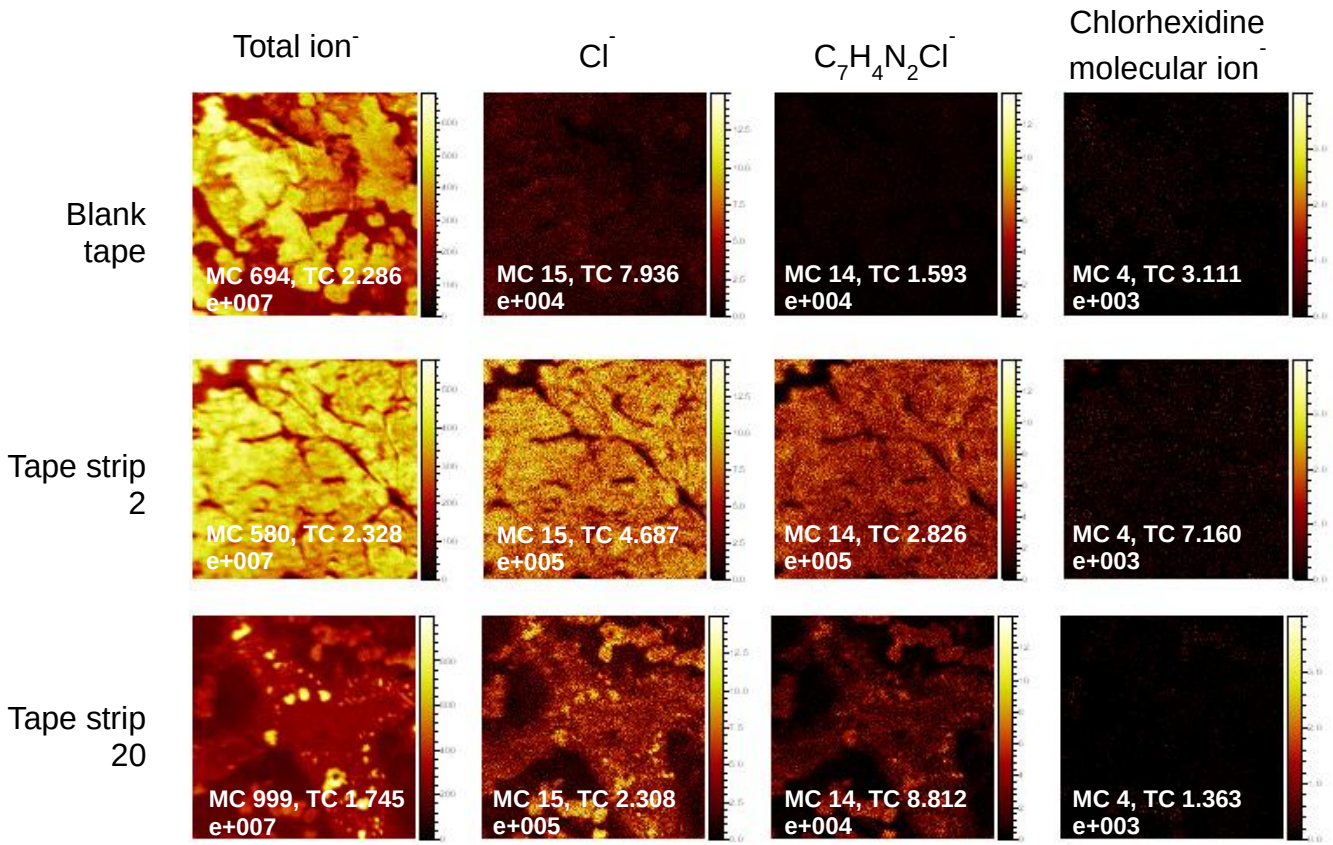

Figure. 5.14 ToF-SIMS images showing the distribution of CHG marker ions across various tape strips. *ToF-SIMS images of various CHG specific ions of the negative control and representative tape strips 2 and 20 taken from 2 % CHG (w/v) dosed porcine dermatomed skin (400 µm thick), MC = maximum ion count per pixel and TC = total ion count for the specific ion of interest.*

The permeation profile obtained from the ROI on the tape strip was plotted on a graph of $C_7H_4N_2Cl^-$ (*m/z* = 151) ion intensity against the tape strip number. The $C_7H_4N_2Cl^-$ (*m/z* = 151) ion intensity decreased dramatically for the first 3 tape strips but then from tape strip 4 to 11 a steady and slight fluctuation in the CHG marker intensity was observed before a gradual ion intensity decrease from tape strip 16 to 21 (Figure 5.15 (b)). This trend was observed for all four samples analysed. This profile was compared to the profile obtained from solvent extraction/ HPLC analysis conducted in Chapter 3 (Figure 5.15 (a)). To ensure the concentration of CHG was

above the LOD of the HPLC, tape strips are typically pooled together. Though the ToF-SIMS analysis is semi-quantitative only, a great deal of complementary data can be obtained as highlighted in Figure 5.15. The ion intensity for each tape strip can be analysed elucidating subtle trends in the permeation profile that can not be achieved by conventional tape strip analysis (Figure 5.15).

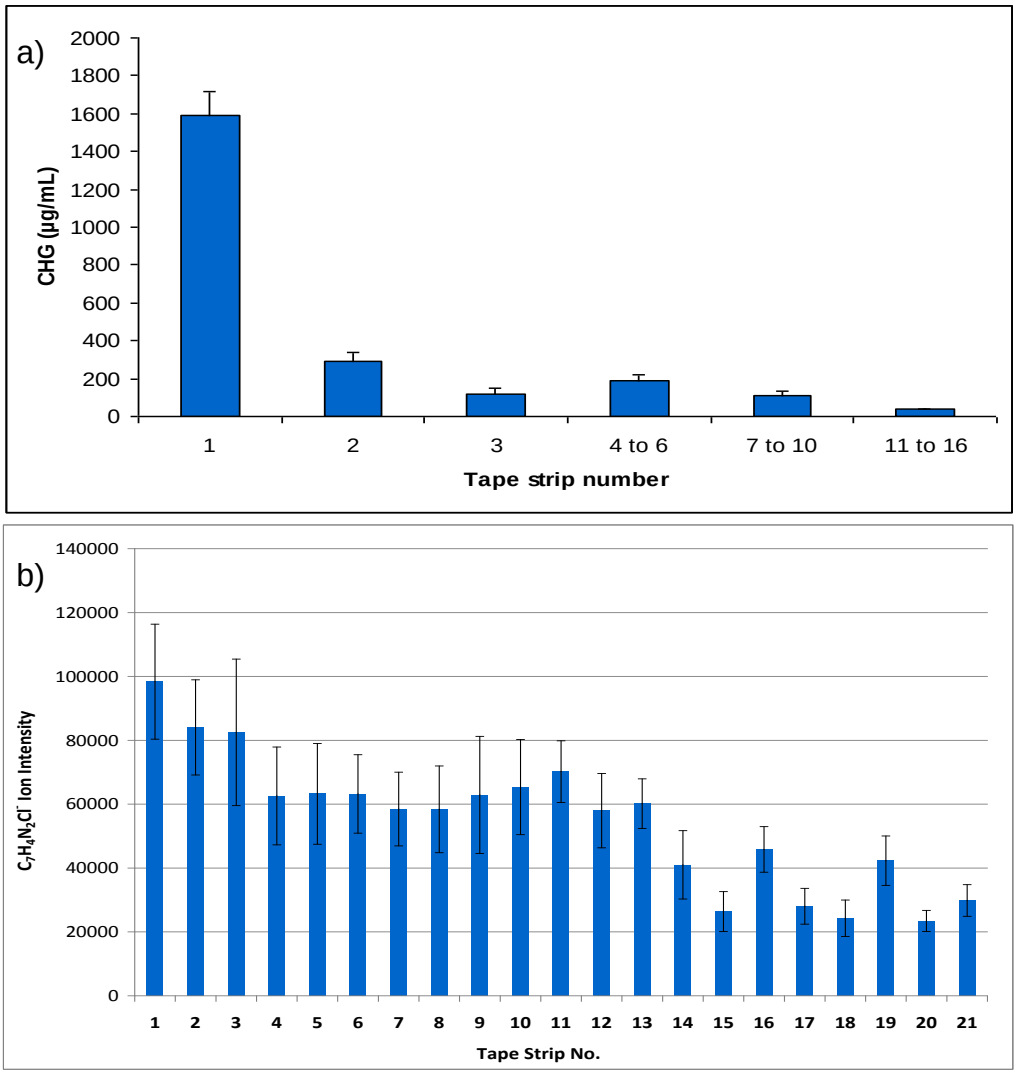

Figure 5.15 Graphs showing the distribution of CHG throughout the SC using two complementary techniques; HPLC and ToF-SIMS. *(a) Concentration of CHG extracted from tape strips and analysed by HPLC see Section 3.3.1 (n=14 ± SEM).(b) Fragment ion ($C_7H_4N_2Cl^-$) assigned to CHG intensity for 21 consecutive tape strips taken from CHG dosed (2 % w/v) porcine skin (n=4 ± SD). Ion intensity normalised against total ion content of SC material on the tape strip giving a semi-quantitative permeation profile.*

Chapter 3 illustrated the use of PAMAM dendrimers as a novel permeation enhancer for CHG. The novel ToF-SIMS method developed as outlined within this Chapter was tested to determine whether it could be applied to observing the permeation enhancement affect of chemical permeation enhancers. The chemical distribution images were used to visualise the enhanced distribution and permeation of CHG after a G3-PAMAM-NH_2 pre-dose treatment (Figure 5.16). For the PAMAM pre-treated skin a more intense distribution of all CHG markers was observed across the upper skin strata. A very intense distribution of CHG markers $^{37}Cl^-$ and $C_7H_4N_2Cl^-$ was observed throughout the SC. When CHG was dosed without a G3-PAMAM-NH_2 pre-treatment the ion intensity for the $[M-H]^-$ was lacking, however after a G3-PAMAM-NH_2 pre-treatment $[M-H]^-$ can be observed throughout the *SC* with good contrast (Figure 5.16). All three replicates of G3-PAMAM-NH_2 pre-treated skin dosed with CHG (2 % w/v) support the results obtained in Chapter 3 in that PAMAM dendrimers act as a permeation enhancer.

Comparison of the distribution images of the G3-PAMAM-NH_2 pre-treated compared to the CHG alone, clearly illustrates a much deeper permeation and ingress of CHG into the upper skin strata. Figure 4.17 shows three replicates of the $C_7H_4N_2Cl^-$ distribution for G3-PAMAM-NH_2 and non G3-PAMAM-NH_2 treated side-by-side, unmistakably the ion intensity is markedly increased for all three G3-PAMAM-NH_2 pre-treated skin Sections. The chemical distribution images have confirmed that PAMAM dendrimers act as a permeation enhancer by visualising an enhanced topical delivery of CHG (Figures 5.16 and 5.17).

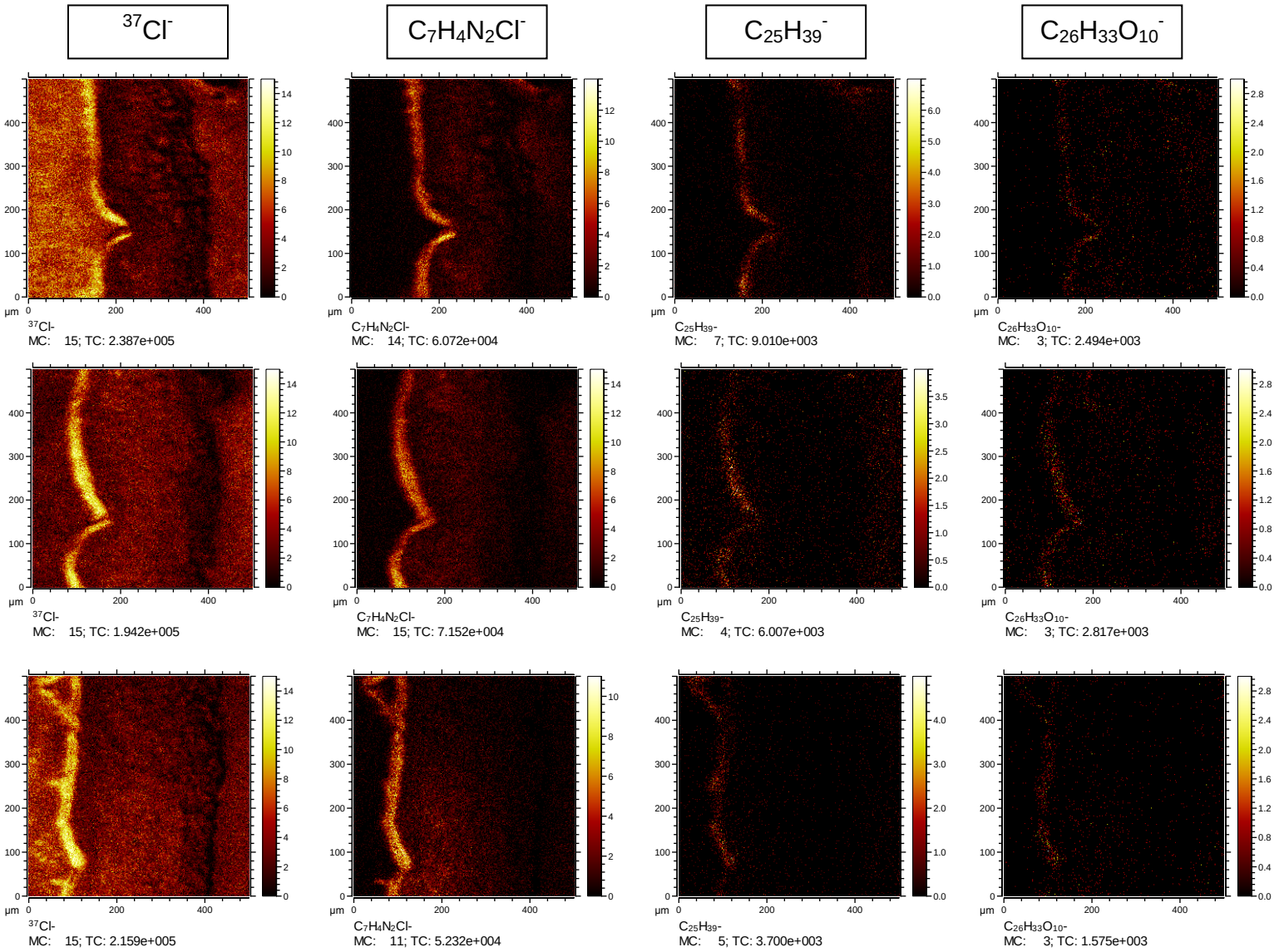

Figure 5.16. ToF-SIMS images showing the distribution of CHG ion markers throughout the upper skin strata after a PAMAM dendrimer skin pre-treatment. *ToF-SIMS images of various CHG markers distributed within skin after a 24 h pre-treatment with G3-PAMAM-NH_2 (10 mM, 0.2 mL dose) followed by an application of 2% CHG (w/v) onto porcine dermatomed skin (400 µm thick). MC = maximum ion count per pixel and TC = total ion count for the specific ion of interest.*

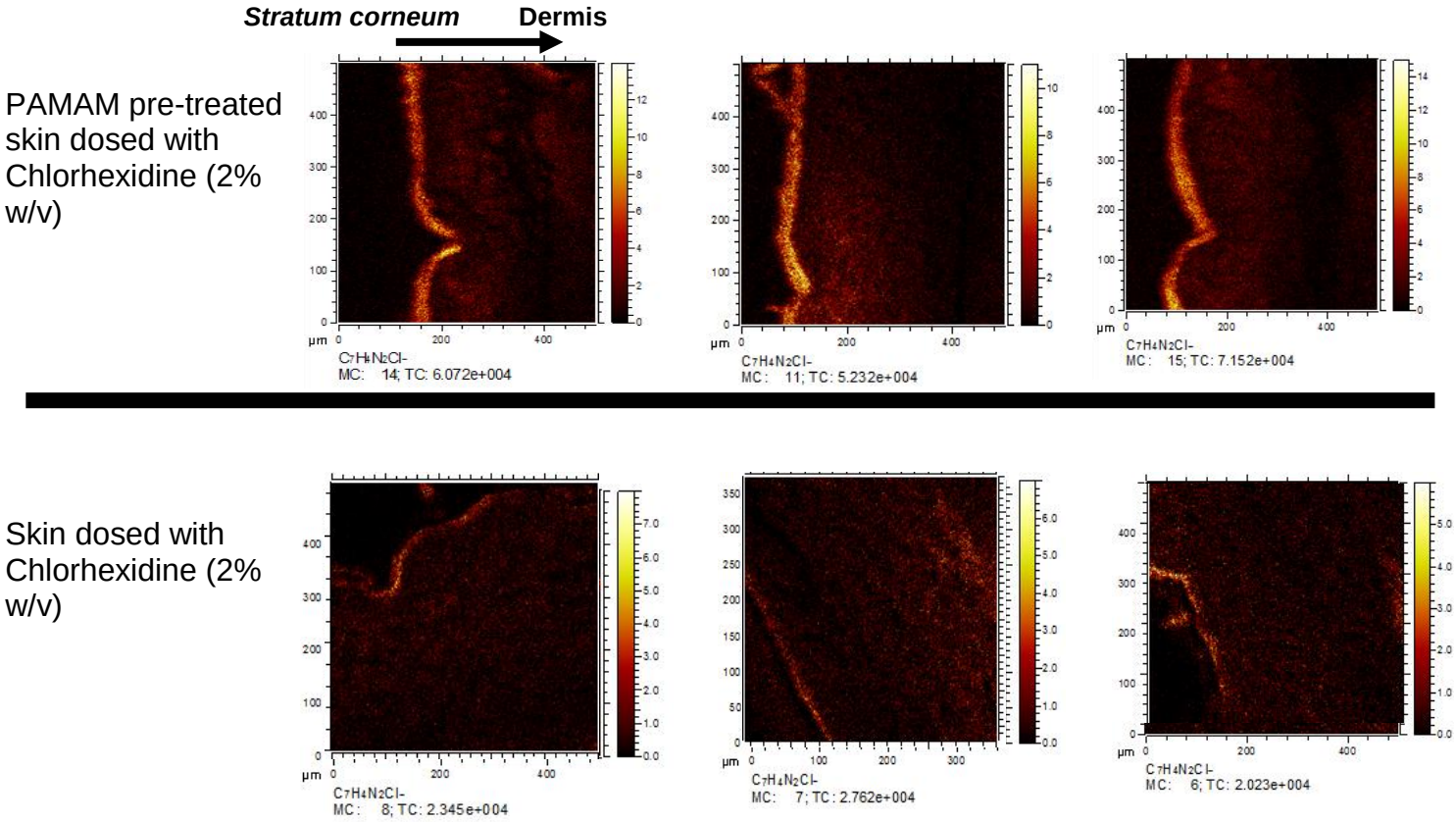

Figure 5.17. A comparison of ToF-SIMS images of various CHG markers distributed within skin with and without a 24 h pre-treatment with PAMAM dendrimer. *A pre-treatment of G3-PAMAM-NH_2 (10 mM, 0.2 mL dose) followed by an application of 2 % CHG (w/v) onto porcine dermatomed skin (400 µm thick) was compared to porcine skin dosed only with 2 % CHG (w/v). Scale bar represents 100 µm, MC = maximum ion count per pixel and TC = total ion count for the specific ion of interest.*

Another interesting feature of the ToF-SIMS is that is can also act as a scanning electron microscope (SEM). The distance in which the CHG had permeated was measured from the chemical distribution images using the SurfaceLab 6 software. The unique $C_7H_4N_2Cl^-$ fragment ion was used as a marker for CHG ingress for the G3-PAMAM-NH_2 pre-treated skin samples and $^{37}Cl^-$ was used as a marker for the CHG alone treated skin samples. This is due to the increase in intensity for the CHG markers when pre-treated with G3-PAMAM-NH_2, the $^{37}Cl^-$ signal was too intense to accurately measure the permeation of the ingress and likewise for the samples where CHG was dosed alone the intensity of $C_7H_4N_2Cl^-$ was too low. The average distance the CHG had permeated into the skin was found to be 32.22 μm ± 1.412 and 47.56 μm ± 3.980 for PAMAM untreated and PAMAM pre-treated skin. The results are reported as the mean ± SEM and are an average of n=9. The average distance the CHG had permeated after a G3-PAMAM-NH_2 pre-treatment was found to be statistically different from the skin samples where CHG was dosed alone (T test, t=4.07, p<0.001).

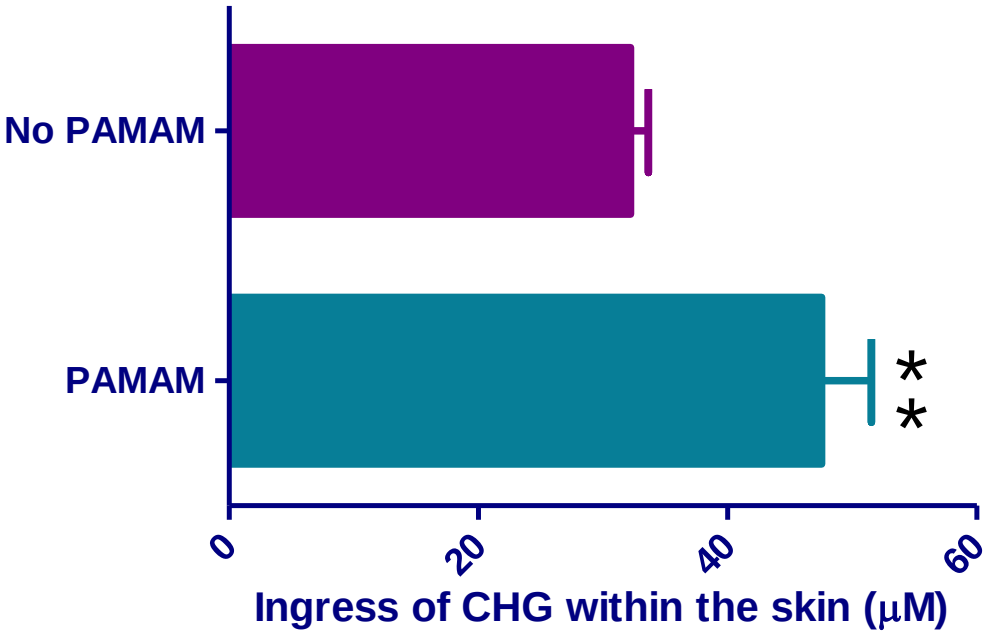

Figure 5.18. A graph showing the depth permeated by CHG (2 % w/v) with and without a G3-PAMAM-NH_2 (10 mM, 0.2 mL) pre-treatment as measured using SufaceLab 6 software. *The Average measurement of ingress for PAMAM untreated and PAMAM treated samples were 32.22 μm ± 1.41 and 47.46 μm ± 3.91, respectively. Data is presented as the mean ± SEM (n=10). The permeation distance of CHG within the PAMAM pre-treated skin is statistically different from the PAMAM untreated skin as shown by a two tailed T test t=4.07, p<0.001.*

5.3.0 Discussion

The ToF-SIMS technique provides a highly detailed mass spectral map of the biological sample being analyzed (Wu *et al.* 2007). Biological material can yield hundreds of secondary ions (Figure 5.2) making the interpretation difficult. This intricacy occurs as a result of fragmentation of larger secondary ions liberated from the complex biological sample surface. These complex spectra hold the detailed chemical information about the composition, distribution and surface order of the sample (Graham *et al.* 2006). In order to identify and assign secondary ion peaks, it is imperative to run reference samples e.g. drug sample, embedding and substrate materials, in order to understand characteristic spectral differences. Control biological tissue should also be analysed in parallel (Piwowar *et al.* 2011). This enables for accurate peak assignments of exogenous and endogenous molecules.

To study the deposition of CHG within the skin it was important to first elucidate characteristic fragment ions unique and indicative to the presence of CHG. The overview of the negative polarity spectra obtained (Figure 5.3(a)) illustrates the secondary ion peaks detected having a mass range 1-160 (amu) from the surface of dosed (2 % (w/v) solution of CHG) and un-dosed porcine skin. Chlorhexidine (Figure 5.4(b)) consists of two chlorinated aromatics; therefore chlorine might be an anticipated ideal marker of the drug within the tissue. This was found not to be the case and chlorine was only used as supplementary supporting data as the element is abundant within tissue and is not unique to the presence of chlorhexidine. Chlorine is observed in the un-dosed control skin surface as highlighted in the survey spectra

(Figure 5.4(a)) and associated chemical images (Figure 5.6). A fragment ion thought to be characteristic of chlorhexidine was observed at 151 amu, with the proposed secondary ion assignment $C_7H_4N_2Cl^-$ (*m/z* = 151) (Figure 5.3). The magnification of the overview spectra for this fragment ion (Figure 5.3(c)) highlights a potential issue of analyzing biological tissue in that a low intensity endogenous peak is detected within the skin tissue itself at 150.8 amu. Great care must be taken integrating the 151- $C_7H_4N_2Cl^-$ (*m/z* = 151) fragment ion to prevent overlap, resulting in noise within the spectral image (Figures 5.3 and 5.5). However, due to the high mass resolution, peak identification and assignment is typically straightforward.

The overview spectrum (Figure 5.4(a)) highlights the $C_{22}N_{10}H_{30}Cl_2^-$ $[M-H]^-$ ion peak for chlorhexidine (*m/z* = 505). This molecular ion peak is clear evidence for the identification and localization of chlorhexidine; however, due to the high molecular weight the intensity is relatively low. The low ion intensity amongst the noise and interference of complex biological substrates results in low chemical contrast and thus impedes the ability to obtain detailed chemical images. Spectral images (Figure 5.5) were generated after the secondary ion peaks were identified and assigned as CHG markers. The spectral images visualize the distribution of chlorhexidine upon the surface of dosed and un-dosed skin. The skin was analysed post-wash therefore the presence of such intense ion intensity for CHG-assigned fragment ions and molecular ions as observed in Figure 5.5 suggests that the cationic CHG strongly binds to the superficial layers of the skin. The strong binding affinity of CHG to the skin protein has been described elsewhere (Lim and Kam, 2008). It is clear in Figure 5.5 that Cl^- is not

a strong candidate as a characteristic CHG marker due to its abundance upon the skin surface, in contrast to the other selected markers, $C_7H_4N_2Cl^-$ and $[M\text{-}H]^-$.

ToF-SIMS analysis can be undertaken in two modes (the bunched mode, with high mass resolution and low spatial resolution, or the burst alignment mode, with high spatial resolution and low mass resolution). The differences in mass and spatial resolution achievable in the two different operational modes are illustrated in Figures 5.6 and 5.7, respectively. The decrease in mass resolution associated with burst alignment mode can result in the inability to discriminate one peak from another, as exemplified in Figure 5.6 where the $^{37}Cl^-$ and C_3H^- ion peaks can not be resolved in the burst alignment spectrum. Figure 5.6 illustrates the mass spectra obtained in both operating modes for chlorine on the surface of the skin. The data obtained in the two operating modes is highly complementary and together offer high mass resolution and high spatial resolution. Sodhi, 2004 discussed the principles behind both operating modes at great length (Sodhi, 2004).

Cryo-Sections of skin were investigated to determine the penetration depth and the distribution of chlorhexidine within the skin. During the method development process it became apparent that the sample preparation stage would be of importance to the integrity and quality of the ToF-SIMS data achieved. Figure 5.7 demonstrates an artefact identified from the cryo-Sectioning process where the SC had ‘curled’. When the skin is not effectively adsorbed onto the cover slip occasionally the SC and upper viable epidermis fold over onto the dermis. The occurrence of this issue is easily identifiable using the ToF-SIMS technique as the change in topography

is readily observable. The ToF-SIMS system can also act as a SEM that can be utilised to check the tissue integrity. Further, complementary histology such as haematoxylin and eosin staining can be performed following ToF-SIMS analysis (Figure 5.8) to confirm tissue integrity or skin structures of interest. Although the Sectioning of the skin sample in Figure 5.6 was found to be sub-standard due to tissue curling, the drug markers assigned from the mass spectra analysed in the bunched mode on the skin surface were found to be of high enough intensity to image the deposition and distribution of CHX within the skin.

Once the sample preparation was optimised, to further validate the results, reference materials of OCT embedding material and a standard solution of CHG were analysed using ToF-SIMS in bunched mode (high mass resolution) revealing characteristic fragment ions. The following mass peaks were assigned as characteristic negative fragment ions within the skin corresponding to chlorhexidine digluconate: chlorine (*m/z* = 35 and 37), $C_7H_4N_2Cl^-$ (*m/z* = 151) and the $[M\text{-}H]^-$ ion (*m/z* = 505). No secondary ion peaks corresponding to the OCT embedding material overlapped with the secondary ions characteristic of the CHG. Figure 5.9 shows a comparison of spectra demonstrating a range of secondary ions that illustrate that the ion peaks are characteristic only of the CHG and are not inherent within the porcine tissue Sections. The OCT embedding material and undosed control skin both show a low intensity secondary ion peak for chlorine as it is abundant within the natural tissue and environment. For this reason it would not act as a discriminatory peak for the compound of interest. The higher molecular weight fragment ion, $C_7H_4N_2Cl^-$ (*m/z* = 151) and the chlorhexidine molecular ion (*m/z* = 505) are very distinctive and unique

respectively to CHG and this specificity is confirmed by their absence in the controls as shown in Figure 5.9. The selected CHG markers are in abundance within the dosed tissue where a clear intensity peak is demonstrated in the mass spectrum of Figure 5.9 (c).

It is possible to use the specific fragment ions to map the permeation of chlorhexidine into dosed porcine tissue. Figure 5.10 shows the distribution and localization of the CHG markers in dosed porcine skin and are absent within the untreated skin. The chlorine (*m/z* = 37) ion intensity for the 2 % CHG (w/v) treated skin sample is much higher and localized to the skin surface in contrast to the untreated sample. The chlorhexidine-treated sample has a higher ion intensity within the upper strata of the skin and there is a clear trend that with each skin sample illustrated the chlorine and the $C_7H_4N_2Cl^-$ ion (*m/z* = 151) are strongly associated with the layers of the SC. The CHG characteristic ions are absent at a significant intensity within the deeper skin strata. The explicit localization trend of the ions characteristic of the CHG was observed repeatedly with the CHG 2 % (w/v) dosed porcine skin samples (Figure 5.10, (b-d)). The three replicate samples dosed with CHG (Figure 5.10, (b-d)) illustrate a very similar distribution trend of CHG that implies reproducibility of the method and a consistent distribution of CHG once topically applied.

The chemical images obtained demonstrate the strong affinity that chlorhexidine has for the skin as it binds to the SC (Aki and Kawasaki, 2004). The lack of CHG associated ions within the deeper skin strata illustrates the need for a

permeation enhancement strategy in order to effectively neutralize bacteria found below the superficial layers of the SC.

ToF-SIMS has the capability to simultaneously image molecular ions associated with the applied compound and native fragment ions occurring within the tissue. A phosphate ion intensity signal was also detected and imaged within the viable epidermis that was utilised to compartmentalize the tissue Section into histological components; in this case, to identify the distinction between the viable epidermis and the SC. Phospholipids are not present in the SC due to the cornification process as free esterified sterols accumulate instead (Elias *et al.* 2005, Lampe *et al.* 1983 and Reinertson, and Wheatson 1959). This interesting feature may aid the understanding of a dosed compound's localization within a complex tissue or highlight the presence of co-localization with native tissue molecules i.e. co-localisation of penetrants within the SC, other dermatological layers or features of the skin such as sebaceous glands.

To further investigate the localization of CHG within the skin, the samples were analyzed using the burst alignment mode (high spatial resolution). Although the overall mass resolution of the burst alignment mode spectra is reduced, each of the characteristic ions for CHG can still be resolved. High resolution chemical images of tissue samples were obtained and are shown in Figure 5.11. Once the ions of interest are assigned in the high mass resolution spectra, the burst alignment mode can offer a wealth of spatial information. For example, Figure 5.11 clearly shows the $^{37}Cl^-$ (*m/z* = 37) attributed CHG is strongly associated with the SC and the chlorine is clearly

observed at a relatively high intensity within the SC layers on the magnified burst-alignment image (Figure 5.11). Again, only very low ion intensity for CHG markers was observed within the deeper skin strata.

To confirm the ingress of the CHG into the upper skin strata as opposed to being adsorbed to superficial outer layers, a conventional tape-stripping experiment was conducted in parallel to the cryo-Sectioning experiments. To remove the SC, 21 tape strips were taken from the dosed and washed skin samples. They were then freeze-dried and analysed using the method previously described (Section 5.5), to visualize the distribution of the characteristic CHG ions across the surface of the tape (Figure 5.12). An overview of the ion intensities for CHG markers $^{37}Cl^-$ and $C_7H_4N_2Cl^-$ (*m/z* = 151) can be observed on all tapes even on tape strip 21 (Figure 5.12). This confirms what was observed within the skin cryo-Sections in that CHG is distributed throughout the SC layer. Interestingly, from tape strips 9-13 there is an observed increase in the signal intensity of the CHG ion marker $C_7H_4N_2Cl^-$ (*m/z* = 151). The applied compound CHG is hydrophilic in nature and this trend of CHG intensity that increases at around tape strip 9 coincides with the SC water gradient. The SC water content is typically around 15-30 % but dramatically increases to 70 % at a depth of around 10-15 µm at the boundary layer of the SC-viable epidermis (Capsers *et al.* 2001). Speculatively, this may be the reason for the residual effect CHG pertains once applied to the skin. It is possible that the SC acts as a depot or reservoir particularly close to the SC-viable epidermis boundary layer where a higher water content is observed. Moisture, however, does impede the tape stripping process as the adhesive fails to adhere to the SC material in the presence of water.

As the tape stripping progresses deeper into the SC a decreasing mass of material was removed from the sample with each tape strip removed, as observed in Figures 5.12 and 5.14. A feature of the ToF-SIMS software is that a region of interest (ROI) can be selected i.e. only the SC material. Once an ROI has been selected the mass spectra can be re-analysed thus removing the background tape that contributes to the overall image and mass spectrum. The intensity of the compound fragment ion of interest within the selected ROI (SC material only) is normalized against the total ion intensity count for the selected ROI. The ability to analyse only the SC material can give a more accurate analysis of the drug deposition and absorption throughout the layers of the SC and can thus confirm the substantivity of a compound within the superficial layers of the skin.

There was a decreasing trend observed for the CHG content for the ROI on tape strips 1 to 21. The $C_7H_4N_2Cl^-$ (*m/z* = 151) fragment ion generally decreases with the number of tape strips taken, with a small increase in ion intensity from tape strip 9 to 13. Tape strips 1 and 2 show a high concentration of $C_7H_4N_2Cl^-$ (*m/z* = 151) that may correspond to adsorbed chlorhexidine that was not completely washed from the superficial layers of the SC due to strong adsorption with skin proteins. It is clear from the tape strip experiment (Figures 5.12 and 5.14) that CHG is localized to the upper layers of the SC that is consistent with the results obtained for the cryo-Sectioned tissue (Figures 5.9 and 5.10). The strong binding within the upper skin strata and poor permeation has also been observed elsewhere (Lafforgue *et al.* 1997) and (Karpanen *et al.* 2008).

Typically, beyond tape strip 5, it would be normal to pool the tape strips together (Trebilcock *et al.* 1994) in order to achieve a concentration higher than the limit of detection (LOD) when using analytical instrumentation such as a high performance liquid chromatography (HPLC). The LOD for CHG extracted form skin Section samples using conventional HPLC assays were 0.016 µg/mL (Reinertson *et al.* 1959) and 0.050 µg/mL (Carret *et al.* 1997). The ppm sensitivity of ToF-SIMS (Chabala *et al.* 1995) circumvents this issue, where significant ion intensity can still be observed at tape strip 20 (Figures 5.12 and 5.14). A semi-quantitative depth profile was obtained from the ToF-SIMS analysis and compared to the depth profile obtained from extracting the CHG and analysing the samples by HPLC (Figure 5.15). The permeation profile obtained from analysing the tape strips by ToF-SIMS offers a highly detailed profile as it is not limited by a high LOD due to the ppm sensitivity. Subtle trends and fluctuations can be observed in the permeation profiles within the *SC* that are not present when the tape strips are analysed by HPLC (Figure 5.15). The enhanced detail achieved from ToF-SIMS analysis could help to establish the dermatopharmacokinetics of a drug and would be an extremely powerful and complementary technique when combined with quantitative HPLC tape strip studies.

The ToF-SIMS data has shown that CHG applied to the skin surface as a 2 % w/w solution binds to the upper layers of the *SC* and demonstrates poor permeation into the deeper tissues of the skin over the duration of the diffusion experiment. This lack of permeation may lead to an inefficient reduction in the microbial flora of the deeper skin strata as described in Section 1.4 (Brown *et al.* 1989), and also within the skin appendages where propionibacteria and staphylococcal bacteria are found

(Touitou *et al.* 1998). This may suggest that the incorporation of a permeation enhancer within a formulation may be required in order to provide a more comprehensive reduction in the skin's microflora, particularly below the SC. This is particularly important for when the skin barrier is impaired such as prior to a surgical site incision or in cases of skin conditions such as eczema or psoriasis.

In Chapter 3 it was shown that a G3-PAMAM-NH_2 skin pre-treatment enhanced the permeation of topically applied CHG. ToF-SIMS data was used to visualise the permeation enhancement of CHG due to the pre-treatment with PAMAM dendrimer to support the findings of the conventional Franz cell studies in Section 3.3.0 (Figures 5.16-18). G3-PAMAM-NH_2 was also analysed by ToF-SIMS as a reference material. The fragment ions detected that correspond to the dendrimer were not sufficiently unique to be distinguished from the endogenous skin components. This is due to PAMAM dendrimers being constituted of polymeric branches of amides and carboxyl groups. As such no evidence of PAMAM permeation was detected. A clear intensity increase of the CHG markers within the upper skin strata was observed (Figure 5.16). This was attributed to the penetration enhancement effect of the PAMAM dendrimer. When the PAMAM dendrimer-treated skin is compared to the skin treated with CHG alone, the considerable penetration and deposition enhancement is clearly evident (Figure 5.17). It is also possible to measure the permeation depth of a topically applied compound using the SurfaceLab 6 software (Figure 5.18). A semi-quantitative permeation depth was obtained from the chemical distribution images of the skin Sections. A statistically significant ($t=4.07$, $p<0.001$) penetration depth increase was observed after the skin was pre-treated with PAMAM dendrimer (Figure 5.18). After a

PAMAM dendrimer pre-treatment on average the CHG had permeated ~15 μm further into the skin than without a PAMAM dendrimer pre-treatment.

The ToF-SIMS method developed and outlined within this Chapter has successfully been applied to visualise the distribution and penetration of the conventional topically applied antiseptic, CHG, and has established the effectiveness of a novel dendrimer permeation enhancer. A higher concentration of CHG within deeper layers of the upper skin strata may result in an increased reduction of opportunistic pathogens within the skin. The ToF-SIMS method has wide ranging potential applications including the ability to investigate the diffusivity of a drug within the skin and the dermatopharmacokinetics of a topically applied drug. Other potential biomedical applications include establishing biochemical differences between healthy and diseased skin and the technique could also be applied to establish whether toxic compounds such as pesticides are systemically absorbed after treatment to the skin surface.

5.4.0 Conclusion

This study has demonstrated that ToF-SIMS is capable of providing rapid, spatially-relevant data for a topically applied compound once dosed on to the skin. Currently, the method is only semi-quantitative, and that is no different to a range of other established skin visualization techniques, including classical histology and spectroscopic methods. ToF-SIMS is a highly sensitive and powerful imaging technique that in this study has shown itself to be highly complementary to conventional Franz-type diffusion cell studies that measure skin penetration. In

addition, the ToF-SIMS approach has provided a detailed qualitative profile of CHG's permeation into the skin, particularly its penetration into the *stratum corneum*. This investigation has also demonstrated that the ToF-SIMS technique can be applied to observe the effects of a novel dendritic permeation enhancer (G3-PAMAM-NH_2) of CHG. This visualisation technique therefore shows great promise for the characterisation of a compound's skin permeation profile. This may in turn allow for the development of more effective topical or transdermal formulations of pharmaceutical compounds.

6.0 An investigation into the co-formulation of a PAMAM dendrimer-CHG skin treatment and the development and optimisation of a suitable topical formulation that will ultimately deliver an increased concentration of CHG within the skin.

6.0 Introduction

6.0.1 PAMAM dendrimers' interactions with small drug molecules

Chapter 3 focused on a PAMAM dendrimer pre-treatment to investigate the physical interactions between the dendrimer and the skin. This Chapter focuses of a co-treatment of PAMAM dendrimer applied in a vehicle with CHG. A one step application would be more convenient, cost-effective and enhance patient compliance and adherence to treatment (Jorge *et al*. 2011).

Numerous research groups have investigated PAMAM dendrimers as a topical or transdermal drug delivery system. The effects of PAMAM dendrimer skin pre-treatment has been discussed in Section 3.1, this chapter will discuss the co-application of PAMAM dendrimers with a range of small molecule drugs. Co-application of ketoprofen and clonidine with G3-PAMAM-NH_2 dendrimer (0.373 µmol solution) within a transdermal patch did not result in an enhanced transdermal drug delivery across an *in vitro* snake skin model (Wang *et al.* 2003a). The same group also investigated the transdermal delivery of tamsulosin complexed to G3-PAMAM-NH_2 dendrimer however the co-application of the PAMAM dendrimer with the drug did not enhance the permeation of the NSAID across snake skin while the PAMAM dendrimer skin pre-treatment did. The authors believe this is due to the interaction of the PAMAM dendrimer with the

drug as opposed to the enhancement effect caused by the PAMAM dendrimer's interaction with the skin (Wang *et al.* 2003b).

Conversely, the flux of indomethacin complexed with G4-PAMAM-NH_2 dendrimer (0.2 % w/v) increased by an enhancement factor of 4.5 when compared to that of the free drug across rat skin in an *in vitro* model. This flux increase was also observed *in vivo* in a Wistar rat model with the dendrimer-drug complex resulting in a $[AUC]_{0\text{-}24h}$ 2.27 times higher for G4-PAMAM-NH_2 when compared to the free drug (Chauhan *et al.* 2003). An enhanced accumulative concentration was observed for G5-PAMAM-NH_2 dendrimer complexed with both ketoprofen and diflunisal *in vitro* from an aqueous rat model and in an *in vivo* rat model the ketoprofen-PAMAM had a 2.73 time higher bioavailability and the diflusinal-PAMAM had a 2.48 time higher bioavailability (Cheng *et al.* 2007). It is interesting to note that in contrast to the Cheng *et al.* 2007 paper no enhancement was observed for ketoprofen complexed to G3-PAMAM-NH_2 across snake skin in a chloroform/methanol vehicle (Wang *et al.* 2003a). The variation in results for the PAMAM dendrimer-ketoprofen complex is likely due to the different model skin membranes used. Pig and rat skin is acknowledged as a surrogate for human skin by the OECD unlike snake skin which is used in the studies above (OECD, 2008). Cnubben *et al.* have shown that rat skin is more permeable than human skin and transdermal absorption *in vivo* in rats is 1.5-2.5 times higher than for human skin. The same authors show that perfused pig ear epidermis is a good surrogate model for human skin (Cnubben *et al.* 2002). Also, the studies utilise different PAMAM dendrimer generations and concentrations throughout the studies.

PAMAM dendrimers co-applied with hydrophilic drugs have also resulted in an enhancement in percutaneous absorption. Co-application of PAMAM dendrimers with 5-Fluorouracil resulted in an increased flux of drug across the porcine skin from a mineral oil and isopropyl myristate vehicle but not from PBS (Venuganti and Perumal, 2008). Again it was found that a PAMAM dendrimer pre-dose was more effective than simultaneous application of the PAMAM-drug. Another hydrophilic drug simultaneously applied with PAMAM dendrimer was riboflavin. A co-treatment of G2-PAMAM-NH_2 and riboflavin in an oil in water emulsion resulted in an increased permeation of riboflavin within porcine ear skin (Filipowicz and Wolowiec, 2011).

PAMAM dendrimers have been formulated into a variety of drug delivery systems. For example PAMAM dendrimers have been incorporated into a polyhydroxyalkanoate matrix into a transdermal drug delivery patch that delivered a clinical concentration of tamsulosin across the skin (Wang *et al.* 2003). Further, Devarakonda *et al.* (2004) characterised hydrogels containing nifedipine, G3-PAMAM-NH_2/ G5-PAMAM-NH_2 with hydroxyl propyl methyl cellulose (HMPC) as a gelling agent. The authors discovered that the amount of nifedipine released from the gels increased with increasing PAMAM dendrimer concentration. A generation dependent effect was also observed with G5-PAMAM-NH_2 resulting in a higher flux of drug release when compared to G3-PAMAM-NH_2. The dendrimer also prevented recrystallization of the drug therefore inferring stability on the formulation. The authors did not test the dendrimer containing hydrogels on an *in vitro* skin model. A detailed review on dendrimers and their effects on the pharmacodynamics and pharmacokinetics once complexed to drugs were compiled by Cheng and Xu (2008).

More recent topical formulations including PAMAM dendrimers include a hydrogel incorporating the antifungal, ketoconazole, and G2 and G3 PAMAM-NH_2 and PAMAM-OH (Winnicka *et al.* 2012). The authors found that the PAMAM dendrimers increased the solubility of ketoconazole and the PAMAM-NH_2 dendrimers resulted in up to a 16 fold enhancement in antifungal properties. The PAMAM-NH_2 dendrimer incorporated hydrogel was found to out-perform the commercially available ketoconazole formulations. Recently, PAMAM dendrimers were also incorporated into a topical crème formulation with silver sulfadiazine and silver nanoparticles for a novel topical treatment for burn-wound infections (Strydom *et al.* 2012). The incorporation of PAMAM dendrimers exerted stability within the formulation and also resulted in an enhanced antimicrobial efficacy.

Dendrimers have found a role in cosmetics and personal care topical formulations. Unlike linear polymers, dendrimers are unique in that the intrinsic viscosity increases with increasing molecular weight to a maximum after which the viscosity decreases with molecular weight in a bell shaped curve (Tolia and Choi, 2008). This is an interesting characteristic that allows for high molecular weight dendrimers to be easily formulated without issues with viscosity. There are a vast number of patents which include amine terminated dendrimers due to their unique characteristics. For example, Revlon filed a patent on amine terminated dendrimers complexed with anti-acne molecules to treat acne vulgaris within a cosmetically acceptable formulation (Wolf and Snyder, 1995). Starpharma have also filed for a patent using amine terminated PAMAM dendrimers in deodorant formulations as the water soluble active odour-reducing agent. This is because some basic compounds have the ability to reduce body odour. PAMAM dendrimers were shown to limit body odour for up to 20 hours (Forestier and

Rollat-Corval, 1999). PAMAM dendrimers are also covered in a patent filed by L'Oreal which outlines a self-tanning formulation, which, combined with the active dihydroxyacetone, forms a more natural looking tan (Allard and Forestier, 1998). PAMAM dendrimers have wide ranging potential within topical drug delivery and cosmetics and personal care.

The advantages of utilising PAMAM dendrimers within a dermatological formulation discussed above are summarised below;

(i) Enhances the permeation of drugs within the skin (Venuganti and Perumal 2008, Wang et al. 2003 and Filipowicz and Wolowiec, 2011).

(ii) Increases drug solubility and bioavailability (Devarakonda et al. 2004, Milhem et al. 2000 and Yiyun et al. 2005).

(iii) Exhibits antimicrobial properties (Observed in Chapter 2 and Calabretta et al. 2007 and Wang et al. 2010).

(iv) Exhibits anti-inflammatory properties (Chauhan et al. 2009).

(v) Has been shown to reduce irritation through binding to anionic surfactants (Derici et al. 2005).

(vi) Odour absorbing properties (Forestier and Rollat-Corval, 1998).

(vii) Ideal intrinsic viscosity properties (Tolia and Choi, 2008).

(viii) Water soluble and compatible with organic solvents (Liu and Fréchet, 1999).

(ix) Good bioadhesion (Vandamme and Brobeck, 2005).

6.02 Rationale for the investigation of a topical preparation using a CHG-PAMAM complex.

In Chapter 2, it was shown that a PAMAM dendrimer skin pre-treatment enhanced the permeation of CHG within the upper skin strata. A PAMAM

dendrimer skin pre-treatment enhances the penetration of therapeutics across the skin (Chapter 2, Wang *et al.* 2003, and Venuganti and Perumal, 2009) though co-application of a drug with the dendrimer enhancer would be more convenient in a one-step application. Various PAMAM dendrimer-drug complexes are discussed in section 6.01 however no *in vitro* skin absorption or drug-dendrimer interaction studies have been conducted on the co-application of an antimicrobial compound-PAMAM dendrimer complex formulation. Moreover, there are limited studies available within the literature where PAMAM dendrimers have been formulated into a cosmetically acceptable topical formulation (Winnicka *et al.* 2012 and Strydom *et al.* 2012).

6.03 Aims and objectives

The aim of this chapter is 2 fold; to firstly investigate whether a PAMAM dendrimer-CHG co-application enhances the permeation of CHG within porcine skin and secondly to develop a cosmetically acceptable formulation for the co-application.

To achieve these aims a number of objectives were necessary;

(i) To investigate the interactions between G3-PAMAM-NH_2 dendrimer and CHG.

(ii) To conduct studies into determining whether a co-application of G3-PAMAM-NH_2 –CHG enhanced the percutaneous absorption of CHG within porcine heat separated epidermis. To also determine whether any enhancement effect is proportional to the PAMAM concentration within the co-dose application.

(iii) To develop a formulation for the co-application of PAMAM dendrimer-CHG that out performs formulations already available in terms of antimicrobial efficacy but is still cosmetically acceptable. The properties of the formulations will be characterised and then an optimal formulation will be tested in an *in vitro* porcine percutaneous absorption model.

6.1 Materials and methods

6.1.0 Investigation into the interactions between chlorhexidine digluconate and PAMAM dendrimers

6.1.1 Imaging and measurement of crystal formation

Within 12 h of contact G3-PAMAM-NH_2 and CHG formed a precipitate in an aqueous solution forming crystals. These crystals were then magnified and imaged on a Leica light microscope (model- MZ8, Milton Keynes, UK) and the crystals were illuminated using a cold light source (Schott light, KL1500, Massachusetts, US). The images were captured on an attached Infinity X camera (Lumenera, Ottawa, Canada). The length of crystals formed was measured using a calibrated graticule on the microscope.

6.1.2 Matrix assisted laser desorption ionization Time of Flight (MALDI-ToF) mass spectrometry

A 10 mg sample of vacuum dried (24 h on a high vacuum line) precipitate was sent to the EPSRC National Mass Spectrometry Service Centre at Swansea University. The sample was analysed on a Voyager De-STR (Applied biosystems) with a nitrogen laser (λ=355 nm) using a 3-indoleacrylic acid, and a 1:1 ethanol: acetonitrile matrix. The spectra were collected in positive linear mode.

6.1.3 Single crystal x-ray diffraction

A sample of the crystals in aqueous solution was sent to the UK National Crystallography Service, University of Southampton. The diffractometer used was the beamline I19 situated on an undulator insertion device with a combination of double crystal monochromator, vertical and horizontal focussing mirrors and a series of beam slits (primary white beam and either side of the focussing mirrors). The experimental hutch (EH1) was equipped with a Crystal Logic 4-circle kappa geometry goniometer with a Rigaku Saturn 724 charged coupled device (CCD) detector and an Oxford Cryosystems Cryostream plus cryostat (80-500 K). The beamline operates at 18 KeV.

6.1.4 Formulation of the co-application (G3-PAMAM-NH_2 dendrimer–CHG) formulation

The G3-PAMAM-NH_2 dendrimer–CHG complex was stabilised in a water: ethanol solution (varying in volume ratio from 10-90 % ethanol content) within 2 mL amber glass vials. The water used in the formulation was ultrapure and the ethanol was HPLC grade (Fisher Scientific, Loughborough). The samples were left for three months at ambient temperature. The ideal organic solvent/water mixture was chosen based on the absence of precipitation.

6.1.5 Recovery of CHG after addition of PAMAM dendrimer in occluded and unoccluded conditions.

G3-PAMAM-NH_2 was added in varying concentrations (0.2 mL of 0.5, 1 and 10 mM) to CHG (0.2 mL, 2 % w/v) in a 50:50 ethanol:water vehicle in a 3 mL vial. The samples were mixed and placed in a water bath at 32°C ± 1°C (skin surface temperature) and were either occluded or unoccluded. The samples were left for 24 h after which they were syringe filtered (0.2 µm, 15 mm diameter polypropylene filters, Fisher Scientific, Loughbrough, UK) and diluted to an appropriate level. An aliquot of each sample was removed and placed in a clean quartz cuvette and after running a blank the absorbance at 254 nm was measured on a UV-VIS Varian Cary® 50 Bio spectrometer (West Sussex, UK). The equation of the line after analysing a series of CHG standards to form a calibration graph was y=0.034x+0.321 which was linear over a concentration range of 0-100 µg/mL (R^2 = 0.9998).

6.1.6 Microdilution broth with viable count assay to determine inhibitory concentration (IC_{50})

To determine whether the addition of the PAMAM dendrimer would result in synergistic or antagonistic antimicrobial effects, a microdilution broth assay with a viable count was conducted. The method is outlined fully in section 2.1.1. Various concentrations ranging from 1-0.005 µg/mL of CHG in a 50:50 water: ethanol vehicle and various concentrations of G3-PAMAM-NH_2 dendrimer and CHG (1-0.005 µg/mL) were tested against *S. aureus.*

6.1.7 Co-application of various dendrimer concentrations (G3-PAMAM-NH_2) formulated with CHG in an ethanolic vehicle to porcine epidermis.

The co-application was dosed onto porcine epidermis to determine whether the addition of PAMAM dendrimer increases the permeation of CHG within the skin. The method is outlined in full in Sections 3.2.1-3.2.3. Various concentrations of G3-PAMAM-NH_2 were tested (0.5-10 mM, 0.2 mL) in combination with CHG (2 % w/v) in a 50:50 water:ethanol vehicle.

6.1.8 Formulation development and characterisation

A range of formulations were developed in high grade 30 mL glass universals and the constituents were all HPLC or reagent grade. Each formulation was created in triplicate. The ethanol used was HPLC grade (Fisher Scientific, Loughborough, UK), the hydroxyl propyl cellulose (HPC, 100,000 mw) was purchased from Sigma Aldrich (Dorset, UK), CHG (20 % w/v) was purchased from Sigma Aldrich (Dorset, UK) also as was the glycerol and the dimethicone. All formulations were mixed on a Retsch mm200 mixer mill (Castleford, UK) for 5 minutes at a frequency of 30 cycle per second and then left to stir over night at 200 RPM on a stirrer plate (Stuart, UC152, Stone, UK).

6.1.8.1 Measurement of the pH of the topical gel formulations

For each formulation 1 g was weighed out (Precisa, 262 SMA-FR, Milton Keynes, UK) in to a clean conical flask (Grade A glassware, 25 mL) and was made up to 10 g with ultra-pure water (SG, HYXO, Kerava, Finland). The conical flask was swirled until the formulation had completely dissolved. The pH was measured using a pH probe (HANA instruments, pH 210 microprocessor, Bedfordshire, UK)

that had been buffered to pH 4.1, 7.1 and 9.1 prior to use, the temperature was accounted for (19.8 °C) by the inclusion of the temperature probe with the pH probe. The pH was measured in triplicate.

6.1.8.2 Measurement of the spreadability of the topical gel formulations

The spreadability of the formulations was determined by weighing out 1 g of the topical gel formulation onto a clean glass plate (20 x 20 cm) after which a top plate (20 x 20 cm) was placed over the top of the bottom glass plate that had been standardised to a weight of 132 g. After 60 seconds the diameter of the formulation spread was measured in mm using a standard ruler (error ± 0.5 mm) in the vertical and horizontal direction. The measurements were recorded and the spreadability capacity was calculated using Equation 1. Again, the measurements were taken in triplicate (Lardy *et al.* 2000 and Garg *et al.* 2002). The spreadability of a commercially available alcohol hand gel 'Safemate original' (151 Products Limited, Manchester, UK) was also measured in parallel for comparative reasons. The 'Safemate original' gel contained ethyl alcohol 62 % as the active ingredient.

6.1.8.3 Extraction of CHG from formulations (drug content and uniformity)

To determine the concentration of CHG available within the formulation (Shafiullah *et al.* 2005), CHG was extracted from 1 g of each formulation. In triplicate 1 g of each formulation was weighed into a 100 mL volumetric flask (grade A glassware) and made up to volume with ultra-pure water. The volumetric flask was inverted until the formulation had dissolved. Then, 1 g of the diluted solution was added to a 25 mL volumetric flask and made up to volume with ultra-pure water and inverted ten times. A 1.5 mL aliquot was removed and placed in a

clean quartz cuvette and after running a blank the absorbance at 254 nm was measured on a UV-VIS Varian Cary® 50 Bio spectrometer (West Sussex, UK). This was repeated for each formulation and the percentage of CHG recovered was calculated from a calibration curve created by measuring the absorbance of 6 CHG standards (1-50 µg/mL). The line equation was y=0.0321x+ 0.0154 (R^2= 0.9991).

6.1.8.4 Viscosity of topical gel formulations

Before measurement of the rheology or viscosity of the formulations was undertaken all formulations were placed in a vacuum for 2 h to ensure removal of any trapped air bubbles. The rheology of the topical formulations (20 mL) was measured from 1-12 RPM and back down from 12-2 RPM on a DV-E Brookfield™ system with an LV spindle set (Essex, UK). The accuracy of the calibrated DV-E Brookfield™ system is ± 0.1 %.

6.1.8.5 Antimicrobial efficacy of topical gel formulations

A modified agar cup method (Orafidiya *et al.* 2001 and Wannachaiyasit and Phaechamud, 2010) was utilised to determine the antimicrobial efficacy of the formulations against three bacteria *Staphylococcus aureus* (ATCC 11832), *Escherichia coli* (ATCC 8277) and *pseudomonas aeruginosa* (ATCC 10848). The bacteria were cultured, harvested and diluted as outlined in Section 2.1.1. For each bacteria, an inoculum of ~10^5 was achieved. Cation adjusted Mueller Hinton agar (MHA) was poured into 90 mm petri dishes (25 mL) and allowed to cool at room temperature. Once the agar was set a sterile borer was used to bore 3 x 10 mm holes within the agar of each petri dish. Each hole was labelled with the

formulation reference and the plate was labelled with the bacteria name. A 1 mL syringe was used to add 0.1 mL of the gel formulation into the hole in the agar taking care not to spill any formulation on the agar surface. Once each of the holes in the agar had been filled, 0.2 mL of the inoculum (~10^5) was vortex mixed with 7 mL of molten MHA that had been cooled to 40 °C. The inoculated MHA was then immediately poured on top of the agar plate and thus the holes filled with the topical gels. Great care was taken as to not disturb the topical gels as the inoculated MHA was poured very slowly. Once the top MHA layer had set the petri dish was inverted and incubated at 37 °C for 24 h. Each formulation was made up in triplicate and each formulation was tested in duplicate therefore for each formulation (*n*=6) against each bacteria. After 24 h the zone of inhibition was measured using a standard ruler (error ± 0.5 mm) and the average and standard deviation as calculated.

6.1.8.6 Attenuated total reflectance Fourier transform infra-red spectroscopy (ATR-FTIR) of topical gel formulations

Each formulation and the corresponding starting materials were measured using the same ATR-FTIR as outlined in Section 4.1.4. After a background spectrum was obtained, 50 µL of the topical gel was transferred onto the diamond and immediately a spectrum was collected. Differences and similarities between the starting materials and the formulations were recorded.

6.1.8.7 Percutaneous absorption of chlorhexidine digluconate from selected formulations determined by tape stripping dermatomed porcine skin after 24 h

The permeation of CHG within dermatomed porcine skin was measured by using a tape stripping procedure as previously detailed in Sections 3.2.3-3.2.4. Three of the developed formulations were selected F4(a), F5 and F6 and 1 mL of each formulation was placed on the skin surface of each Franz cell for 24 h (*n*=5).

6.1.9 Analysis of results

All data is presented as the mean ± SEM unless otherwise stated and were analysed using GraphPad Prism® version 5 (San Diego, USA). Prior to statistical analysis all data were placed in to a histogram to check for normality. To compare the percentage recovery of CHG after addition of the PAMAM dendrimer under occluded and uncoccluded conditions (section 6.2.6) a one way ANOVA with a Dunnett's post test was conducted (*n*=3). The calculation of the IC_{50} of the co-formulation of G3-PAMAM-NH_2 –CHG (section 6.2.7) was conducted as outlined in section 2.2.1 (*n*=3). In section 6.2.8 a Kruskal-Wallis ANOVA with an *ad hoc* Dunn's test was used to show significance between the PAMAM dendrimer-CHG co-treated skin compared to the CHG control (*n*=6) (Figure 6.9). Also in section 6.2.8, a one way ANOVA (normally distributed data) was conducted on the total concentration of CHG (µg/cm^2) detected within the receptor fluid at 24 h after co-application of G3-PAMAM-NH_2-CHG as well as CHG (*n*=6) (Figure 6.10). No post test was conducted however due to $p>0.05$. In Section 6.2.9.2 a one way ANOVA was conducted to confirm any significant difference between the spreadability diameters as a function of altering the formulation compositions. Further, a

Tukey's multiple comparison was utilised to determine specific significant intracomparisons (p<0.05). A one way ANOVA analysis was also used in Section 6.2.9.3 to analyse the differences within the uniformity and concentration of CHG within the formulation.

6.2 Results

6.2.1 Investigation into the interactions between chlorhexidine digluconate and PAMAM dendrimers

A 10 mM solution of G3-PAMAM-NH_2 was slowly added to a solution of a clinically relevant concentration of CHG (2 % w/v) (Figure 6.1). Immediately on contact it was observed that the solution had turned cloudy and after 6 h a crystalline precipitation occurred. The precipitate was magnified and photographed and the micrograph is illustrated in Figures 6.2 and 6.3. It was discovered that shard crystals formed and that the crystal shape was dependent on the order of addition. Crystal formation occurred at 10, 1 and 0.5 mM concentration of G3-PAMAM-NH_2. It was discovered that the crystal shape was dependent on the order of addition for example Figure 6.2 shows the crystal formation when the formulation was added in the following order: water-G3-PAMAM-NH_2-CHG and Figure 6.3 shows the crystal structure after an addition order of CHG-G3-PAMAM-NH_2 water.

(a)

(b)

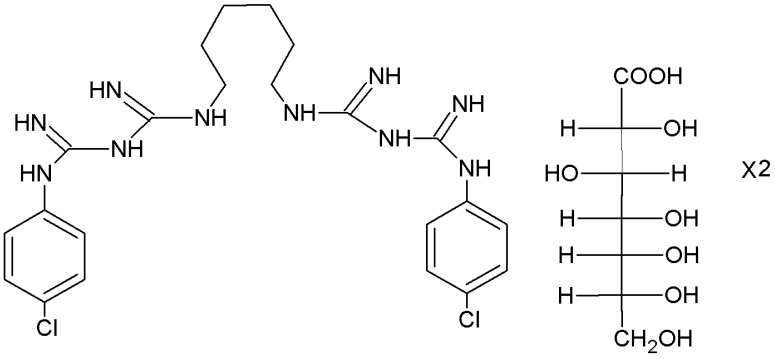

Figure 6.1. Chemical structure of a PAMAM dendrimer and CHG *(a) Chemical structure of G3-PAMAM-NH_2 dendrimer linear formula: [NH2(CH2)2NH2]:(G=3);dendriPAMAM(NH2)32, molecular Weight: 6908.84 and (b) Chemical structure of chlorhexidine digluconate, molecular formula: C22H30Cl2N10.2(C6H12O7), molecular weight: 897.56.*

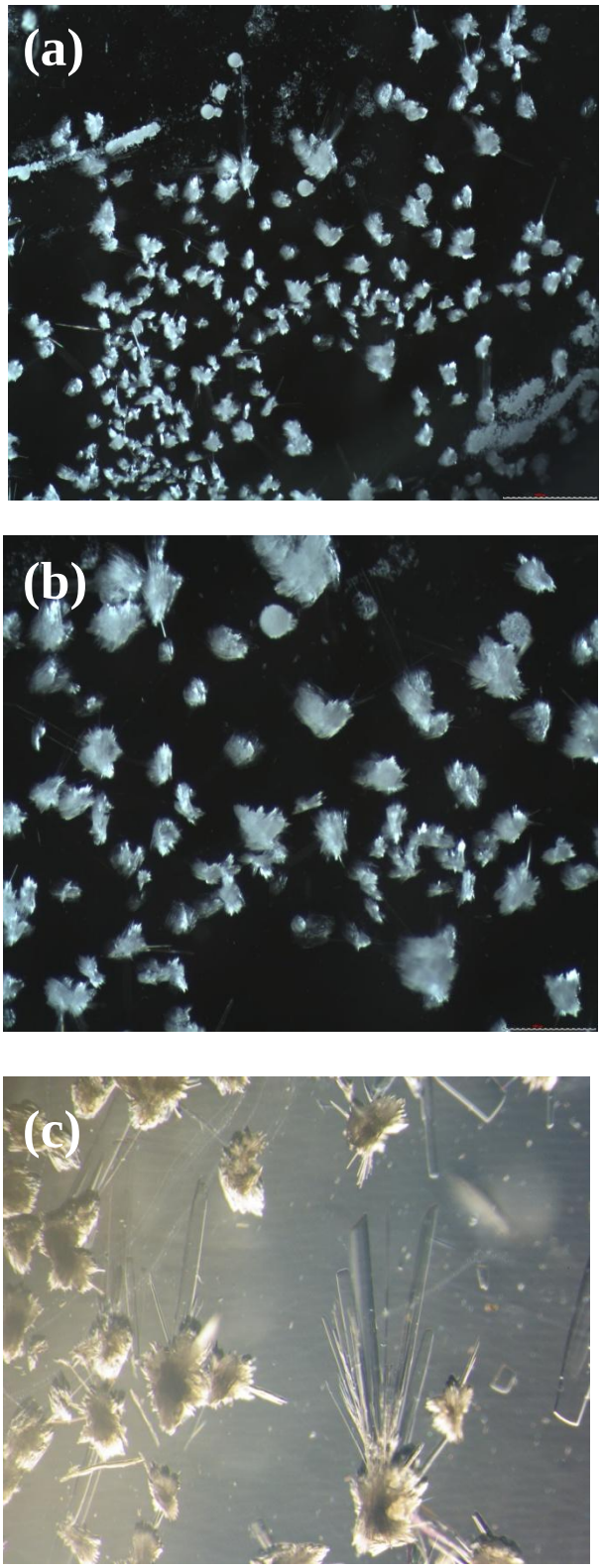

Figure 6.2. Photograph of shard crystals formed on addition of CHG to PAMAM dendrimer. *Crystallised precipitate after addition of water (up to 200 µL) followed by G3-PAMAM-NH_2 followed by CHG. Images were taken 24 h after contact at a magnification of (a) x2, (b) x4 and (c) x11. Shards of transparent crystal can be observed emanating from a focal point.*

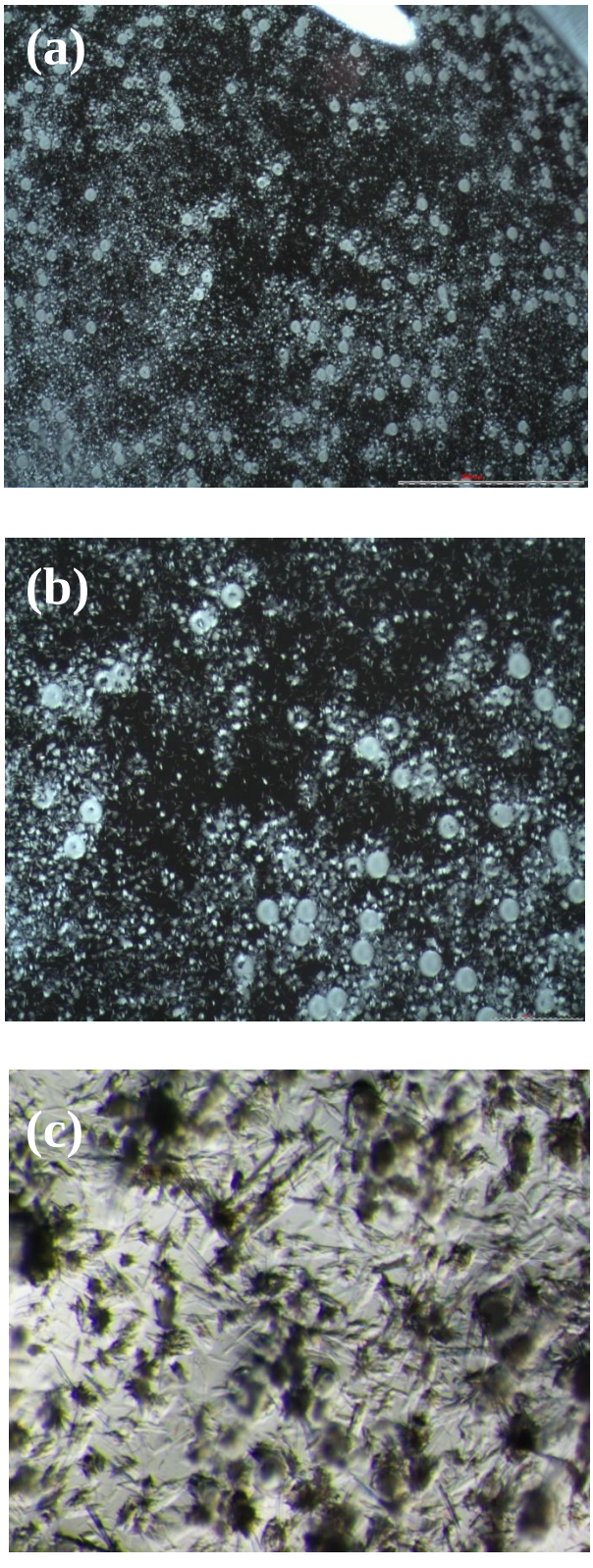

Figure 6.3. Photograph of short shard crystals emanating from a focal core after addition of CHG to PAMAM dendrimer. *Crystallised precipitate after addition of CHG, G3-PAMAM-NH_2 and then water (up to 200 µL). Images were taken 24 h after contact at a magnification of (a) x2, (b) x4 and (c) x11. Small shards of crystal emanating from a rounded single focal core much like that of petals of a flower can be observed.*

6.2.2 Measurement of the melting point

The crystalline precipitate was dried under vacuum at 50°C and the melting point was determined. The crystals began to melt at 109°C and had completely melted at 115°C; two further replicates of each crystal shape confirmed the melting point.

6.2.3 Measurement of crystal lengths

The length of the crystals was measured on a calibrated Leica microscope at a 6.4 x magnification. The mean shard crystal length obtained in from Figure 6.2 was 0.578 ± 0.0013 mm (mean ± SD, *n*=5) and the mean diameter of the 'flower' shaped crystals from Figure 6.3 was 0.128 ± 0.0022 mm (mean ± SD, *n*=5).

6.2.4 MALDI-ToF analysis of precipitate

The crystalline precipitate was dried under vacuum at 50°C and was analysed in parallel with G3-PAMAM-NH_2 dendrimer reference material. The mass spectra for G3-PAMAM-NH_2 reference material and the precipitate can be observed in Figures 6.4 and 6.5. The mass accuracy of this particular mass spectral system is +/- 2 Da. Isotopically resolved species could not be obtained in reflectron mode. The sample appears to be a mixture and the species are likely to be $[PAMAM+H]^+$ and possibly $[PAMAM+Na]^+$. Figure 6.4 illustrates the mass spectra of G3-PAMAM-NH_2 reference material with the overview spectrum (a) and (b) magnified spectrum showing a mass of 1000-4400 (m/z) and (c) magnified spectrum showing 4855-7525 (m/z). Figure 6.5 shows the spectra corresponding to the vacuum dried precipitate after addition of CHG to G3-PAMAM-NH_2

dendrimer; (a) is an overview spectra, (b) magnification at 1000- 2475 (m/z) and (c) magnification of spectrum at 5970- 7505 (m/z).

(a)

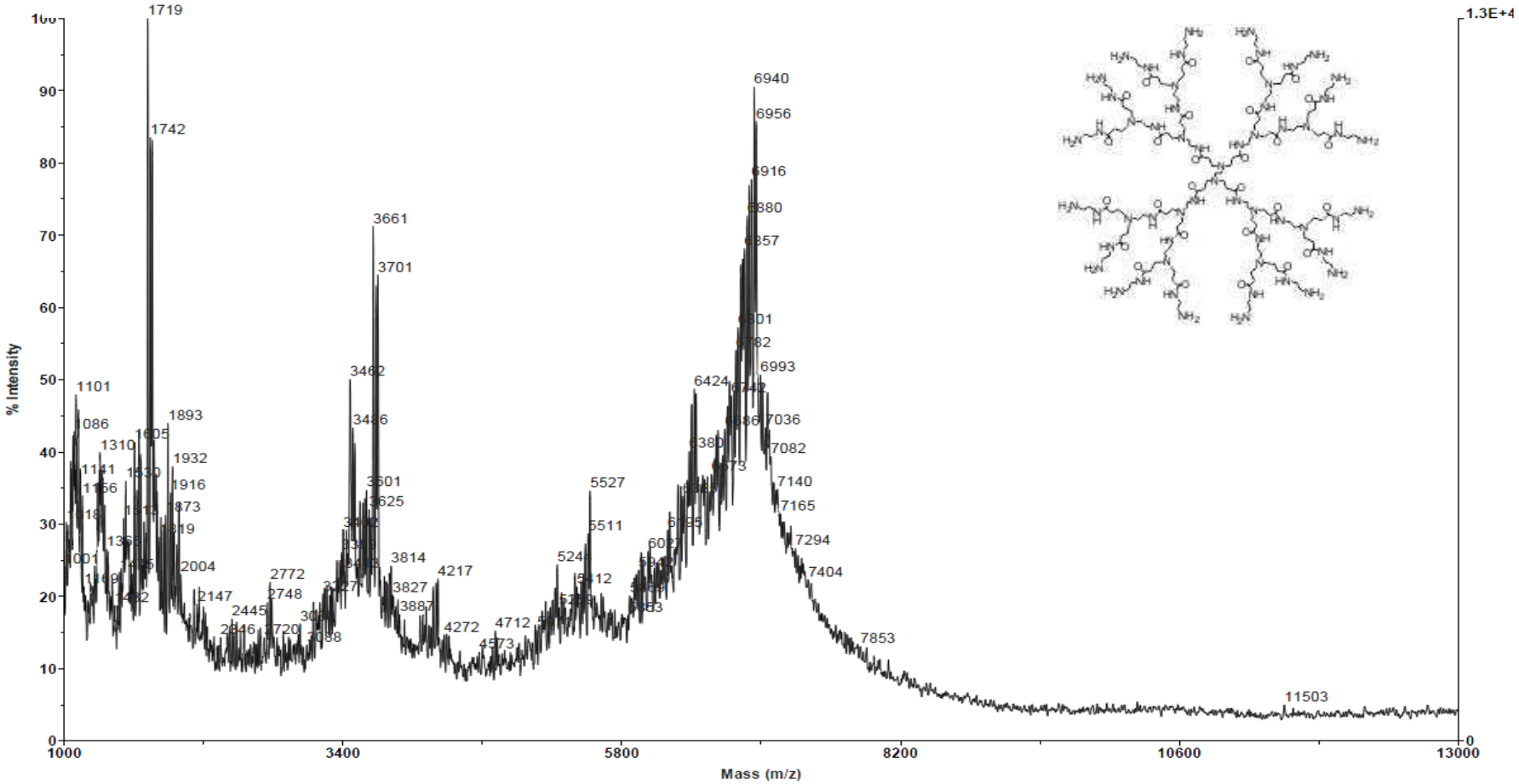

Figure 6.4. MALDI-ToF mass spectra of G3-PAMAM-NH_2 dendrimer *(a) overview spectrum*

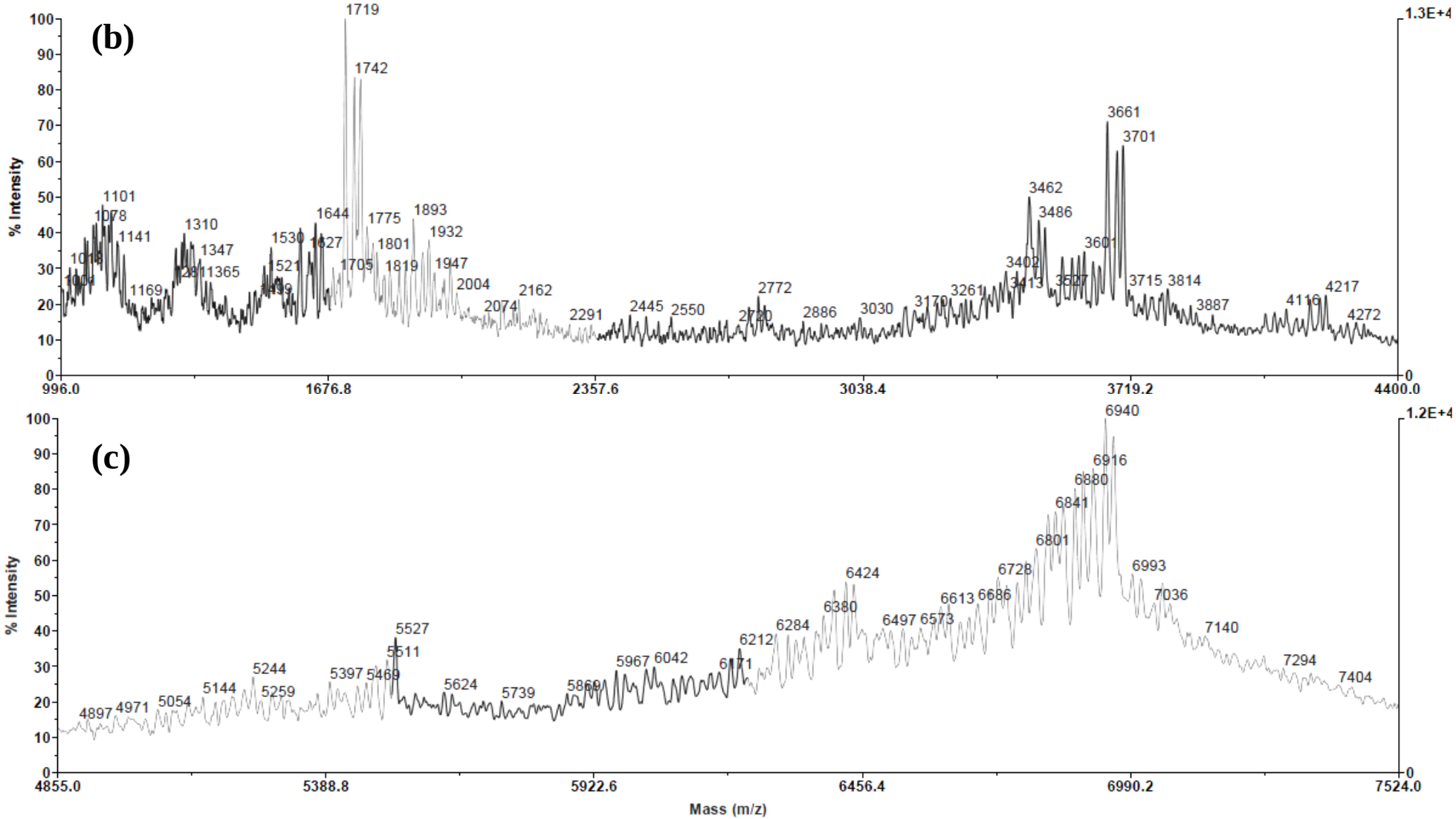

Figure 6.4. MALDI-ToF mass spectra of G3-PAMAM-NH_2 dendrimer *(b) magnified spectrum showing a mass of 1000-4400 (m/z) and (c) magnified spectrum showing 4855-7525 (m/z).*

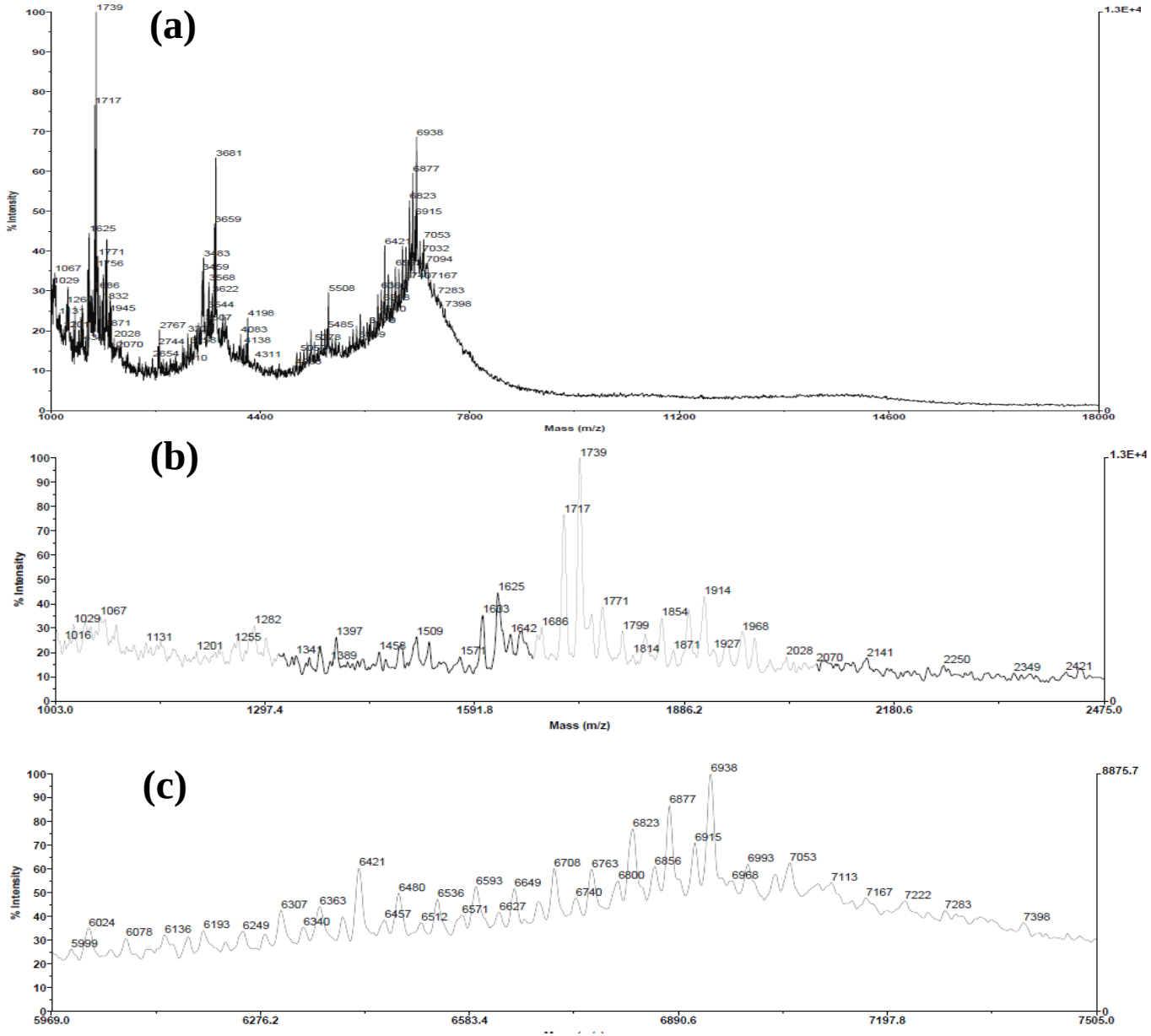

Figure 6.5. MALDI-ToF mass spectra of G3-PAMAM-NH_2 and CHG precipitate *(a) is an overview spectrum, (b) spectrum magnification at 1000- 2475 (m/z) and (c) magnification of spectrum at 5970- 7505 (m/z).*

6.2.5 Single crystal x-Ray Diffraction (XRD) on precipitate

The XRD results of the crystalline precipitate analysis are illustrated below in Table 6.1. The crystal system was found to be a monoclinic system that is a rectangular prism with a parallelogram at its base. The crystal was a colourless platelet and was found to have a molecular weight of 639.55 Da. The two nitrogen atoms closest to the 4-chlorophenyl group are protonated. CHX (base), four water molecules and an oxocarbon anion were detected within the crystal. For full details on the XRD data please refer to Appendix 3 A structure built from the XRD data is displayed in Figure 6.6 as a ball and stick structure.

Table 6.1 Crystal data obtained from XRD analysis.

Crystal data	
Empirical formula	$C_{23}H_{40}Cl_2N_{10}O_7$
Formula weight	639.55
Crystal system	Monoclinic
Crystal	Platelet; Colourless
Crystal size	$0.10 \times 0.04 \times 0.01$ mm^3

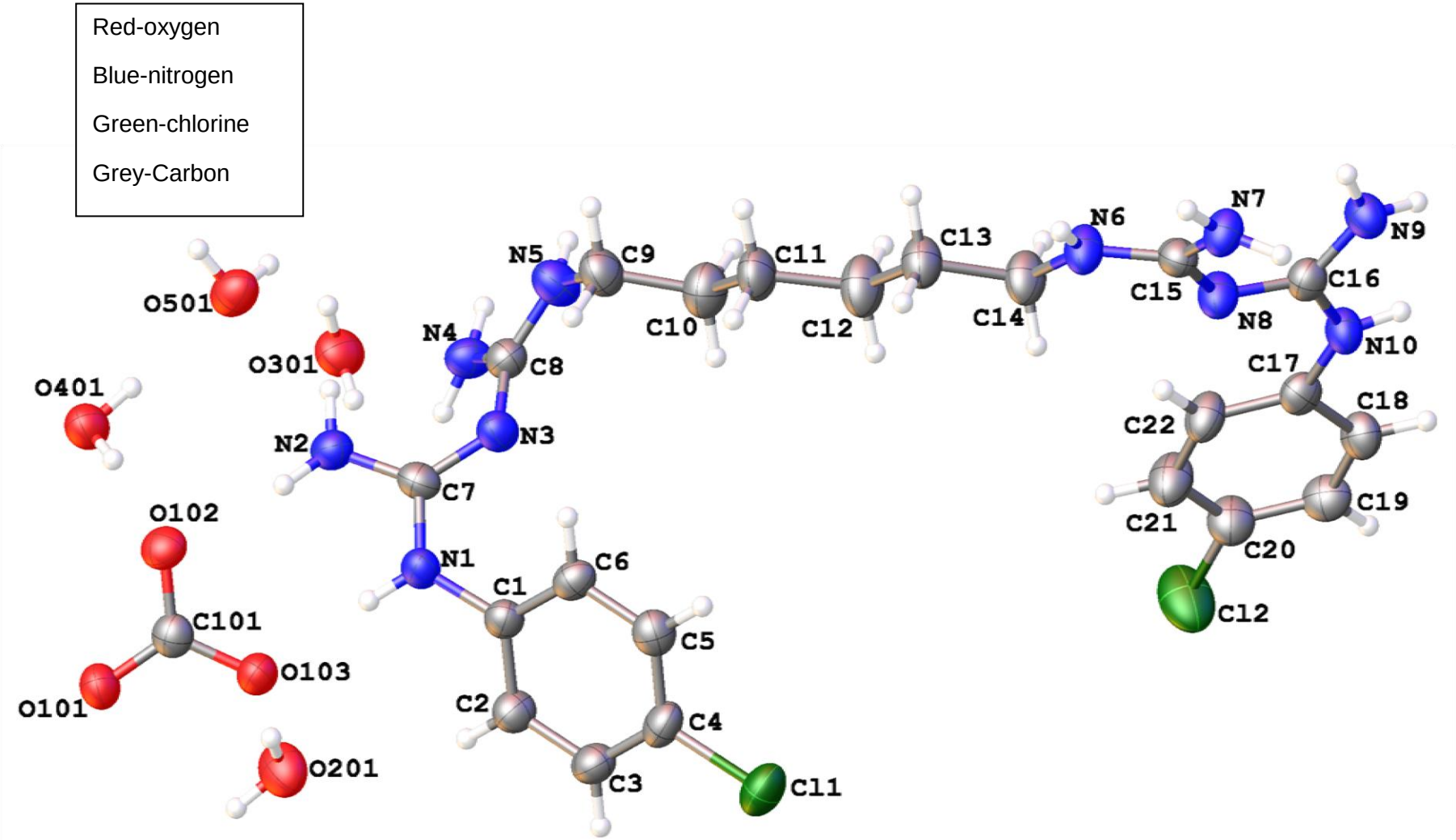

Figure 6.6 Chemical structure obtained from XRD analysis of a single crystal of the precipitate.

6.2.6 Formulation of CHG-PAMAM dendrimer

On addition of CHG to a G3-PAMAM-NH_2 dendrimer solution it was shown that the CHG precipitates out of solution. Once the two components were added to an ethanol:water solution (50:50), the co-dose formulation became stable. No precipitate was observed over a 3 month period under occluded conditions, stored away from light at ambient temperature. A lower percentage of CHG was recovered from the unoccluded samples with the lowest being the control containing only CHG and no PAMAM dendrimer (Table 6.2). Under unoccluded conditions the formulation containing 0.5 mM G3-PAMAM-NH_2 resulted in the highest recovery of CHG from the formulation (59.22 ± 2.00 %) followed by 10 mM (51.77 ± 2.63 %) and lastly 1 mM G3-PAMAM- NH_2 dendrimer (47.25 ± 5.44 %). This is compared to a recovery of only 34.44 ± 3.33 % for the formulation containing no PAMAM dendrimer and only CHG. Under occluded conditions a significantly higher recovery of CHG was observed for all formulations. The lowest recovery was observed for the 10 mM G3-PAMAM-NH_2 formulation at 79.24 ± 1.23 % but it was observed that the solution had turned white and pearlescent in appearance. The 0.5 and 1 mM G3-PAMAM-NH_2 dendrimer formulations enhanced the recovery of CHG (85.94 ± 1.16 % and 92.56 ± 1.84 % respectively) when compared to the control formulation that contained no PAMAM dendrimer (84.27 ± 1.96 %).

Table 6.2 Percentage recovery of CHG after addition of PAMAM dendrimer under occluded and unoccluded conditions. *Recovery of CHG from a co-formulation of various concentrations of G3-PAMAM-NH_2 that were maintained in occluded or unoccluded conditions at 32°C ± 1°C (skin temperature) for 24 h.*

Co-formulation	Percentage recovery of CHG from co-formulation (%)			
Sample (*n*=3)	Unoccluded at 32°C Mean	SEM	Occludded at 32°C Mean	SEM
No PAMAM dendrimer	34.44	3.33	84.27	1.96
0.5 mM + CHG	59.22	2.00	85.94	1.16
1 mM + CHG	47.25	5.44	92.56	1.84
10 mM + CHG	51.77	2.63	79.24*	1.23

* Formulation turned white and pearlescent.

Figure 6.7 displays the CHG recovery data in which the difference between the occluded and unoccluded formulations is evident. A one way ANOVA with a Dunnett's post test (F=12.02, df=11, 332.8, p<0.05) showed a statistically significant difference between the formulation without PAMAM dendrimer and the 1 mM G3-PAMAM-NH_2. Further, statistical significance was observed between the control and the 0.5 mM and 1 mM G3-PAMAM-NH_2 (one way ANOVA with a Dunnett's post test F=7.046, df=11, 1126 and p<0.05). Interestingly under occluded conditions only the 1 mM G3-PAMAM-NH_2 dendrimer formulation resulted in a significant CHG percentage recovery. Conversely under unoccluded conditions it was only the 1 mM G3-PAMAM-NH_2 dendrimer formulation that didn't result in a significant enhanced recovery of CHG.

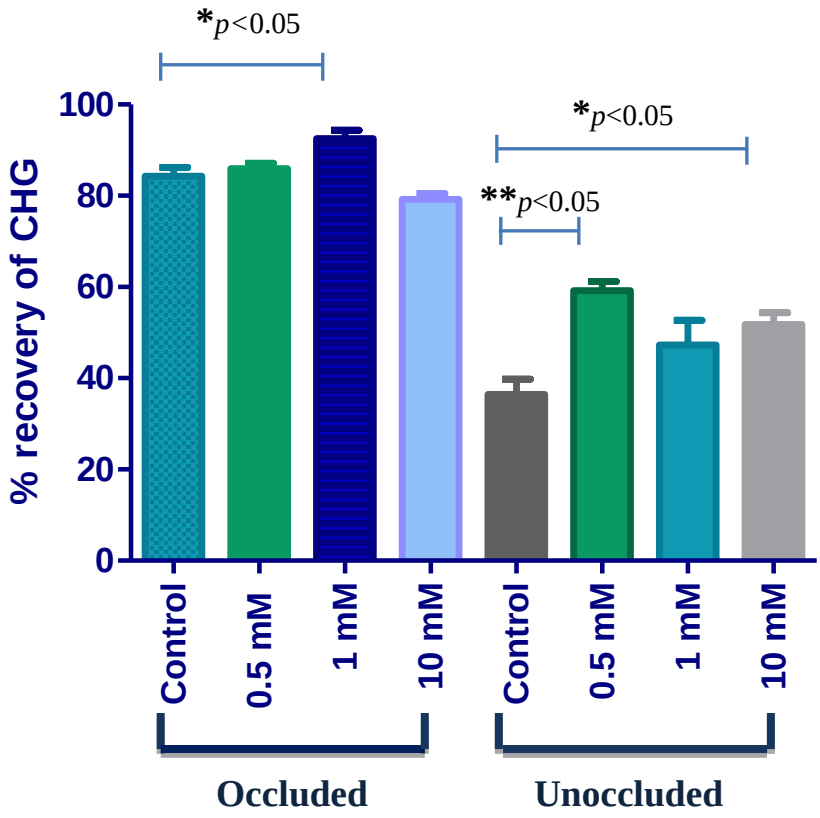

Figure 6.7. Bar chart of percentage recovery of CHG from a co-formulation of various concentrations of G3-PAMAM-NH_2 and CHG. *The formulations were maintained in occluded or unoccluded conditions at 32°C for 24 h. Data are shown as the mean ± SEM (n=3). Statistical significance was observed when 1 mM was compared to the CHG control (p<0.05) under occluded conditions and also significance was observed when comparing 0.5 and 10 mM PAMAM dendrimer to the CHG control under unoccluded conditions (p<0.05).*

6.2.7 The effect of PAMAM dendrimer on the efficacy of CHG

It was determined that the addition of CHG to G3-PAMAM-NH_2 did not alter the antimicrobial efficacy of CHG. The IC_{50} concentration was calculated to be 0.056 µg/mL and for CHG in an ethanol:water (50:50) vehicle and 0.057 µg/mL for CHG-G3-PAMAM-NH_2 complex in an ethanol:water (50:50) vehicle. Thus the calculated IC_{50} were within 0.001 µg/mL of each other. (Figure 6.8)

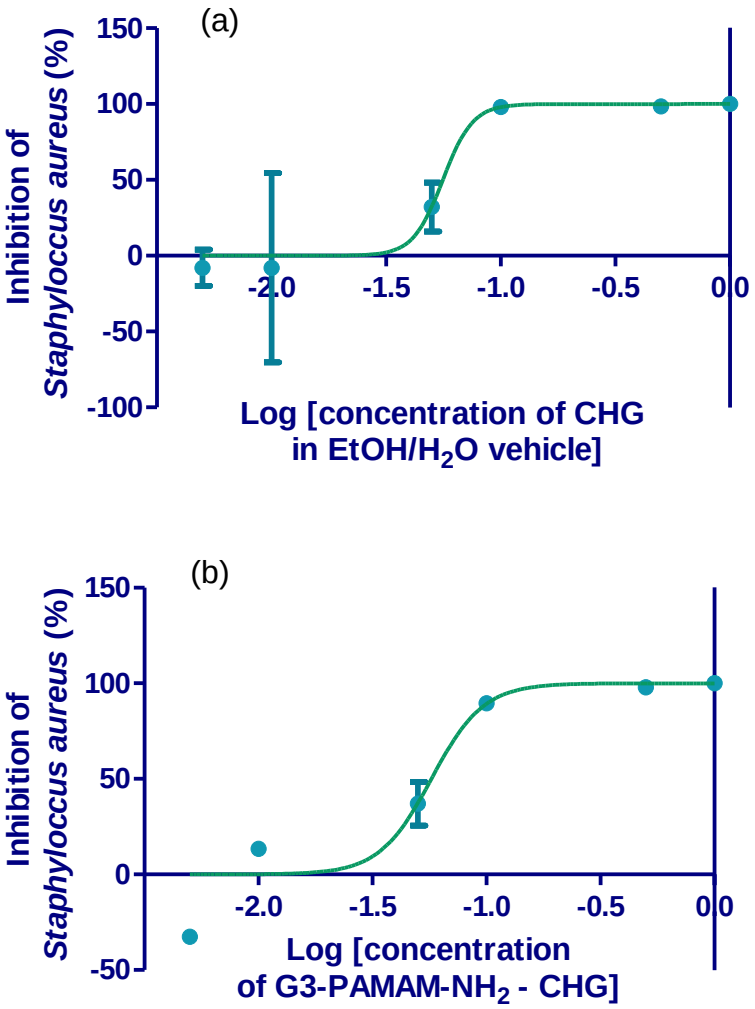

Figure 6.8. Inhibition curves used to calculate the IC_{50} concentrations of CHG alone in an ethanol:water (50:50) vehicle and for G3-PAMAM-NH_2 –CHG in an ethanol: water (50:50) vehicle *(a) CHG in ethanol:water vehicle the IC_{50} was calculated to be 0.056 µg/mL (95 %CI: 0.02582-0.1212 µg/mL) and (b) CHG-G3-PAMAM-NH_2 formulation calculated IC_{50} 0.057 µg/mL (95 %CI: 0.04620-0.07120 µg/mL) Results are represented as the mean ± SEM (n=3).*

6.2.8 Co-application of various dendrimer concentrations (G3-PAMAM-NH_2) formulated with CHG in an ethanolic vehicle, applied to porcine epidermis

A co-application of PAMAM dendrimer was added in combination with CHG (2 % w/v) at three different concentrations (0.5, 1 and 10 mM) in an ethanol:water solution (50:50). The data from the studies is shown in Tables 6.3, 6.4, 6.5 and 6.6, corresponding to no PAMAM dendrimer, 0.5, 1 and 10 mM respectively. A much lower concentration of CHG was recovered across all skin treatment groups with a mean of around 57 % in the amount of CHG dosed recovered. The highest concentration of CHG was detected within the skin wash at 24 h, and the second highest was extracted from the glass donor chamber. A mean concentration of CHG permeated into the porcine epidermis for the formulation without the presence of PAMAM dendrimer was 211.370 ± 33.189 µg/cm^2 compared to 775.857 ± 283.070 µg/cm^2, 384.209 ± 153.937 µg/cm^2 and 621.711 ± 98.818 µg/cm^2 for 0.5, 1 and 10 mM PAMAM dendrimer co-application respectively (Figure 6.9). A Kruskal-Wallis ANOVA test showed that the median concentration of CHG within the epidermis for CHG dosed alone compared to 10 mM G3-PAMAM-NH_2 dendrimer was statistically lower. A high variability for the CHG concentration within the epidermis for the 1 mM G3-PAMAM-NH_2-CHG formulation was observed after application to porcine skin.

Table 6.3. Percutaneous absorption (mass balance) of CHG within porcine epidermis after a 24 h of CHG (2 % w/v) formulation in ethanol:water (50:50). *Data is represented as the mean ± SEM (n=6) for each diffusion cell compartment for both the CHG concentration (µg/cm^2) and for the percentage of dosed applied.*

Compartment (*n*=6)	CHG (µg/cm^2)		% of applied dose	
	Mean	SEM	Mean	SEM
Donor chamber	632.610	60.470	8.010	0.810
Skin wash	3189.095	355.540	40.500	1.440
Epidermis	211.370	33.189	2.684	0.421
Receptor fluid	9.100	2.087	0.116	0.026
Total recovered	4042.175	451.286	51.310	2.679

Table 6.4 Percutaneous absorption (mass balance) of CHG within porcine epidermis after a 24 h treatment with 0.5 mM-PAMAM dendrimer CHG formulation in ethanol:water (50:50). *Data is represented as the mean ± SEM (n=6) for each diffusion cell compartment for both the CHG concentration (µg/cm^2) and for the percentage of dosed applied.*

Compartment (*n*=6)	CHG (µg/cm^2)		% of applied dose	
	Mean	SEM	Mean	SEM
Donor chamber	910.700	144.835	11.623	1.815
Skin wash	2738.010	419.365	34.888	5.305
Epidermis	775.857	283.070	9.853	3.594
Receptor fluid	6.574	1.899	0.083	0.024
Total recovered	4431.141	849.169	56.447	10.738

Table 6.5 Percutaneous absorption (mass balance) of CHG within porcine epidermis after a 24 h treatment with 1 mM-PAMAM dendrimer- CHG formulation in ethanol:water (50:50). *Data is represented as the mean ± SEM (n=6) for each diffusion cell compartment for both the CHG concentration (µg/cm^2) and for the percentage of dosed applied.*

Compartment (*n*=6)	CHG (µg/cm^2)		% of applied dose	
	Mean	SEM	Mean	SEM
Donor chamber	1123.050	431.425	14.333	5.505
Skin wash	3600.000	621.857	45.786	7.999
Epidermis	384.209	153.937	4.879	1.954
Receptor fluid	9.047	5.076	0.115	0.064
Total recovered	5116.306	1212.295	65.113	15.522

Table 6.6 Percutaneous absorption (mass balance) of CHG within porcine epidermis after a 24 h treatment with 10 mM-PAMAM dendrimer- CHG formulation in ethanol:water (50:50). *Data is represented as the mean ± SEM (n=6) for each diffusion cell compartment for both the CHG concentration (µg/cm^2) and for the percentage of dosed applied.*

Compartment (*n*=6)	CHG (µg/cm^2)		% of applied dose	
	Mean	SEM	Mean	SEM
Donor chamber	754.335	140.909	9.695	1.805
Skin wash	2980.024	266.673	37.800	3.487
Epidermis	621.711	98.818	7.895	1.255
Receptor fluid	17.980	2.407	0.228	0.030
Total recovered	4374.050	508.807	55.618	6.577

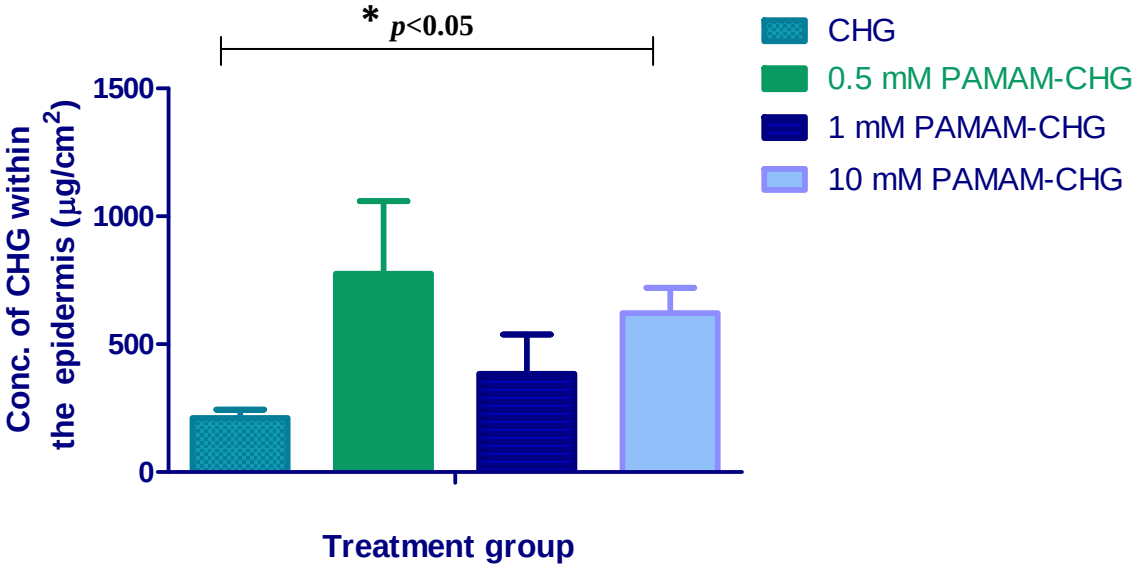

Figure 6.9. Total concentration of CHG within the epidermis (µg/cm^2) at 24 h after application of CHG alone, 0.5 mM, 1 mM and 10 mM PAMAM dendrimer with CHG in an ethanol: water vehicle (50:50). *Data is presented as the mean ± SEM (n=6). A Kruskal-Wallis test with an ad hoc Dunn's post test (histogram showed the data was non-parametric) derived that the medians between CHG and 10 mM-PAMAM-NH$_2$ –CHG formulations were statistically different from one another (p<0.05).*

The PAMAM dendrimer-CHG co-treatment did not result in a significant increase in the concentration of CHG that had permeated the epidermis into the receptor fluid at 24 h (Figure 6.10). Without the presence of PAMAM dendrimer a total concentration of 9.100 ± 2.087 µg/cm^2 of CHG was detected within the receptor fluid at 24 h compared to 6.574 ± 1.899, 9.047 ± 5.076 and 17.980 ± 2.407 for 0.5, 1 and 10 mM of G3-PAMAM-NH$_2$ respectively.

Application of the CHG in parallel to PAMAM dendrimer did not significantly enhance the permeation through the epidermis into the receptor fluid but did significantly increase the deposition of CHG within the epidermis for the 10 mM G3-PAMAM-NH$_2$-CHG co-treatment (p<0.05) (Figure 6.9). The total concentration of CHG increased within the receptor fluid at 24 h with increasing concentration of PAMAM dendrimer within the co-treatment. The total concentration of CHG within

the receptor fluid at 24 h for 10 mM-PAMAM-NH_2 dendrimer was ~2 x higher than for the CHG dosed without PAMAM dendrimer (Figure 6.10).

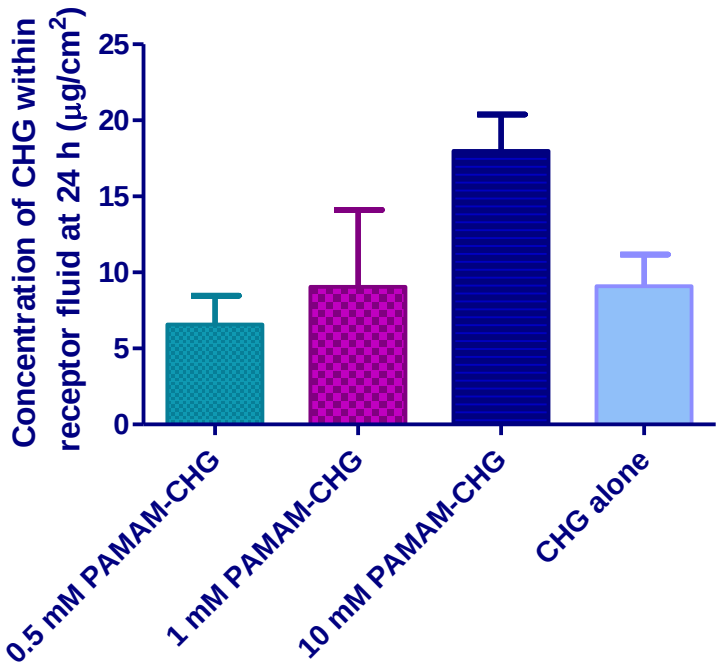

Figure 6.10. Total concentration of CHG absorbed within the receptor fluid (µg/cm^2) at 24 h after application of, 0.5, 1 and 10 mM PAMAM dendrimer and CHG alone. T*he dose preparation consisted of CHG in an ethanol:water vehicle (50:50) with the aforementioned PAMAM dendrimer concentrations. Data is presented as the mean ± SEM (n=6). No significant difference (p>0.05) was observed using a one-way ANOVA test (normally distributed data).*

6.2.9 Formulation Development and characterisation

After formulating an alcoholic hand gel, an ointment, a cream and a lotion it was decided that an alcohol hand gel would be the ideal formulation for a PAMAM dendrimer-CHG complex. Alcohol hand gels are antimicrobial, widely used clinically and the PAMAM dendrimer is likely to be more stable in an ethanolic solution (according to the manufacturer's specification). A range of alcohol gels were formulated (20 g in total). Each formulation was formulated in triplicate see below (Tables 6.7-9). No PAMAM dendrimer was added to the formulations in the

developmental stage until the formulations were optimised due to the high cost of the dendrimer.

Table 6.7 Weight of constituents of formulations F-F4 with alteration of the ethanol content of the formulation.

Constituent	Weight of constituent in formulation (F) in grams				
	F (60 % EtOH)	F1 (65 % EtOH)	F2 (70 % EtOH)	F3 (75 % EtOH)	F4 (80 % EtOH)
Ethanol (Absolute)	12	13	14	15	16
Hydroxy propyl cellulose (HPC)	1.6	1.6	1.6	1.6	1.6
Water (ultrapure)	4.4	3.4	2.4	1.4	0.4
Chlorhexidine digluconate	2	2	2	2	2

In appearance formulation F4 turned cloudy after 12 h at room temperature. It was observed that at concentrations above 75 % ethanol the CHG precipitates out therefore an optimal concentration of 70 % ethanol was chosen (Table 6.7).

Table 6.8 Weight of constituents of formulations F4(a) to F6(a) with the alteration of HPC content in formulation (mw of HPC was 100,000).

Constituent	Weight of constituent in formulation (F) in grams				
	F 4(a)	F5	F6*	F7*	F6a
Ethanol (Absolute)	14	14	14	14	14
Hydroxy propyl cellulose (HPC)	2	2.5	3.0	3.5	1.4
Water (ultrapure)	2	1.5	1	0.5	2.6
Chlorhexidine digluconate	2	2	2	2	2

*It was observed that formulation F6 and F7 turned opaque immediately (and the HPC had not dissolved after 24 h of shaking and 15 minutes of vigorous mixing on a mixer mill) and were discarded. F6a was formulated with a lower HPC concentration. The formulations were shaken overnight at 250 RPM to ensure the HPC had dissolved. Table 6.8 shows the range of different HPC compositions within the formulations.

Table 6.9. Weight of constituents of formulations F7 and F8 with the addition of glycerol

Constituent	Weight of constituent in formulation (F) in grams	
	F 7	F8
Ethanol (Absolute)	14	14
Hydroxy propyl cellulose	1.6	1.6
Water (ultrapure)	2.2	1.8
Chlorhexidine digluconate	2	2
Glycerol	0.2	0.6

Initial observations were that the formulations appeared stable (with the exception of the noted formulations), were all transparent in appearance and had a strong alcohol odour. In my personal experience when applied to the skin the formulations were easy to spread across the skin surface and were fully evaporated within 30-60 seconds of application. A thin, flexible and transparent film was left on the surface of the skin which was again non-irritating and water soluble (White, 1994). The film was formed due to an interaction between CHG and the HPC in which the CHG acts as a plasticiser. The control formulation which did not include CHG formed no film. The film formed with formulations 7 and 8 that included glycerol and remained tacky for a prolonged period of time possibly due

to the hygroscopic nature of the glycerol (Table 6.9). The formulations that contained dimethicone are not included as they were disregarded due to effervescing on addition to the formulation.

The formulations were characterised by the following parameters-

- Appearance
- Odour
- pH (1 in 10 dilution in ultrapure water)
- Available CHG (uniformity of CHG concentration)
- Spreadability diameters
- Antimicrobial affect (modified agar cup method)
- ATR-FTIR
- Viscosity profile

6.2.9.1 pH of formulations

To ensure that the formulations were compatible with the skin, the pH was determined for each formulation and can be found below in Table 6.10. All formulations were found to be within the neutral range. A general trend was observed where the pH decreased by 2.27 with increasing ethanol content (from 60-80 % ethanol) with formulations F-F4.

Table 6.10. Measured pH for the formulations after a 1 in 10 dilution in ultrapure water. *The results are presented as the mean ± SD (n=3).*

Formulation	Mean pH ± SD (*n*=3)
F	7.79 ± 0.02
F1	7.72 ± 0.03
F2	7.62 ± 0.07
F3	6.93 ± 0.07
F4	5.52 ± 0.14
F5	5.67 ± 0.06
F4(a)	7.04 ± 0.28
F6(a)	6.96 ± 0.01
F7	6.99± 0.07
F8	6.91 ± 0.07
Control no CHG (*n*=1)	7.04
Control no HPC (*n*=1)	6.93

6.2.9.2 Spreadability of formulations

The spreadability of the gel formulations were determined by measuring the spread diameter under set conditions for each formulation (Table 6.11). The highest mean diameter corresponded to the formulation with the lowest HPC content (Formulation F6(a)). Formulation 4 and formulation 3 had the highest ethanol content and therefore resulted in the second and third highest mean spreadability diameters, respectively, after formulation 6(a) that consisted of the lowest HPC polymer concentration. All formulations with Φ >70 mm are classified as fluid gels. Formulation 4a and formulation 5 have a mean of 70 $\geq$ Φ > 55 mm and are therefore considered to be semi-fluid gels. This was anticipated as these two formulations contained the highest HPC content and was therefore more viscous resulting in a lower spreadability diameter. The addition of glycerol within formulation 7 (mean diameter of 83.17 ± 1.17 mm) and formulation 8 (mean diameter of 81.00 ± 2.79 mm) significantly increased the spreadability diameter

when compared to formulation 2 (mean diameter 76.17 ± 1.02) that had the same composition minus the glycerol (p<0.05). A one way ANOVA confirmed that the spreadability diameters were different as a function of altering the ethanol and HPC content as well as the inclusion of glycerol (F=72.20, d=65, 345.7 p<0.05). Intracomparisons were made by conducting a Tukey's multiple comparison test. There was no significant difference between formulations 4(a), 6(a) and 7 when compared to the commercially available alcohol gel 'Safemate original' (p>0.05). Based on a subjective personal experience the 'Safemate original' and formulations with a comparable spreadability (formulations 4(a), 6(a) and 7) were possibly the least favourable in terms of skin application as a lack of viscosity resulted in the formulation running from the site of application. All of the formulations tested however resulted in excellent skin coverage due to an agreeable spreadability capacity.

Table 6.11. Displays the calculated spreadability diameter of the formulations after application of a known weight and time period. *The spreadability diameter was calculated from a mean ± SEM (n=3).*

Formulation	Diameter ↕ (mm)	Mean ± SEM ↕ (mm)	Diameter ↔ (mm)	Mean ± SEM ↔ (mm)	Total mean ± SEM (mm)
Fa	69	73.33 ± 2.19	71	72.67 ± 0.88	73.00 ± 1.53
Fb	76		74		
Fc	75		73		
F1a	76	76.67 ± 0.67	79	77.67 ± 1.33	77.17 ± 1.00
F1b	78		79		
F1c	76		75		
F2a	75	75.33 ± 0.88	77	77.00 ± 1.16	76.17 ± 1.02
F2b	77		79		
F2c	74		75		
F3a	84	82.33 ± 1.20	87	85.00 ± 1.00	83.67 ± 1.10
F3b	80		84		
F3c	83		84		
F4a	86	84.67 ± 0.67	89	86.67 ± 1.20	85.67 ± 0.94
F4b	84		86		
F4c	84		85		
F4(a)a	70	70.00 ± 0.58	68	69.33 ± 0.88	69.67 ± 0.73
F4(a)b	71		71		
F4(a)c	69		69		
F5a	65	63.33 ± 0.88	63	63.67 ± 1.33	63.50 ± 1.11
F5b	65		64		
F5c	61		63		
F6(a)a	90	89.00 ± 0.58	90	89.67 ± 0.33	89.34 ± 0.46
F6(a)b	89		89		
F6(a)c	88		90		
F7a	83	82.67 ± 0.88	81	83.67 ± 1.45	83.17 ± 1.17
F7b	81		84		
F7c	84		86		
F8a	83	79.67 ± 2.40	85	82.33 ± 3.18	81.00 ± 2.79
F8b	81		86		
F8c	75		76		
control no CHG a	81	81.67 ± 0.67	82	82.33 ± 0.88	82.00 ± 0.78
b	83		81		
c	81		84		
'Safemate' a	89	87.67 ± 0.67	90	90.33 ± 0.88	89.00 ± 0.77
b	87		92		
c	87		89		

6.2.9.3 Concentration of available CHG within formulation (CHG concentration and uniformity).

The available CHG concentration within the formulation was determined (Table 6.12). After extraction of CHG from 1 g of each formulation it was established that there was a consistent loss of ~14 % of CHG. The loss in CHG was not due to the interaction with HPC but perhaps due to adsorption of CHG to the glass of the volumetric flasks. CHG strongly binds to glass resulting in loss of the biocide (Denton, 1991). Future work should ideally utilise silanized glassware to reduce the amount of CHG adsorbed onto glass surfaces (Musial *et al.* 2012). The control formulation without addition of HPC to the formulation resulted in a 5.52 ± 0.51 % loss of CHG.

Table 6.12. Recovered CHG from formulations after dissolving 1 g of each formulation in ultra-pure water. *The results are displayed as the mean CHG concentration extracted ± standard deviation (n=3).*

Formulation	Extracted CHG from formulation (µg/mL)	Percentage recovery (%)
F	16847.06 ± 138.8	84.24 ± 0.69
F1	17099.58 ± 267.1	85.49 ± 1.35
F2	16819.11 ± 98.92	84.10 ± 0.50
F3	17193.22 ± 496.5	85.97 ± 2.58
F4	17665.84 ± 313.9	88.32 ± 1.57
F5	17660.25 ± 232.6	88.30 ± 1.16
F4(a)	17477.11 ± 67.5	87.39 ± 0.34
F6	17067.31 ± 547.8	85.34 ± 0.43
F7	17679.57 ± 412.2	88.39 ± 2.06
F8	18359.52 ± 844.3	91.79 ± 4.22
Control no CHG (*n*=1)	0	0
Control no HPC	18897.87 ± 101.5	94.48 ± 0.51

6.2.9.4 Viscosity of formulations

All formulations exhibited non Newtonian behaviour; a typical example is illustrated in Table 6.13 and Figure 6.11 corresponding to formulation F (a-c). Shear thinning was observed as the viscosity decreased with increasing RPM. Figure 6.11 shows a plot of the viscosity (m.Pas) against the RPM. A hysteresis was observed however it is not indicative of thixotropy but is due to the variability observed between the replicate formulations as the error bars (SEM) overlap. Despite measuring the viscosity under experimental conditions (temperature 19 ± 1°C) variability was observed between replicate formulations. The rate of evaporation over a 10-15 minute period (an approximate time to conduct the viscosity analysis) was minimal (<0.1 % loss in weight of the formulation). This may have contributed to the variability observed however the effect would likely be negligible.

Table 6.13. Measured torque for increasing and then decreasing shear rates for formulation F(a-c). *The data is presented as the mean ± SEM (n=3).*

RPM	Viscosity (mPas) Mean (*n*=3)	SEM
2	1550.000	102.632
2.5	1510.000	104.083
3	1466.667	96.148
4	1373.000	120.000
5	1378.000	76.000
6	1366.667	73.277
10	1344.000	68.235
12	1312.000	63.319
12	1313.667	61.431
10	1318.000	61.830
6	1348.333	70.848
5	1362.000	77.149
4	1427.667	98.930
3	1513.333	97.696
2.5	1583.333	69.841
2	1586.667	113.186

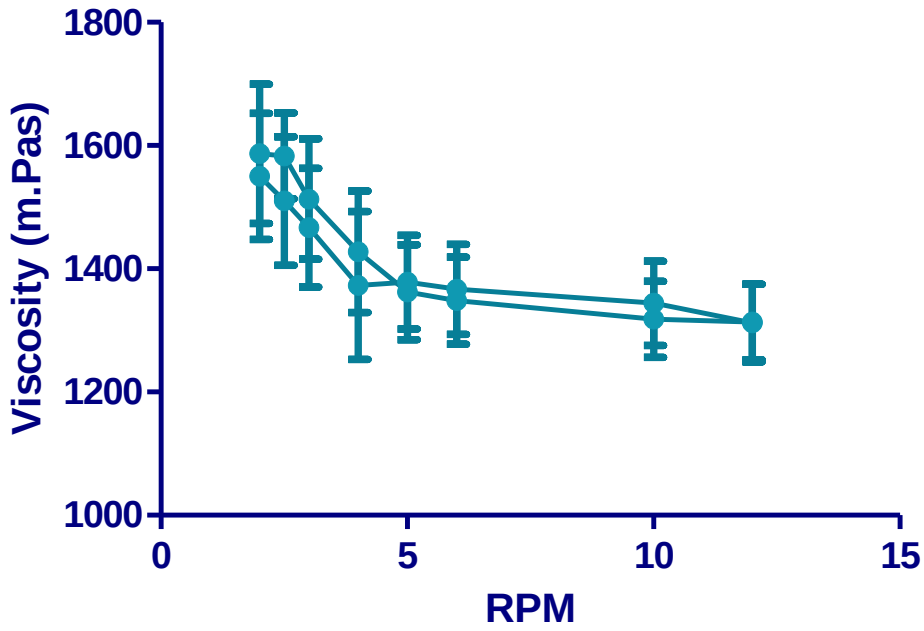

Figure 6.11. RPM plotted with the viscosity (m.Pas) for formulation F illustrating non Newtonian behaviour. *Data is represented as the mean ± SEM (n=3).*

6.2.9.5 Antimicrobial efficacy of formulations.

It was necessary to determine whether CHG still exhibited antimicrobial characteristics after interaction with HPC within the formulations. A modified agar cup method was conducted and established that the formulations did possess antimicrobial properties. Figure 6.12 is a photograph taken of a typical agar plate after formulation F (*n*=3) was challenged against *P*. *aeruginosa.* A large inhibition zone (halo effect) can be observed whereby the CHG had diffused through the agar until a sub-lethal concentration was achieved. That is the point where *P. aeruginosa* persists. In parallel with the formulations 'Safemate' original sanitising gel was also tested using the same method; Safemate was the hand sanitiser used after an antimicrobial hand wash in the microbiology laboratory. The inhibitory zones were measured with a ruler (accuracy ± 0.5 mm) and recorded in

Table 6.14 for each formulation against three opportunistic human pathogens; *S. aureus, E. coli* and *P. aeruginosa*.

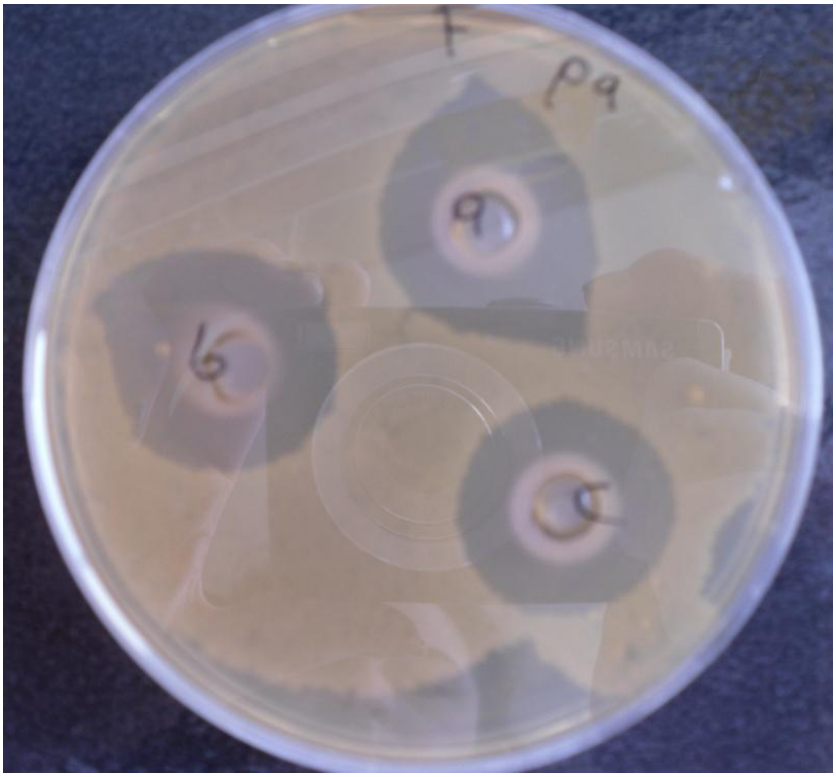

Figure 6.12. Photograph of an agar plate (cationic adjusted Mueller Hinton agar) illustrating formulation F challenged against *P. aeruginosa* using a modified agar cup method. *The diameter of the zone of inhibition was measured and the results of all formulations tested can be observed in Table 6.14.*

Table 6.14 displays the zones of inhibition that is evidence for CHG still retaining antimicrobial efficacy despite the interaction of CHG with HPC to act as a plasticizer. All formulations exhibited antimicrobial activity against all three pathogens. The control formulation that did not contain CHG did not show any antimicrobial activity. Further, a solution of 75 % ethanol and 'Safemate' that contains 62 % ethanol also did not result in a zone of inhibition for any of the bacteria tested. Formulation F2 (70 % ethanol) was the most effective antimicrobial formulation across all three bacteria (mean 30.3 ± 1.06 mm inhibition

zone across all three bacteria *n*=18), however there was no observable trend between the formulation composition and antimicrobial efficacy.

Table 6.14. Diffusion zone of formulations challenged against the Gram negative *E. coli* and *P. aeruginosa* and the Gram positive *S. aureus*. *The semi-quantitative results are presented as mean ± SD (n=6).*

	Zone of inhibition mm (mean ± SD, *n*=6)		
Formulation	*Escherichia coli*	*Staphylococcus aureus*	*Pseudomonas aeruginosa*
F	24.50 ± 0.87	25.00 ± 0.87	23.83 ± 0.60
F1	24.00 ± 0.87	24.17 ± 0.33	24.33 ± 1.67
F2	28.50 ± 2.29	29.00 ± 0.16	33.33 ± 0.73
F3	19.33 ± 3.01	26.33 ± 1.59	20.00 ± 2.29
F4	19.00 ± 1.32	27.33 ± 0.67	20.17 ± 0.88
F5	20.50 ± 1.80	20.67 ± 0.17	24.17 ± 0.60
F4(a)	25.17 ± 0.76	20.50 ± 0.76	21.34 ± 0.72
F6	31.00 ± 1.32	26.33 ± 0.44	23.50 ± 0.58
F7	24.17 ± 0.76	26.17 ± 1.36	22.17 ± 0.17
F8	22.50 ± 1.73	25.17 ± 0.60	23.00 ± 0.50
Control- no CHG	0	0	0
Control-75 % EtOH	0	0	0
Safemate alcohol hand gel	0	0	0

6.2.9.6 ATR-FTIR of formulations

ATR-FTIR analysis was conducted to visualize the interactions between CHG and HPC within the formulations. There are differences between the free drug (Figure 6.13 (a)) and the formulation (F used as an example) Figure 6.13 (b). Peaks corresponding to the C-H and C-O stretch of ethanol can be observed on the spectra. Peaks corresponding to CHG shift when the CHG is formulated in ethanol with HPC for example the C=N stretch peak for free CHG is found at 1633 cm^{-1} but in the formulation after interaction with HPC the C=N peak shifts to 1647 cm^{-1} (Shafiullah, 2005). The vibrational modes of the chlorophenyl group can

be observed at 1492-1533 cm^{-1} in Figure 6.13 (a) (Suci *et al.* 2001) but these peaks change when the CHG is added within the formulation with HPC and a peak at 1380 cm^{-1} is apparent. Figure 6.13 (b) also shows additional peaks corresponding to the (aliphatic) C-H stretch for HPC and ethanol at 2975 and 2896 cm^{-1}. Further, C-H bending due to the aromatic ring on CHG can be observed at 878 cm^{-1} within the formulation that is not present in the CHG alone spectrum. The minor peak shifts observed in the spectra in Figure 6.13 indicate an interaction between CHG and HPC in the presence of ethanol and water. The range of formulations were very similar when the spectra were overlaid therefore no differences were observed in the spectra between formulations.

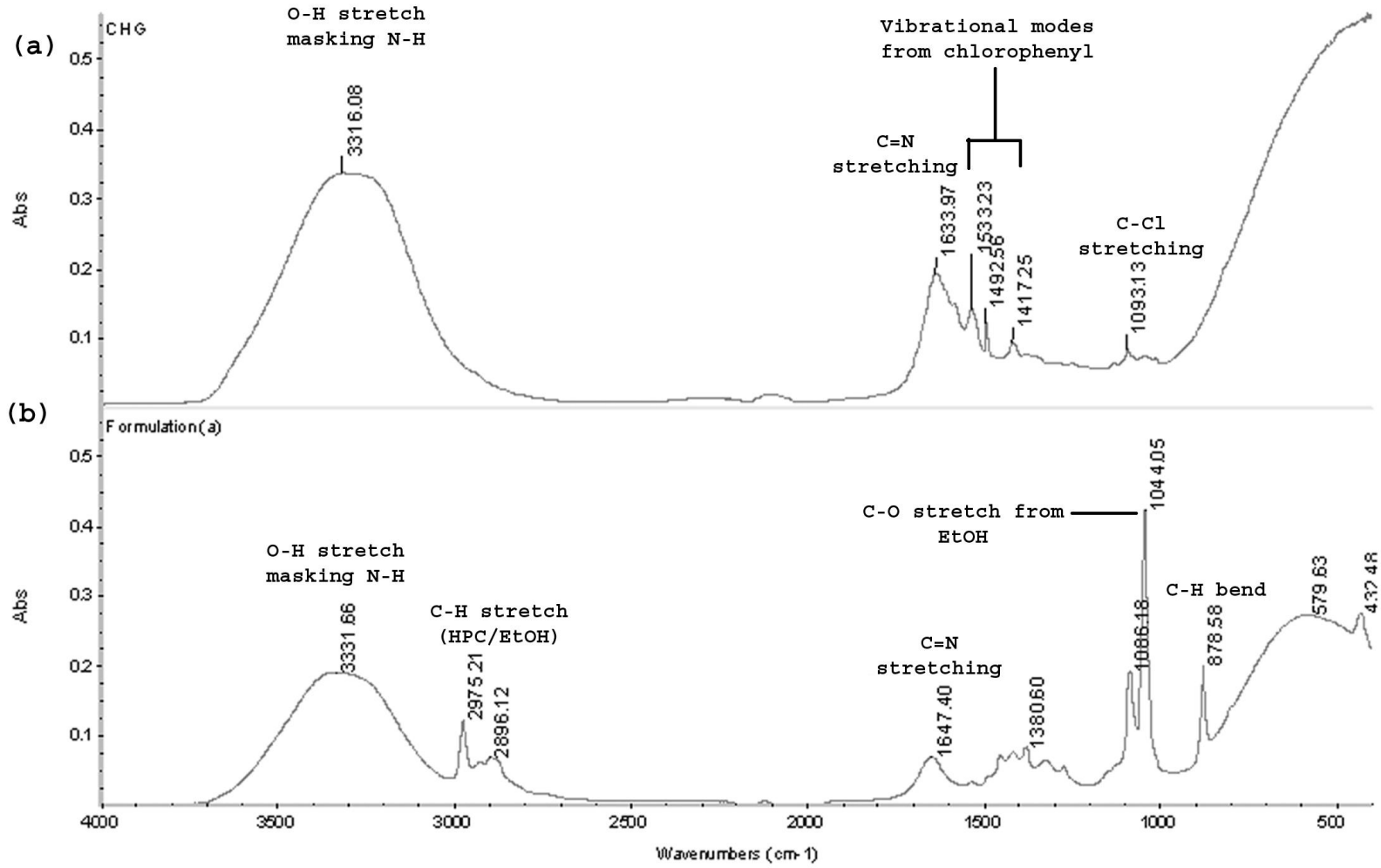

Figure 6.13. ATR-FTIR spectra of (a) a CHG (2 % w/v) solution and (b) Formulation a. *The spectra were collected as a result of 32 scans resulting in a resolution of 8 cm^{-1}.*

6.2.9.7 Percutaneous absorption of chlorhexidine digluconate from selected formulations determined by tape stripping dermatomed porcine skin after 24 h

The permeation of CHG within porcine dermatomed skin was determined from the formulations F4, F5 and F6 (Tables 6.15, 6.16 and 6.17). Previously within this chapter it was observed that the CHG interacts with HPC to form a plasticizer that results in film formation after solvent evaporation. It was of interest to the project to characterise the penetration of CHG into the skin from the film formed across the skin surface. Across all three formulations tested, no CHG was detected within the 21 tape strips removed from the SC or the remaining epidermis/dermis. It was observed that after 6 h the solvents had evaporated leaving a film across the skin. At 24 h it was attempted to remove the film by washing the skin surface however hydration caused the film to become tacky and removal by water was not sufficient. The films were then carefully removed from the skin surface at 24 h using tweezers and the CHG was extracted from the film. The highest concentration of CHG was recovered from the washed films. The concentrations within the film were; 3110.062 ± 347.9 µg/cm^2 for F4, 3561.948 ± 278.4 µg/cm^2 for F5 and 3200.972 ± 298.4 µg/cm^2 for F6. These concentrations are equivalent to ~ 40 % of the applied CHG dose.

A high concentration of CHG was extracted from the glass donor chambers. The mean concentration across the three formulations was 2589.71 ± 167.45 µg/cm^2 that is equivalent to around 33 % of the applied dose of CHG. This can be accounted for as it was observed that on deconstruction of the Franz cell a proportion of the film was removed with the donor chamber. Attempts were made

to recover the film from the donor chamber however this was not achieved due to the strong adhesion of the film to the glass. In previous studies conducted in chapter 3 (section 3.3.0 and 3.3.1) the highest concentration of CHG was recovered within the 24 skin wash. With regards to this study, only low concentrations of CHG was recovered within the 24 h skin wash with an average percentage of applied dose recovered of 6.03 ± 1.63 %. The mass recovery of CHG was consistent with the CHG concentrations recovered from the formulations under occluded conditions in section 6.2.6.

Table 6.15 Concentration of CHG extracted from the different compartments of the *in vitro* diffusion cell after dosing with formulation 4 for 24 h. *Data is represented as the mean ± SEM (n=5) for each diffusion cell compartment for both the CHG concentration (µg/cm^2) and for the percentage of dose applied.*

Formulation F4 (*n*=5)	CHG (µg/cm^2) Mean	CHG (µg/cm^2) SEM	% of applied dose Mean	% of applied dose SEM
Donor chamber	2603.558	211.921	33.065	2.691
Skin wash	355.3078	58.090	4.512	0.738
Film	3110.062	347.901	39.498	4.418
Epidermis & tape strips	<LOQ*	<LOQ	<LOQ	<LOQ
Receptor fluid	<LOQ	<LOQ	<LOQ	<LOQ
Total recovered	6068.928	617.912	77.075	7.847

Limit of quantification calculated from HPLC validation data found in appendix 1 using the equation 10(STD/slope of line). LOQ was calculated to be 0.168 µg/mL.

Table 6.16 Concentration of CHG extracted from the different compartments of the *in vitro* diffusion cell after dosing with formulation 5 for 24 h. *Data is represented as the mean ± SEM (n=5) for each diffusion cell compartment for both the CHG concentration (µg/cm^2) and for the percentage of dose applied.*

Formulation F5 (*n*=5)	CHG (µg/cm^2)		% of applied dose	
	Mean	SEM	Mean	SEM
Donor chamber	2560.291	101.621	32.516	1.290
Skin wash	714.382	473.923	9.073	6.019
Film	3561.948	278.400	45.237	3.536
Epidermis & tape strips	<LOQ	<LOQ	<LOQ	<LOQ
Receptor fluid	<LOQ	<LOQ	<LOQ	<LOQ
Total recovered	6836.621	853.944	86.826	10.845

Table 6.17 Concentration of CHG extracted from the different compartments of the *in vitro* diffusion cell after dosing with formulation 6 for 24 h. *Data is represented as the mean ± SEM (n=5) for each diffusion cell compartment for both the CHG concentration (µg/cm^2) and for the percentage of dose applied.*

Formulation F6 (*n*=5)	CHG (µg/cm^2)		% of applied dose	
	Mean	SEM	Mean	SEM
Donor chamber	2604.653	188.801	33.079	3.790
Skin wash	353.456	47.823	4.489	0.607
Film	3200.972	298.410	40.652	2.398
Epidermis and tape strips	<LOQ	<LOQ	<LOQ	<LOQ
Receptor fluid	<LOQ	<LOQ	<LOQ	<LOQ
Total recovered	6159.081	535.034	78.22	6.795

6.3 Discussion

On addition of the PAMAM dendrimer to CHG a crystalline material formed in aqueous solution. Different crystalline shapes and particle sizes confer different physiochemical properties which can in turn effect the bioavailability of drugs (Khankari and Grant, 1995). Crystallisation of the drug is also important in terms of stability of any formulation. It is of paramount importance that the crystal structures are fully characterised to not only understand the interaction between CHG and the PAMAM dendrimer but to also understand the differences in crystal structures formed and any possible effects on the bioavailability of the drug. Co-crystals of water-drug molecules within an aqueous environment are important in determining the stability of such hydrate crystal systems (Han, 2006). The crystals formed in the hydro-methanolic solution on the addition of the CHG solution.

Two different crystal structures were observed depending on the order of addition of the CHG, G3-PAMAM-NH_2 dendrimer (in methanol) and the water (Figures 6.2 and 6.3). Previously it has been shown that the water activity (energy status of water within a system) is very important in the formation of such drug crystals in an organic solvent and water mixture. The organic solvent and the water mixture compositions affect the physical stability of the drug crystalline phases. It has been shown to affect the nature of the crystallising drug phase for drugs such as theophylline (Zhu *et al.* 1996) and ampicillin (Zhu and Grant, 1996). As such the composition of the organic solvent and water mixtures are likely to affect the crystallisation of CHG and may account for the differences observed in Figures 6.2 and 6.3. Longer shards of microcrystalline material formed after there was an initial excess of water whereas shorter shards radiating form a focal point

occurred as the PAMAM dendrimer was added to CHG in a reduced volume of water before the addition of water up to full volume.

The aqueous solubility (% w/w) of CHG is >70 % (Farkas *et al.* 2001). It is also soluble in alcohol(s), however the addition of CHG to neat alcohol(s) will result in precipitation (Denton, 1991). The CHG was not added to neat alcohol as the water was added to the dendrimer in methanol in the first instance before the addition of CHG. CHG is soluble in water and methanol solutions. The control co-formulation without the addition of PAMAM dendrimer did not form a crystalline material. The crystal formation was therefore attributed to the addition of the G3-PAMAM-NH_2 dendrimer and crystal formation occurred at a range of dendrimer concentrations (0.5- 10 mM). Figures 6.2 and 6.3 are micrographs illustrating the differences in crystal shape and size after addition of the CHG in a differing order. The length of the crystals was measured and the crystals formed in Figure 6.2 were on average 4.5 times longer than those formed in Figure 6.3. The crystals formed were fully characterised. The melting points were obtained from vacuum-dried crystalline material and were both determined to be between 109-115 °C; CHX has a melting point between 132-136 °C (Lam *et al.* 1993). CHG does not exist as a solid but as a viscous liquid therefore the melting point data may suggest that the precipitate is not just a case of the CHX base having precipitated out of solution.

A vacuum-dried sample of the crystalline precipitate and G3-PAMAM-NH_2 dendrimer reference material was sent to the EPSRC National Mass Spectrometry Centre for MALDI-ToF analysis to determine the molecular weight of the samples. Figures 6.4 and 6.5 show the resulting spectra and it was determined that the

vacuum-dried sample was a mixture. It is possible that the G3-PAMAM-NH_2 dendrimer in solution was dried *in vacuo* conditions onto the precipitate resulting in a mixture of CHX and dendrimer. The theoretical molecular weight of G3-PAMAM-NH_2 dendrimer is 6909 Da but the spectra shows that the molecular weight determined was 6940 Da for the reference material and 6938 Da for the CHG-PAMAM mixture. The mass resolution of the system was ± 2 Da which may account for the discrepancy between the two spectra. The observed species that are higher in mass than the theoretical mass may be $[PAMAM+K]^+$ or possibly $[PAMAM+Na]^+$ which are a result of ionisation of salt impurities within the sample or they may be a result of a minor structural defect within the dendrimer (Peterson *et al.* 2003).

The MALDI-ToF spectra indicating a mixture was sent for analysis therefore in order to determine the actual composition of the crystalline material it was sent for single crystal X-Ray diffraction analysis. The crystalline material was sent in aqueous solution to the EPSRC National Crystallography Centre that was in turn forwarded the sample to the Diamond beam line in Oxford. Table 6.1 and Figure 6.6 exhibit the crystal data and structure respectively. The XRD data clearly shows the chlorhexidine structure which is associated with four water molecules and an oxocarbon anion with a calculated molecular weight of 639.55 Da. The molecular weight of the dosed CHG within the formulation was 897.8 Da, on removal of the oxocarbon anion and the water molecule's molecular weight the resulting molecular weight is 507 Da that corresponds to the CHX base with two nitrogen positions protonated. The XRD data shows that the digluconic acid is missing from the structure and in its place are four water molecules and an oxocarbon anion. It is possible that the polycationic PAMAM dendrimer had scavenged the gluconic

acid resulting in precipitation of the CHX base due to a lack of solubility in aqueous solution (solubility; 0.008 % w/v in water, Farkas *et al.* 2001). The crystalline precipitate may have occurred due to the oxocarbon anion (the counter ion) forming a salt through an anion exchange group such as –NHR- present on the CHX structure (Yoshimura, 2011). Further, another reason could be that the pH was too high and that the counter ion-CHX base had precipitated out. The pH of the G3-PAMAM-NH_2-CHG co-formulation was ~ pH 9 as analysed by a standard pH universal indicator test strip. It has previously been reported that the CHX base can precipitate out in high pH conditions i.e. > pH 8 (Denton, 2000).

The results within this chapter have shown that a PAMAM dendrimer-CHG complex does not form in aqueous solution but that the CHX loses its gluconic acid salt, possibly through interaction with the polycationic PAMAM dendrimer or possibly due to the high pH. No precipitate formed when the CHG was added to the PAMAM dendrimer in ethanol, methanol or isopropanol. This is interesting as the CHX free base is also practically insoluble in alcohols (Modak and Sampath, 2007). This result may question the proposed idea that the PAMAM dendrimer scavenged the gluconic acid from the CHG as that would likely have occurred in an alcoholic solution also. Previously, to graft gluconic acid to a G3-PAMAM-NH_2 dendrimer a coupling agent (1-ethyl-3-(dimethylaminopropyl)carbodiimide) was required in conjunction with an activating agent (*N*-Hydroxysuccinimide). The coupling reaction was then left overnight in a sonicator to activate the condensation reaction (Tao *et al.* 2013). The coupling agents are required as the condensation reaction between a carboxylic acid such as that of gluconic acid and an amine group such as that on the PAMAM dendrimer surface is a very slow reaction. This suggests that the interaction demonstrated in Sections 6.2.1-6.2.5 is

likely to be an electrostatic interaction between the amine groups of the PAMAM dendrimer and the carboxyl group of the gluconic acid.The presence of an oxocarbon anion may indicate an interaction between the gluconic acid of CHG with the PAMAM dendrimer. The carbonate anion $(CO_3)^{2-}$ detected within the crystal structure using XRD is due to the removal of all protons from a corresponding acid carbonic acid (Moore and Khanna, 1991) that was possibly provided by the gluconic acid (Figure 6.14).

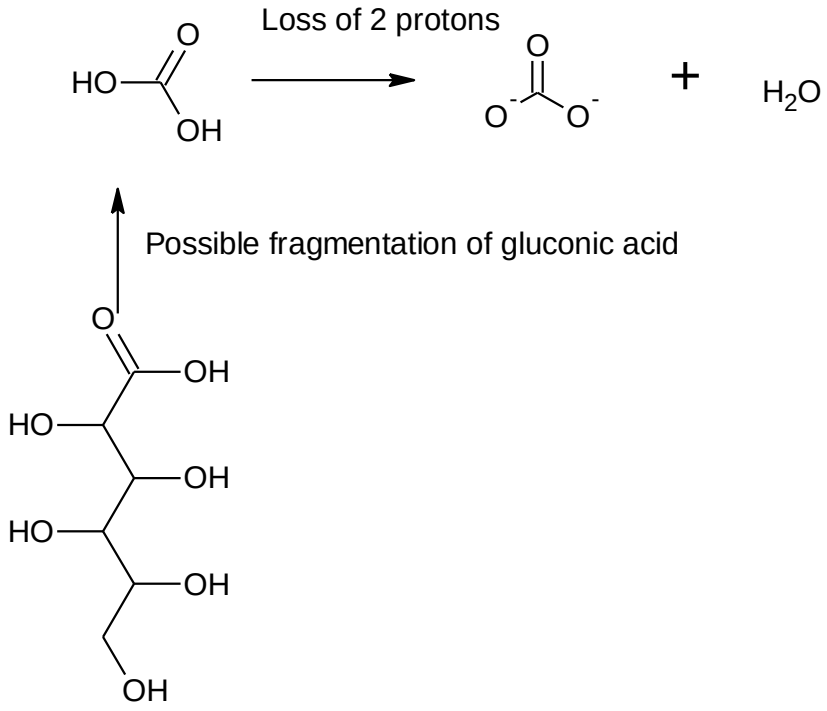

Figure 6.14 A possible schematic for the formation of the oxocarbon anion detected within the single molecule crystal using XRD analysis.

There was an electrostatic interaction between the carbon anion and the protonated nitrogen next to the 4-chlorophenyl due to the electron withdrawal characteristic of this moiety. Four water molecules were also detected within the crystal that was hydrogen bonded to the electron dense 4-chlorophenyl moiety. The electrostatic potential of CHX can be observed in Figure 6.15. The red areas

correspond to the delocalised positive charge of the amine groups on the biguanide structure and the blue regions correspond to the electron dense chlorophenyl moieties (Blackburn *et al.* 2007). Though only one molecule of CHX was presented it is likely that the crystal structure is a repetitive pattern of CHX with carbonate anions associated with any of the red areas corresponding to the amines of the biguanide structure and water molecules that have hydrogen bonded to the blue electron dense chlorophenyl groups.

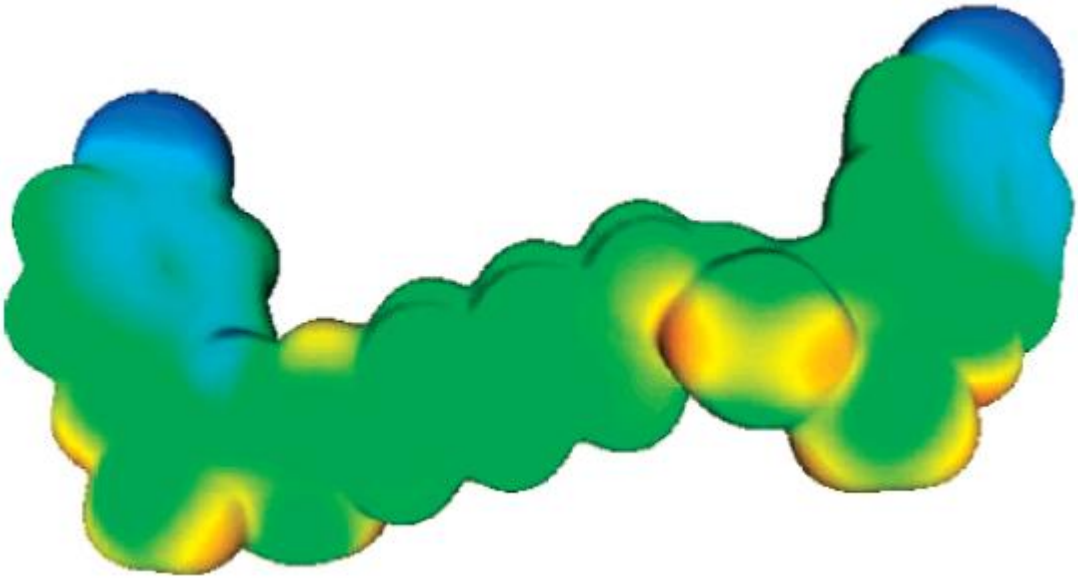

Figure 6.15 Image showing the electrostatic potential plotted on an electrostatic density image of CHX. *The structure is represented as space occupied by the Van Der Waals radius of the molecule. Green corresponds to neutral, blue corresponds to the strongest negative electrostatic potential and red corresponds to the strongest positive electrostatic potential. Taken from Blackburn et al. (2007).*

In an ethanol-water solution no precipitate was formed on addition of PAMAM dendrimer to CHG. No precipitate was formed for 3 months within a 50:50 water: ethanol vehicle, therefore this was the chosen vehicle for the co-dose application. The recovery of CHG was determined for a variety of PAMAM dendrimer concentrations under occluded and unoccluded conditions (Table 6.2). At a skin surface temperature of 32°C ± 1°C under occluded conditions the

recovery of CHG was comparable to that of the control where PAMAM dendrimer was absent (~10-20 % loss of CHG). The ~15 % loss of the dosed CHG in the control solution without the PAMAM dendrimer (in occluded conditions) may be due to degradation of the compound in light at 32°C ± 1°C. It is unlikely that such a high loss of CHG would occur solely from adsorption on to the glass surface of the vial. The lowest percentage recovery of CHG was at the higher 10 mM PAMAM dendrimer concentration, but it was observed that the formulation had turned a pearlescent white colour indicating precipitation of a constituent. Perhaps the semi-solid formulation appeared pearlescent due to the dispersion of particles of the incompatible polymer (excess G3-PAMAM-NH_2 dendrimer) (Lu, 1986).

Under unoccluded conditions a low recovery of CHG was achieved for the control corresponding to 2 % CHG (w/v) in an ethanol: water (50:50) vehicle. Only 34.44 ± 3.33 % of the dosed CHG was recovered at 24 h which was likely due to evaporation of the vehicle at 32°C ± 1°C resulting in precipitation of CHG. Under unoccluded conditions a higher concentration of CHG was recovered from the CHG-PAMAM dendrimer formulations than from the control without the addition of PAMAM dendrimer. For example, the addition of 0.5 mM PAMAM dendrimer to 2 % CHG (w/v) significantly enhanced (p<0.05) the percentage recovery of dosed CHG by ~25 % (Figure 6.7). The extremely hygroscopic PAMAM dendrimer possibly extracted atmospheric moisture allowing a higher concentration of CHG to be dissolved within the hydrated PAMAM dendrimer layer rather than precipitate into an insoluble salt or the CHX base.

It was established that the interaction between CHG and G3-PAMAM-NH_2 dendrimer did not have synergistic nor antagonistic effects on the antimicrobial

efficacy of CHG. The calculated IC_{50} against *S. aureus* for the CHG-PAMAM dendrimer was only 0.001 µg/mL higher than for the calculated IC_{50} for CHG in the same water: ethanol (50: 50) vehicle. Therefore the PAMAM dendrimer does not inhibit or enhance the antimicrobial efficacy of CHG in a co-formulation. The PAMAM dendrimer did not enhance the antimicrobial efficacy of CHG because the IC_{50} of CHG (0.056 µg/mL, 95 % CI: 0.02582-0.1212 µg/mL against *S. aureus*) is much lower than the IC_{50} of G3-PAMAM-NH_2 dendrimer (9.374 µg/mL 95 % CI: 7.88-11.15 µg/mL against *S. aureus* within an ethanol:water vehicle). PAMAM dendrimers have been observed to enhance the antimicrobial efficacy of silver sulfadiazine (Strydom *et al.* 2012). This may be due to the biocide having a much higher IC_{50} than the PAMAM dendrimer; silver sulfadiazine was shown to have an IC_{50} of 85 µg/mL against *S. aureus* (Maple *et al.* 1992). Thus after the addition of the PAMAM dendrimer, that has a calculated IC_{50} of 9.374 µg/mL (see Section 2.2.1), to the silver sulfadiazine it is not unexpected that the dendrimer would enhance the antimicrobial efficacy.

The co-formulation was applied to porcine skin to determine whether the PAMAM dendrimer would still act as a permeation enhancer of CHG when applied in a one-step application as opposed to a skin pre-treatment. Previously in Section 6.2.6 it was shown that G3-PAMAM-NH_2 enhanced the recovery of CHG under unoccluded conditions. This was also observed after the co-dose formulation had been applied to porcine skin *in vitro* for 24 h, though there was still a 37- 45 % loss of CHG across all 3 PAMAM dendrimer concentrations. Without the presence of PAMAM dendrimer there was ~49 % of the dosed CHG that was not recovered. This is very low compared to the ~75-85 % of dosed CHG recovered after a PAMAM dendrimer pre-treatment in sections 3.3.0 and 3.3.1 The low percentage

recovery of CHG may be due to a number of reasons; there is the possibility that an increase in the permeation of CHG occurred within the epidermis due to the penetration enhancement effects of the ethanolic vehicle and possibly due to the action of the PAMAM dendrimer. The extraction procedure may not have been effective in extracting CHG from the deeper layers of the porcine epidermis therefore resulting in a reduction of CHG recovery and an underestimate of the CHG concentration within the epidermis. Another possibility for the loss of CHG could be that once the ethanol: water vehicle had evaporated, the interaction of CHG with the PAMAM dendrimer in aqueous solution caused the loss of the digluconic acid from the CHG resulting in the insoluble crystalline precipitate of oxocarbon anion associated with the CHX base (Figure 4.16). This precipitate would therefore be syringe filtered out and discarded before HPLC analysis resulting in a high loss of applied CHG. This is also consistent with the recovery values observed in Table 6.2 where the available CHG (after addition of PAMAM dendrimer in unoccluded conditions) was found to approximately half the dosed CHG concentration. It should be noted however that ~1 % CHG solution (w/v) does still exhibit strong antimicrobial effects.

The one-step co-application did result in an increase in the concentration of CHG within the skin for 0.5 and 10 mM G3-PAMAM-NH_2 dendrimer (Figure 6.9). A 10 mM PAMAM dendrimer co-treatment with CHG resulted ~3 fold increase of CHG within the epidermis that was statistically significant when compared to CHG dosed alone (p<0.05). A high variability was observed for the 0.5 and 1 mM PAMAM dendrimer-CHG formulations. This may be due to the inherent variability between the two porcine donor skins utilised within the study. Another possible explanation for the high variability may be due to the vehicle evaporating from the

skin at different rates (forming an unstable saturated solution) therefore leaving the CHG and PAMAM dendrimer to form an insoluble salt at different time points.

Speculatively, perhaps the significant increase (p<0.05) of CHG within the epidermis after a 10 mM G3-PAMAM-NH_2- CHG co-application was due to the PAMAM dendrimer acting as an anti-nucleant polymer. It is possible that the 10 mM PAMAM dendrimer solution retarded the formation of crystal growth for longer as the vehicle evaporated from the skin. This would allow a prolonged time frame for the CHG to permeate the skin compared to CHG dosed alone from an ethanolic vehicle before the saturated solution becomes unstable. Perhaps the saturated solution (caused by evaporation or skin absorption of the ethanolic vehicle), which the 10 mM PAMAM dendrimer solution prolonged the stability of, enhanced the flux of CHG into the skin due to the formulation possessing a high thermodynamic activity (Kemken *et al.* 1992). This has been observed previously for piroxicam in supersaturated solutions whereby HPC prevented the formation of pseudopolymorphs such as the hydrate form of the drug that is less stable than the anhydrous form in aqueous solution. The addition of the HPC within the saturated solutions was shown to enhance the drug's flux concentrations *in vitro* using excised human skin as a membrane (Pellet *et al.* 1997).

A concentration increase of 564.487 µg/cm^2 of CHG within the skin was recorded for the 0.5 mM G3-PAMAM-NH_2 dendrimer-CHG formulation when compared to the CHG dosed alone. This however was not statistically significant due to the high variability observed between each of the diffusion cells as previously mentioned. There was no significant increase in the concentration of CHG after a co-treatment with PAMAM dendrimer within the receptor fluid at 24 h

when compared to the control (Figure 6.10). The 10 mM-PAMAM-NH_2 –CHG formulation resulted in the highest CHG concentration within the receptor fluid at 24 h (17.980 ± 2.407 µg/mL) that was a marginal increase compared to CHG dosed alone (9.100 ± 2.087 µg/mL). The concentrations of CHG detected within the receptor fluid would still exhibit considerable antimicrobial inhibitory effects (Odore *et al.* 2000).

The aim of the PAMAM dendrimer skin treatment is to increase the CHG deposition within the skin to enhance the antiseptic's efficacy. The CHG concentrations detected within the epidermis were much lower for the co-treatment than for the pre-treatment concentrations detailed in Chapter 3. For example when comparing the no PAMAM dendrimer controls, the physiological saline pre-treated skin followed by application of CHG 2 % (w/v) in aqueous solution resulted in 1030.668 ± 130.017 µg/mL of CHG within the epidermis whereas the CHG co-treatment control (CHG dosed in a 50:50 ethanol: water vehicle) resulted in a CHG concentration of 211.370 ± 33.189 µg/mL of CHG within the epidermis. The 24 h pre-treatment of physiological saline before the addition of the CHG may have contributed to the ~ 5 fold increase in CHG within the epidermis. Another possible explanation for the increase may be due to the difference in vehicle that the CHG is applied to the skin within. Karpanen *et al.* (2009) observed a significant reduction (p=0.008) in the permeation of CHG within excised human full thickness skin when CHG was delivered from a 70 % isopropanol vehicle when compared to CHG delivered from an aqueous vehicle. Though alcohols are considered a penetration enhancer (Benson, 2005) it appears that CHG permeates the skin in a higher concentration when applied in an aqueous vehicle compared to an alcohol-aqueous vehicle.

When developing a formulation inclusive of CHG it is important to first consider the large number of CHX incompatible materials that would typically be used within topical formulations. Chlorhexidine is considered to be compatible with cationic materials such as PAMAM dendrimers but as observed in Section 6.2.1 compatibility is dependent on the vehicle and the nature of the second cationic species (Denton, 2000). CHG is inactivated in the presence of non-ionic surfactants and may form insoluble salts with inorganic anions including phosphates and chlorides, carbonates, nitrates, sulphates and dyes. It is also incompatible with organic anions, due to micelle formation, that includes many soaps, sodium carboxymethyl cellulose, tragacanth and alginates (Larson, 1988). Within a formulation CHG must retain its antimicrobial efficacy and not become neutralised by incompatible detergents or anions.

A number of formulations were developed including a cream, lotion and hydrogel however based on the skin feel, aesthetics, stability of CHG and ultimately PAMAM dendrimer within the formulation, an alcohol hand gel was chosen as an ideal formulation. PAMAM dendrimers are more stable long term in ethanol than water (according to manufacturer's specification) and ethanol also has the advantage of being antimicrobial in its own right. Alcohol gels are also readily accepted in the healthcare sector for use as an antiseptic (Larson *et al.* 2006) and have been used to reduce HCAIs within hospital wards (MacDonald *et al.* 2004, Bischoff *et al.* 2000 and Girou *et al.* 2002). Alcohol gels are cost effective (Johnson *et al.* 2005) and low risk with regards to contamination when compared to other topical antiseptic strategies (Kampf *et al.* 2005). Alcohol gels have been shown to be better tolerated and have even been used to reduce dermatitis

caused by antiseptic soaps (Pittet *et al.* 2000, Jungbauer *et al.* 2004 and Newman and Seitz, 1990).

A range of alcohol gels were developed with HPC (hydroxypropyl cellulose, ~100,000 mw) as it is a cellulose derivative that has shown to be compatible with CHG and is typically used in synergy within toothpastes (Lehmann, 2000). Hydroxyethyl cellulose (HEC) has also been shown previously using Raman spectroscopy to solubilise the protonated CHX (dication) that was a consequence of protonation caused by a second polymer, polycarbophil within an aqueous semi-solid formulation (Jones *et al.* 2000). The first variable to be optimised was the concentration of ethanol. Formulations with a high ethanol concentration possess the highest antimicrobial efficacy (i.e. 70-90 %), with the exception of absolute ethanol (Kramer *et al.* 2002). At a concentration of 80 % and 75 % ethanol the formulation turned cloudy on addition of HPC and CHG, even after stirring for 24 h at 200 RPM followed by a 15 minute period of vigorous shaking in a mixing mill, the CHG and HPC did not fully dissolve. Therefore the optimal concentration of ethanol was determined to be 70 % as the CHG and HPC had fully dissolved. This would be considered the lowest concentration that would be considered an effective against a broad spectrum of microorganisms (Reynolds *et al.* 2006). The consistency and viscosity are important parameters for a topical gel in terms of acceptability by consumers (whether that be patients or healthcare workers) and antimicrobial efficacy. It has been shown that antimicrobial activity is lower for alcohol gels when compared to alcohol liquids due to the lower concentration of ethanol within the formulation as a result of the inclusion of a thickener (Pietsch, 2001). A thickener system may also inhibit the release of alcohol in turn reducing the antimicrobial efficacy of the formulation (Maiwald,

2008 and Guilhermetti *et al.* 2010). It is for this reason that a number of formulations were produced with a range of HPC concentrations (Table 6.8). Further, to improve the perceived feeling of the formulations glycerol, a known humectant that hydrates the skin, was incorporated as well as dimethicone. Formulations including dimethicone were not used due to incompatibility as an unknown gas effervesced from the sample.

The appearance of all formulations was determined by visual inspection; all were transparent, free from particulates and fibres. All formulations had a strong alcohol odour. The formulations was applied to the skin and unexpectedly after evaporation of the solvents (ethanol: water) a transparent and flexible film formed across the skin surface within 30-60 seconds of application (after physically rubbing a thin layer of the formulation across the skin). The film formed containing glycerol within the formulations was tacky and not agreeable with regards to acceptability by a consumer. After a further patent search it was reported that HPC is an ideal viscosifying agent that retards the evaporation of alcohol thus increasing the exposure time to microorganisms. The formulations were described as evaporation-stabilised (White, 1994). Also reported was an antimicrobial film formation for the prevention of surgical site incision infections. The formulations incorporated CHG and ethyl cellulose which was shown to interact and form a plasticiser, CHG has a strong affinity for cellulose and its derivatives. The resulting films that had formed were antimicrobial, allowed for TEWL and were ductile, smooth and flexible (Khan and Hoang, 1998). An advantage of the CHG-HPC film is that it is easily removed from laundry and would not decolourise and stain on contact with sodium hydroxide which is a significant problem for the healthcare laundry sector. The film-forming compositions developed within this chapter were

found to be covered by a patent however until this chapter there have not been studies investigating the permeation of CHG from the films into skin.

The pH of all the formulations was determined to ensure compatibility with the skin. The SC is described as an ‘acid mantle’ as the pH of the skin surface is around 4.5-5.3 that increases with increasing depth into the SC (Fluhr and Elias, 2002). It is important the pH of the skin is not altered as the acidic pH plays an integral part in the antimicrobial barrier of the skin (Schmid-Wendtner and Schmid-Wendtner, 2007). The pH of the formulations varied from the highest being 7.787 ± 0.02 for formulation F to 5.517 ± 0.14 the lowest pH detected that corresponds to formulation F4. Formulations F4 and F5 had a pH of around 5.5 which would be an ideal and compatible pH for a topical skin preparation.

The spreadability of a formulation is an important factor not only in terms of sensation upon application but also so that a user can spread an even layer across the skin for optimal drug delivery (Garg *et al.* 2002). Acceptability of a semisolid formulation is based upon a range of characteristics including; greasiness, appearance, odour, stickiness, spreadability and sensation on application (Barry and Grace, 1972). Efficacy and ultimately the success of a semisolid formulation are also based on rheological properties, spreadability and bioadhesion (Jones *et al.* 1997). Cellulose polymers such as HPC, sodium carboxymethyl cellulose (Na CMC) and hydroxyethyl cellulose (HEC) exhibit a range of excellent bioadhesive, textural and viscoelastic properties (Jones *et al.* 1997). The spreadability was measured to ensure the formulation’s behaviour was optimised with a compromise between viscosity and thus retention upon the skin for drug delivery but also spreadability and the stiffness of the formulation texture.

Measuring spreadability of a formulation upon skin is very difficult because individuals apply a different pressure or motion on application however a parallel plate method can be used to approximate the spreadability of a semisolid formulation (Vennat *et al.* 1998 and Vennat *et al.* 1995). A simple study was conducted as described elsewhere whereby the diameter of the spread was measured under experimental conditions and interpreted against the following terms; Φ >70 mm corresponds to a fluid gel, 70 $\geq$ Φ > 55 mm would be classed as a semi fluid gel and 55 $\geq$ Φ > 47 mm a semi stiff gel (Lardy *et al.* 2000). All formulations were classified as fluid gels with the exception of F4 and F5 that are classified as semi-fluid gels. The gels were easy to spread across a volunteer's skin (the author) and high coverage and distribution was achieved. The spreadability diameters were significantly different from one another depending on the ethanol and HPC content and the inclusion of glycerol (p<0.05).

The available concentration of CHG within the formulations (to investigate CHG concentration and uniformity) was determined by extracting CHG from 1 g of each formulation as it is known that CHG interacts with HPC to act as a plasticiser (Khan and Hoang, 1998). Across all formulations there was ~14 % deficit of CHG not recovered from the formulation though a formulation inclusive of 1.72 % CHG would still exhibit a strong antimicrobial effect. A percentage recovery of CHG from a control formulation that did not include HPC yielded a CHG recovery at 94.48 ± 0.51 %. This suggests that the CHG-HPC interaction does not alone affect the extraction of CHG from the formulations but that it may be due to adsorption on to glass or ineffective extraction of CHG from formulation. The CHG concentration and uniformity of the gels were comparable across all formulations as there was no difference in CHG recovery as a function of formulation (p>0.05). The CHG

recoveries observed from the film formulations are comparable to that demonstrated elsewhere from carbohydrate based films where the recovery of CHG was between 76 – 87 % of applied dose (Shafiullah, 2005).

A formulation under an applied shear stress flow will occur at a shear rate that is determined by the viscosity and/or the rheology (Morrison, 2001). The gel formulations exhibited non Newtonian behaviour which means that there was a non-linear relationship between the shear stress and the shear rate (Figure 6.11). Table 6.13 shows the viscosity of formulation F(a) but as the formulations exhibit non-Newtonian behaviour, the viscosity is not an absolute constant and instantaneously changes depending on the shear conditions. The viscosity is not an absolute constant and instantaneously changes depending on the shear conditions. The viscosity of the formulations showed shear thinning, with viscosity decreasing as the shear rate was increased. The viscosity modifier used in the formulation was hydroxypropyl cellulose (HPC) polymer, which been shown by Paradkar *et al.* 2009 to possess shear thinning properties. The process of shear thinning was described by Osswald as a reduction of the entanglement of the polymer chains as the shear force aligns them, allowing them to pass over one another more readily and thus reducing the viscosity (Osswald, 1998). The rheology of the HPC-CHG semi-solid formulations could not be fully characterised as there was only a viscometer available for use.

The gel formulation's antimicrobial efficacy was determined using a modified agar cup method against three opportunistic pathogens (Orafidiya *et al.* 2001 and Wannachaiyasit and Phaechamud, 2010). The agar cup method determines the diffusivity of an antimicrobial component from a topical preparation

added to a bore within standardised MHA (Figure 6.12). A zone of microbial inhibition can be observed and the concentration of the antimicrobial compound decreases logarithmically until a point is reached where bacterial growth occurs (Bhende and Spangler, 2004). The zone of inhibition whereby the presence of CHG is high enough to prevent microbial growth was measured in triplicate for each formulation. All formulations were antimicrobial against the three opportunistic pathogens tested; *S. aureus*, *E. coli* and *P. aeruginosa.* The zones of inhibition were similar across all formulations and all bacteria were susceptible to the formulations. The results indicate that CHG is not inactivated within the formulations and still exhibits a strong inhibitory effect against Gram negative and Gram positive bacteria.

The modified agar cup method is not suitable for measuring the antimicrobial efficacy of instantaneous biocides such as alcohol solutions. As Table 6.14 shows for the control and commercially available alcohol gel, the alcohol had evaporated from the agar as opposed to diffusing through it so that it does not inhibit microbial growth. The agar cup method is semi quantitative as with the disk diffusion method as it is likely that the zone of inhibition is an underestimate of the inhibitory effect of CHG. This is because of the presence of inorganic components within the agar required by microorganisms for growth, such as casein that contains calcium, phosphorous (Anon, 2013) and anionic agaropectin chains within the agar (Samiey and Ashoori, 2012) that may be incompatible with CHG. Further, the agar cup assay relies on the ability of the drug to diffuse through the agar.

The interaction between CHG and HPC within the ethanolic formulation was investigated using ATR-FTIR. It was observed that peaks corresponding to CHG, notably the region at 1492-1533 cm^{-1} attributed to the chlorophenyl group, are dramatically reduced in intensity and the peak shapes had altered on contact with HPC. It has been reported that CHG binds to cellulosic material (Khan and Hoang,. 1998) and as discussed below the interaction and affinity of CHG to the HPC results in no permeation of CHG into the SC (see section 6.2.9.7). The strong sorption of CHG to cellulose materials is because of electrostatic interactions between the amine groups of CHG and the carboxylic acid groups of the cellulose and in minor contribution, hydrogen bonding between the biguanide residues and the *para*-chlorophenyl moieties of CHG with the hydroxyl groups of the cellulose (Blackburn *et al.* 2007). The same authors also determined that at a high CHG concentration there is evidence of monolayer and bilayer aggregation upon cellulosic materials. The electrostatic and hydrogen bonding interactions between CHG and HPC was likely to have caused the C=N stretching peak shift. The C=N bonds on the biguanide moiety are protonated due to the electron withdrawing nature of the *para*-chloropheynl group and is therefore the most likely site for electrostatic interaction with the carboxyl groups of the cellulosic material HPC. A minor contribution of the interaction is between the 4-chlorophenyl group and the hydroxyl groups of the HPC (Yoshida forces) (Blackburn *et al.* 2007). The C-Cl stretching observed in Figure 6.13 (a) for the free CHG is masked by the dominate C-O stretch from the ethanol within the formulation therefore this interaction was not evident ATR-FTIR spectrum.

After characterisation of the formulations they were then applied to porcine dermatomed skin and a tape stripping assay was conducted to determine the permeation of CHG within the skin from the films. Formulation 4(a), 5 and 6(a) were chosen for the studies and after application of the topical gels to the porcine skin it was noted that a thick film deposited across the skin surface after evaporation of the vehicle. At 24 h a 10 mL wash (2 mL aliquots) of ultra-pure water was agitated across the surface of the films in an attempt to remove any excess drug not absorbed within the skin. Previously, for all other skin studies the highest concentration of CHG was recovered from the 24 h wash (typically >50 % of dose applied). For formulation 4(a) and 6(a) only ~5 % of the dosed CHG was recovered from the 24 h wash and ~9 % of the applied CHG was detected within the formulation 5 wash. This suggests that the CHG-HPC film formed strongly retains the CHG. The highest concentration of CHG was extracted from the films that were previously washed then prised from the skin surface using tweezers. It was noted that on removal of the film superficial layers of the SC were also removed because they adhered to the underside of the film.

Around a third of the dosed CHG was recovered from the glass donor chamber. The reason for the high concentration associated with the donor chamber was because the film had strongly adhered to the glass. Removal of the film from the glass was only possible after the donor chamber was dissolved in HPLC mobile phase as an extraction solvent overnight. No CHG was detected on the tape strips removed from the SC or the remaining epidermis/dermis across all three formulations. Further, no CHG was detected within the receptor fluid. The data presented in Tables 6.15-17 indicates that the CHG is strongly associated with HPC within the film adhered to the superficial layers of the SC. No CHG had

permeated into the SC and was thus confined to the skin surface interface. The film forming alcohol gels did not enhance the deposition of CHG within the upper skin strata but would have potential benefits for surgical incision antisepsis. The antimicrobial film-forming formulations developed within this chapter would form a ‘breathable’, flexible and transparent protective layer from transient microorganisms. The antimicrobial film could prevent skin infections by offering an antimicrobial barrier to the colonisation of transient pathogens.

Previously, Khan and Hoang (1998) incorporated pluronic surfactants within the film forming formulation (containing HEC) that aided the release of CHG. Non-ionic surfactants although not incompatible can reduce the antimicrobial efficacy of antiseptics depending on concentration and surfactant type (Denton, 1991). The next step in this study would be to add in a CHG compatible non-ionic surfactant and test to determine if the surfactant added reduces the efficacy of CHG. Once an optimised formulation is developed and fully characterised, including measuring the tensile strength etc., then the PAMAM dendrimer may be added and experiments could then be conducted into the stability, compatibility and CHG release once applied to the skin in future work. Speculatively, perhaps the polycationic PAMAM dendrimer would interact with the HPC becoming immobilised within the film allowing for the skin permeation of CHG.

6.4 Conclusion

The objective of this chapter was to characterise the interaction between CHG and G3-PAMAM-NH_2 dendrimer. It was discovered that the choice of solvent was an important factor with regards to instilling stability within the co-formulation. The antimicrobial activity of CHG was not altered when combined with the G3-PAMAM-NH_2 dendrimer. It was observed that the co-application of G3-PAMAM-NH_2 dendrimer-CHG enhanced the deposition of CHG within the upper skin strata. This has the potential to increase the contact between the antiseptic and bacteria and, as such, increase the effectiveness of skin antisepsis. The characterisation of the drug-dendrimer interactions may help to design more efficient topical drug delivery platforms. A range of cosmetically acceptable formulations were investigated for the co-application of the antiseptic and dendrimer. Whilst these were not ideally suitable for the topical delivery of CHG, they may well have significant potential as an effective approach in the prevention or treatment of surgical site infections.

7.0 Conclusions and general discussion

7.1 Summary of findings

It has been shown within this thesis that PAMAM dendrimers are a novel topical drug delivery platform of the model antiseptic, chlorhexidine digluconate. The aims and objectives of my research have been addressed within this thesis and are briefly summarised below.

Firstly, this investigation has established that PAMAM dendrimers are antimicrobial without complexation or conjugation to a conventional antimicrobial compound and that the mechanism of action is most likely due to bacterial membrane permeabilisation/disruption (Chapter 2). In addition, PAMAM dendrimers have been shown to enhance the permeation of CHG within porcine skin by either skin pre-treatment or by co-application of CHG within a hydro-ethanolic vehicle (Chapter 3 and 6). The mechanisms of action of the dendrimer-enhanced penetration enhancement effect have been investigated. The effect is likely to be multifactorial, including perturbation of intercellular lipids and hydration of the *stratum corneum* (SC) (Chapter 4). Further elucidation of the dendrimer's action on the skin is required.

The key findings of this thesis include the confirmation that PAMAM dendrimers are antimicrobial in their own right against the opportunistic skin pathogens *Staphylococcus aureus* and *Escherichia coli*. The dendrimer's antimicrobial efficacy was shown to increase with increasing concentration and also increases with increasing PAMAM dendrimer generation i.e. the number of amine surface groups. SEM micrographs and cell membrane integrity studies demonstrated that the mechanism of action of PAMAM dendrimers was severe

membrane permeabilisation and cell membrane disruption (Chapter 2). This was shown to lead to leakage and precipitation of the bacterial cells' cytoplasmic contents resulting in inhibition and, in bactericidal concentrations, cell death. The inner membrane permeabilisation assay was used to discover that the PAMAM dendrimers' effect was once again not only concentration dependent but also generation dependent. G3-PAMAM-NH_2 and G5-PAMAM-NH_2 possessed a very similar inner membrane permeabilisation effect that is due to a compromise between the number of surface amine groups and molecular size and weight for ease of diffusion into the bacterial cells. The inner membrane permeabilisation assay also confirmed that PAMAM dendrimers diffuse within the bacterial cell after reducing the integrity of the cell membrane.

This thesis has also established that a PAMAM dendrimer pre-treatment significantly enhanced the permeation and deposition of the antiseptic CHG within porcine skin compared to CHG pre-treated with physiological saline. An increase in the concentration and depth of permeation of CHG within the skin will increase the contact between the biocide and the flora within the skin layers. Disinfection of deeper layers of the skin strata, as opposed to just the superficial layers of the SC, as observed for conventional antiseptics, would reduce the microbial load of the skin. The strategy to reduce the bio-burden of the skin through more effective antisepsis may have considerable benefit to reduce the incidence of skin and soft tissue infections.

It was observed that PAMAM dendrimers did not incite any major changes in the skin integrity that significantly altered the TEER or TEWL measurements that are indicative of significant damage to the barrier properties of the skin. The

ATR-FTIR analysis did however suggest that the PAMAM dendrimers may perturb the intercellular lipid packing and organization due to observed peak shifts. The suggested ultrastructural alterations such as lipid disorder within the SC barrier were attributed to the presence of the PAMAM dendrimers (both G3-PAMAM-NH_2 and G3.5-PAMAM-COOH) as made evident by the ATR-FTIR spectra. Speculatively, this mechanism may be reversible on removal of the PAMAM dendrimer as their size and charge retards their permeation into the skin resulting in a transient effect. OCT imaging revealed that PAMAM dendrimers (G3-PAMAM-NH_2 and G3.5-PAMAM-COOH) temporarily reduced the attenuation of light on the skin, for example through a reduction in the back-scattering of light at the SC-air interface. This change in the optical characteristics at the air-skin interface was shown to be temporary. A transient penetration enhancement effect would be ideal as to not cause significant skin barrier impairment that may allow for the ingress of other toxic xenobiotics or micro-organisms. Further experimentation may determine if the temporary nature of the optical properties at the SC-air interface transpires as a temporary penetration enhancement effect. The OCT results also suggest that the PAMAM dendrimers are not evenly distributed across the skin surface but accumulate within furrows and pores. Future investigation into whether there are any changes in surface tension after application of CHG with the PAMAM dendrimer would aid understanding of deposition of the PAMAM dendrimer across the skin surface. The OCT images suggest that PAMAM dendrimers (nanoparticles that are 3.6 nm in diameter) may preferentially accumulate within the undulations of the skin. This effect after application of PAMAM dendrimers to the skin has been previously observed using confocal microscopy (Venuganti *et al.* 2011). The skin appendages act as a

bacterial reservoir (Selwyn and Elias, 1972) therefore accumulation of antimicrobial dendrimers (observed with Chapter 2) within these follicles, pores and furrows will aid skin disinfection. The PAMAM dendrimers may also be exploited for the delivery of other drugs to the follicles such as anti-acne drugs, anti-fungal drugs or hair re-growth drugs.

A novel ToF-SIMS method was developed to chemically map the distribution and localisation of a topically applied drug within the skin. The ToF-SIMS method was used to characterise the distribution of CHG once applied to the skin and also to visualise and measure the enhanced permeation of CHG following PAMAM/dendrimer skin pre-treatment. The ToF-SIMS images supported the observations in the quantitative Franz cell studies with porcine skin and the *in vitro* skin tape stripping studies. All the evidence gained within this study supports the hypothesis that the PAMAM dendrimer acts as a penetration enhancer for CHG.

During the co-dose formulation development investigations a microcrystalline precipitate formed on addition of CHG to a PAMAM dendrimer solution. The crystals were fully characterised by MALDI-ToF and single crystal XRD. It was found that in aqueous solution PAMAM dendrimers scavenge the gluconic acid resulting in a carbon anion-CHX hydrate precipitate. It was discovered that PAMAM dendrimers and CHG were stable when co-applied in a hydro-ethanolic vehicle. The co-application of CHG and PAMAM dendrimers enhanced the permeation of CHG within porcine skin. The degree of permeation enhancement was found to be dependent on the PAMAM dendrimer's concentration within the co-dose formulation (Chapter 6). The only statistically significant enhancement of CHG permeation within the epidermis (for the

co-application) was observed for the highest PAMAM dendrimer concentration (10 mM G3-PAMAM-NH_2). A series of hydro-ethanolic gel formulations were developed with the ultimate aim of incorporating the co-application of CHG with PAMAM dendrimers after optimisation. Antimicrobial film-forming alcohol gels (without the presence of PAMAM dendrimers) were characterised and optimised that would have potential use in pre-surgical incision skin disinfection.

7.2 Implications of research and future work

The implications of specific findings of this project have been discussed within each relevant chapter. A number of the novel findings of the thesis potentially have broader implications for topical drug delivery and the wider Healthcare sector which will be discussed further. PAMAM dendrimers have been used previously as drug carriers for topical or transdermal drug delivery for a very limited range of therapeutics (Sun *et al.* 2012). The results presented within this thesis investigate their use as a novel topical delivery platform for CHG. For this reason, the permeation enhancement effect is seen in co-dosing but is not specifically dependent on the drug-dendrimer interaction as the research within this thesis has also shown that as a skin pre-treatment, PAMAM dendrimers enhanced the penetration of subsequently applied CHG within the skin. This illustrates a physical enhancement effect (and possibly a depot effect) due to modulation of the superficial layers of the SC and not as a result of drug-dendrimer interactions. It is therefore expected that a PAMAM dendrimer skin pre-treatment will enhance the permeation of a vast range of topically applied therapeutics including antimicrobial compounds.

There is also very little evidence that PAMAM dendrimers permeate the SC. No evidence was observed for this within this thesis and it is suspected that this limited permeation is due to the dense surface charge and the high molecular weight of the PAMAM dendrimers. This would be an ideal property for a penetration enhancer to possess so that irritation and toxicity problems are avoided.

When synthesising any dendritic architecture inclusive of PAMAM dendrimers there is great scope to tailor and functionalise the nanoparticles for sustained and targeted release. For example, an anti-cancer dendritic pro-drug comprising of G5-PAMAM-NH_2 dendrimer functionalised with fluorescein isothiocyanate (FITC) for fluorescent imaging, folic acid as an active targeting ligand and the anti-cancer drug methotrexate for therapeutic effect were previously designed (Gurdag *et al.* 2006). This pro-drug system was designed for injection though there is scope for the pro-drug system to be exploited for topical and transdermal drug delivery. For example the OCT data within this thesis showed that the PAMAM dendrimers may accumulate within the undulations and pores of the skin. This could be used as a passive targeted drug delivery mechanism to the hair follicles. Additionally, a fluorescent tag conjugated to the PAMAM dendrimer would enable visualisation of the complexed or conjugated dendrimer-drug's localisation and distribution. Further, esterase enzymes are distributed throughout the SC and the viable epidermis (Lau *et al.* 2012 and Morris *et al.* 2009). The resulting hydrolysis of esterase linkages once the dendrimer pro-drug had been topically applied could be exploited to cleave the drug from the dendritic carrier after distribution within the hair follicles or across the skin surface.

Drug-dendrimer interactions such as those that increase the solubility of a drug may be responsible for an enhancing effect, as well as physical effects such as perturbation of the intercellular lipid packing (as observed within the ATR-FTIR work within this thesis). Further work would be required to fully elucidate the multiple factors involved with regards to the PAMAM dendrimer's skin penetration enhancement effects. One approach could include investigations to delineate the interactions of PAMAM dendrimers with SC lipids using atomic force microscopy (AFM) and differential scanning calorimetry (DSC). These methods would further clarify the dendrimers' interactions with SC lipids. Elucidation of the mechanism of action is imperative to optimise the design of synthetically tailored dendrimers aimed at improving topical and transdermal delivery.

For a one step co-application of PAMAM dendrimers with CHG, a range of hydro-ethanolic gels were first developed. It was discovered that due to the electrostatic interactions and to a lower extent, hydrogen bonding between HPC and CHG, no CHG was detected within the SC. The CHG was retained within the films that had formed across the skin surface. Though the designed films were shown to be unsuitable for the topical delivery of CHG they have the potential for widespread application in forming an antimicrobial skin barrier prior to surgical site incisions. It would also be of interest to investigate whether addition of the PAMAM dendrimer in the film-forming formulation would react with the HPC instead of the CHG to allow it to permeate into the upper skin strata. Whether or not the PAMAM dendrimer would still act as a penetration enhancer whilst immobilised within a polymeric film on the skin surface would also require further experimentation. Once a formulation for the co-application had been determined and optimised it would be of interest to perform a bioequivalence test to ascertain the efficacy of

the formulation containing PAMAM dendrimer against a commercially available formulation.

The ToF-SIMS method used CHG as a model drug in this instance and as such this method may be applied to a vast range of topically applied compounds. This method would have significant benefits in determining whether pesticides on contact with skin would permeate to the depth of the microcirculation of the viable epidermis. This could conclude to a high sensitivity (femtomolar detection limit) as to whether a pesticide would be available for systemic absorption. Further, the method could also be utilised to determine the distribution of other topically applied compounds and to reveal any co-localisation with specific biomolecules. Information such as affinity for particular biomolecules and distribution within the different histological tissue compartments can aid elucidation of mechanisms of action. As such, more effective formulation strategies or physiochemical alterations to drugs could be employed in light of such valuable chemical distribution information. As ToF-SIMS also detects secondary ions from endogenous biomolecules it would also be of interest to investigate biopsied skin due to a range of pathologies and compare them to that of healthy skin. Chemical distribution maps may aid characterisation of pathological conditions such as basal cell carcinoma or psoriasis that could support the investigation into treatment or prevention of such skin diseases.

The novel findings within this thesis, notably that the PAMAM dendrimer acts as an effective topical biocide delivery platform and the ToF-SIMS method developed to image this, have the potential for widespread biomedical applications. One area that is clearly important in healthcare institutions is

effective antisepsis to reduce the incidence of skin and soft tissue infections. More effective treatment regimes, including the approaches described in this thesis, could have a positive impact on morbidity and mortality rates due to hospital-acquired infections.

Appendix 1 CHG HPLC validation

Replicate calibration standards

CHG conc. µg/mL	1	2	3	4
1	14439	13875	14188	13910
5	118606	117841	118689	117685
10	198679	198982	197655	196938
50	783109	779946	779962	777602
100	1666449	1667049	1673436	1675335
500	7905666	7885445	7879440	7896623

Average calibration graph

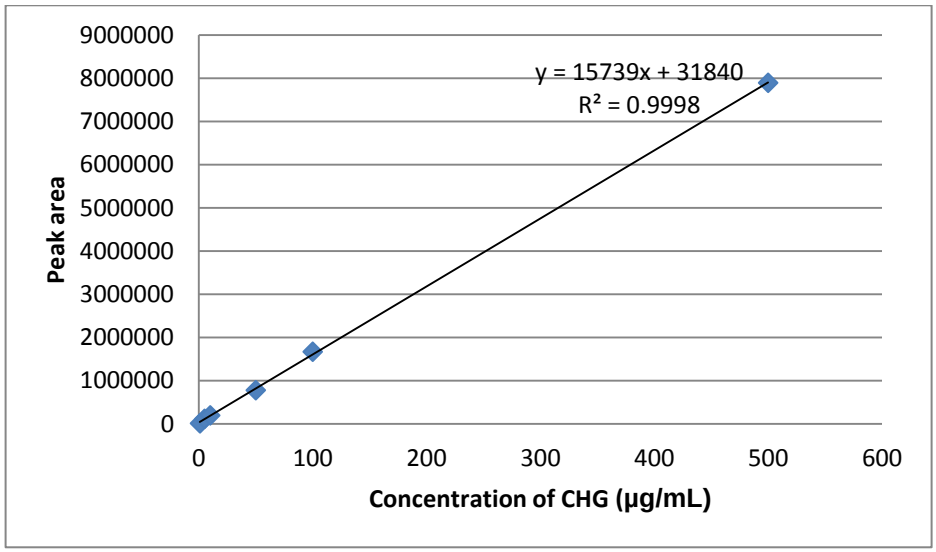

Reproducibility check of a mid-range CHG standard

CHG conc. µg/mL	Peak area
10	198649
10	198756
10	198860
10	198679
10	196938
10	198982
SD	763.9978
Mean	198477.3
RSD %	0.40 %

Appendix 2 Cholesterol HPLC validation

Replicate calibration standards

Cholesterol conc. µg/mL	1	2	3	4	5	6
1	11878	12242	10334	15904	15805.3	14312.3
5	53007	51986	55511.6	54474.5	54103.9	53571.3
10	106637	111163	107249.2	107995.9	107969.9	107880.4
25	252090	248911	Mis-sample	249356.5	252602.1	253165
50	502508	492690	491906.5	488131.8	493188.9	490044.4
100	1038812	1020199	1044811	1035963	1044405	1040312

Average calibration graph

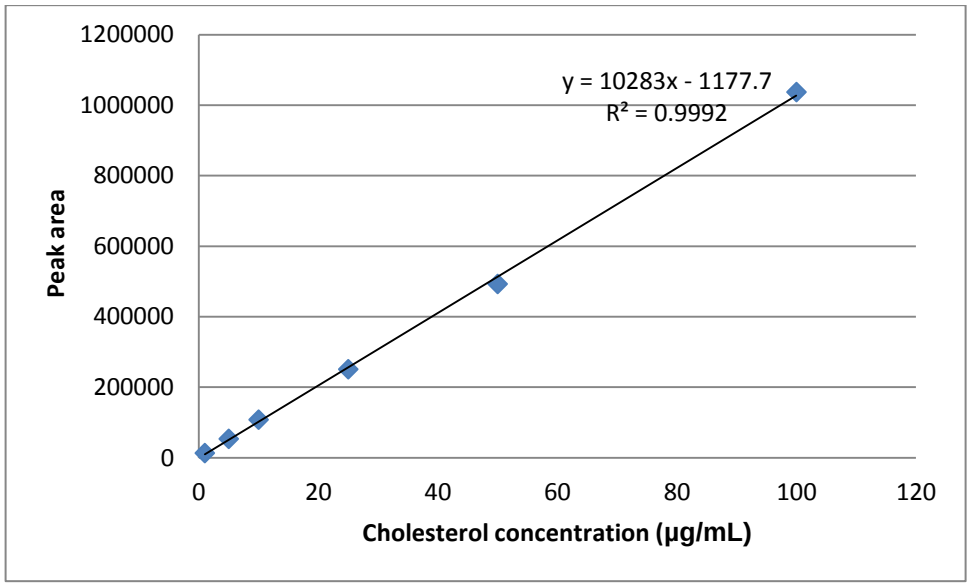

Reproducibility check of a mid-range CHG standard

Chol. Conc. µg/mL	Peak area
10	106637
10	111163
10	107249.2
10	107995.9
10	107969.9
10	107880.4
Mean	108149.2
SD	1568.926
RSD %	1.450705

Appendix 3 – x Ray diffraction information

UK National Crystallography Service

Table 1. Crystal data and structure refinement details.

Identification code	**2012ncs0132dlsaa**	
Empirical formula	$C_{23}H_{40}Cl_2N_{10}O_7$	
Formula weight	639.55	
Temperature	100(2) K	
Wavelength	0.68890 Å	
Crystal system	Monoclinic	
Space group	*P*21/*c*	
Unit cell dimensions	a = **17.727(13) Å**	α = **90°**
	b = **21.018(15) Å**	β = **92.296(6)°**
	c = **8.447(6) Å**	γ = **90°**
Volume	3145(4) Å^3	
Z	4	
Density (calculated)	1.351 Mg / m^3	
Absorption coefficient	0.263 mm^{-1}	
F(000)	1352	
Crystal	Platelet; Colorless	
Crystal size	0.10 × 0.04 × 0.01 mm^3	
θ range for data collection	2.92 – 24.21°	
Index ranges	$-21 \le h \le 21$, $-25 \le k \le 23$, $-10 \le l \le 9$	
Reflections collected	25271	
Independent reflections	5508 [R_{int} = 0.1394]	
Completeness to θ = 24.21°	99.5 %	
Absorption correction	Semi–empirical from equivalents	

Max. and min. transmission	0.9974 and 0.9742
Refinement method	Full-matrix least-squares on F^2
Data / restraints / parameters	5508 / 24 / 439
Goodness-of-fit on F^2	1.055
Final *R* indices [$F^2 > 2\sigma(F^2)$]	*R1* = 0.0801, *wR2* = 0.1921
R indices (all data)	*R1* = 0.1246, *wR2* = 0.2214
Largest diff. peak and hole	0.389 and −0.419 e Å^{-3}

Diffractometer: Beamline I19 situated on an undulator insertion device with a combination of double crystal monochromator, vertical and horizontal focussing mirrors and a series of beam slits (primary white beam and either side of the focussing mirrors). The experimental hutch (EH1) is equipped with a Crystal Logic 4-circle kappa geometry goniometer with a Rigaku Saturn 724 CCD detector and an Oxford Cryosystems Cryostream plus cryostat (80-500K). For conventional service crystallography the beamline operates at a typical energy of 18 keV (Zr K absorption edge) and a Rigaku ACTOR robotic sample changing system is available. **Cell determination and data collection**: *CrystalClear-SM Expert 2.0 r5* (Rigaku, 2010). **Data reduction, cell refinement and absorption correction**: *CrystalClear-SM Expert 2.0 r5* (Rigaku, 2010). **Structure solution**: *SUPERFLIP* (Palatinus, L. & Chapuis, G. (2007). J. Appl. Cryst. 40, 786-790). **Structure refinement**: *SHELXL97* (Sheldrick, G.M. (2008). Acta Cryst. A64, 112-122). **Graphics:** *OLEX2* (Dolomanov, O. V., Bourhis, L. J., Gildea, R. J., Howard, J. A. K. & Puschmann, H. (2009). J. Appl. Cryst. 42, 339-341).

References

ABRAMS, K., HARVELL, J.D., SHRINER, D., WERTZ, P., MAIBACH, H., MAIBACH, H.I. and REHFELD, S., 1993. Effect of organic solvents on in vitro human skin water barrier function. *Journal of Investigative Dermatology,* **101**(4), pp. 609-613.

AKI, H. and KAWASAKI, Y., 2004. Thermodynamic clarification of interaction between antiseptic compounds and lipids consisting of stratum corneum. *Thermochimica Acta,* **416**(1-2), pp. 113-119.

ALBERTI, I., KALIA, Y.N., NAIK, A. and GUY, R.H., 2001. Assessment and prediction of the cutaneous bioavailability of topical terbinafine, in vivo, in man. *Pharmaceutical Research,* **18**(10), pp. 1472-1475.

ALIBARDI, L., DOCKAL, M., REINISCH, C., TSCHACHLER, E. and ECKHART, L., 2004. Ultrastructural localization of caspase-14 in human epidermis. *Journal of Histochemistry & Cytochemistry,* **52**(12), pp. 1561-1574.

ALLARD, D. and FORESTIER, S., 1998. *Artificial tanning compositions,* US Patent 6399048.

AL-REFU, K., 2011. General Methods in Preparation of Skin Biopsies for Haematoxylin & Eosin Stain and Immunohistochemistry, *InTech open* http://www.intechopen.com/books/skin-biopsy-perspectives/general-methods-in-preparation-of-skin-biopsies-for-haematoxylin-eosin-stain-and-immunohistochemistr [Accessed on 1/3/12].

ALVAREZ-ROMAN, R., NAIK, A., KALIA, Y.N., GUY, R.H. and FESSI, H., 2004. Enhancement of topical delivery from biodegradable nanoparticles. *Pharmaceutical Research,* **21**(10), pp. 1818-1825.

ALVAREZ-ROMÁN, R., NAIK, A., KALIA, Y., GUY, R.H. and FESSI, H., 2004. Skin penetration and distribution of polymeric nanoparticles. *Journal of Controlled Release,* **99**(1), pp. 53-62.

ALVAREZ-ROMÁN, R., NAIK, A., KALIA, Y., FESSI, H. and GUY, R.H., 2004. Visualization of skin penetration using confocal laser scanning microscopy. *European Journal of Pharmaceutics and Biopharmaceutics,* **58**(2), pp. 301-316.

ALVAREZ-ROMÁN, R., BARRÉ, G., GUY, R.H. and FESSI, H., 2001. Biodegradable polymer nanocapsules containing a sunscreen agent: preparation and photoprotection. *European Journal of Pharmaceutics and Biopharmaceutics,***52**(2), pp. 191-195.

ALVAREZ-ROMÁN, R., NAIK, A., KALIA, Y.N., GUY, R.H. and FESSI, H., 2004. Skin penetration and distribution of polymeric nanoparticles. *Journal of Controlled Release,* **99**(1), pp. 53-62.

AMAGAI, M., MATSUYOSHI, N., WANG, Z., ANDL, C. and STANLEY, J., 2000. Toxin in bullous impetigo and staphylococcal scalded-skin syndrome targets desmoglein 1. *Nature Medicine,* **6**(11), pp. 1275-1277.

ANDANSON, J., HADGRAFT, J. and KAZARIAN, S.G., 2009. Errata: In situ permeation study of drug through the stratum corneum using attenuated total reflection Fourier transform infrared spectroscopic imaging. *Journal of Biomedical Optics,* **14**(3), pp. 039801-039801-1.

ANONYMOUS (2012) http://www.sigmaaldrich.com/etc/medialib/docs/ Sigma/Bulletin/tp0300bul.Par.0001.File.tmp/tp0300bul.pdf [online] [Accessed on 11/06/12]).

ANONYMOUS (2013)http://www.oxoid.com/UK/blue/prod_detail /prod_detail.asp?pr=Cm0337 [online][accessed on 24/2/13]

ANONYMOUS, Mueller-Hinton agar details [Homepage of Oxoid], [Online]. Available: http://www.oxoid.com/UK/blue/prod_detail/prod_detail.asp?pr=Cm0337 [02/24, 2013].

AOYAGI, T., TERASHIMA, O., SUZUKI, N., MATSUI, K. and NAGASE, Y., 1990. Polymerization of benzalkonium chloride-type monomer and application to percutaneous drug absorption enhancer. *Journal of Controlled Release,* **13**(1), pp. 63-71.

ARORA, P. and MUKHERJEE, B., 2002. Design, development, physicochemical, and in vitro and in vivo evaluation of transdermal patches containing diclofenac diethylammonium salt. *Journal of pharmaceutical sciences,* **91**(9), pp. 2076-2089.

ART, G., 2005. Combination povidone-iodine and alcohol formulations more effective, more convenient versus formulations containing either iodine or alcohol alone: a review of the literature. *Journal of Infusion Nursing,* **28**(5), pp. 314-320.

BADRAN, M., KUNTSCHE, J. and FAHR, A., 2009. Skin penetration enhancement by a microneedle device (Dermaroller< sup>®</sup>) in vitro: Dependency on needle size and applied formulation. *European Journal of Pharmaceutical Sciences,* **36**(4), pp. 511-523.

BAE, Y., PARK, C.S., LEE, J.K., JEONG, E., KIM, T., CHO, Y.S. and MOON, H., 2008. A case of anaphylaxis to chlorhexidine during digital rectal examination. *Journal of Korean Medical Science,* **23**(3), pp. 526-528.

BAGNANINCHI, P., YANG, Y., ZGHOUL, N., MAFFULLI, N., WANG, R. and HAJ, A.E., 2007. Chitosan microchannel scaffolds for tendon tissue engineering characterized using optical coherence tomography. *Tissue Engineering,* **13**(2), pp. 323-331.

BAKO, J., SZEPESI, M., VERES, A.J., CSERHATI, C., BORBELY, Z.M., HEGEDUS, C. and BORBELY, J., 2008. Synthesis of biocompatible nanocomposite hydrogels as a local drug delivery system. *Colloid and Polymer Science,* **286**(3), pp. 357-363.

BALAKRISHNAN, P., SHANMUGAM, S., LEE, W.S., LEE, W.M., KIM, J.O., OH, D.H., KIM, D., KIM, J.S., YOO, B.K. and CHOI, H., 2009. Formulation and in vitro assessment of minoxidil niosomes for enhanced skin delivery.*International Journal of Pharmaceutics,* **377**(1), pp. 1-8.

BALOGH, L., SWANSON, D.R., TOMALIA, D.A., HAGNAUER, G.L. and MCMANUS, A.T., 2001. Dendrimer-silver complexes and nanocomposites as antimicrobial agents. *Nano Letters,* **1**(1), pp. 18-21.

BARBER, E.D., TEETSEL, N.M., KOLBERG, K.F. and GUEST, D., 1992. A comparative study of the rates of< i> in vitro</i> percutaneous absorption of eight chemicals using rat and human skin. *Fundamental and Applied Toxicology,* **19**(4), pp. 493-497.

BARNES, T.J., KEMPSON, I.M. and PRESTIDGE, C.A., 2011. Surface analysis for compositional, chemical and structural imaging in pharmaceutics with mass spectrometry: A ToF-SIMS perspective. *International Journal of Pharmaceutics,* **417**(1–2), pp. 61-69.

BARRY, B.W., 2004. Breaching the skin's barrier to drugs. *Nature biotechnology,* **22**(2), pp. 165-167.

BARRY, B., 1987. Mode of action of penetration enhancers in human skin. *Journal of Controlled Release,* **6**(1), pp. 85-97.

BARRY, B. and GRACE, A., 1972. Sensory testing of spreadability: Investigation of rheological conditions operative during application of topical preparations. *Journal of Pharmaceutical Sciences,* **61**(3), pp. 335-341.

BEETGE, E., DU PLESSIS, J., MÜLLER, D.G., GOOSEN, C. and VAN RENSBURG, F.J., 2000. The influence of the physicochemical characteristics and pharmacokinetic properties of selected NSAID's on their transdermal absorption. *International Journal of Pharmaceutics,* **193**(2), pp. 261-264.

BELAZI, D., 2009. Visualizing and profiling tissue lipids by ToF-SIMS imaging mass spectrometry.Thesis, Karolinska, Sweden.

BENABDELLAH, F., SEYER, A., QUINTON, L., TOUBOUL, D., BRUNELLE, A. and LAPRÉVOTE, O., 2010. Mass spectrometry imaging of rat brain sections: nanomolar sensitivity with MALDI versus nanometer resolution by TOF–SIMS. *Analytical and Bioanalytical Chemistry,* **396**(1), pp. 151-162.

BENECH-KIEFFER, F., WEGRICH, P., SCHWARZENBACH, R., KLECAK, G., WEBER, T., LECLAIRE, J. and SCHAEFER, H., 2000. Percutaneous absorption of sunscreens in vitro: interspecies comparison, skin models and reproducibility aspects. *Skin Pharmacology and Physiology,* **13**(6), pp. 324-335.

BENNINGHOVEN, A., 1994. Chemical-Analysis of Inorganic and Organic-Surfaces and Thin-Films by Static Time-Of-Flight Secondary-Ion Mass-Spectrometry (ToF-SIMS). *Angewandte Chemie-International Edition in English,***33**(10), pp. 1023-1043.

BENSON, H.A.E., 2005. Transdermal drug delivery: penetration enhancement techniques. *Current Drug Delivery,* **2**(1), pp. 23-33.

BENTLEY, M., VIANNA, R.F., WILSON, S. and COLLETT, J.H., 1997. Characterization of the influence of some cyclodextrins on the stratum corneum from the hairless mouse. *Journal of Pharmacy and Pharmacology,* **49**(4), pp. 397-402.

BERGSSON, G., STEINGRIMSSON, O. and THORMAR, H., 2002. Bactericidal effects of fatty acids and monoglycerides on Helicobacter pylori. *International Journal of Antimicrobial Agents,* **20**(4), pp. 258-262.

BETTINGER, J., GLOOR, M., PETER, C., KLEESZ, P., FLUHR, J. and GEHRING, W., 1998. Opposing effects of glycerol on the protective function of the horny layer against irritants and on the penetration of hexyl nicotinate.*Dermatology,* **197**(1), pp. 18-24.

BEVERIDGE, T.J., 1999. Structures of gram-negative cell walls and their derived membrane vesicles. *Journal of Bacteriology,* **181**(16), pp. 4725.

BHATTI, A., SCOTT, R. and DYER, A., 1988. In-vitro percutaneous absorption: pig epidermal membrane as a model for human skin. *Journal of Pharmacy and Pharmacology,* **40**, pp. 45.

BHENDE, S. and SPANGLER, D., 2004. In vitro assessment of chlorhexidine gluconate-impregnated polyurethane foam antimicrobial dressing using zone of inhibition assays. *Infection control and hospital epidemiology : the official journal of the Society of Hospital Epidemiologists of America,* **25**(8), pp. 664-667.

BIELINSKA, A.U., CHEN, C., JOHNSON, J. and BAKER JR, J.R., 1999. DNA complexing with polyamidoamine dendrimers: implications for transfection. *Bioconjugate Chemistry,* **10**(5), pp. 843-850.

BISCHOFF, W.E., REYNOLDS, T.M., SESSLER, C.N., EDMOND, M.B. and WENZEL, R.P., 2000. Handwashing compliance by health care workers: the impact of introducing an accessible, alcohol-based hand antiseptic. *Archives of Internal Medicine,* **160**(7), pp. 1017.

BLACKBURN, R.S., HARVEY, A., KETTLE, L.L., MANIAN, A.P., PAYNE, J.D. and RUSSELL, S.J., 2007. Sorption of chlorhexidine on cellulose: mechanism of binding and molecular recognition. *The Journal of Physical Chemistry B,***111**(30), pp. 8775-8784.

BLUME, L., DENKER, M., GIESELER, F. and KUNZE, T., 2010. Temperature corrected transepithelial electrical resistance (TEER) measurement to quantify rapid changes in paracellular permeability. *Die Pharmazie-An International Journal of Pharmaceutical Sciences,* **65**(1), pp. 19-24.

BOAS, U. and HEEGAARD, P.M.H., 2004. Dendrimers in drug research. *Chemical Society Reviews,* **33**(1), pp. 43-63.

BOMMANNAN, D., POTTS, R.O. and GUY, R.H., 1990. Examination of stratum corneum barrier function in vivo by infrared spectroscopy. *Journal of Investigative Dermatology,* **95**(4), pp. 403-408.

BOROWSKA, K., LASKOWSKA, B., MAGOŃ, A., MYSLIWIEC, B., PYDA, M. and WOŁOWIEC, S., 2010. PAMAM dendrimers as solubilizers and hosts for 8-methoxypsoralene enabling transdermal diffusion of the guest. *International Journal of Pharmaceutics,* **398**(1–2), pp. 185-189.

BOS, J.D. and MEINARDI, M.M.H.M., 2000. The 500 Dalton rule for the skin penetration of chemical compounds and drugs. *Experimental Dermatology,* **9**(3), pp. 165-169.

BOUCHEMAL, K., BRIANÇON, S., PERRIER, E. and FESSI, H., 2004. Nano-emulsion formulation using spontaneous emulsification: solvent, oil and surfactant optimisation. *International Journal of Pharmaceutics,* **280**(1), pp. 241-251.

BOURNE, N., STANBERRY, L., KERN, E., HOLAN, G., MATTHEWS, B. and BERNSTEIN, D., 2000. Dendrimers, a new class of candidate topical microbicides with activity against herpes simplex virus infection. *Antimicrobial Agents and Chemotherapy,* **44**(9), pp. 2471-2474.

BOUWSTRA, J.A., DE GRAAFF, A., GOORIS, G.S., NIJSSE, J., WIECHERS, J.W. and VAN AELST, A.C., 2003. Water distribution and related morphology in human stratum corneum at different hydration levels. *Journal of Investigative Dermatology,* **120**(5), pp. 750-758.

BOUWSTRA, J.A., HONEYWELL-NGUYEN, P.L., GOORIS, G.S. and PONEC, M., 2003. Structure of the skin barrier and its modulation by vesicular formulations. *Progress in Lipid Research,* **42**(1), pp. 1-36.

BOUWSTRA, J., GOORIS, G., BRAS, W. and DOWNING, D., 1995. Lipid organization in pig stratum corneum. *Journal of Lipid Research,* **36**(4), pp. 685-695.

BOUWSTRA, J.A., GOORIS, G.S., VAN DER SPEK, JOOP A and BRAS, W., 1991. Structural investigations of human stratum corneum by small-angle X-ray scattering. *Journal of Investigative Dermatology,* **97**(6), pp. 1005-1012.

BOUWSTRA, J.A., GOORIS, G., DUBBELAAR, F., WEERHEIM, A., IJZERMAN, A. and PONEC, M., 1998. Role of ceramide 1 in the molecular organization of the stratum corneum lipids. *Journal of Lipid Research,* **39**(1), pp. 186-196.

BOUWSTRA, J.A. and PONEC, M., 2006. The skin barrier in healthy and diseased state. *Biochimica et biophysica acta,* **1758**(12), pp. 2080.

BOYCE, J.M., PITTET, D. and HEALTHCARE INFECTION CONTROL PRACTICES ADVISORY COMMITTEE. SOCIETY FOR HEALTHCARE EPIDEMIOLOGY OF AMERICA. ASSOCIATION FOR PROFESSIONALS IN INFECTION CONTROL. INFECTIOUS DISEASES SOCIETY OF AMERICA. HAND HYGIENE TASK FORCE, 2002. Guideline for Hand Hygiene in Health-Care Settings: recommendations of the Healthcare Infection Control Practices Advisory Committee and the HICPAC/SHEA/APIC/IDSA Hand Hygiene Task Force. *Infection control and hospital epidemiology : the official journal of the Society of Hospital Epidemiologists of America,* **23**(12 Suppl), pp. S3-40.

BRIGGS, D., 1998. *Surface analysis of polymers by XPS and static SIMS.* Cambridge University Press.

BROWN, E., WENZEL, R.P. and HENDLEY, J.O., 1989. Exploration of the Microbial Anatomy of Normal Human Skin by Using Plasmid Profiles of Coagulase-Negative Staphylococci: Search for the Reservoir of Resident Skin Flora [with Discussion]. *The Journal of Infectious Diseases,* **160**(4), pp. 644-650.

BUCKS, D. and MAIBACH, H.I., 1999. 4 Occlusion Does Not Uniformly Enhance Penetration In Vivo. *Drugs and the Pharmaceutical Sciences,* **97**, pp. 81-106.

BUNCH, J., CLENCH, M.R. and RICHARDS, D.S., 2004. Determination of pharmaceutical compounds in skin by imaging matrix-assisted laser desorption/ionisation mass spectrometry. *Rapid Communications in Mass Spectrometry,* **18**(24), pp. 3051-3060.

CALABRETTA, M.K., KUMAR, A., MCDERMOTT, A.M. and CAI, C., 2007. Antibacterial activities of poly (amidoamine) dendrimers terminated with amino and poly (ethylene glycol) groups. *Biomacromolecules,* **8**(6), pp. 1807.

CAMPBELL, J., SINGH, A.K., SWOBODA, J.G., GILMORE, M.S., WILKINSON, B.J. and WALKER, S., 2012. An Antibiotic That Inhibits a Late Step in Wall Teichoic Acid Biosynthesis Induces the Cell Wall Stress Stimulon in Staphylococcus aureus. *Antimicrobial Agents and Chemotherapy,* **56**(4), pp. 1810-1820.

CARLOTTI, D. and MAFFART, P., 1996. Chlorhexidine. *Pratique Medicale et Chirurgicale de l animan de compagnie,* **31**, pp. 553-563.

CARRET, L., REVERDY, M., LAFFORGUE, C., FALSON, F., FLEURETTE, J. and FRENEY, J., 1997. Kinetics of chlorhexidine on intact skin following a single application. *Pathologie et Biologie,* **45**(9), pp. 737-740.

CARS, O., HÖGBERG, L.D., MURRAY, M., NORDBERG, O., SIVARAMAN, S., LUNDBORG, C.S., SO, A.D. and TOMSON, G., 2008. Meeting the challenge of antibiotic resistance. *British Medical Journal,* **337**.

CARSON, C.F., MEE, B.J. and RILEY, T.V., 2002. Mechanism of action of Melaleuca alternifolia (tea tree) oil on Staphylococcus aureus determined by time-kill, lysis, leakage, and salt tolerance assays and electron microscopy.*Antimicrobial Agents and Chemotherapy,* **46**(6), pp. 1914-1920.

CASE, D., 1977. Safety of hibitane I. Laboratory experiments. *Journal of Clinical Periodontology,* **4**(5), pp. 66-72.

CASPERS, P.J., LUCASSEN, G.W., CARTER, E.A., BRUINING, H.A. and PUPPELS, G.J., 2001. In vivo confocal Raman microspectroscopy of the skin: noninvasive determination of molecular concentration profiles. *Journal of Investigative Dermatology,* **116**(3), pp. 434-442.

CATZ, P. and FRIEND, D.R., 1990. Transdermal delivery of levonorgestrel. VIII. Effect of enhancers on rat skin, hairless mouse skin, hairless guinea pig skin, and human skin. *International Journal of Pharmaceutics,* **58**(2), pp. 93-102.

CEVC, G. and VIERL, U., 2010. Nanotechnology and the transdermal route: A state of the art review and critical appraisal. *Journal of Controlled Release,* **141**(3), pp. 277-299.

CHABALA, J.M., SONI, K.K., LI, J., GAVRILOV, K.L. and LEVISETTI, R., 1995. High-Resolution Chemical Imaging with Scanning Ion Probe Sims. *International Journal of Mass Spectrometry and Ion Processes,* **143**, pp. 191-212.

CHAIYAKUNAPRUK, N., VEENSTRA, D.L., LIPSKY, B.A. and SAINT, S., 2002. Chlorhexidine compared with povidone-iodine solution for vascular catheter-site care: a meta-analysis. *Annals of Internal Medicine,* **136**(11), pp. 792.

CHAUHAN, A.S., JAIN, N.K., DIWAN, P.V. and KHOPADE, A.J., 2004. Solubility enhancement of indomethacin with poly (amidoamine) dendrimers and targeting to inflammatory regions of arthritic rats. *Journal of Drug Targeting,* **12**(9-10), pp. 575-583.

CHAUHAN, A.S., SRIDEVI, S., CHALASANI, K.B., JAIN, A.K., JAIN, S.K., JAIN, N. and DIWAN, P.V., 2003. Dendrimer-mediated transdermal delivery: enhanced bioavailability of indomethacin. *Journal of Controlled Release,* **90**(3), pp. 335-343.

CHAUHAN, A.S., JAIN, N.K. and DIWAN, P.V., 2010. Pre-clinical and behavioural toxicity profile of PAMAM dendrimers in mice. *Proceedings of the Royal Society A: Mathematical, Physical and Engineering Science,* **466**(2117), pp. 1535-1550.

CHAUHAN, A.S., DIWAN, P.V., JAIN, N.K. and TOMALIA, D.A., 2009. Unexpected in vivo anti-inflammatory activity observed for simple, surface functionalized poly(amidoamine) dendrimers. *Biomacromolecules,* **10**(5), pp. 1195-1202.

CHAURAND, P., NORRIS, J.L., CORNETT, D.S., MOBLEY, J.A. and CAPRIOLI, R.M., 2006. New developments in profiling and imaging of proteins from tissue sections by MALDI mass spectrometry. *Journal of Proteome Research,***5**(11), pp. 2889-2900.

CHEN, C.Z., BECK-TAN, N.C., DHURJATI, P., VAN DYK, T.K., LAROSSA, R.A. and COOPER, S.L., 2000. Quaternary ammonium functionalized poly (propylene imine) dendrimers as effective antimicrobials: structure-activity studies. *Biomacromolecules,* **1**(3), pp. 473-480.

CHEN, C.Z. and COOPER, S.L., 2002. Interactions between dendrimer biocides and bacterial membranes. *Biomaterials,* **23**(16), pp. 3359-3368.

CHEN, C.Z., COOPER, S.L. and TAN, N.C.B., 1999. Incorporation of dimethyldodecylammonium chloride functionalities onto poly (propylene imine) dendrimers significantly enhances their antibacterial properties.*Chemistry Communications,* (16), pp. 1585-1586.

CHENG, Y., QU, H., MA, M., XU, Z., XU, P., FANG, Y. and XU, T., 2007(a). Polyamidoamine (PAMAM) dendrimers as biocompatible carriers of quinolone antimicrobials: an in vitro study. *European Journal of Medicinal Chemistry,***42**(7), pp. 1032-1038.

CHENG, Y. and XU, T., 2008. The effect of dendrimers on the pharmacodynamic and pharmacokinetic behaviors of non-covalently or covalently attached drugs. *European Journal of Medicinal Chemistry,* **43**(11), pp. 2291-2297.

CHENG, Y., XU, Z., MA, M. and XU, T., 2007(b). Dendrimers as drug carriers: applications in different routes of drug administration. *Journal of Pharmaceutical Sciences,* **97**(1), pp. 123-143.

CHENG, Y., WU, Q., LI, Y. and XU, T., 2008. External electrostatic interaction versus internal encapsulation between cationic dendrimers and negatively charged drugs: which contributes more to solubility enhancement of the drugs? *The Journal of Physical Chemistry B,* **112**(30), pp. 8884-8890.

CHENG, Y. and XU, T., 2008. The effect of dendrimers on the pharmacodynamic and pharmacokinetic behaviors of non-covalently or covalently attached drugs. *European Journal of Medicinal Chemistry,* **43**(11), pp. 2291-2297.

CHILCOTT, R., JENNER, J., HOTCHKISS, S. and RICE, P., 2001. In vitro skin absorption and decontamination of sulphur mustard: comparison of human and pig-ear skin. *Journal of Applied Toxicology,* **21**(4), pp. 279-283.

CHOI, W.I., LEE, J.H., KIM, J., KIM, J., KIM, Y.H. and TAE, G., 2012. Efficient skin permeation of soluble proteins via flexible and functional nano-carrier. *Journal of Controlled Release,* **157**(2), pp. 272-278.

CHOW, C.P., BUTTAR, H.S. and DOWNIE, R.H., 1978. Percutaneous absorption of chlorhexidine in rats. *Toxicology letters,* **1**(4), pp. 213-216.

CHRISTOPHERS, E., WOLFF, H.H. and LAURENCE, E.B., 1974. The formation of epidermal cell columns. *Journal of Investigative Dermatology,* **62**(6), pp. 555-559.

CLIMO, M.W., YOKOE, D.S., WARREN, D.K., PERL, T.M., BOLON, M., HERWALDT, L.A., WEINSTEIN, R.A., SEPKOWITZ, K.A., JERNIGAN, J.A., SANOGO, K. and WONG, E.S., 2013. Effect of daily chlorhexidine bathing on hospital-acquired infection. *The New England journal of medicine,* **368**(6), pp. 533-542.

CLONINGER, M.J., 2002. Biological applications of dendrimers. *Current Opinion in Chemical Biology,* **6**(6), pp. 742-748.

CNUBBEN, N.H.P., ELLIOTT, G.R., HAKKERT, B.C., MEULING, W.J.A. and VAN DE SANDT, J.J.M., 2002. Comparative *in Vitro–in Vivo* Percutaneous Penetration of the Fungicide *ortho*-Phenylphenol.*Regulatory Toxicology and Pharmacology,* **35**(2), pp. 198-208.

CODLING, C.E., HANN, A.C., MAILLARD, J.Y. and RUSSELL, A., 2005. An investigation into the antimicrobial mechanisms of action of two contact lens biocides using electron microscopy. *Contact Lens and Anterior Eye,* **28**(4), pp. 163-168.

COOKSEY, C., 2010. Hematoxylin and related compounds-an annotated bibliography concerning their origin, properties, chemistry, and certain applications. *Biotechnic & Histochemistry,* **85**(1), pp. 65-82.

COUVREUR, R.G.P., 2006. Nanocapsules: preparation, characterization and therapeutic applications. *Nanoparticulates As Drug Carriers,* pp. 255.

COWEN, J., ELLIS, S.H. and MCAINSH, J., 1979. Absorption of chlorhexidine from the intact skin of newborn infants. *Archives of Disease in Childhood,* **54**(5), pp. 379-383.

CRISCIONE, J.M., LE, B.L., STERN, E., BRENNAN, M., RAHNER, C., PAPADEMETRIS, X. and FAHMY, T.M., 2009. Self-assembly of pH-responsive fluorinated dendrimer-based particulates for drug delivery and noninvasive imaging.*Biomaterials,* **30**(23), pp. 3946-3955.

DAS, M., BHATTACHARYA, A. and GHOSAL, S., 2006. Transdermal delivery of trazodone hydrochloride from acrylic films prepared from aqueous latex. *Indian Journal of Pharmaceutical Sciences,* **68**(1), pp. 41.

DAVIES, D., WARD, R. and HEYLINGS, J., 2004. Multi-species assessment of electrical resistance as a skin integrity marker for in vitro percutaneous absorption studies. *Toxicology in Vitro,* **18**(3), pp. 351-358.

DAVIES, S.C., 2013. *Annual Report of the Chief Medical Officer, Volume Two, 2011, infections and the rise of antimicrobial resistance.* Volume 2. London: Department of Health.

DAVIES, S.C., 2012. *Annual Report of the Chief Medical Officer, Volume One, 2011, On the State of the Public's Health.* Volume 1. London: Department of Health.

DAVIES, G.E., FRANCIS, J., MARTIN, A.R., ROSE, F.L. and SWAIN, G., 1954. 1:6-Di-4'-chlorophenyldiguanidohexane (hibitane); laboratory investigation of a new antibacterial agent of high potency. *British Journal of Pharmacology and Chemotherapy,* **9**(2), pp. 192-6.

DAVIS, K.A., STEWART, J.J., CROUCH, H.K., FLOREZ, C.E. and HOSPENTHAL, D.R., 2004. Methicillin-resistant Staphylococcus aureus (MRSA) nares colonization at hospital admission and its effect on subsequent MRSA infection.*Clinical Infectious Diseases,* **39**(6), pp. 776-782.

DE JALÓN, E.G., BLANCO-PRIETO, M., YGARTUA, P. and SANTOYO, S., 2001. PLGA microparticles: possible vehicles for topical drug delivery. *International Journal of Pharmaceutics,* **226**(1), pp. 181-184.

DE SOUZA, E.L., DE BARROS, J.C., DE OLIVEIRA, C.E.V. and DA CONCEIÇÃO, M.L., 2010. Influence of *Origanum vulgare* L. essential oil on enterotoxin production, membrane permeability and surface characteristics of *Staphylococcus aureus*. *International Journal of Food Microbiology,* **137**(2), pp. 308-311.

DENTON, G.W., 2000. Chlorhexidine. In: S. BLOCK, ed, *Disinfection, sterilization, and preservation* 5th edn. Lippincott Williams & Wilkins, pp. 321.

DENTON, G. W.,1991 Chlorhexidine. In: S. BLOCK, ed, *Disinfection, sterilization and preservation* 4th edn. pp. 274–289. Philadelphia: Lea and Febiger.

DEPARTMENT OF HEALTH, 2006. *Code of practice for the prevention and control of healthcare associated*
infection. http://www.dh.gov.uk/en/Publicationsandstatistics/Publications/PublicationsPolicyAndGuidance/DH_4139336: Department of Health.

DERICI, L., HARCUP, J.P., HILL, S.P. and KHOSHDEL, E., 2009. *Hair care composition comprising a dendritic macromolecule,* WO2006018063, patent.

DEVARAKONDA, B., HILL, R.A. and DE VILLIERS, M.M., 2004. The effect of PAMAM dendrimer generation size and surface functional group on the aqueous solubility of nifedipine. *International Journal of Pharmaceutics,* **284**(1), pp. 133-140.

DIALLO, M.S., CHRISTIE, S., SWAMINATHAN, P., BALOGH, L., SHI, X., UM, W., PAPELIS, C., GODDARD III, W.A. and JOHNSON JR, J.H., 2004. Dendritic chelating agents. 1. Cu (II) binding to ethylene diamine core poly (amidoamine) dendrimers in aqueous solutions. *Langmuir,* **20**(7), pp. 2640-2651.

DIALLO, M.S., CHRISTIE, S., SWAMINATHAN, P., JOHNSON JR, J.H. and GODDARD III, W.A., 2005. Dendrimer enhanced ultrafiltration. 1. Recovery of Cu (II) from aqueous solutions using PAMAM dendrimers with ethylene diamine core and terminal NH2 groups. *Environmental Science & Technology,* **39**(5), pp. 1366-1377.

DIASPRO, A., FEDERICI, F. and ROBELLO, M., 2002. Influence of refractive-index mismatch in high-resolution three-dimensional confocal microscopy. *Applied Optics,* **41**(4), pp. 685-690.

DICK, I.P. and SCOTT, R.C., 1992. Pig ear skin as an in-vitro model for human skin permeability. *Journal of Pharmacy and Pharmacology,* **44**(8), pp. 640-645.

DOMADIA, P.N., BHUNIA, A., RAMAMOORTHY, A. and BHATTACHARJYA, S., 2010. Structure, interactions, and antibacterial activities of MSI-594 derived mutant peptide MSI-594F5A in lipopolysaccharide micelles: role of the helical hairpin conformation in outer-membrane permeabilization. *Journal of the American Chemical Society,* **132**(51), pp. 18417-18428.

DOUGLAS, M. and CHEN, P., 1998. Quantitative trace metal analysis of silicon surfaces by ToF-SIMS. *Surface and Interface Analysis,* **26**(13), pp. 984-994.

DOWHAN, W., 1997. Molecular basis for membrane phospholipid diversity: why are there so many lipids? *Annual Review of Biochemistry,* **66**(1), pp. 199-232.

DREHER, F., 2007. Quantification of *stratum corneum* removed by tape stripping. In: WILHELM K.P, ZHAI, H., AND MAIBACH, H.I, ed, *Dermatotoxicology.* seventh edn. CRC press Taylor and Francis group, pp. 343.

DREHER, F., MODJTAHEDI, B.S., MODJTAHEDI, S.P. and MAIBACH, H.I., 2005. Quantification of stratum corneum removal by adhesive tape stripping by total protein assay in 96-well microplates. *Skin Research and Technology,* **11**(2),.

DRYDEN, M.S., 2009. Skin and soft tissue infection: microbiology and epidemiology. *International Journal of Antimicrobial Agents,* **34**(1), pp. 2.

DUNCAN, I.W., CULBRETH, P.H. and BURTIS, C.A., 1979. Determination of free, total, and esterified cholesterol by high-performance liquid chromatography. *Journal of Chromatography B: Biomedical Sciences and Applications,* **162**(3), pp. 281-292.

DUNCAN, R. and IZZO, L., 2005. Dendrimer biocompatibility and toxicity. *Advanced Drug Delivery Reviews,* **57**(15), pp. 2215-2237.

EADY, E. and COVE, J., 2003. Staphylococcal resistance revisited: community-acquired methicillin resistant Staphylococcus aureus - an emerging problem for the management of skin and soft tissue infections. *Current Opinion in Infectious Diseases,* **16**(2), pp. 103-124.

EBO, D.G., STEVENS, W.J., BRIDTS, C.H. and MATTHIEU, L., 1998. Contact allergic dermatitis and life-threatening anaphylaxis to chlorhexidine. *Journal of Allergy and Clinical Immunology,* **101**(1), pp. 128-129.

EGBARIA, K. and FRIEDMAN, M., 1990. Sustained in vitro activity of human albumin microspheres containing chlorhexidine dihydrochloride against bacteria from cultures of organisms that cause urinary tract infections.*Antimicrobial Agents and Chemotherapy,* **34**(11), pp. 2118-2121.

EGBARIA, K. and FRIEDMAN, M., 1990. Sustained release albumin microspheres containing antibacterial drugs: Effects of preparation conditions on kinetics of drug release. *Journal of Controlled Release,* **14**(1), pp. 79-94.

EGELRUD, T., 2000. Desquamation in the stratum corneum. *Acta Dermato Venereologica-Supplement,* (208), pp. 44-45.

EICHMAN, J.D., BIELINSKA, A.U., KUKOWSKA-LATALLO, J.F. and BAKER JR, J.R., 2000. The use of PAMAM dendrimers in the efficient transfer of genetic material into cells. *Pharmaceutical Science & Technology today,* **3**(7), pp. 232-245.

EL MAGHRABY, G., BARRY, B. and WILLIAMS, A., 2008. Liposomes and skin: from drug delivery to model membranes. *European Journal of Pharmaceutical Sciences,* **34**(4), pp. 203-222.

ELIAS, P.M., 1983. Epidermal lipids, barrier function, and desquamation. *Journal of Investigative Dermatology,* **80**, pp. 44s-49s.

ELLIS, C.N., WEISS, J.S., HAMILTON, T.A., HEADINGTON, J.T., ZELICKSON, A.S. and VOORHEES, J.J., 1990. Sustained improvement with prolonged topical tretinoin (retinoic acid) for photoaged skin. *Journal of the American Academy of Dermatology,* **23**(4), pp. 629-637.

ELMAHJOUBI, E., FRUM, Y., ECCLESTON, G.M., WILKINSON, S.C. and MEIDAN, V.M., 2009. Transepidermal water loss for probing full-thickness skin barrier function: Correlation with tritiated water flux, sensitivity to punctures and diverse surfactant exposures. *Toxicology in Vitro,* **23**(7), pp. 1429-1435.

EL-SAYED, M., GINSKI, M., RHODES, C. and GHANDEHARI, H., 2002. Transepithelial transport of poly (amidoamine) dendrimers across Caco-2 cell monolayers. *Journal of Controlled Release,* **81**(3), pp. 355-365.

ELSAYED, M., ABDALLAH, O.Y., NAGGAR, V.F. and KHALAFALLAH, N.M., 2006. Deformable liposomes and ethosomes: mechanism of enhanced skin delivery. *International Journal of Pharmaceutics,* **322**(1), pp. 60-66.

ELSAYED, M.M.A., ABDALLAH, O.Y., NAGGAR, V.F. and KHALAFALLAH, N.M., 2007. Lipid vesicles for skin delivery of drugs: Reviewing three decades of research. *International Journal of Pharmaceutics,* **332**(1–2), pp. 1-16.

ESFAND, R. and TOMALIA, D.A., 2001. Poly (amidoamine)(PAMAM) dendrimers: from biomimicry to drug delivery and biomedical applications. *Drug Discovery Today,* **6**(8), pp. 427-436.

ESPOSITO, E., CORTESI, R., DRECHSLER, M., PACCAMICCIO, L., MARIANI, P., CONTADO, C., STELLIN, E., MENEGATTI, E., BONINA, F. and PUGLIA, C., 2005. Cubosome dispersions as delivery systems for percutaneous administration of indomethacin. *Pharmaceutical Research,* **22**(12), pp. 2163-2173.

FARKAS, E., SCHUBERT, R. and ZELKO, R., 2004. Effect of β-sitosterol on the characteristics of vesicular gels containing chlorhexidine. *International Journal of Pharmaceutics,* **278**(1), pp. 63-70.

FARKAS, E., ZELKO, R., TÖRÖK, G., RÁCZ, I. and MARTON, S., 2001. Influence of chlorhexidine species on the liquid crystalline structure of vehicle. *International Journal of Pharmaceutics,* **213**(1), pp. 1-5.

FARKAS, E., KISS, D. and ZELKO, R., 2007. Study on the release of chlorhexidine base and salts from different liquid crystalline structures. *International journal of pharmaceutics,* **340**(1-2), pp. 71-75.

FEDERAL REGISTER, 1994. *Topical Antimicrobial Drug Products for Over-the-Counter Human Use: Tentative Final Monograph for Health-Care Antiseptic Drug Products.* Vol. 59, No. 116, p. 31402-52. 21 CFR Parts 333 and 369. edn. USA: Food and Drug Administration.

FILIPOWICZ, A. and WOŁOWIEC, S., 2011. Solubility and *in vitro* transdermal diffusion of riboflavin assisted by PAMAM dendrimers. *International Journal of Pharmaceutics,* **408**(1), pp. 152-156.

FINNIN, B.C. and MORGAN, T.M., 1999. Transdermal penetration enhancers: applications, limitations, and potential. *Journal of Pharmaceutical Sciences,* **88**(10), pp. 955-958.

FITZPATRICK, T.B., WOLFF, K., JOHNSON, R.A. and SUURMOND, D., 2005. *Fitzpatrick's color atlas and synopsis of clinical dermatology.* McGraw-Hill Medical Pub. New York.

FLETCHER, J.S., HENDERSON, A., BIDDULPH, G.X., VAIDYANATHAN, S., LOCKYER, N.P. and VICKERMAN, J.C., 2008. Uncovering new challenges in bio-analysis with ToF-SIMS. *Applied Surface Science,* **255**(4), pp. 1264-1270.

FLETCHER, J.S., LOCKYER, N.P., VAIDYANATHAN, S. and VICKERMAN, J.C., 2007. TOF-SIMS 3D biomolecular imaging of Xenopus laevis oocytes using buckminsterfullerene (C-60) primary ions. *Analytical Chemistry,* **79**(6), pp. 2199-2206.

FLUHR, J.W. and ELIAS, P.M., 2002. Stratum corneum pH: formation and function of the 'acid mantle'. *Exogenous Dermatology,* **1**(4), pp. 163-175.

FLUHR, J.W., KAO, J., JAIN, M., AHN, S.K., FEINGOLD, K.R. and ELIAS, P.M., 2001. Generation of free fatty acids from phospholipids regulates stratum corneum acidification and integrity. *Journal of Investigative Dermatology,***117**(1), pp. 44-51.

FORESTIER, S. and ROLLAT-CORVOL, I., 1999. *Deodorant composition and use thereof,* US patent US6001342.

FRAZEE, B.W., LYNN, J., CHARLEBOIS, E.D., LAMBERT, L., LOWERY, D. and PERDREAU-REMINGTON, F., 2005. High prevalence of methicillin-resistant Staphylococcus aureus in emergency department skin and soft tissue infections. *Annals of Emergency Medicine,* **45**(3), pp. 311-320.

FRÉCHET, J.M. and TOMALIA, D.A., 2001. *Dendrimers and other dendritic polymers.* Wiley New York.

FREUDIGER, C.W., MIN, W., SAAR, B.G., LU, S., HOLTOM, G.R., HE, C., TSAI, J.C., KANG, J.X. and XIE, X.S., 2008. Label-Free Biomedical Imaging with High Sensitivity by Stimulated Raman Scattering Microscopy. *Science,***322**(5909),.

FRITSCH, W.C., STOUGHTON, R.B. and STAPELFELDT, A., 1963. The Effect of Temperature and Humidity on the Penetration of C14 Acetylsalicylic Acid in Excised Human Skin1. *Journal of Investigative Dermatology,* **41**(5), pp. 307-311.

FRYKLUND, B., TULLUS, K. and BURMAN, L., 1995. Survival on skin and surfaces of epidemic and nonepidemic strains of enterobacteria from neonatal special care units. *Journal of Hospital Infection,* **29**(3), pp. 201-208.

GAO, Z., TSENG, C., PEI, Z. and BLASER, M.J., 2007. Molecular analysis of human forearm superficial skin bacterial biota. *Proceedings of the National Academy of Sciences,* **104**(8), pp. 2927-2932.

GAO, S. and SINGH, J., 1997. Mechanism of transdermal transport of 5-fluorouracil by terpenes: Carvone, 1,8-cineole and thymol. *International Journal of Pharmaceutics,* **154**(1), pp. 67-77.

GARDELLA, D., HATTON, W.J., RIND, H.B., ROSEN, G.D. and VON BARTHELD, C.S., 2003. Differential tissue shrinkage and compression in the *z*-axis: implications for optical disector counting in vibratome-, plastic-and cryosections. *Journal of Neuroscience Methods,* **124**(1), pp. 45-59.

GARDIKIS, K., HATZIANTONIOU, S., VIRAS, K., WAGNER, M. and DEMETZOS, C., 2006. A DSC and Raman spectroscopy study on the effect of PAMAM dendrimer on DPPC model lipid membranes. *International Journal of Pharmaceutics,* **318**(1–2), pp. 118-123.

GARDINER, J., FREEMAN, S., LEACH, M., GREEN, A., ALCOCK, J. and D'EMANUELE, A., 2008. PAMAM dendrimers for the delivery of the antibacterial Triclosan. *Journal of Enzyme Inhibition and Medicinal Chemistry,* **23**(5), pp. 623-628.

GARG, A., AGGARWAL, D., GARG, S. and SINGLA, A.K., 2002. Spreading of semisolid formulations: an update. *Pharmaceutical Technology,* **26**(9), pp. 84-105.

GIBBS, B. and STUTTARD, L., 1967. Evaluation of skin germicides. *Journal of Applied Microbiology,* **30**(1), pp. 66-77.

GILLIES, E.R. and FRECHET, J.M.J., 2005. Dendrimers and dendritic polymers in drug delivery. *Drug Discovery today,* **10**(1), pp. 35-43.

GIROU, E., LOYEAU, S., LEGRAND, P., OPPEIN, F. and BRUN-BUISSON, C., 2002. Efficacy of handrubbing with alcohol based solution versus standard handwashing with antiseptic soap: randomised clinical trial. *British Medicine Journal,***325**(7360), pp. 362.

GONGWER, L., HUBBEN, K., LENKIEWICZ, R., HART, E. and COCKRELL, B., 1980. The effects of daily bathing of neonatal rhesus monkeys with an antimicrobial skin cleanser containing chlorhexidine gluconate. *Toxicology and Applied Pharmacology,* **52**(2), pp. 255-261.

GONZALEZ ENSENAT, P., MAIERHOFER, G., OLIVÉ, M.J. and ECHEVERRIA GARCIA, J.J., 1998. *Chlorhexidine diacetate or chlorhexidine digluconate containing liposomes,*US patent EP0613685.

GONZALEZ, E.P., 2000. *Skin-cleaning towels impregnated with liposomes containing compositions,* EU patent EP1000605.

GOON, A., WHITE, I., RYCROFT, R. and MCFADDEN, J., 2004. Allergic contact dermatitis from chlorhexidine. *Dermatitis,* **15**(1), pp. 45-47.

GRAHAM, D.J., WAGNER, M.S. and CASTNER, D.G., 2006. Information from complexity: Challenges of TOF-SIMS data interpretation. *Applied Surface Science,* **252**(19), pp. 6860-6868.

GRAMS, J., 2007. *New trends and potentialities of ToF-SIMS in surface studies.* Nova Science Pub Incorporated NEW YORK.

GRDADOLNIK, J., 2002. ATR-FTIR spectroscopy: Its advantage and limitations. *Acta Chimica Slovenica,* **49**(3), pp. 631-642.

GRENIER, D., BERTRAND, J. and MAYRAND, D., 2007. Porphyromonas gingivalis outer membrane vesicles promote bacterial resistance to chlorhexidine. *Oral Microbiology and Immunology,* **10**(5), pp. 319-320.

GRICE, K., SATTAR, H., SHARRATT, M. and BAKER, H., 1971. Skin temperature and transepidermal water loss. *Journal of Investigative Dermatology,* **57**(2), pp. 108-110.

GRICE, E.A., KONG, H.H., RENAUD, G., YOUNG, A.C., BOUFFARD, G.G., BLAKESLEY, R.W., WOLFSBERG, T.G., TURNER, M.L., SEGRE, J.A. and NISC COMPARATIVE SEQUENCING, 2008. A diversity profile of the human skin microbiota. *Genome Research,* **18**(7), pp. 1043-1050.

GROSS, M., CRAMTON, S.E., GÖTZ, F. and PESCHEL, A., 2001. Key Role of Teichoic Acid Net Charge inStaphylococcus aureus Colonization of Artificial Surfaces. *Infection and Immunity,* **69**(5), pp. 3423-3426.

GUILHERMETTI, M., MARQUES WIIRZLER, L., CASTANHEIRA FACIO, B., DA SILVA FURLAN, M., CAMPO MESCHIAL, W., BRONHARO TOGNIM, M., BOTELHO GARCIA, L. and LUIZ CARDOSO, C., 2010. Antimicrobial efficacy of alcohol-based hand gels. *Journal of Hospital Infection,* **74**(3), pp. 219-224.

GUPTA, P., VERMANI, K. and GARG, S., 2002. Hydrogels: from controlled release to pH-responsive drug delivery. *Drug Discovery Today,* **7**(10), pp. 569-579.

GUPTA, U., AGASHE, H.B., ASTHANA, A. and JAIN, N., 2006. Dendrimers: novel polymeric nanoarchitectures for solubility enhancement. *Biomacromolecules,* **7**(3), pp. 649-658.

GURDAG, S., KHANDARE, J., STAPELS, S., MATHERLY, L.H. and KANNAN, R.M., 2006. Activity of dendrimer-methotrexate conjugates on methotrexate-sensitive and-resistant cell lines. *Bioconjugate Chemistry,* **17**(2), pp. 275-283.

GUSTAFSON, J., LIEW, Y., CHEW, S., MARKHAM, J., BELL, H., WYLLIE, S. and WARMINGTON, J., 1998. Effects of tea tree oil on Escherichia coli. *Letters in Applied Microbiology,* **26**(3), pp. 194-198.

GUTERRES, S.S., ALVES, M.P. and POHLMANN, A.R., 2007. Polymeric nanoparticles, nanospheres and nanocapsules, for cutaneous applications. *Drug Target Insights,* **2**, pp. 147.

GUY, R. and HADGRAFT, J., 1989. Structure-activity correlations in percutaneous absorption. *Percutaneous Absorption,* pp. 95-109.

HADDADI, A., ABOOFAZELI, R., ERFAN, M. and FARBOUD, E.S., 2008. Topical delivery of urea encapsulated in biodegradable PLGA microparticles: O/W and W/O creams. *Journal of Microencapsulation,* **25**(6), pp. 379-386.

HADGRAFT, J. and VALENTA, C., 2000. pH, pKa and dermal delivery. *International Journal of Pharmaceutics,* **200,** pp. 243-247.

HADGRAFT, J., 2001. Skin, the final frontier. *International Journal of Pharmaceutics,* **224**(1-2), pp. 1-18.

HAHN, B.L., ONUNKWO, C.C., WATTS, C.J. and SOHNLE, P.G., 2009. Systemic dissemination and cutaneous damage in a mouse model of staphylococcal skin infections. *Microbial Pathogenesis,* **47**(1), pp. 16-23.

HAHN, T., HANSEN, S., NEUMANN, D., KOSTKA, K., LEHR, C., MUYS, L. and SCHAEFER, U., 2010. Infrared densitometry: a fast and non-destructive method for exact stratum corneum depth calculation for in vitro tape-stripping.*Skin Pharmacology and Physiology,* **23**(4), pp. 183-192.

HAIGH, J., BEYSSAC, E., CHANET, L. and AIACHE, J., 1998. In vitro permeation of progesterone from a gel through the shed skin of three different snake species. *International Journal of Pharmaceutics,* **170**(2), pp. 151-156.

HAIGH, J.M. and SMITH, E.W., 1994. The selection and use of natural and synthetic membranes for in vitro diffusion experiments. *European Journal of Pharmaceutical Sciences,* **2**(5), pp. 311-330.

HAN, J., 2006. Advances in Characterization of Pharmaceutical Hydrates. *Trends in Bio/Pharmaceutical Industry,* **3**, pp. 25-29.

HARA, M. and VERKMAN, A., 2003. Glycerol replacement corrects defective skin hydration, elasticity, and barrier function in aquaporin-3-deficient mice. *Proceedings of the National Academy of Sciences,* **100**(12), pp. 7360-7365.

HEALTH PROTECTION AGENCY, 2012. *Quarterly Epidemiological Commentary: Mandatory MRSA, MSSA and E. coli bacteraemia, and C. difficile infection data (up to October – December 2011).*http://www.hpa.org.uk/web/HPAweb&HPAwebStandard/HPAweb_C/1259151891722: Health Protection Agency.

HEARD, D. and ASHWORTH, R., 1968. The colloidal properties of chlorhexidine and its interaction with some macromolecules. *Journal of Pharmacy and Pharmacology,* **20**(7), pp. 505-512.

HEISIG, M., LIECKFELDT, R., WITTUM, G., MAZURKEVICH, G. and LEE, G., 1996. Non steady-state descriptions of drug permeation through stratum corneum. I. The biphasic brick-and-mortar model. *Pharmaceutical Research,***13**(3), pp. 421-426.

HELANDER, I., NURMIAHO-LASSILA, E.L., AHVENAINEN, R., RHOADES, J. and ROLLER, S., 2001. Chitosan disrupts the barrier properties of the outer membrane of Gram-negative bacteria. *International Journal of Food Microbiology,* **71**(2), pp. 235-244.

HEO, S., KIM, S., JEONG, Y., BAE, I., JIN, J. and LEE, J., 2008. Hospital outbreak of Burkholderia stabilis bacteraemia related to contaminated chlorhexidine in haematological malignancy patients with indwelling catheters. *Journal of Hospital Infection,* **70**(3), pp. 241.

HIGO, N., NAIK, A., BOMMANNAN, D.B., POTTS, R.O. and GUY, R.H., 1993. Validation of Reflectance Infrared-Spectroscopy as a Quantitative Method to Measure Percutaneous-Absorption In-Vivo. *Pharmaceutical Research,***10**(10),.

HOFFMAN, P., 2001. Skin disinfection and acupuncture. *Acupuncture in Medicine,* **19**(2), pp. 112-116.

HONG, S., BIELINSKA, A.U., MECKE, A., KESZLER, B., BEALS, J.L., SHI, X., BALOGH, L., ORR, B.G., BAKER JR, J.R. and HOLL, M.M.B., 2004. Interaction of poly (amidoamine) dendrimers with supported lipid bilayers and cells: hole formation and the relation to transport. *Bioconjugate Chemistry,* **15**(4), pp. 774-782.

HONG, S., BIELINSKA, A.U., MECKE, A., KESZLER, B., BEALS, J.L., SHI, X., BALOGH, L., ORR, B.G., BAKER, J.R. and BANASZAK HOLL, M.M., 2004. Interaction of poly (amidoamine) dendrimers with supported lipid bilayers and cells: hole formation and the relation to transport. *Bioconjugate Chemistry,* **15**(4), pp. 774-782.

HONG, S., LEROUEIL, P.R., ELIZABETH, K., PETERS, J.L., KOBER, M., ISLAM, M.T., ORR, B.G., BAKER JR, J.R. and HOLL, M.M.B., 2006. Interaction of polycationic polymers with supported lipid bilayers and cells: nanoscale hole formation and enhanced membrane permeability. *Bioconjugate Chemistry,* **17**(3), pp. 728-734.

HUGO, W. and LONGWORTH, A., 1964. Effect of chlorhexidine diacetate on “protoplasts” and spheroplasts of Escherichia coli, protoplasts of Bacillus megaterium and the gram staining reaction of Staphylococcus aureus.*Journal of Pharmacy and Pharmacology,* **16**(11), pp. 751-758.

HUYNH, T.T.N., PADOIS, K., SONVICO, F., ROSSI, A., ZANI, F., PIROT, F., DOURY, J. and FALSON, F., 2010. Characterization of a polyurethane-based controlled release system for local delivery of chlorhexidine diacetate.*European Journal of Pharmaceutics and Biopharmaceutics,* **74**(2), pp. 255-264.

IDSON, B., 1971. Biophysical factors in skin penetration. *Journal of the Society of. Cosmetic.Chemists,* **22**, pp. 615-618.

IGARASHI, Y. and OKA, Y., 1988. Vestibular ototoxicity following intratympanic applications of chlorhexidine gluconate in the cat. *European Archives of Oto-Rhino-Laryngology,* **245**(4), pp. 210-217.

IKEDA, T., HIRAYAMA, H., YAMAGUCHI, H., TAZUKE, S. and WATANABE, M., 1986. Polycationic biocides with pendant active groups: molecular weight dependence of antibacterial activity. *Antimicrobial Agents and Chemotherapy,***30**(1), pp. 132-136.

IMFELD,T., 2006. Chlorhexidine-containing chewing gum. *Schweizer Monatsschrift Fur Zahnmedizin,* **116**(5), pp. 476.

IOANNOU, C.J., HANLON, G.W. and DENYER, S.P., 2007. Action of disinfectant quaternary ammonium compounds against Staphylococcus aureus. *Antimicrobial Agents and Chemotherapy,* **51**(1), pp. 296-306.

IWATSUKI, K., YAMASAKI, O., MORIZANE, S. and OONO, T., 2006. Staphylococcal cutaneous infections: invasion, evasion and aggression. *Journal of Dermatological Science,* **42**(3), pp. 203.

J.G.E.PHILLIPS, 2013-last update, National Physical Laboratory- Properties of organic compounds. [Homepage of National Physical Laboratory], [Online]. Available: http://www.kayelaby.npl.co.uk/chemistry/3_3/3_3.html[27/12, 2013].

JAIN, K.K., 2012. *The Handbook of Nanomedicine.* Springer New York.

JAIN, R., AQIL, M., AHAD, A., ALI, A. and KHAR, R.K., 2008. Basil oil is a promising skin penetration enhancer for transdermal delivery of labetolol hydrochloride. *Drug Development and Industrial Pharmacy,* **34**(4), pp. 384-389.

JAIN, K., KESHARWANI, P., GUPTA, U. and JAIN, N.K., 2010. Dendrimer toxicity: Let's meet the challenge. *International Journal of Pharmaceutics,* **394**(1–2), pp. 122-142.

JANG, W., KAMRUZZAMAN SELIM, K., LEE, C. and KANG, I., 2009. Bioinspired application of dendrimers: from bio-mimicry to biomedical applications. *Progress in Polymer Science,* **34**(1), pp. 1-23.

JAYATHILLAKE, A., MASON, D.F.C. and BROOME, K., 2003. Allergy to chlorhexidine gluconate in urethral gel: report of four cases and reviewof the literature. *Urology,* **61**(4), pp. 837.

JE, J.Y. and KIM, S.K., 2006. Chitosan derivatives killed bacteria by disrupting the outer and inner membrane. *Journal of Agricultural and Food Chemistry,* **54**(18), pp. 6629-6633.

JENNING, V., GYSLER, A., SCHÄFER-KORTING, M. and GOHLA, S.H., 2000. Vitamin A loaded solid lipid nanoparticles for topical use: occlusive properties and drug targeting to the upper skin. *European journal of Pharmaceutics and Biopharmaceutics,* **49**(3), pp. 211-218.

JEVPRASESPHANT, R., PENNY, J., JALAL, R., ATTWOOD, D., MCKEOWN, N. and D'EMANUELE, A., 2003. The influence of surface modification on the cytotoxicity of PAMAM dendrimers. *International Journal of Pharmaceutics,* **252**(1-2), pp. 263-266.

JI, Q.X., ZHAO, Q.S., DENG, J. and LÜ, R., 2010. A novel injectable chlorhexidine thermosensitive hydrogel for periodontal application: preparation, antibacterial activity and toxicity evaluation. *Journal of Materials Science: Materials in Medicine,* **21**(8), pp. 2435-2442.

JOHNSON, P.D.R., MARTIN, R., BURRELL, L.J., GRABSCH, E.A., KIRSA, S.W., O KEEFFE, J., MAYALL, B.C., EDMONDS, D., BARR, W. and BOLGER, C., 2005. Efficacy of an alcohol/chlorhexidine hand hygiene program in a hospital with high rates of nosocomial methicillin-resistant Staphylococcus aureus (MRSA) infection. *Medical Journal of Australia,* **183**(10), pp. 509.

JONES, C.G., 2007. Chlorhexidine: is it still the gold standard? *Periodontology 2000,* **15**(1), pp. 55-62.

JONES, D., 2004. *Pharmaceutical applications of polymers for drug delivery.*15(6) Rapra review, Smithers Rapra Technology. Shropshire, UK.

JONES, D.S., BROWN, A.F., WOOLFSON, A.D., DENNIS, A.C., MATCHETT, L.J. and BELL, S.E., 2000. Examination of the physical state of chlorhexidine within viscoelastic, bioadhesive semisolids using Raman spectroscopy.*Journal of Pharmaceutical Sciences,* **89**(5), pp. 563-571.

JONES, D.S., LORIMER, C.P., MCCOY, C.P. and GORMAN, S.P., 2008. Characterization of the physicochemical, antimicrobial, and drug release properties of thermoresponsive hydrogel copolymers designed for medical device applications. *Journal of Biomedical Materials Research Part B: Applied Biomaterials,* **85**(2), pp. 417-426.

JONES, D.S., WOOLFSON, A.D. and BROWN, A.F., 1997. Textural, viscoelastic and mucoadhesive properties of pharmaceutical gels composed of cellulose polymers. *International Journal of Pharmaceutics,* **151**(2), pp. 223-233.

JONES, M.N., SONG, Y., KASZUBA, M. and REBOIRAS, M.D., 1997. The interaction of phospholipid liposomes with bacteria and their use in the delivery of bactericides. *Journal of Drug Targeting,* **5**(1), pp. 25-34.

JOOSTEN, J.A.F., LOIMARANTA, V., APPELDOORN, C.C.M., HAATAJA, S., EL MAATE, F.A., LISKAMP, R.M.J., FINNE, J. and PIETERS, R.J., 2004. Inhibition of Streptococcus s uis Adhesion by Dendritic Galabiose Compounds at Low Nanomolar Concentration. *Journal of Medicinal Chemistry,* **47**(26), pp. 6499-6508.

JORGE, L.L., FERES, C.C. and TELES, V.E., 2011. Topical preparations for pain relief: efficacy and patient adherence. *Journal of Pain Research,* **4**, pp. 11.

JOSWICK, H.L., CORNER, T.R., SILVERNA.JN and GERHARDT, P., 1971. Antimicrobial Actions of Hexachlorophene - Release of Cytoplasmic Materials. *Journal of Bacteriology,* **108**(1), pp. 492.

JUNGBAUER, F., VAN DER HARST, J., GROOTHOFF, J. and COENRAADS, P., 2004. Skin protection in nursing work: promoting the use of gloves and hand alcohol. *Contact Dermatitis,* **51**(3), pp. 135-140.

KAI, J., SATOH, M. and TSUKIDATE, K., 1999. A new method for preparing electron microscopic specimens of Helicobacter pylori. *Medical Electron Microscopy,* **32**(1), pp. 62-65.

KALAB, M., YANG, A.F. and CHABOT, D., 2008. Conventional Scanning Electron Microscopy of Bacteria. *Infocus Magazine,* (10), pp. 42-61.

KAMPF, G., 2008. What is left to justify the use of chlorhexidine in hand hygiene? *Journal of Hospital Infection,* **70**, pp. 27-34.

KAMPF, G., 2006. Are biofilms relevant for skin disinfection? *Journal of Hospital Infection,* **63**(1), pp. 106-108.

KAMPF, G., JAROSCH, R. and RÜDEN, H., 1998. Limited effectiveness of chlorhexidine based hand disinfectants against methicillin-resistant Staphylococcus aureus (MRSA). *Journal of Hospital Infection,* **38**(4), pp. 297-303.

KAMPF, G., MCDONALD, C. and OSTERMEYER, C., 2005. Bacterial in-use contamination of an alcohol-based hand rub under accelerated test conditions. *The Journal of Hospital Infection,* **59**(3), pp. 271-272.

KAPADIA, B.H., JOHNSON, A.J., DALEY, J.A., ISSA, K. and MONT, M.A., 2013. Pre-admission Cutaneous Chlorhexidine Preparation Reduces Surgical Site Infections In Total Hip Arthroplasty. *The Journal of Arthroplasty,* **28**(3), pp. 490-493.

KARANDE, P., JAIN, A. and MITRAGOTRI, S., 2006. Relationships between skin's electrical impedance and permeability in the presence of chemical enhancers. *Journal of Controlled Release,* **110**(2), pp. 307-313.

KARPANEN, T.J., CONWAY, B.R., WORTHINGTON, T., HILTON, A.C., ELLIOTT, T.S.J. and LAMBERT, P.A., 2010. Enhanced chlorhexidine skin penetration with eucalyptus oil. *BMC Infectious Diseases,* **10**(1), pp. 278.

KARPANEN, T., WORTHINGTON, T., CONWAY, B., HILTON, A., ELLIOTT, T. and LAMBERT, P., 2009. Permeation of chlorhexidine from alcoholic and aqueous solutions within excised human skin. *Antimicrobial Agents and Chemotherapy,* **53**(4), pp. 1717.

KARPANEN, T.J., WORTHINGTON, T., CONWAY, B.R., HILTON, A.C., ELLIOTT, T.S.J. and LAMBERT, P.A., 2008. Penetration of chlorhexidine into human skin. *Antimicrobial Agents and Chemotherapy,* **52**(10), pp. 3633-3636.

KATSU, T., NAKAGAWA, H. and YASUDA, K., 2002. Interaction between polyamines and bacterial outer membranes as investigated with ion-selective electrodes. *Antimicrobial Agents and Chemotherapy,* **46**(4), pp. 1073-1079.

KATSU, T., YOSHIMURA, S. and FUJITA, Y., 1984. Increases in permeability of *Escherichia coli* outer membrane induced by polycations. *FEBS letters,* **166**(1), pp. 175-178.

KAZARIAN, S. and CHAN, A.K., 2013. ATR-FTIR spectroscopic imaging: recent advances and applications to biological systems. *Analyst,* **138,** pp. 1940-1952.

KE, W., ZHAO, Y., HUANG, R., JIANG, C. and PEI, Y., 2007. Enhanced oral bioavailability of doxorubicin in a dendrimer drug delivery system. *Journal of Pharmaceutical Sciences,* **97**(6), pp. 2208-2216.

KEMKEN, J., ZIEGLER, A. and MULLER, B.W., 1992. Influence of Supersaturation on the Pharmacodynamic Effect of Bupranolol After Dermal Administration using Microemulsions as Vehicle. *Pharmaceutical research,* **9**(4), pp. 554-558.

KHAN, M.A. and HOANG, M.Q.,1998. *Film-forming composition containing chlorhexidine gluconate,* US5763412 US patent.

KHAN, R., KAZI, T. and O'DONOHOE, B., 2011. Near fatal intra-operative anaphylaxis to chlorhexidine—is it time to change practice? *BMJ Case Reports 2011*.

KHANKARI, R.K. and GRANT, D.J., 1995. Pharmaceutical hydrates. *Thermochimica Acta,* **248**, pp. 61-79.

KHUNKITTI, W., HANN, A.C., LLOYD, D., FURR, J.R. and RUSSELL, A.D., 1998. Biguanide-induced changes in Acanthamoeba castellanii: an electron microscopic study. *Journal of Applied Microbiology,* **84**(1), pp. 53-62.

KIM, B.S., WON, M., LEE, K.M. and KIM, C.S., 2008. In vitro permeation studies of nanoemulsions containing ketoprofen as a model drug. *Drug Delivery,* **15**(7), pp. 465-469.

KIM, S.H., LEE, H.S., RYU, D.S., CHOI, S.J. and LEE, D.S., 2011. Antibacterial Activity of Silver-nanoparticles Against Staphylococcus aureus and Escherichia coli. *Korean Journal Microbiolology Biotechnology,* **39**(1), pp. 77-85.

KING, M.D., HUMPHREY, B.J., WANG, Y.F., KOURBATOVA, E.V., RAY, S.M. and BLUMBERG, H.M., 2006. Emergence of community-acquired methicillin-resistant Staphylococcus aureus USA 300 clone as the predominant cause of skin and soft-tissue infections. *Annals of Internal Medicine,* **144**(5), pp. 309.

KIREMITÇI, A.S., ÇIFTÇI, A., ÖZALP, M. and GÜMÜŞDERELIOĞLU, M., 2007. Novel chlorhexidine releasing system developed from thermosensitive vinyl ether-based hydrogels. *Journal of Biomedical Materials Research Part B: Applied Biomaterials,* **83**(2), pp. 609-614.

KLAJNERT, B. and EPAND, R., 2005. PAMAM dendrimers and model membranes: Differential scanning calorimetry studies. *International Journal of Pharmaceutics,* **305**(1), pp. 154-166.

KNORR, F., LADEMANN, J., PATZELT, A., STERRY, W., BLUME-PEYTAVI, U. and VOGT, A., 2009. Follicular transport route–Research progress and future perspectives. *European Journal of Pharmaceutics and Biopharmaceutics,***71**(2), pp. 173-180.

KNU, A. and BOEHLAU-GODAU, M., 2000. Spatially confined and temporally resolved refractive index and scattering evaluation in human skin performed with optical coherence tomography. *Journal of Biomedical Optics,* **5**(1), pp. 83-92.

KOCH A.L., 1994. Growth Measurement. In: P.E.A. GERHARDT, ed, *Methods for General and Molecular Bacteriology.* American Society for Microbiology Washington, DC., pp. 248.

KRAFFT, C., STEINER, G., BELEITES, C. and SALZER, R., 2009. Disease recognition by infrared and Raman spectroscopy. *Journal of Biophotonics,* **2**(1-2), pp. 13-28.

KRAMER, A., RUDOLPH, P., KAMPF, G. and PITTET, D., 2002. Limited efficacy of alcohol-based hand gels. *The Lancet,* **359**(9316), pp. 1489-1490.

KRAUTHEIM, A., JERMANN, T. and BIRCHER, A., 2004. Chlorhexidine anaphylaxis: case report and review of the literature. *Contact Dermatitis,* **50**(3), pp. 113-116.

KÜCHLER, S., RADOWSKI, M.R., BLASCHKE, T., DATHE, M., PLENDL, J., HAAG, R., SCHÄFER-KORTING, M. and KRAMER, K.D., 2009. Nanoparticles for skin penetration enhancement–a comparison of a dendritic core-multishell-nanotransporter and solid lipid nanoparticles. *European Journal of Pharmaceutics and Biopharmaceutics,* **71**(2), pp. 243-250.

KUMAR, P.V., ASTHANA, A., DUTTA, T. and JAIN, N.K., 2006. Intracellular macrophage uptake of rifampicin loaded mannosylated dendrimers. *Journal of Drug Targeting,* **14**(8), pp. 546-556.

KUYYAKANOND, T. and QUESNEL, L.B., 1992. The mechanism of action of chlorhexidine. *FEMS Microbiology Letters,* **100**(1), pp. 211-215.

LABIENIEC, M., ULICNA, O., VANCOVA, O., GLOWACKI, R., SEBEKOVA, K., BALD, E., GABRYELAK, T. and WATALA, C., 2008. PAMAM G4 dendrimers lower high glucose but do not improve reduced survival in diabetic rats. *International Journal of Pharmaceutics,* **364**(1), pp. 142-149.

LADEMANN, J., JACOBI, U., SURBER, C., WEIGMANN, H.J. and FLUHR, J., 2009. The tape stripping procedure–evaluation of some critical parameters. *European Journal of Pharmaceutics and Biopharmaceutics,* **72**(2), pp. 317-323.

LADEMANN, J., MEINKE, M., SCHANZER, S., RICHTER, H., DARVIN, M., HAAG, S., FLUHR, J., WEIGMANN, H.J., STERRY, W. and PATZELT, A., 2012. In vivo methods for the analysis of the penetration of topically applied substances in and through the skin barrier. *International Journal of Cosmetic Science,* **34**(6), pp. 551-559.

LADEMANN, J., JACOBI, U., SURBER, C., WEIGMANN, H. and FLUHR, J., 2009. The tape stripping procedure–evaluation of some critical parameters. *European Journal of Pharmaceutics and Biopharmaceutics,* **72**(2), pp. 317-323.

LADEMANN, J., RICHTER, H., TEICHMANN, A., OTBERG, N., BLUME-PEYTAVI, U., LUENGO, J., WEIß, B., SCHAEFER, U.F., LEHR, C. and WEPF, R., 2007. Nanoparticles--an efficient carrier for drug delivery into the hair follicles.*European Journal of Pharmaceutics and Biopharmaceutics: official journal of Arbeitsgemeinschaft fur Pharmazeutische Verfahrenstechnik eV,* **66**(2), pp. 159.

LAFFORGUE, C., CARRET, L., FALSON, F., REVERDY, M. and FRENEY, J., 1997. Percutaneous absorption of a chlorhexidine digluconate solution. *International Journal of Pharmaceutics,* **147**(2), pp. 243-246.

LAGARRIGUE, M., BECKER, M., LAVIGNE, R., DEININGER, S.O., WALCH, A., AUBRY, F., SUCKAU, D. and PINEAU, C., 2011. Revisiting Rat Spermatogenesis with MALDI Imaging at 20-µm Resolution. *Molecular & Cellular Proteomics,***10**(3),.

LAM, Y., CHAN, D.C., RODRIGUEZ, S.Y., LINTAKOON, J.H. and LAM, T., 1993. Sensitive high-performance liquid chromatographic assay for the determination of chlorhexidine in saliva. *Journal of Chromatography B: Biomedical Sciences and Applications,* **612**(1), pp. 166-171.

LAM, Y., CHAN, D.C., RODRIGUEZ, S.Y., LINTAKOON, J.H. and LAM, T., 1993. Sensitive high-performance liquid chromatographic assay for the determination of chlorhexidine in saliva. *Journal of Chromatography B: Biomedical Sciences and Applications,* **612**(1), pp. 166-171.

LAMPE, M.A., BURLINGAME, A., WHITNEY, J., WILLIAMS, M.L., BROWN, B.E., ROITMAN, E. and ELIAS, P.M., 1983. Human stratum corneum lipids: characterization and regional variations. *Journal of Lipid Research,* **24**(2), pp. 120-130.

LARDY, F., VENNAT, B., POUGET, M. and POURRAT, A., 2000. Functionalization of hydrocolloids: Principal component analysis applied to the study of correlations between parameters describing the consistency of hydrogels. *Drug Development and Industrial Pharmacy,* **26**(7), pp. 715-721.

LARSON, E., 1988. Guideline for use of topical antimicrobial agents. *American Journal of Infection Control,* **16**(6), pp. 253-266.

LARSON, E., GIRARD, R., PESSOA-SILVA, C.L., BOYCE, J., DONALDSON, L. and PITTET, D., 2006. Skin reactions related to hand hygiene and selection of hand hygiene products. *American Journal of Infection Control,* **34**(10), pp. 627-635.

LAU, W.M., NG, K.W., SAKENYTE, K. and HEARD, C.M., 2012. Distribution of esterase activity in porcine ear skin; and the effects of freezing and heat separation. *International Journal of Pharmaceutics,* .

LAUER, A.C., LIEB, L.M., RAMACHANDRAN, C., FLYNN, G.L. and WEINER, N.D., 1995. Transfollicular drug delivery. *Pharmaceutical Research,* **12**(2), pp. 179-186.

LAVRIJSEN, A., BOUWSTRA, J., GOORIS, G., WEERHEIM, A., BODDE, H. and PONEC, M., 1995. Reduced Skin Barrier Function Parallels Abnormal Stratum-Corneum Lipid Organization in Patients with Lamellar Ichthyosis. *Journal of Investigative Dermatology,* **105**(4), pp. 619-624.

LBOUTOUNNE, H., CHAULET, J.F., PLOTON, C., FALSON, F. and PIROT, F., 2002. Sustained ex vivo skin antiseptic activity of chlorhexidine in poly (ϵ-caprolactone) nanocapsule encapsulated form and as a digluconate. *Journal of Controlled Release,* **82**(2), pp. 319-334.

LBOUTOUNNE, H., GUILLAUME, Y., MICHEL, L., MAKKI, S., HUMBERT, P. and MILLET, J., 2004. Study and development of encapsulated forms of 4, 5′, 8-Trimethylpsoralen for topical drug delivery. *Drug Development Research,***61**(2), pp. 86-94.

LEE, C.C., MACKAY, J.A., FRÉCHET, J.M.J. and SZOKA, F.C., 2005a. Designing dendrimers for biological applications. *Nature Biotechnology,* **23**(12), pp. 1517-1526.

LEE, D., SPÅNGBERG, L.S., BOK, Y., LEE, C. and KUM, K., 2005b. The sustaining effect of three polymers on the release of chlorhexidine from a controlled release drug device for root canal disinfection. *Oral Surgery, Oral Medicine, Oral Pathology, Oral Radiology, and Endodontology,* **100**(1), pp. 105-111.

LEE, J.W., PARK, J. and PRAUSNITZ, M.R., 2008a. Dissolving microneedles for transdermal drug delivery. *Biomaterials,* **29**(13), pp. 2113-2124.

LEE, J.W., HAN, M. and PARK, J., 2012. Polymer microneedles for transdermal drug delivery. *Journal of Drug Targeting,* (00), pp. 1-13.

LEE, T.G., PARK, J., SHON, H.K., MOON, D.W., CHOI, W.W., LI, K. and CHUNG, J.H., 2008b. Biochemical imaging of tissues by SIMS for biomedical applications. *Applied Surface Science,* **255**(4), pp. 1241-1248.

LEEMHS, A., HARLANMS, R., BREAUDMS, A.R., SPECKMPH, K., PERLMD, T.M., CLARKEPHD, W. and MILSTONEMD, A.M., 2011. Blood concentrations of chlorhexidine in hospitalized children undergoing daily chlorhexidine bathing.*Blood,* **32**(4), pp. 395-397.

LEGENDRE, J., RAULT, I., PETIT, A., LUIJTEN, W., DEMUYNCK, I., HORVATH, S., GINOT, Y. and CUINE, A., 1995. Effects of β-cyclodextrins on skin: implications for the transdermal delivery of piribedil and a novel cognition enhancing-drug, S-9977. *European Journal of Pharmaceutical Sciences,* **3**(6), pp. 311-322.

LEHMANN, R., 2000. Synergism in disinfectant formulation. In: S.S. BLOCK, ed, *Disinfection, sterilization, and preservation.* 5th edn. Lippincott Williams & Wilkins, pp. 465.

LEVANG, A.K., ZHAO, K. and SINGH, J., 1999. Effect of ethanol/propylene glycol on the in vitro percutaneous absorption of aspirin, biophysical changes and macroscopic barrier properties of the skin. *International Journal of Pharmaceutics,* **181**(2), pp. 255-263.

LEYDEN, J.J., MARPLES, R.R. and KLIGMAN, A.M., 2006. Staphylococcus aureus in the lesions of atopic dermatitis. *British Journal of Dermatology,* **90**(5), pp. 525-525.

LEYDON, J.J, MCGINLEY, K., WENSTER, G., 1983. Cutaneous microbiology. In: J. GOLDSMITH, ed, *1. Biochemistry and Physiology of the skin* Volume II edn. New York: Oxford University Press.

LI, J., PIEHLER, L., QIN, D., BAKER JR, J., TOMALIA, D. and MEIER, D., 2000. Visualization and characterization of poly (amidoamine) dendrimers by atomic force microscopy. *Langmuir,* **16**(13), pp. 5613-5616.

LIEB, L.M., RAMACHANDRAN, C., EGBARIA, K. and WEINER, N., 1992. Topical delivery enhancement with multilamellar liposomes into pilosebaceous units: I. In vitro evaluation using fluorescent techniques with the hamster ear model. *Journal of Investigative Dermatology,* **99**(1), pp. 108-113.

LIIPPO, J., KOUSA, P. and LAMMINTAUSTA, K., 2011. The relevance of chlorhexidine contact allergy. *Contact Dermatitis,* **64**(4), pp. 229-234.

LIM, K.-. and KAM, P.C.A., 2008. Chlorhexidine - pharmacology and clinical applications. *Anaesthesia and Intensive Care,* **36**(4), pp. 502-512.

LIN, S., DUAN, K. and LIN, T., 1996. Simultaneous determination of the protein conversion process in porcine stratum corneum after pretreatment with skin enhancers by a combined microscopic FT-IR/DSC system.*Spectrochimica Acta Part A: Molecular and Biomolecular Spectroscopy,* **52**(12), pp. 1671-1678.

LINDEMANN, U., WILKEN, K., WEIGMANN, H.J., SCHAEFER, H., STERRY, W. and LADEMANN, J., 2003. Quantification of the horny layer using tape stripping and microscopic techniques. *Journal of Biomedical Optics,* **8**(4),.

LIU, H., DU, Y., WANG, X. and SUN, L., 2004. Chitosan kills bacteria through cell membrane damage. *International Journal of Food Microbiology,* **95**(2), pp. 147-155.

LIU, J., HU, W., CHEN, H., NI, Q., XU, H. and YANG, X., 2007. Isotretinoin-loaded solid lipid nanoparticles with skin targeting for topical delivery. *International Journal of Pharmaceutics,* **328**(2), pp. 191-195.

LIU, M. and FRÉCHET, J.M.J., 1999. Designing dendrimers for drug delivery. *Pharmaceutical Science & Technology Today,* **2**(10), pp. 393-401.

LIU, Y., BRYANTSEV, V.S., DIALLO, M.S. and GODDARD III, W.A., 2009. PAMAM dendrimers undergo pH responsive conformational changes without swelling. *Journal of the American Chemical Society,* **131**(8), pp. 2798-2799.

LLOYD-LAVERY, A. and REED, J., 2012. A case of chlorhexidine-induced anaphylaxis to mouthwash. *British Journal of Dermatology,* **167**, pp. 143-143.

LÖFFLER, H., DREHER, F. and MAIBACH, H., 2004. Stratum corneum adhesive tape stripping: influence of anatomical site, application pressure, duration and removal. *British Journal of Dermatology,* **151**(4), pp. 746-752.

LOPEZ, A.I., REINS, R.Y., MCDERMOTT, A.M., TRAUTNER, B.W. and CAI, C., 2009. Antibacterial activity and cytotoxicity of PEGylated poly (amidoamine) dendrimers. *Molecular BioSystems,* **5**(10), pp. 1148-1156.

LOTHIAN-TOMALIA, M.K., HEDSTRAND, D.M., TOMALIA, D.A., PADIAS, A.B. and HALL, H., 1997. A contemporary survey of covalent connectivity and complexity. The divergent synthesis of poly (thioether) dendrimers. Amplified, genealogically directed synthesis leading to the de Gennes dense packed state. *Tetrahedron,* **53**(45), pp. 15495-15513.

LOWRY, O.H., ROSEBROUGH, N.J., FARR, A.L. and RANDALL, R.J., 1951. Protein measurement with the Folin phenol reagent. *Journal of biological chemistry,* **193**(1), pp. 265-275.

LU, P., 1986. *Opaque pearlescent films containing dispersed incompatible polymer and polymeric interfacial agent.,* EP 0188123 EU patent.

LUO, Y., KIRKER, K.R. and PRESTWICH, G.D., 2000. Cross-linked hyaluronic acid hydrogel films: new biomaterials for drug delivery. *Journal of Controlled Release,* **69**(1), pp. 169-184.

MA, M., CHENG, Y., XU, Z., XU, P., QU, H., FANG, Y., XU, T. and WEN, L., 2007. Evaluation of polyamidoamine (PAMAM) dendrimers as drug carriers of anti-bacterial drugs using sulfamethoxazole (SMZ) as a model drug.*European Journal of Medicinal Chemistry,* **42**(1), pp. 93-98.

MA, Z., WANG, R., WU, Z., CHEN, D., ZHANG, B., HE, W., WANG, X., LIU, Q., XU, J. and ZHU, H., 2007. Preparation of functional chitosan thermosensitive hydrogel for slow release both rhBMP-2 and chlorhexidine. *Sheng wu gong cheng xue bao = Chinese Journal of Biotechnology,* **23**(6), pp. 1049-54.

MACDONALD, A., DINAH, F., MACKENZIE, D. and WILSON, A., 2004. Performance feedback of hand hygiene, using alcohol gel as the skin decontaminant, reduces the number of inpatients newly affected by MRSA and antibiotic costs. *Journal of Hospital Infection,* **56**(1), pp. 56-63.

MAGHRABY, G.M.E., WILLIAMS, A.C. and BARRY, B.W., 2001. Skin delivery of 5-fluorouracil from ultradeformable and standard liposomes in-vitro. *Journal of Pharmacy and Pharmacology,* **53**(8), pp. 1069-1077.

MAINS, J., WILSON, C. and URQUHART, A., 2011. ToF-SIMS analysis of ocular tissues reveals biochemical differentiation and drug distribution. *European Journal of Pharmaceutics and Biopharmaceutics,* **79**(2), pp. 328-333.

MAITI, P.K., CAGIN, T., WANG, G. and GODDARD III, W.A., 2004. Structure of PAMAM dendrimers: Generations 1 through 11. *Macromolecules,* **37**(16), pp. 6236-6254.

MAIWALD, M., 2008. Alcohol-based hand hygiene and nosocomial infection rates. *Alcohol,* **29**(6), pp. 579-580.

MALIK, N., WIWATTANAPATAPEE, R., KLOPSCH, R., LORENZ, K., FREY, H., WEENER, J.W., MEIJER, E.W., PAULUS, W. and DUNCAN, R., 2000. Dendrimers:: Relationship between structure and biocompatibility in vitro, and preliminary studies on the biodistribution of 125I-labelled polyamidoamine dendrimers in vivo. *Journal of Controlled Release,* **65**(1–2), pp. 133-148.

MALMBERG, P., JENNISCHE, E., NILSSON, D. and NYGREN, H., 2011. High-resolution, imaging TOF-SIMS: novel applications in medical research. *Analytical and Bioanalytical Chemistry,* **399**(8), pp. 2711-2718.

MAMMEN, M., CHOI, S.K. and WHITESIDES, G.M., 1998. Polyvalent interactions in biological systems: implications for design and use of multivalent ligands and inhibitors. *Angewandte Chemie International Edition,* **37**(20), pp. 2754-2794.

MAO-QIANG, M., ELIAS, P.M. and FEINGOLD, K.R., 1993. Fatty acids are required for epidermal permeability barrier function. *Journal of Clinical Investigation,* **92**(2), pp. 791.

MAPLE, P., HAMILTON-MILLER, J. and BRUMFITT, W., 1992. Comparison of the in-vitro activities of the topical antimicrobials azelaic acid, nitrofurazone, silver sulphadiazine and mupirocin against methicillin-resistant Staphylococcus aureus. *Journal of Antimicrobial Chemotherapy,* **29**(6), pp. 661-668.

MARKS, R., 2004. The stratum corneum barrier: the final frontier. *The Journal of Nutrition,* **134**(8), pp. 2017-2021.

MARTTIN, E., NEELISSENSUBNEL, M.T.A., DEHAAN, F.H.N. and BODDE, H.E., 1996. A critical comparison of methods to quantify stratum corneum removed by tape stripping. *Skin Pharmacology,* **9**(1), pp. 69-77.

MCCARTHY, T.D., KARELLAS, P., HENDERSON, S.A., GIANNIS, M., O'KEEFE, D.F., HEERY, G., PAULL, J.R.A., MATTHEWS, B.R. and HOLAN, G., 2005. Dendrimers as drugs: discovery and preclinical and clinical development of dendrimer-based microbicides for HIV and STI prevention. *Molecular.Pharmacology,* **2**(4), pp. 312-318.

MEHNERT, W. and MÄDER, K., 2001. Solid lipid nanoparticles: production, characterization and applications. *Advanced Drug Delivery Reviews,* **47**(2), pp. 165-196.

MEIDAN, V.M., BONNER, M.C. and MICHNIAK, B.B., 2005. Transfollicular drug delivery—is it a reality? *International Journal of Pharmaceutics,* **306**(1), pp. 1-14.

MENDELSOHN, R., REREK, M.E. and MOORE, D.J., 2000. Infrared spectroscopy and microscopic imaging of stratum corneum models and skin. Invited Lecture. *Phys.Chem.Chem.Phys.,* **2**(20), pp. 4651-4657.

MENDELSOHN, R., FLACH, C.R. and MOORE, D.J., 2006. Determination of molecular conformation and permeation in skin via IR spectroscopy, microscopy, and imaging. *Biochimica Et Biophysica Acta-Biomembranes,* **1758**(7), pp. 923-933.

MEYER, W. and ZSCHEMISCH, N., 2002. Skin layer thickness at the ear of the domesticated pig, with special reference to the use of the ear integument for human dermatological research. *Berl Munch Tierarztl Wochenschr,***115**, pp. 401-406.

MEYERS, S.R., JUHN, F.S., GRISET, A.P., LUMAN, N.R. and GRINSTAFF, M.W., 2008. Anionic amphiphilic dendrimers as antibacterial agents. *Journal of the American Chemical Society,* **130**(44), pp. 1444-1445.

MEZEI, M. and GULASEKHARAM, V., 1980. Liposomes-a selective drug delivery system for the topical route of administration I. Lotion dosage form. *Life Sciences,* **26**(18), pp. 1473-1477.

MILHEM, O., MYLES, C., MCKEOWN, N., ATTWOOD, D. and D'EMANUELE, A., 2000. Polyamidoamine Starburst® dendrimers as solubility enhancers. *International Journal of Pharmaceutics,* **197**(1), pp. 239-241.

MILLER, L.G., QUAN, C., SHAY, A., MOSTAFAIE, K., BHARADWA, K., TAN, N., MATAYOSHI, K., CRONIN, J., TAN, J. and TAGUDAR, G., 2007. A prospective investigation of outcomes after hospital discharge for endemic, community-acquired methicillin-resistant and-susceptible Staphylococcus aureus skin infection. *Clinical Infectious diseases,* **44**(4), pp. 483-492.

MILSTONE, A.M., PASSARETTI, C.L. and PERL, T.M., 2008. Chlorhexidine: Expanding the armamentarium for infection control and prevention. *Clinical Infectious Diseases,* **46**(2), pp. 274-281.

MINNOCK, A., VERNON, D.I., SCHOFIELD, J., GRIFFITHS, J., PARISH, J.H. and BROWN, S.B., 2000. Mechanism of Uptake of a Cationic Water-Soluble Pyridinium Zinc Phthalocyanine across the Outer Membrane ofEscherichia coli.*Antimicrobial Agents and Chemotherapy,* **44**(3), pp. 522-527.

MINTZER, M.A., DANE, E.L., O'TOOLE, G.A. and GRINSTAFF, M.W., 2011. Exploiting Dendrimer Multivalency To Combat Emerging and Re-Emerging Infectious Diseases. *Molecular Pharmaceutics,* **9**(3), pp. 342-354.

MIYAZAKI, S., TAKAHASHI, A., KUBO, W., BACHYNSKY, J. and LÖBENBERG, R., 2003. Poly n-butylcyanoacrylate (PNBCA) nanocapsules as a carrier for NSAIDs: in vitro release and in vivo skin penetration. *Journal of Pharmaceutical Science,* **6**(2), pp. 238-245.

MODAK, S.M. and SAMPATH, L.A., 2007. *Antimicrobial Medical Devices Containing Chlorhexidine Free Base And Salt,* EP1343547, EU patent .

MOORE, D.J., REREK, M.E. and MENDELSOHN, R., 2001. Role of ceramides 2 and 5 in the structure of the stratum corneum lipid barrier. *International Journal of Cosmetic Science,* **21**(5), pp. 353-368.

MOORE, D.J. and REREK, M.E., 2000. Insights into the molecular organization of lipids in the skin barrier from infrared spectroscopy studies of stratum corneum lipid models. *Acta Dermato Venereologica-Supplement,* (208), pp. 16-22.

MOORE, M. and KHANNA, R., 1991. Infrared and mass spectral studies of proton irradiated H< sub> 2</sub> O CO< sub> 2</sub> ice: Evidence for carbonic acid. *Spectrochimica Acta Part A: Molecular Spectroscopy,* **47**(2), pp. 255-262.

MORGAN, M.T., NAKANISHI, Y., KROLL, D.J., GRISET, A.P., CARNAHAN, M.A., WATHIER, M., OBERLIES, N.H., MANIKUMAR, G., WANI, M.C. and GRINSTAFF, M.W., 2006. Dendrimer-encapsulated camptothecins: increased solubility, cellular uptake, and cellular retention affords enhanced anticancer activity in vitro. *Cancer Research,* **66**(24), pp. 11913-11921.

MORONES, J.R., ELECHIGUERRA, J.L., CAMACHO, A., HOLT, K., KOURI, J.B., RAMÍREZ, J.T. and YACAMAN, M.J., 2005. The bactericidal effect of silver nanoparticles. *Nanotechnology,* **16**(10), pp. 2346.

MORRIS, A.P., BRAIN, K.R. and HEARD, C.M., 2009. Skin permeation and ex vivo skin metabolism of O-acyl haloperidol ester prodrugs. *International Journal of Pharmaceutics,* **367**(1–2), pp. 44-50.

MORRISON, F.A., 2001. *Understanding rheology.* Oxford University Press, USA.

MUKHERJEE, S.P. and BYRNE, H.J., 2012. Polyamidoamine Dendrimer Nanoparticle Cytotoxicity, Oxidative Stress, Caspase Activation and Inflammatory Response: Experimental Observation and Numerical Simulation.*Nanomedicine: Nanotechnology, Biology and Medicine,*9**(2)**, pp.202-211.

MÜLLER, R.H., RADTKE, M. and WISSING, S.A., 2002. Solid lipid nanoparticles (SLN) and nanostructured lipid carriers (NLC) in cosmetic and dermatological preparations. *Advanced Drug Delivery Reviews,* **54, Supplement**(0), pp. 131-155.

MUSIAL, W., VONCINA, B., PLUTA, J. and KOKOL, V., 2012. The Study of Release of Chlorhexidine from Preparations with Modified Thermosensitive Poly-N-isopropylacrylamide Microspheres. *The Scientific World Journal,* **2012**.

MYER, K.A., DREHER, F., PELOSI, A., MIO, K., BERARDESCA, E. and MAIBACH, H.I.,2012. Adhesive tape stripping reveals differences in stratum corneum cohesion between Caucasians, Blacks, and Hispanics as a function of age. In: Dermatotoxicology 8th edn. Ed. Farage and Maibach CRC Press, New York.

NAIK, A., KALIA, Y.N., GUY, R.H. and FESSI, H., 2004. Enhancement of topical delivery from biodegradable nanoparticles. *Pharmaceutical Research,* **21**(10), pp. 1818-1825.

N'DRI-STEMPFER, B., NAVIDI, W.C., GUY, R.H. and BUNGE, A.L., 2009. Improved Bioequivalence Assessment of Topical Dermatological Drug Products Using Dermatopharmacokinetics. *Pharmaceutical Research,* **26**(2), pp.316-328.

NETZLAFF, F., KOSTKA, K.H., LEHR, C.M. and SCHAEFER, U.F., 2006. TEWL measurements as a routine method for evaluating the integrity of epidermis sheets in static Franz type diffusion cells in vitro. Limitations shown by transport data testing. *European Journal of Pharmaceutics and Biopharmaceutics,* **63**(1), pp. 44-50.

NEWMAN, J.L. and SEITZ, J.C., 1990. Intermittent use of an antimicrobial hand gel for reducing soap-induced irritation of health care personnel. *American Journal of Infection Control,* **18**(3), pp. 194-200.

NHUNG, D.T.T., FREYDIERE, A., CONSTANT, H., FALSON, F. and PIROT, F., 2007. Sustained antibacterial effect of a hand rub gel incorporating chlorhexdine-loaded nanocapsules (Nanochlorex®). *International Journal of Pharmaceutics,* **334**(1), pp. 166-172.

NIKAIDO, H., 1996. Multidrug efflux pumps of gram-negative bacteria. *Journal of Bacteriology,* **178**(20), pp. 5853.

NISHIOKA, K. and KATAYAMA, I., 2006. Histamine release in contact urticaria. *Contact Dermatitis,* **11**(3), pp. 191-191.

NORLÉN, L., NICANDER, I., ROZELL, B.L., OLLMAR, S. and FORSLIND, B., 1999. Inter-and intra-individual differences in human stratum corneum lipid content related to physical parameters of skin barrier function in vivo.*Journal of Investigative Dermatology,* **112**(1), pp. 72-77.

NYGREN, H., BORNER, K., HAGENHOFF, B., MALMBERG, P. and MANSSON, J.E., 2005. Localization of cholesterol, phosphocholine and galactosylceramide in rat cerebellar cortex with imaging TOF-SIMS equipped with a bismuth cluster ion source. *Biochimica Et Biophysica Acta-Molecular and Cell Biology of Lipids,* **1737**(2-3), pp. 102-110.

OCHOA, M., MOUSOULIS, C. and ZIAIE, B., 2012. Polymeric microdevices for transdermal and subcutaneous drug delivery. *Advanced Drug Delivery Reviews,* **64**(14), pp. 1603-1616.

ODORE, R., VALLE, V.C. and RE, G., 2000. Efficacy of chlorhexidine against some strains of cultured and clinically isolated microorganisms. *Veterinary Research Communications,* **24**(4), pp. 229-238.

OECD ORGANISATION FOR ECONOMIC CO-OPERATION AND DEVELOPMENT, 2004. *Guidance Document No. 28: The Conduct of Skin Absorption Studies.* Paris, France.

OECD. PUBLISHING, 2008. *OECD Science, Technology and Industry Outlook 2008.* Organisation for Economic Co-operation and Development.

OGASE, H., NAGAI, I., KAMEDA, K., KUME, S. and ONO, S., 1992. Identification and quantitative analysis of degradation products of chlorhexidine with chlorhexidine-resistant bacteria with three-dimensional high performance liquid chromatography. *Journal of Applied Microbiology,* **73**(1), pp. 71-78.

OHMAN, H. and VAHLQUIST, A., 1994. In vivo studies concerning a pH gradient in human stratum corneum and upper epidermis. *Acta Dermato-Venereologica,* **74**(5), pp. 375.

OKAMOTO, M., TANJI, N., KATAYAMA, Y. and OKADA, J., 2006. TOF-SIMS investigation of the distribution of a cosmetic ingredient in the epidermis of the skin. *Applied Surface Science,* **252**(19), pp. 6805-6808.

OKANO, M., NOMURA, M., HATA, S., OKADA, N., SATO, K., KITANO, Y., TASHIRO, M., YOSHIMOTO, Y., HAMA, R. and AOKI, T., 1989. Anaphylactic symptoms due to chlorhexidine gluconate. *Archives of Dermatology,* **125**(1), pp. 50.

ORAFIDIYA, L.O., OYEDELE, A., SHITTU, A. and ELUJOBA, A., 2001. The formulation of an effective topical antibacterial product containing Ocimum gratissimum leaf essential oil. *International Journal of Pharmaceutics,* **224**(1-2), pp. 177-183.

OSSWALD, T., 1998. *Polymer processing fundamentals.* Hanser Verlag. Munich, Germany.

PANCHAGNULA, R., BOKALIAL, R., SHARMA, P. and KHANDAVILLI, S., 2005. Transdermal delivery of naloxone: skin permeation, pharmacokinetic, irritancy and stability studies. *International Journal of Pharmaceutics,* **293**(1), pp. 213-223.

PARADKAR, A., KELLY, A., COATES, P. and YORK, P., 2009. Shear and extensional rheology of hydroxypropyl cellulose melt using capillary rheometry. *Journal of Pharmaceutical and Biomedical Analysis,* **49**(2), pp. 304-310.

PARDEIKE, J., HOMMOSS, A. and MÜLLER, R.H., 2009. Lipid nanoparticles (SLN, NLC) in cosmetic and pharmaceutical dermal products. *International Journal of Pharmaceutics,* **366**(1), pp. 170-184.

PARK, J., ALLEN, M.G. and PRAUSNITZ, M.R., 2005. Biodegradable polymer microneedles: fabrication, mechanics and transdermal drug delivery. *Journal of Controlled Release,* **104**(1), pp. 51-66.

PATEL, G.K. and FINLAY, A.Y., 2003. Staphylococcal scalded skin syndrome: diagnosis and management. *American Journal of Clinical Dermatology,* **4**(3), pp. 165-175.

PATRI, A.K., MAJOROS, I.J. and BAKER, J.R., 2002. Dendritic polymer macromolecular carriers for drug delivery. *Current opinion in chemical biology,* **6**(4), pp. 466-471.

PAULSON, D.S., 2002. *Handbook of Topical Antimicrobials: Industrial Applications in Consumer Products and Pharmaceuticals.* CRC Press, New York.

PELLETT, M., DAVIS, A. and HADGRAFT, J., 1994. Effect of supersaturation on membrane transport: 2. Piroxicam. *International Journal of Pharmaceutics,* **111**(1), pp. 1-6.

PELLETT, M.A., CASTELLANO, S., HADGRAFT, J. and DAVIS, A.F., 1997. The penetration of supersaturated solutions of piroxicam across silicone membranes and human skin in vitro. *Journal of Controlled Release,* **46**(3), pp. 205-214.

PERRIN, J. and WITZKE, E., 1971. The aggregation of chlorhexidine digluconate in aqueous solution from optical rotatory dispersion measurements. *Journal of Pharmacy and Pharmacology,* **23**(1), pp. 76-77.

PETERSON, G.L., 1977. A simplification of the protein assay method of Lowry et al. which is more generally applicable. *Analytical Biochemistry,* **83**, pp. 346-356.

PETERSON, J., ALLIKMAA, V., SUBBI, J., PEHK, T. and LOPP, M., 2003. Structural deviations in poly (amidoamine) dendrimers: a MALDI-TOF MS analysis. *European Polymer Journal,* **39**(1), pp. 33-42.

PETERSON, J., EBBER, A., ALLIKMAA, V. and LOPP, M., 2001. Synthesis and CZE analysis of PAMAM dendrimers with an ethylenediamine core, *Proceedings-Estonian Academy of Sciences Chemistry* 2001, TRUEKITUD OU, pp. 156-166.

PETERSON, J., ALLIKMAA, V., SUBBI, J., PEHK, T. and LOPP, M., 2003. Structural deviations in poly (amidoamine) dendrimers: a MALDI-TOF MS analysis. *European Polymer Journal,* **39**(1), pp. 33-42.

PIANTADOSI, C. and SMART, R.S.C., 2002. Statistical comparison of hydrophobic and hydrophilic species on galena and pyrite particles in flotation concentrates and tails from TOF-SIMS evidence. *International Journal of Mineral Processing,* **64**(1), pp. 43-54.

PIERS, K.L., BROWN, M.H. and HANCOCK, R., 1994. Improvement of outer membrane-permeabilizing and lipopolysaccharide-binding activities of an antimicrobial cationic peptide by C-terminal modification. *Antimicrobial Agents and Chemotherapy,* **38**(10), pp. 2311-2316.

PIETSCH, H., 2001. Hand antiseptics: rubs versus scrubs, alcoholic solutions versus alcoholic gels. *Journal of Hospital Infection,* **48**, pp. S33-S36.

PIROT, F., KALIA, Y.N., STINCHCOMB, A.L., KEATING, G., BUNGE, A. and GUY, R.H., 1997. Characterization of the permeability barrier of human skin in vivo. *Proceedings of the National Academy of Sciences,* **94**(4), pp. 1562-1567.

PITTET, D., HUGONNET, S., HARBARTH, S., MOUROUGA, P., SAUVAN, V., TOUVENEAU, S. and PERNEGER, T.V., 2000. Effectiveness of a hospital-wide programme to improve compliance with hand hygiene. *Lancet,* **356**(9238), pp. 1307-1312.

PIWOWAR, A., FLETCHER, J., LOCKYER, N. and VICKERMAN, J., 2011. Top-down approach to studying biological components using ToF-SIMS. *Surface and Interface Analysis,* **43**(1-2), pp. 265-268.

POTTS, R.O. and GUY, R.H., 1992. Predicting skin permeability. *Pharmaceutical Research,* **9**(5), pp. 663-669.

PRATT, R., HOFFMAN, P. and ROBB, F., 2005. The need for skin preparation prior to injection: point—counterpoint. *British Journal of Infection Control,* **6**(4), pp. 18-20.

PRAUSNITZ, M.R. and LANGER, R., 2008. Transdermal drug delivery. *Nature Biotechnology,* **26**(11), pp. 1261-1268.

PRAUSNITZ, M.R., MITRAGOTRI, S. and LANGER, R., 2004. Current status and future potential of transdermal drug delivery. *Nature Reviews Drug Discovery,* **3**(2), pp. 115-124.

PRESTIDGE, C.A., BARNES, T.J. and SKINNER, W., 2010. Time-of-flight secondary-ion mass spectrometry for the surface characterization of solid-state pharmaceuticals. *Journal of Pharmacy and Pharmacology,* **59**(2), pp. 251-259.

PROW, T.W., GRICE, J.E., LIN, L.L., FAYE, R., BUTLER, M., BECKER, W., WURM, E.M., YOONG, C., ROBERTSON, T.A. and SOYER, H.P., 2011. Nanoparticles and microparticles for skin drug delivery. *Advanced Drug Delivery Reviews,***63**(6), pp. 470-491.

RAGHAVAN, S.L., TRIVIDIC, A., DAVIS, A.F. and HADGRAFT, J., 2000. Effect of cellulose polymers on supersaturation and in vitro membrane transport of hydrocortisone acetate. *International Journal of Pharmaceutics,* **193**(2), pp. 231-237.

RAJAN, S., 2012. Skin and soft-tissue infections: Classifying and treating a spectrum. *Cleveland Clinic Journal of Medicine,* **79**(1), pp. 57-66.

RANGANATHAN, N., 1996. Chlorhexidine. *Handbook of disinfectants and antiseptics.New York, Marcel Dekker,* pp. 235-264.

RASTOGI, R., ANAND, S. and KOUL, V., 2009. Flexible polymerosomes—An alternative vehicle for topical delivery. *Colloids and Surfaces B: Biointerfaces,* **72**(1), pp. 161-166.

REDDY, M.B., STINCHCOMB, A.L., GUY, R.H. and BUNGE, A.L., 2002. Determining dermal absorption parameters in vivo from tape strip data. *Pharmaceutical Research,* **19**(3), pp. 292-298.

REDDY, M.B., GUY, R.H. and BUNGE, A.L., 2000. Does epidermal turnover reduce percutaneous penetration? *Pharmaceutical Research,* **17**(11), pp. 1414-1419.

REINERTSON, R.P. and WHEATLEY, V.R., 1959. Studies on the chemical composition of human epidermal lipids. *The Journal of Investigative Dermatology,* **32**(1), pp. 49-59.

RELLER, L.B., SCHOENKNECHT, F.D., KENNY, M.A. and SHERRIS, J.C., 1974. Antibiotic susceptibility testing of Pseudomonas aeruginosa: selection of a control strain and criteria for magnesium and calcium content in media.*Journal of Infectious Diseases,* **130**(5), pp. 454-463.

RENNIE, R., 2001. *M32-P Evaluation of lots of Mueller Hinton broth for antimicrobial susceptibility testing; proposed guideline.* first edn. USA: Clinical and Laboratory Standards Institute.

REYBROUCK, G., 1986. Handwashing and hand disinfection. *The Journal of Hospital Infection,* **8**(1), pp. 5.

REYNOLDS, S.A., LEVY, F. and WALKER, E.S., 2006. Hand sanitizer alert. *Emerging Infectious Diseases,* **12**(3), pp. 527.

RICE, L.B., 2009. The clinical consequences of antimicrobial resistance. *Current Opinion in Microbiology,* **12**(5), pp. 476-481.

RIGG, P.C. and BARRY, B.W., 1990. Shed snake skin and hairless mouse skin as model membranes for human skin during permeation studies. *Journal of Investigative Dermatology,* **94**(2), pp. 235-240.

RIGGS, P., BRADEN, M. and PATEL, M., 2000. Chlorhexidine release from room temperature polymerising methacrylate systems. *Biomaterials,* **21**(4), pp. 345-351.

ROBERTS, J.C., BHALGAT, M.K. and ZERA, R.T., 1996. Preliminary biological evaluation of polyamidoamine (PAMAM) StarburstTM dendrimers. *Journal of Biomedical Materials Research,* **30**(1), pp. 53-65.

ROBERTS, M. and WALKER, M., 1993. Water. The most natural penetration enhancer. *Drugs and the Pharmaceutical Sciences,* **59**, pp. 1-30.

ROTHMAN, S., 1954. Physiology and biochemistry of the skin, University of Chicago Press. Chicago, USA.

SAAR, B.G., CONTRERAS-ROJAS, L.R., XIE, X.S. and GUY, R.H., 2011. Imaging Drug Delivery to Skin with Stimulated Raman Scattering Microscopy. *Molecular Pharmaceutics,* **8**(3), pp. 969-975.

SAJJA, H.K., EAST, M.P., MAO, H., WANG, A.Y., NIE, S. and YANG, L., 2009. Development of Multifunctional Nanoparticles for Targeted Drug Delivery and Non-invasive Imaging of Therapeutic Effect. *Current Drug Discovery Technologies,* **6**(1), pp. 43.

SAKEENA, M., FA, M., ZA, G., MM, K., AS, M. and MN, A., 2010. Formulation and in vitro evaluation of ketoprofen in palm oil esters nanoemulsion for topical delivery. *Journal of Oleo Science,* **59**(4), pp. 223-228.

SALAMI, A.A., IMOSEMI, I.O., OWOEYE, O.O., SALAMI, A., IMOSEMI, I. and OWOEYE, O., 2006. A comparison of the effect of chlorhexidine, tap water and normal saline on healing wounds. *International Journal of Morphology,* **24**(4), pp. 673-676.

SALMINEN, A., LOIMARANTA, V., JOOSTEN, J.A.F., KHAN, A.S., HACKER, J., PIETERS, R.J. and FINNE, J., 2007. Inhibition of P-fimbriated Escherichia coli adhesion by multivalent galabiose derivatives studied by a live-bacteria application of surface plasmon resonance. *Journal of Antimicrobial Chemotherapy,* **60**(3), pp. 495-501.

SAMAD, A., SULTANA, Y. and AQIL, M., 2007. Liposomal drug delivery systems: an update review. *Current Drug Delivery,* **4**(4), pp. 297-305.

SAMIEY, B. and ASHOORI, F., 2012. Adsorptive removal of methylene blue by agar: effects of NaCl and ethanol. *Chemistry Central Journal,* **6**(1), pp. 14.

SAND, M., GAMBICHLER, T., MOUSSA, G., BECHARA, F., SAND, D., ALTMEYER, P. and HOFFMANN, K., 2006. Evaluation of the epidermal refractive index measured by optical coherence tomography. *Skin Research and Technology,***12**(2), pp. 114-118.

SARKER, D.K., 2005. Engineering of nanoemulsions for drug delivery. *Current Drug Delivery,* **2**(4), pp. 297-310.

SATO, J., DENDA, M., NAKANISHI, J., NOMURA, J. and KOYAMA, J., 1998. Cholesterol sulfate inhibits proteases that are involved in desquamation of stratum corneum. *Journal of Investigative Dermatology,* **111**(2), pp. 189-193.

SCHMID-WENDTNER, M. and KORTING, H., 2007. *pH and skin care.* ABW Wissenschaftsverlag, Berlin, Germany. pp. 15-25.

SCHMOOK, F.P., MEINGASSNER, J.G. and BILLICH, A., 2001. Comparison of human skin or epidermis models with human and animal skin in in-vitro percutaneous absorption. *International Journal of Pharmaceutics,* **215**(1), pp. 51-56.

SCHREIER, H. and BOUWSTRA, J., 1994. Liposomes and niosomes as topical drug carriers: dermal and transdermal drug delivery. *Journal of Controlled Release,* **30**(1), pp. 1-15.

SCHUELER, B.W., 1992. Microscope imaging by time-of-flight secondary ion mass spectrometry. *Microscopy Microanalysis Microstructures,* **3**, pp. 119-119.

SCHURER, N. and ELIAS, P., 1991. The biochemistry and function of stratum corneum lipids. *Advances in Lipid Research,* **24**, pp. 27.

SCHWARB, F., GABARD, B., RUFLI, T. and SURBER, C., 1999. Percutaneous absorption of salicylic acid in man after topical administration of three different formulations. *Dermatology,* **198**(1), pp. 44-51.

SCOTT, R.C. and CLOWES, H.M., 1992. In vitro percutaneous absorption experiments: a guide to the technique for use in toxicology assessments. *Toxicology Mechanisms and Methods,* **2**(2), pp. 113-123.

SCOTT, R.C., DUGARD, P.H., RAMSEY, J.D. and RHODES, C., 1987. In vitro absorption of some o-phthalate diesters through human and rat skin. *Environmental Health Perspectives,* **74**, pp. 223.

SEED, B., 2001. Silanizing glassware. *Current Protocols in Immunology,* pp. A. 3K.1-A. 3K.2.

SELWYN, S. and ELLIS, H., 1972. Skin Bacteria and Skin Disinfection Reconsidered. *British medical Journal,* **1**(5793), pp. 136-&.

ŞENEL, S., IKINCI, G., KAŞ, S., YOUSEFI-RAD, A., SARGON, M. and HINCAL, A., 2000. Chitosan films and hydrogels of chlorhexidine gluconate for oral mucosal delivery. *International Journal of Pharmaceutics,* **193**(2), pp. 197-203.

SHABALA, L., ROSS, T., NEWMAN, I., MCMEEKIN, T. and SHABALA, S., 2001. Measurements of net fluxes and extracellular changes of H+, Ca2+, K+, and NH4+ in Escherichia coli using ion-selective microelectrodes. *Journal of Microbiological Methods,* **46**(2), pp. 119-129.

SHAFIULLAH, D., 2005. *Formulation and evaluation of chlorhexidine mucoadhesive drug delivery systems*, Rajiv Gandhi University of Health Sciences.

SHAH, P., BHALODIA, D. and SHELAT, P., 2010. Nanoemulsion: a pharmaceutical review. *Systematic Reviews in Pharmacy,* **1**(1), pp. 24.

SHAKEEL, F., BABOOTA, S., AHUJA, A., ALI, J. and SHAFIQ, S., 2008. Skin permeation mechanism and bioavailability enhancement of celecoxib from transdermally applied nanoemulsion. *Journal of Nanobiotechnology,* **6**(8).

SHAKEEL, F., BABOOTA, S., AHUJA, A., ALI, J., AQIL, M. and SHAFIQ, S., 2007. Nanoemulsions as vehicles for transdermal delivery of aceclofenac. *AAPS Pharmaceutical Science and Technology,* **8**(4), pp. 191-199.

SHAKEEL, F. and RAMADAN, W., 2010. Transdermal delivery of anticancer drug caffeine from water-in-oil nanoemulsions. *Colloids and Surfaces B: Biointerfaces,* **75**(1), pp. 356-362.

SHAKHBAZAU, A., ISAYENKA, I., KARTEL, N., GONCHAROVA, N., SEVIARYN, I., KOSMACHEVA, S., POTAPNEV, M., SHCHARBIN, D. and BRYSZEWSKA, M., 2010. Transfection efficiencies of PAMAM dendrimers correlate inversely with their hydrophobicity. *International Journal of Pharmaceutics,* **383**(1), pp. 228-235.

SHCHARBIN, D., DRAPEZA, A., LOBAN, V., LISICHENOK, A. and BRYSZEWSKA, M., 2006. The breakdown of bilayer lipid membranes by dendrimers. *Cellular & Molecular Biology Letters,* **11**(2), pp. 242-248.

SHIM, E.K., BARNETTE, D., HUGHES, K. and GREENWAY, H.T., 2001. Microdermabrasion: a clinical and histopathologic study. *Dermatologic Surgery,* **27**(6), pp. 524-530.

SHOCKMAN, G.D. and BARREN, J., 1983. Structure, function, and assembly of cell walls of gram-positive bacteria. *Annual Reviews in Microbiology,* **37**(1), pp. 501-527.

SIDDIQUI, O., ROBERTS, M. and POLACK, A., 1989. Percutaneous absorption of steroids: relative contributions of epidermal penetration and dermal clearance. *Journal of Pharmacokinetics and Pharmacodynamics,* **17**(4), pp. 405-424.

SILHAVY, T.J., KAHNE, D. and WALKER, S., 2010. The bacterial cell envelope. *Cold Spring Harbor perspectives in biology,* **2**(5),.

SILVESTRO, L., WEISER, J.N. and AXELSEN, P.H., 2000. Antibacterial and antimembrane activities of cecropin A in Escherichia coli. *Antimicrobial Agents and Chemotherapy,* **44**(3), pp. 602-607.

SMITH, J. and IRWIN, W., 2000. Ionisation and the effect of absorption enhancers on transport of salicylic acid through silastic rubber and human skin. *International Journal of Pharmaceutics,* **210**(1-2), pp. 69-82.

SOBEL, J.D., HASHMAN, N., REINHERZ, G. and MERZBACH, D., 1982. Nosocomial Pseudomonas cepacia infection associated with chlorhexidine contamination. *The American Journal of Medicine,* **73**(2), pp. 183-186.

SODHI, R.N.S., 2004. Time-of-flight secondary ion mass spectrometry (TOF-SIMS): versatility in chemical and imaging surface analysis. *Analyst,* **129**(6), pp. 483-487.

SÖZGEN, K., CEKIC, S.D., TÜTEM, E. and APAK, R., 2006. Spectrophotometric total protein assay with copper(II)–neocuproine reagent in alkaline medium. *Talanta,* **68**(5), pp. 1601-1609.

STEVENS, D.L., BISNO, A.L., CHAMBERS, H.F., EVERETT, E.D., DELLINGER, P., GOLDSTEIN, E.J., GORBACH, S.L., HIRSCHMANN, J.V., KAPLAN, E.L. and MONTOYA, J.G., 2005. Practice guidelines for the diagnosis and management of skin and soft-tissue infections. *Clinical Infectious Diseases,* **41**(10), pp. 1373-1406.

STONE, C.A., WRIGHT, H., DEVARAJ, V.S., CLARKE, T. and POWELL, R., 2000. Healing at skin graft donor sites dressed with chitosan. *British Journal of Plastic Surgery,* **53**(7), pp. 601-606.

STOUGHTON, R., 1989. Percutaneous absorption of drugs. *Annual Review of Pharmacology and Toxicology,* **29**(1), pp. 55-69.

STRYDOM, S.J., ROSE, W.E., OTTO, D.P., LIEBENBERG, W. and DE VILLIERS, M.M., 2012. Poly (amidoamine) dendrimer-mediated synthesis and stabilization of silver sulfonamide nanoparticles with increased antibacterial activity. *Nanomedicine: Nanotechnology, Biology and Medicine,*9(1), pp. 85-93.

STULBERG, D.L., PENROD, M.A. and BLATNY, R.A., 2002. Common bacterial skin infections. *American Family Physician,* **66**(1), pp. 119-128.

SUCI, P.A., GEESEY, G.G. and TYLER, B.J., 2001. Integration of Raman microscopy, differential interference contrast microscopy, and attenuated total reflection Fourier transform infrared spectroscopy to investigate chlorhexidine spatial and temporal distribution in< i> Candida albicans</i> biofilms. *Journal of Microbiological Methods,* **46**(3), pp. 193-208.

SULEA, D., ALBU, M.G., GHICA, M.V., BRAZDARU, L., LECA, M. and POPA, L., 2011. Characterization and in Vitro Release of Chlorhexidine Digluconate Contained in Type i Collagen Porous Matrices. *Revue Roumaine De Chimie,***56**(1), pp. 65.

SUN, M., FAN, A., WANG, Z. and ZHAO, Y., 2012. Dendrimer-mediated drug delivery to the skin. *Soft Matter,* **8**(16), pp. 4301-4305.

SURIYAPHOL, G., SARIKAPUTI, M. and SURIYAPHOL, P., 2009. Differential responses of cells from human skin keratinocyte and bovine mammary epithelium to attack by pore-forming< i> Staphylococcus aureus</i> α-toxin. *Comparative Immunology, Microbiology and Infectious Diseases,* **32**(6), pp. 491-502.

SVENSON, S., 2009. Dendrimers as versatile platform in drug delivery applications. *European Journal of Pharmaceutics and Biopharmaceutics,* **71**(3), pp. 445-462.

SVENSON, S. and TOMALIA, D.A., 2005. Dendrimers in biomedical applications—reflections on the field. *Advanced Drug Delivery Reviews,* **57**(15), pp. 2106-2129.

SWEETMAN, S., ed, 2011. *Martindale: The complete drug reference.* 37th edn. London: Pharmaceutical Press.

TABBAKHIAN, M., TAVAKOLI, N., JAAFARI, M.R. and DANESHAMOUZ, S., 2006. Enhancement of follicular delivery of finasteride by liposomes and niosomes: 1. In vitro permeation and in vivo deposition studies using hamster flank and ear models. *International Journal of Pharmaceutics,* **323**(1), pp. 1-10.

TAKEUCHI, H., MANO, Y., TERASAKA, S., SAKURAI, T., FURUYA, A., URANO, H. and SUGIBAYASHI, K., 2011. Usefulness of Rat Skin as a Substitute for Human Skin in the in Vitro Skin Permeation Study. *Experimental Animals,* **60**(4), pp. 373-384.

TAN, G., XU, P., LAWSON, L.B., HE, J., FREYTAG, L.C., CLEMENTS, J.D. and JOHN, V.T., 2009. Hydration effects on skin microstructure as probed by high-resolution cryo-scanning electron microscopy and mechanistic implications to enhanced transcutaneous delivery of biomacromolecules. *Journal of Pharmaceutical Sciences,* **99**(2), pp. 730-740.

TANAKA, T., ISHII, M., NAKANO, S., MORI, Y., YANO, Y., IIJIMA, T., TAKEDA, K. and KIDO, Y., 2006. Microbial degradation of disinfectants: two new aromatic degradation products of chlorhexidine, chlorhexidine aromatic degradation product (CHADP)-4 and CHADP-6, produced by Pseudomonas sp. strain No. A-3. *Journal of Health Science,* **52**(1), pp. 58-62.

TANAKA, T., MURAYAMA, S., TUDA, N., NISHIYAMA, M., NAKAGAWA, K., MATSUO, Y., ISOHAMA, Y. and KIDO, Y., 2005. Microbial degradation of disinfectants. A new chlorhexidine degradation intermediate (CHDI), CHDI-C, produced by Pseudomonas sp. strain No. A-3. *Journal of Health Science,* **51**(3), pp. 357-361.

TANJI, N., OKAMOTO, M., KATAYAMA, Y., HOSOKAWA, M., TAKAHATA, N. and SANO, Y., 2008. Investigation of the cosmetic ingredient distribution in the stratum corneum using NanoSIMS imaging. *Applied Surface Science,***255**(4), pp. 1116-1118.

TAO, X., YANG, Y., LIU, S., ZHENG, Y., FU, J. and CHEN, J., 2013. Poly (amidoamine) dendrimer-grafted porous hollow silica nanoparticles for enhanced intracellular photodynamic therapy. *Acta Biomaterialia,* **9**(1), pp. 85-93.

TATTAWASART, U., HANN, A., MAILLARD, J.Y., FURR, J. and RUSSELL, A., 2000. Cytological changes in chlorhexidine-resistant isolates of Pseudomonas stutzeri. *Journal of Antimicrobial Chemotherapy,* **45**(2), pp. 145-152.

TATTAWASART, U., MAILLARD, J.-., FURR, J.R. and RUSSELL, A.D., 1999. Development of resistance to chlorhexidine diacetate and cetylpyridinium chloride in Pseudomonas stutzeri and changes in antibiotic susceptibility.*Journal of Hospital Infection,* **42**(3), pp. 219-229.

TEARNEY, G., BREZINSKI, M., SOUTHERN, J., BOUMA, B., HEE, M. and FUJIMOTO, J., 1995. Determination of the refractive index of highly scattering human tissue by optical coherence tomography. *Optics Letters,* **20**(21), pp. 2258-2260.

TEICHMANN, A., JACOBI, U., WEIGMANN, H., STERRY, W. and LADEMANN, J., 2005. Reservoir function of the stratum corneum: development of an in vivo method to quantitatively determine the stratum corneum reservoir for topically applied substances. *Skin Pharmacology and Physiology,* **18**(2), pp. 75-80.

THOMAS, L., MAILLARD, J.-., LAMBERT, R.J.W. and RUSSELL, A.D., 2000. Development of resistance to chlorhexidine diacetate in Pseudomonas aeruginosa and the effect of a 'residual' concentration. *Journal of Hospital Infection,* **46**(4), pp. 297-303.

THOMPSON, J.P. and SCHENGRUND, C.L., 1998. Inhibition of the adherence of cholera toxin and the heat-labile enterotoxin of< i> Escherichia coli</i> to cell-surface GM1 by oligosaccharide-derivatized dendrimers.*Biochemical Pharmacology,* **56**(5), pp. 591-597.

THOMPSON, J.P. and SCHENGRUND, C.L., 1997. Oligosaccharide-derivatized dendrimers: defined multivalent inhibitors of the adherence of the cholera toxin B subunit and the heat labile enterotoxin of E. coli to GM1.*Glycoconjugate Journal,* **14**(7), pp. 837-845.

THOMPSON, P.M., 1991. Quantitative surface analysis of organic polymer blends using a time-of-flight static secondary ion mass spectrometer. *Analytical Chemistry,* **63**(21), pp. 2447-2456.

TOLIA, G.T. and CHOI, H.H., 2008. The role of dendrimers in topical drug delivery. *Pharmaceutical Technology,* **32**(11), pp. 88-98.

TOMALIA, D.A., DEWALD, J.R., HALL, M.R., MARTIN, S.J. and SMITH, P.B., 1984. Preprints of the 1st SPSJ International Polymer Conference, Society of Polymer Science Japan, Kyoto. , pp. 64.

TOMALIA, D. and DURST, H., 1993. Genealogically directed synthesis: starburst/cascade dendrimers and hyperbranched structures. *Supramolecular Chemistry I—Directed Synthesis and Molecular Recognition,* , pp. 193-313.

TOMALIA, D.A. and FRÉCHET, J.M.J., 2001. Dendrimers and other dendritic polymers. Wiley, New York, USA.

TOMALIA, D.A., NAYLOR, A.M. and GODDARD III, W.A., 1990. Starburst dendrimers: molecular-level control of size, shape, surface chemistry, topology, and flexibility from atoms to macroscopic matter. *Angewandte Chemie International Edition in English,* **29**(2), pp. 138-175.

TOMALIA, D., BAKER, H., DEWALD, J., HALL, M., KALLOS, G., MARTIN, S., ROECK, J., RYDER, J. and SMITH, P., 1985. A new class of polymers: Starburst-dendritic macromolecules. *Polymer Journal,* **17**(1), pp. 117-132.

TOPP, A., BAUER, B.J., TOMALIA, D.A. and AMIS, E.J., 1999. Effect of solvent quality on the molecular dimensions of PAMAM dendrimers. *Macromolecules,* **32**(21), pp. 7232-7237.

TORCHILIN, V.P., 2005. Recent advances with liposomes as pharmaceutical carriers. *Nature Reviews Drug Discovery,* **4**(2), pp. 145-160.

TOUITOU, E., MEIDAN, V.M. and HORWITZ, E., 1998. Methods for quantitative determination of drug localized in the skin. *Journal of Controlled Release,* **56**(1-3), pp. 7-21.

TREBILCOCK, K.L., HEYLINGS, J.R. and WILKS, M.F., 1994. In-Vitro Tape Stripping as a Model for In-Vivo Skin Stripping. *Toxicology in Vitro,* **8**(4), pp. 665-667.

TSUJIMOTO, H., HARA, K., TSUKADA, Y., HUANG, C., KAWASHIMA, Y., ARAKAKI, M., OKAYASU, H., MIMURA, H. and MIWA, N., 2007. Evaluation of the permeability of hair growing ingredient encapsulated PLGA nanospheres to hair follicles and their hair growing effects. *Bioorganic & Medicinal Chemistry Letters,* **17**(17), pp. 4771-4777.

UPPULURI, S., KEINATH, S.E., TOMALIA, D.A. and DVORNIC, P.R., 1998. Rheology of dendrimers. I. Newtonian flow behavior of medium and highly concentrated solutions of polyamidoamine (PAMAM) dendrimers in ethylenediamine (EDA) solvent. *Macromolecules,* **31**(14), pp. 4498-4510.

URQUHART, A.J., TAYLOR, M., ANDERSON, D.G., LANGER, R., DAVIES, M.C. and ALEXANDER, M.R., 2008. TOF-SIMS analysis of a 576 micropatterned copolymer array to reveal surface moieties that control wettability. *Analytical Chemistry,* **80**(1), pp. 135-142.

VAARA, M., 1992. Agents that increase the permeability of the outer membrane. *Microbiological Reviews,* **56**(3), pp. 395-411.

VALENTA, C., SIMAN, U., KRATZEL, M. and HADGRAFT, J., 2000. The dermal delivery of lignocaine: influence of ion pairing. *International Journal of Pharmaceutics,* **197**(1–2), pp. 77-85.

VAN DER MAADEN, K., JISKOOT, W. and BOUWSTRA, J., 2012. Microneedle technologies for (trans) dermal drug and vaccine delivery. *Journal of Controlled Release,* **161**(2), pp. 645-655.

VAN DER MERWE, D., BROOKS, J., GEHRING, R., BAYNES, R., MONTEIRO-RIVIERE, N. and RIVIERE, J., 2006. A physiologically based pharmacokinetic model of organophosphate dermal absorption. *Toxicological Sciences,* **89**(1), pp. 188-204.

VAN HAL, D.A., JEREMIASSE, E., JUNGINGER, H.E., SPIES, F. and BOUWSTRA, J.A., 1996. Structure of fully hydrated human stratum corneum: a freeze-fracture electron microscopy study. *Journal of Investigative Dermatology,***106**(1), pp. 89-95.

VANDAMME, T.F. and BROBECK, L., 2005. Poly (amidoamine) dendrimers as ophthalmic vehicles for ocular delivery of pilocarpine nitrate and tropicamide. *Journal of Controlled Release,* **102**(1), pp. 23-38.

VANDERMOLEN, R.G., SPIES, F., VANTNOORDENDE, J.M., BOELSMA, E., MOMMAAS, A.M. and KOERTEN, H.K., 1997. Tape stripping of human stratum corneum yields cell layers that originate from various depths because of furrows in the skin. *Archives of Dermatological Research,* **289**(9), pp. 514-518.

VARGAS, G., CHAN, E.K., BARTON, J.K., RYLANDER, H.G. and WELCH, A.J., 1999. Use of an agent to reduce scattering in skin. *Lasers in Surgery and Medicine,* **24**(2), pp. 133-141.

VENDITTO, V.J., REGINO, C.A.S. and BRECHBIEL, M.W., 2005. PAMAM dendrimer based macromolecules as improved contrast agents. *Molecular Pharmaceutics,* **2**(4), pp. 302-311.

VENNAT, B., GROSS, D., POUGET, M., POURRAT, A. and POURRAT, H., 1995. Comparison of the physical stability of astringent hydrogels based on cellulose derivatives. *Drug Development and Industrial Pharmacy,* **21**(5), pp. 559-570.

VENNAT, B., LARDY, F., ARVOUET-GRAND, A. and POURRAT, A., 1998. Comparative texturometric analysis of hydrogels based on cellulose derivatives, carraghenates, and alginates: Evaluation of adhesiveness. *Drug Development and Industrial Pharmacy,* **24**(1), pp. 27-35.

VENUGANTI, V.V.K. and PERUMAL, O.P., 2009. Poly (amidoamine) dendrimers as skin penetration enhancers: Influence of charge, generation, and concentration. *Journal of Pharmaceutical Sciences,* **98**(7), pp. 2345-2356.

VENUGANTI, V.V.K. and PERUMAL, O.P., 2008. Effect of poly (amidoamine)(PAMAM) dendrimer on skin permeation of 5-fluorouracil. *International Journal of Pharmaceutics,* **361**(1-2), pp. 230-238.

VENUGANTI, V.V., SAHDEV, P., HILDRETH, M., GUAN, X. and PERUMAL, O., 2011. Structure-skin permeability relationship of dendrimers. *Pharmaceutical Research,* **28**(9), pp. 2246-2260.

VIGEANT, P., LOO, V.G., BERTRAND, C., DIXON, C., HOLLIS, R., PFALLER, M.A., MCLEAN, A.P.H., BRIEDIS, D.J., PERL, T.M. and ROBSON, H.G., 1998. An outbreak of Serratia marcescens infections related to contaminated chlorhexidine. *Infection Control and Hospital Epidemiology,* pp. 791-794.

VITKOVA, Z., OREMUSOVA, J., VITKO, A. and BEZAKOVA, Z., 2011. Influence of Surfactants on Release of Chlorhexidine from Hydrogels. *Tenside Surfactants Detergents,* **48**(1), pp. 48-52.

VITKOVA, Z., OREMUSOVA, J., HERDOVA, P. and KODADOVA, A., 2013. Release and Rheological Properties of Topical Drugs Part 1: Influence of the surfactant (benzethonium chloride) and temperature on the drug (chlorhexiding dihydrochloride) release kinetics. *Tenside Surfactants Detergents,* **50**(1), pp. 39-44.

VOEGELI, R., HEILAND, J., DOPPLER, S., RAWLINGS, A.V. and SCHREIER, T., 2007. Efficient and simple quantification of stratum corneum proteins on tape strippings by infrared densitometry. *Skin Research and Technology,***13**(3),.

VON EIFF, C., BECKER, K., MACHKA, K., STAMMER, H. and PETERS, G., 2001. Nasal carriage as a source of Staphylococcus aureus bacteremia. *New England Journal of Medicine,* **344**(1), pp. 11-16.

WAHLBERG, J. and WENNERSTEN, G., 1971. Hypersensitivity and photosensitivity to chlorhexidine. *Dermatology,* **143**(6), pp. 376-379.

WALCH, A., RAUSER, S., DEININGER, S.O. and HÖFLER, H., 2008. MALDI imaging mass spectrometry for direct tissue analysis: a new frontier for molecular histology. *Histochemistry and cell biology,* **130**(3), pp. 421-434.

WALSH, C., 2000. Molecular mechanisms that confer antibacterial drug resistance. *Nature,* **406**(6797), pp. 775-781.

WALTERS, K.A.R., M.S, 2005. The structure and function of the skin. In: K.A. WALTERS, ed, *Dermatological and Transdermal Formulations.* Volume 119 edn. Marcel Dekker, pp. 1-40.

WANG, B., NAVATH, R.S., MENJOGE, A.R., BALAKRISHNAN, B., BELLAIR, R., DAI, H., ROMERO, R., KANNAN, S. and KANNAN, R.M., 2010. Inhibition of bacterial growth and intramniotic infection in a guinea pig model of chorioamnionitis using PAMAM dendrimers. *International Journal of Pharmaceutics,* **395**(1), pp. 298-308.

WANG, J.C., WILLIAMS, R.R., WANG, L. and LODER, J., 1990. In vitro skin permeation and bioassay of chlorhexidine phosphanilate, a new antimicrobial agent. *Pharmaceutical Research,* **7**(10), pp. 995-1002.

WANG, X., MILNER, T.E., CHANG, M.C. and NELSON, J.S., 1996. Group refractive index measurement of dry and hydrated type I collagen films using optical low-coherence reflectometry. *Journal of Biomedical Optics,* **1**(2), pp. 212-216.

WANG, Z., ITOH, Y., HOSAKA, Y., KOBAYASHI, I., NAKANO, Y., MAEDA, I., UMEDA, F., YAMAKAWA, J., KAWASE, M. and YAG, K., 2003. Novel transdermal drug delivery system with polyhydroxyalkanoate and starburst polyamidoamine dendrimer. *Journal of Bioscience and Bioengineering,* **95**(5), pp. 541-543.

WANG, Z., ITOH, Y., HOSAKA, Y., KOBAYASHI, I., NAKANO, Y., MAEDA, I., UMEDA, F., YAMAKAWA, J., NISHIMINE, M., SUENOBU, T., FUKUZUMI, S., KAWASE, M. and YAGI, K., 2003. Mechanism of enhancement effect of dendrimer on transdermal drug permeation through polyhydroxyalkanoate matrix. *Journal of Bioscience and Bioengineering,* **96**(6), pp. 537-540.

WANNACHAIYASIT, S. and PHAECHAMUD, T., 2010. Development of chlorhexidine thermosensitive gels as a mouth antiseptic. *J Metals Materials Minerals,* **20**, pp. 165-168.

WEIGMANN, H.J., LADEMANN, J., MEFFERT, H., SCHAEFER, H. and STERRY, W., 1999. Determination of the horny layer profile by tape stripping in combination with optical spectroscopy in the visible range as a prerequisite to quantify percutaneous absorption. *Skin Pharmacology and Physiology,* **12**(1-2), pp. 34-45.

WEIGMANN, H.J., LINDEMANN, U., ANTONIOU, C., TSIKRIKAS, G.N., STRATIGOS, A.I., KATSAMBAS, A., STERRY, W. and LADEMANN, J., 2003. UV/VIS absorbance allows rapid, accurate, and reproducible mass determination of corneocytes removed by tape stripping. *Skin Pharmacology and Applied Skin Physiology,* **16**(4),.

WEINSTEIN, R.A., MILSTONE, A.M., PASSARETTI, C.L. and PERL, T.M., 2008. Chlorhexidine: expanding the armamentarium for infection control and prevention. *Clinical Infectious Diseases,* **46**(2), pp. 274-281.

WEIR, E., LAWLOR, A., WHELAN, A. and REGAN, F., 2008. The use of nanoparticles in anti-microbial materials and their characterization. *Analyst,* **133**(7), pp. 835-845.

WELZEL, J., REINHARDT, C., LANKENAU, E., WINTER, C. and WOLFF, H., 2004. Changes in function and morphology of normal human skin: evaluation using optical coherence tomography. *British Journal of Dermatology,***150**(2), pp. 220-225.

WELZEL, J., 2001. Optical coherence tomography in dermatology: a review. *Skin Research and Technology,* **7**(1), pp. 1-9.

WESTER, R. and MAIBACH, H., 1995. Penetration enhancement by skin hydration. *Percutaneous Penetration Enhancers,* CRC press, Boca Raton, FL.pp.21-28*.*

WHEATLEY, V.R., 1963. The nature, origin and possible functions of the cutaneous lipids, *Proceedings Science Section. Toilet Goods Association*, pp. 25-28.

WHITE, J.H., 1994. *Alcohol-based antimicrobial compositions,* US5288486 US patent.

WIEN, K., 1997. TOF-SIMS analysis of polymers. *Nuclear Instruments and Methods in Physics Research Section B: Beam Interactions with Materials and Atoms,* **131**(1), pp. 38-54.

WIENER, E., AUTERI, F., CHEN, J., BRECHBIEL, M., GANSOW, O., SCHNEIDER, D., BELFORD, R., CLARKSON, R. and LAUTERBUR, P., 1996. Molecular dynamics of ion-chelate complexes attached to dendrimers. *Journal of the American Chemical Society,* **118**(33), pp. 7774-7782.

WIENER, E., BRECHBIEL, M., BROTHERS, H., MAGIN, R., GANSOW, O., TOMALIA, D. and LAUTERBUR, P., 2005. Dendrimer-based metal chelates: A new class of magnetic resonance imaging contrast agents. *Magnetic Resonance in Medicine,* **31**(1), pp. 1-8.

WILLIAMS, A.C. and BARRY, B.W., 2012. Penetration enhancers. *Advanced Drug Delivery Reviews,* 64, pp. 128-137.

WILLIAMS, A.C., 2003. *Transdermal and topical drug delivery from theory to clinical practice.* 1 Lambeth High Street, London.: Pharmaceutical Press.

WINNICKA, K., SOSNOWSKA, K., WIECZOREK, P., SACHA, P.T. and TRYNISZEWSKA, E., 2011. Poly (amidoamine) dendrimers increase antifungal activity of clotrimazole. *Biological and Pharmaceutical Bulletin,* **34**(7), pp. 1129-1133.

WINNICKA, K., WROBLEWSKA, M., WIECZOREK, P., SACHA, P.T. and TRYNISZEWSKA, E., 2012. Hydrogel of ketoconazole and PAMAM dendrimers: formulation and antifungal activity. *Molecules,* **17**(4), pp. 4612-4624.

WINTERS, A.L. and MINCHIN, F.R., 2005. Modification of the Lowry assay to measure proteins and phenols in covalently bound complexes. *Analytical Biochemistry,* **346**(1), pp. 43-48.

WIWATTANAPATAPEE, R., CARREÑO-GÓMEZ, B., MALIK, N. and DUNCAN, R., 2000. Anionic PAMAM dendrimers rapidly cross adult rat intestine in vitro: a potential oral delivery system? *Pharmaceutical Research,* **17**(8), pp. 991-998.

WOLF, B.A. and SNYDER, F., 1995. *Cosmetic compositions having keratolytic and anti-acne activity,* EP0696451, EU patent.

WOLLER, E.K., WALTER, E.D., MORGAN, J.R., SINGEL, D.J. and CLONINGER, M.J., 2003. Altering the strength of lectin binding interactions and controlling the amount of lectin clustering using mannose/hydroxyl-functionalized dendrimers. *Journal of the American Chemical Society,* **125**(29), pp. 8820-8826.

WONG, W., GOH, C. and CHAN, K., 1990. Contact urticaria from chlorhexidine. *Contact Dermatitis,* **22**(1), pp. 52-52.

WORLD HEALTH ORGANIZATION, 2001. *Global Strategy for Containment of Antimicrobial Resistance. WHO/CDS/CSR/DRS/2001.2 (http://www.who.int/csr/resources/publications/drugresist/en/EGlobal_Strat.pdf, accessed 9 January 2012).* Geneva: .

WU, H., RAMACHANDRAN, C., WEINER, N.D. and ROESSLER, B.J., 2001. Topical transport of hydrophilic compounds using water-in-oil nanoemulsions. *International Journal of Pharmaceutics,* **220**(1), pp. 63-75.

WU, L., LU, X., KULP, K.S., KNIZE, M.G., BERMAN, E.S.F., NELSON, E.J., FELTON, J.S. and WU, K.J.J., 2007. Imaging and differentiation of mouse embryo tissues by ToF-SIMS. *International Journal of Mass Spectrometry,* **260**(2-3), pp. 137-145.

XIA, L., JU, X., LIU, J., XIE, R. and CHU, L., 2010. Responsive hydrogels with poly(N-isopropylacrylamide-co-acrylic acid) colloidal spheres as building blocks. *Journal of Colloid and Interface Science,* **349**(1), pp. 106-113.

XU, F., KANG, E. and NEOH, K., 2006. pH-and temperature-responsive hydrogels from crosslinked triblock copolymers prepared via consecutive atom transfer radical polymerizations. *Biomaterials,* **27**(14), pp. 2787-2797.

XU, W., RANGER-MOORE, J.R., SABODA, K., SALASCHE, S.J., WARNEKE, J.A. and ALBERTS, D.S., 2003. Investigating sun-damaged skin and actinic keratosis with optical coherence tomography: a pilot study. *Technology in Cancer Research & Treatment,* **2**(6),.

XU, X. and ZHU, Q., 2007. Evaluation of skin optical clearing enhancement with Azone as a penetration enhancer. *Optics Communications,* **279**(1), pp. 223-228.

YAMANE, M., WILLIAMS, A. and BARRY, B., 1995. Effects of terpenes and oleic acid as skin penetration enhancers towards 5-fluorouracil as assessed with time; permeation, partitioning and differential scanning calorimetry.*International Journal of Pharmaceutics,* **116**(2), pp. 237-251.

YANG, H. and LOPINA, S., 2003. Penicillin V-conjugated PEG-PAMAM star polymers. *Journal of Biomaterials Science, Polymer Edition,* **14**(10), pp. 1043-1056.

YASUDA, K., OHMIZO, C. and KATSU, T., 2004. Mode of action of novel polyamines increasing the permeability of bacterial outer membrane. *International Journal of Antimicrobial Agents,* **24**(1), pp. 67-71.

YIYUN, C., TONGWEN, X. and RONGQIANG, F., 2005. Polyamidoamine dendrimers used as solubility enhancers of ketoprofen. *European Journal of Medicinal Chemistry,* **40**(12), pp. 1390-1393.

YOSHIMURA, K., 2011. *Composition containing oxocarbon and use thereof,* EP1845135, EU patent.

YUE, I.C., POFF, J., CORTÉS, M.E., SINISTERRA, R.D., FARIS, C.B., HILDGEN, P., LANGER, R. and SHASTRI, V.P., 2004. A novel polymeric chlorhexidine delivery device for the treatment of periodontal disease. *Biomaterials,* **25**(17), pp. 3743-3750.

ZANDERIGO, F., FERRARI, S., QUEIROLO, G., PELLO, C. and BORGINI, M., 2000. Quantitative TOF-SIMS analysis of metal contamination on silicon wafers. *Materials Science and Engineering: B,* **73**(1), pp. 173-177.

ZENG, P., ZHANG, G., RAO, A., BOWLES, W. and WIEDMANN, T.S., 2009. Concentration dependent aggregation properties of chlorhexidine salts. *International Journal of Pharmaceutics,* **367**(1–2), pp. 73-78.

ZGODA, J. and PORTER, J., 2001. A convenient microdilution method for screening natural products against bacteria and fungi. *Pharmaceutical Biology,* **39**(3), pp. 221-225.

ZHANG, L., PORNPATTANANANGKUL, D., HU, C. and HUANG, C., 2010. Development of Nanoparticles for Antimicrobial Drug Delivery. *Current Medicinal Chemistry,* **17**(6), pp. 585-594.

ZHANG, G., MOORE, D.J., SLOAN, K.B., FLACH, C.R. and MENDELSOHN, R., 2007. Imaging the prodrug-to-drug transformation of a 5-fluorouracil derivative in skin by confocal Raman microscopy. *Journal of Investigative Dermatology,* **127**(5), pp. 1205-1209.

ZHAO, C., ZHUANG, X., HE, P., XIAO, C., HE, C., SUN, J., CHEN, X. and JING, X., 2009. Synthesis of biodegradable thermo-and pH-responsive hydrogels for controlled drug release. *Polymer,* **50**(18), pp. 4308-4316.

ZHAO, Y., FAN, X., LIU, D. and WANG, Z., 2011. PEGylated thermo-sensitive poly(amidoamine) dendritic drug delivery systems. *International Journal of Pharmaceutics,* **409**(1-2), pp. 229-236.

ZHU, H. and GRANT, D.J., 1996. Influence of water activity in organic solvent water mixtures on the nature of the crystallizing drug phase. 2. Ampicillin. *International Journal of Pharmaceutics,* **139**(1), pp. 33-43.

ZHU, H., YUEN, C. and GRANT, D.J., 1996. Influence of water activity in organic solvent water mixtures on the nature of the crystallizing drug phase. 1. Theophylline. *International Journal of Pharmaceutics,* **135**(1), pp. 151-160.

ZIMELIS, V.M. and JACKSON, G.G., 1973. Activity of aminoglycoside antibiotics against Pseudomonas aeruginosa: specificity and site of calcium and magnesium antagonism. *Journal of Infectious Diseases,* **127**(6), pp. 663-669.